Quantifying Redox Signals: a tool to investigate adaptive responses to oxidative stress

By

Diane Lind

MSc. (Genetics)

Submitted in fulfilment of the academic requirements for the degree of Doctor of Philosophy

in Genetics

School of Life Sciences

College of Agriculture, Engineering and Science

University of KwaZulu-Natal

Pietermaritzburg

South Africa

April 2024

Preface

The research contained in this dissertation was completed by the candidate while based in the discipline of Genetics, School of Life Sciences of the College of Agriculture, Engineering and Science, University of KwaZulu-Natal, Pietermaritzburg, South Africa under the supervision of Dr C. S. Pillay.

These studies represent original work by the candidate and have not otherwise been submitted in any form to another University. Where use has been made of the work by other authors it has been duly acknowledged in the text.

Supervisor: Dr C. S. Pillay

Signature: _____

Date: _____

College of Agriculture, Engineering, and Science Declaration of Plagiarism

I, Diane Lind, declare that:

(i) the research reported in this dissertation, except where otherwise indicated or acknowledged, is my original work;

(ii) this dissertation has not been submitted in full or in part for any degree or examination to any other university;

(iii) this dissertation does not contain other persons' data, pictures, graphs or other information, unless specifically acknowledged as being sourced from other persons;

(iv) this dissertation does not contain other persons' writing, unless specifically acknowledged as being sourced from other researchers. Where other written sources have been quoted, then:

a) their words have been re-written but the general information attributed to them has been referenced;

b) where their exact words have been used, their writing has been placed inside quotation marks, and referenced;

c) where I have used material for which publications followed, I have indicated in detail my role in the work;

(v) this dissertation is primarily a collection of material, prepared by myself, published as journal articles or presented as a poster and oral presentations at conferences. In some cases, additional material has been included;

(vi) this dissertation does not contain text, graphics or tables copied and pasted from the Internet, unless specifically acknowledged, and the source being detailed in the dissertation and in the References sections.

___ _____

Signature: Diane Lind

Date: __19/04/2024_____

List of Publications

Lind, D. J, Naidoo, K. C, Tomalin, L. E, Rohwer, J. R, Veal, E. A & Pillay, C. S. Quantifying redox transcription factor dynamics as a tool to investigate redox signalling. (2024). *Free radical biology and medicine*, *218,* 16-25. https://doi.org/10.1016/j.freeradbiomed.2024.04.004

Lind, D. J, Rohwer, J. R & Pillay, C. S. (2024). Quantifying the profiles of genetically encoded redox sensors. *(Manuscript in preparation).*

Lind, D. J, Rohwer, J. R & Pillay, C. S. (2024). Quantifying pre-treatment effects in the NRF2/Keap1 pathway for assessing cellular adaption to oxidative stress. *(Manuscript in preparation).*

Acknowledgements

"It is the glory of God to conceal things, but the glory of Kings (Scientists) is to search things out – Proverbs 25:2 $_{ESV,MSG}$ *"*

I would like to express my thanks and appreciation to the following people who without this thesis would not have been possible:

First and foremost, to my supervisor Dr Ché Pillay who has walked the long road with me from Honours to PhD. You have been an incredible mentor, and I truly appreciate the investment you've made in helping me become a better scientist. I have thoroughly enjoyed my time in your lab it really has been my second home over the last few years and I'll definitely miss it.

To Dr Elizabeth Veal and Prof Johann Rohwer for your valuable inputs into the experimental and computational aspects of this project. To Faiaz for help with the chickens and tips on all things antibodies. To Dr Lucky Murefu, I miss the corridor catch-ups and general comradery that came with all the experimental challenges; you are truly missed. To Megan Brunkhorst for technical help and advice over the years.

To Pat, Renny, for ordering and processing our precious reagents without which none of our projects can happen.

To the following lab members of B23 (past and present), Nolyn, TJ, Limpho, Erin, Keli and Sarvana. The lab has been one of my favourite places and each of you made the day-to-day labwork so much more fun than just running experiments and troubleshooting.

To Tim and Limpho for the many wine nights and writing parties, they got me through more than you know. Along with all the other fun times and adventures.

To Bam and Erin, I'm so grateful for both of your ongoing friendships from undergrad. I miss having you two around UKZN, but I guess it's finally my turn to say goodbye to old agric.

To my friends, Kerry A, Kerry B, Zel, Katherine, Caity C, Lauren, Mark, Jared, John, and anyone who's ever had the patience to listen to me explain my thesis. I've truly valued all

the fun times that have happened along the way, from hikes, camping trips, coffees, game nights and holiday adventures.

Lastly to my parents Justin and Ingrid Lind. Thank you both for your unwavering support throughout my postgraduate journey I really can't thank you both enough for everything you do. To Julia and Bradley Lind for your encouragement to keep going even when I had run out of steam. Finally, to Pops, you've been a great source of strength over the last year, and I appreciate our long discussions.

This thesis is dedicated to the loving memory of Prudence Lind (Nana), Gloria and Keith Boutle (Granny & Grandpa)

List of Abbreviations

AUC	Area under the curve
AEBSF	4-(2-aminoethyl)benzenesulfonyl fluoride hydrochloride
BSA	Bovine serum albumin
ddH_2O	Double distilled water
DEM	Diethyl malonate
dH2O	Distilled water
DTT	Dithiothreitol
ECL	Electrochemiluminescence
EDTA	Ethylenediaminetetraacetic acid
EMM	Edinburgh minimal media
EPR	Electron paramagnetic resonance
ER	Endoplasmic reticulum
GAPDH	Glyceraldehyde 3-phosphate dehydrogenase
GFP	Green fluorescent protein
GSH	Glutathione
GSSG	Glutathione disulfide
H_2O	Water
H_2O_2	Hydrogen peroxide
HRP	Horseradish peroxidase
HyPer	Hydrogen peroxide sensor
IAA	Iodoacetamide
IgG	Immunoglobulin G
MAPK	mitogen-activated protein kinase
NAC	N-acetylcysteine
NADPH	Nicotinamide adenine dinucleotide phosphate
NOX	NADPH oxidase
OD	Optical density
OxD	Degrees of oxidation
PEG	Polyethylene glycol

PKC	Protein kinase C
PTPs	Protein tyrosine phosphatases
R	Ratiometric value
roGFP	Redox-sensitive green fluorescent protein
ROS	Reactive oxygen species
SDS-PAGE	Sodium dodecyl-sulfate polyacrylamide gel electrophoresis
SH	Sulfhydryl residues
SOH	Sulfenic acid
SOOH	Sulfinic acid
*t*BHQ	*tert*-Butylhydroquinone
t-BOOH	*tert*-Butyl hydroperoxide
TCA	Trichloroacetic acid
TEMED	Tetramethylethylenediamine

List of Tables

List of Figures

Abstract

In the context of redox biology's oxidative eustress/distress model, the contrasting roles of ROS, such as hydrogen peroxide, under normoxic and toxic oxidative stress conditions has been more clearly elucidated. However, a fundamental question in the field has been understanding how dynamic redox signalling processes contribute to balancing the cellular response to oxidative eustress/distress. We employed a quantitative approach, evaluating redox signals based on area under the curve (AUC), signal amplitude, time, and duration. These parameters allowed us to investigate how dynamic profiles changed in response to various oxidants across three distinct experimental contexts. First, quantifying the dynamic response of the Tpx1/Pap1 redox-regulated pathway in *Schizosaccharoymyces pombe* revealed a graded signal and transcriptional response to input peroxide concentrations. Secondly, we applied this method to establish the upper and lower limits of detection for the redox probes HyPer7 and roGFP-TSA2/Tpx1 in *Saccharomyces cerevisiae* and *S. pombe*, providing a set of criteria for improved selection and comparison of probes. Thirdly, we quantitatively evaluated the dynamic response of the mammalian NRF2/Keap1 pathway following pre-exposure to DEM and tBHQ. Our findings revealed that, unlike the Tpx1/Pap1 pathway, this pathway showed that the timing of oxidant exposure influenced the NRF2 response. These metrics have therefore provided useful insights to several different pathways in both experimental and analytical contexts. Importantly, these measures allow for further exploratory questions to be asked and provide a fundamental framework for assessing dynamic responses of redox-regulated pathways associated with cell physiology and disease.

Contents

Chapter 1

Literature Review

"Progress in science depends on new techniques, new discoveries and new ideas, probably in that order" ~ Sydney Brenner

1.1 Introduction

A predominant concept in redox biology is that organisms utilising oxygen for energy production generate reactive oxygen species (ROS), which play a role in various diseases (Szechyńska-Hebda et al., 2022; Brieger et al., 2012). Interestingly, it has also become evident that ROS also play crucial roles in normal cellular functions (Valko et al., 2007). The discovery of key ROS species, antioxidant proteins, and cellular redox signalling pathways spurred the emergence of several theories aiming to explain the links between redox processes and disease (Flohé, 2020; Holmström & Finkel, 2014). These prevalent theories are the Free Radical Theory of Aging, the Oxidative Stress Theory, and the Oxidative Eustress and Distress Theory (Figure 1.1), which are discussed below.

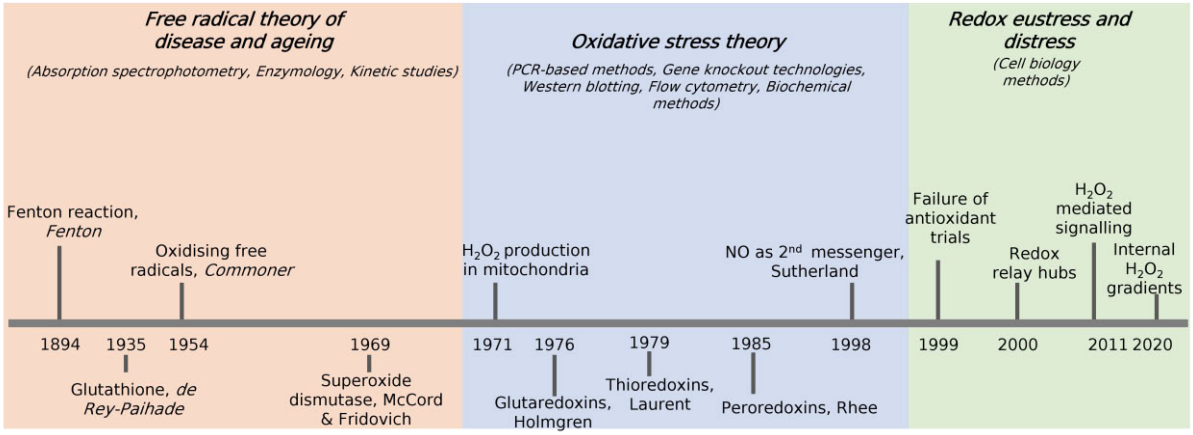

Figure 1.1: The timeline of significant discoveries within redox biology.

Redox biology has three major theories to explain the role of ROS in cell physiology that were informed by methodological advances. The discovery of ROS species by absorption spectrophotometry, enzymology and kinetic studies led to the Free Radical Theory of Disease and Aging. The characterisation of antioxidants like superoxide dismutase (McCord & Fridovich), glutaredoxins (Holmgren), thioredoxins (Laurent), peroxiredoxins (Rhee), and the

tripeptide glutathione (de Rey-Paihade), through (bio)chemical, genetic and cellular techniques culminated in the Oxidative Stress Theory. Lastly, the redox Eustress and Distress Theory was informed by discoveries in cell biology. This figure was adapted from Berndt et al, (2022).

This review will explore these themes in redox biology and the methodologies that informed them. We will also highlight where there are limitations in our current approaches, and the additional methods required for a better understanding of redox-regulated processes.

1.1.1 Free radical theory of disease and ageing

The initial concept of free radicals dates back to the late 1800s with the Fenton reaction. In a series of experiments, Fenton combined ferrous ions, hydrogen peroxide, and tartic acid with the addition of sodium hydroxide, resulting in a bright purple solution, which indicated the presence of hydroxyl radicals (Fenton, 1894). Additional intermediate compounds were discovered using manometric readings, such as the reduction of hydrogen peroxide by catalase to water (Figure 1.2) (Keilin & Hartree, 1939). These studies highlighted the significance of oxygen being reduced into unstable by-products. However, the link between these harmful compounds and the cellular environment was unclear.

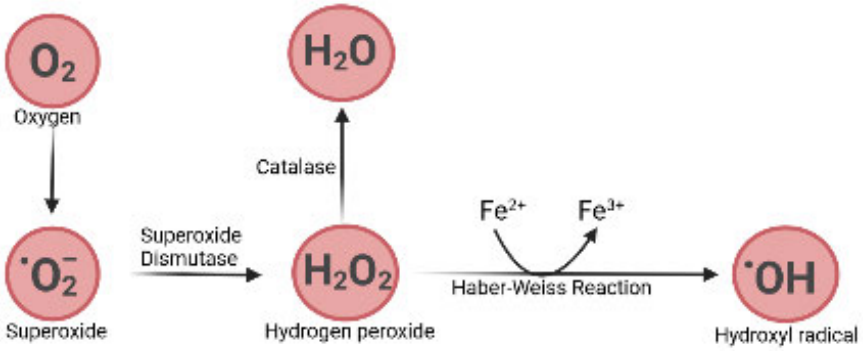

Figure 1.2: The reduction of oxygen into reactive oxygen species.
Oxygen is metabolized into superoxide which is converted to hydrogen peroxide by superoxide dismutase. Hydrogen peroxide combined with iron has the propensity to form hydroxyl radicals or is degraded to water by catalase. Figure adapted from Bardaweel et al., (2018).

It was only by the 1950's that the connection between cellular damage, radiation exposure and the generation of oxidising free radicals was fully understood. Gerschman and colleagues demonstrated that mice exposed to high oxygen concentrations had life expectancies similar to those exposed to ionising radiation (Gerschman et al., 1954). These data began to clarify the link between ROS formation and their negative effects on living organisms. However, the specific molecular mechanisms involved, and whether these processes occurred under normoxic conditions were poorly understood. Interestingly, the toxic effects of ROS could be mitigated by protective agents like glutathione, β-mercaptoethylamine, cysteine, and oxytryamine which increased the life expectancy in mice exposed to toxic oxygen levels (Gerschman et al., 1954). Following a series of studies showing similar results, the Free Radical Theory of Disease and Aging was developed (Alper, 1956; Bacq & Herve, 1951; Boyland & Sargent, 1951; George & Irivine, 1954; Harman, 1956). The theory proposed that ageing and age-related diseases result from cumulative damage caused by exposure to exogenous ROS (Gladyshev, 2014; Ivanova & Yankova, 2013). As a result, efforts shifted toward mitigating these effects in diseased or aged organisms (Halliwell & Gutteridge, 2015).

1.1.1.1 Intracellular generation of ROS

The first steps to offset the effects of ROS was to identify these species in a biological setting. The paramagnetic resonance spectroscopy (EPR) technique enabled researchers to study chemical species with unpaired electrons. An initial demonstration of this capability was seen with riboflavin complexes, which formed free radicals showing that endogenous proteins were capable of generating ROS (Isenberg & Szent-Gyorgyi, 1958). Using spectrophotometric analysis, McCord and Fridovich also showed how superoxide dismutase, an innate cellular protein, was capable of converting superoxide to hydrogen peroxide (Mccords & Fridovich, 1969). This study highlighted that ROS, like superoxide were substrates for enzymes which changed the view that ROS were only a result of external stressors. Further studies highlighted how cellular antioxidant systems counteracted the effects of ROS. For example, inhibition of superoxide dismutase caused spinal neural death and degeneration *in vitro* (Rothstein et al., 1994).

A significant source of ROS production is the mitochondrial electron transport chain, where oxygen is the terminal electron acceptor for energy production (Matsuzaki et al., 2009). Initially, indirect methods were used to identify this ROS formation in the mitochondria. Specifically, Clark oxygen sensors in bovine heart tissue revealed that the ATP production,

which is coupled to oxygen consumption during oxidative phosphorylation, was less than expected (Jensen, 1966). This discrepancy was attributed to 'electron leaks' which then lead to superoxide formation (Finikova et al., 2007). In recent studies, the efflux of hydrogen peroxide from the mitochondrial electron transport chain has been better measured by using enzyme-coupled assays or fluorescent probes (Tabassum et al., 2020).

Further use of EPR demonstrated that molecular oxygen undergoes reduction by NADPH, producing superoxide, which, in turn, leads to respiratory bursts of superoxide that serve as a protective mechanism against pathogens (Rossi & Zatti, 1964; Berndt et al., 2022;). This protective role of ROS complicated the perspective of ROS solely being harmful by-products of aerobic metabolism. Significantly, these methods established the foundation for the discovery of NADPH oxidase (NOX) enzymes, which transfer of electrons to molecular oxygen, leading to the formation of superoxide (Figure 1.3; Sumimoto, 2008; Vermot et al., 2021) and are significant producers of hydrogen peroxide by cells (Wong et al., 2019).

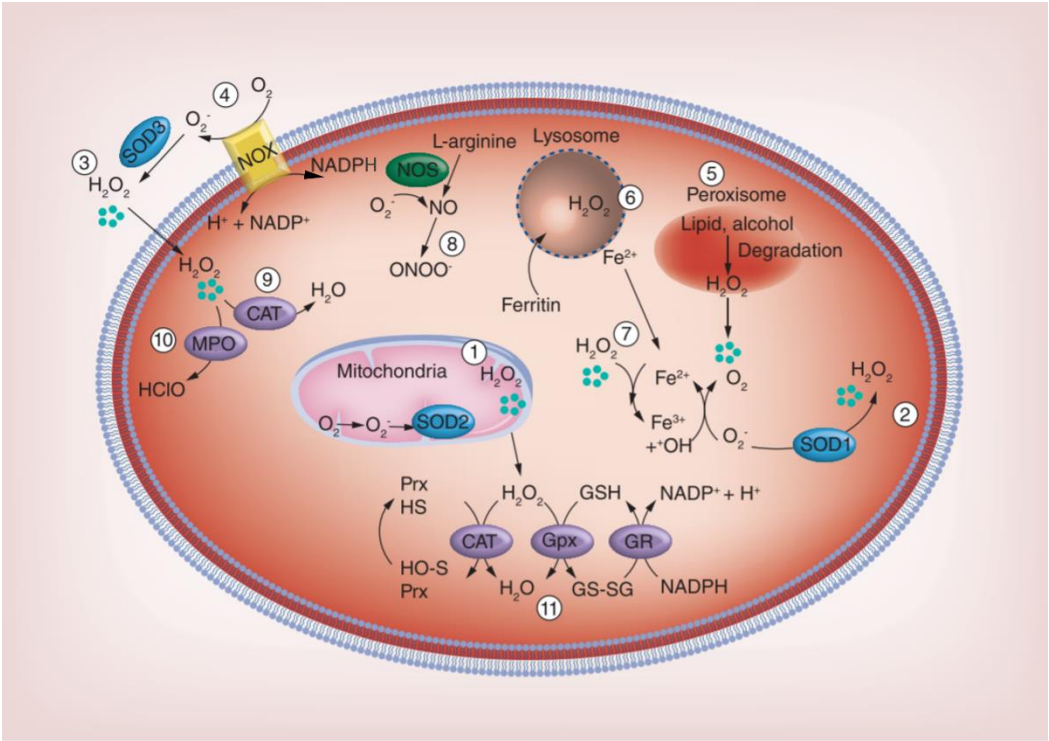

Figure 1.3: Intracellular generation of ROS from metabolic processes.

Superoxide is converted to hydrogen peroxide by SOD1, SOD2 and SOD3 in the mitochondria, cytosol and across the lipid membrane, respectively (1, 2, 3). NADPH oxidase (NOX) catalyses the production of superoxide from oxygen (4), and lipid oxidation in peroxisomes results in hydrogen peroxide (5). Fenton chemistry in the lysosome leads to ROS production from

interactions with iron (6, 7), and peroxynitrite is formed from nitric oxide synthase (NOS) (8). Hydrogen peroxide is degraded to water by catalase (9) and can also form hypochlorous acid by myeloperoxidase (10). The reduction of hydrogen peroxide is undertaken by many systems including glutathione peroxidase (Gpx) and catalase (CAT) (11). Permission to reproduce this image from Kim et al, (2015) was obtained by Elsevier.

The endoplasmic reticulum (ER) actively engages in oxidative protein folding, a process associated with the production of hydrogen peroxide (Pluquet et al., 2015; Shergalis et al., 2020). Using ferrothiocyanate, cytochrome c peroxidase assays and scopoletin fluorescence, hepatic microsomes (fragments of the ER) were found to generate hydrogen peroxide (Thurman et al., 1972). In several mammalian cells, a combination of genetic and biochemical investigations established that the formation of eukaryotic disulfide bonds during protein folding was facilitated by protein disulfide isomerase (PDI) and endoplasmic reticulum oxidoreductin-1 (ERO-1), which transfer electrons from molecular oxygen to PDI (Shergalis et al., 2020). Another source of hydrogen peroxide within cells is fatty acid oxidation within peroxisomes (Figure 1.3). The oxidation rates of purified peroxisomes from rat liver tissue were assessed in response to various substrates such as glycolate and L-lactate (Baumgart et al., 1996; Mcgroarty et al., 1974). By calculating the oxidation rate of peroxisomes in relation to glycolate and L-lactate concentrations, hydrogen peroxide generation could be inferred as a by-product of fatty acid oxidation process within peroxisomes (Oshino et al., 1975). These critical discoveries provided evidence that ROS were indeed produced in the cellular environment and prompted researchers to investigate the potential role of ROS in disease.

1.1.2 The role of ROS in disease

ROS, particularly high levels of hydrogen peroxide, have been implicated in various diseases such as cardiovascular diseases, neurological disorders, and cancer (Brieger et al., 2012; Berndt et al., 2022; Kawagishi & Finkel, 2014). For example, the heart, requiring high oxygen levels for efficient energy production, contains thousands of mitochondria per cell (Pohjoismäki & Goffart, 2017). Tissue samples associated with atherosclerosis (Yu et al., 2013), ischemia (Rodrigo et al., 2013), and hypertension (Rawat et al., 2014) were either measured for ROS and/or assessed for damage to proteins, lipids, and DNA. Elevated ROS and molecular oxidation levels were identified in these studies linking ROS to these diseases. Similarly, elevated monoamine oxidase (MAO) protein expression was assessed using

chemiluminescence and western blotting of heart tissue from aged mice. The study revealed an increase in MAO-dependent hydrogen peroxide production, suggesting that MAO acts as a significant source of hydrogen peroxide in aging hearts.(Maurel et al., 2003). ROS production in human erythrocytes was also elevated in patients with Alzheimer's disease (Sultana & Perluigi, 2006).

Given the high energy demands of the brain, several studies aimed to explore the connection between ROS levels and neurological disorders. Assessments of DNA damage in brain tissue samples were conducted using immunohistochemistry and found that the DNA damage markers, 8-hydroxyl-2'-deoxyguanosine (8-OHdG) and apurine/apyrimidine (AP), were elevated in mice with brain injuries (Leak et al., 2015). Additionally, protein oxidation, as measured by western blotting using anti-dinitrophenyl (DNP) antibodies (Shacter et al., 1994), linked oxidative stress to brain injuries (Nakamura et al., 2005). In post-mortem samples of Parkinson's disease brains, the measurement of glutathionyl and cysteinyl conjugates using HPLC revealed elevated oxidation of L-DOPA (a precursor to dopamine) and D-aspartate in Parkinson's disease patients compared to control patients (Sian et al., 1999). These findings and others provided supporting evidence that ROS contribute to disease development, leading to the widespread acceptance of the Free Radical Theory of Disease (Forman & Zhang, 2021). However, and in parallel, the discovery that manganese superoxide dismutase (MnSOD) was required for cell proliferation, revolutionised the understanding of ROS in redox biology showing that ROS were required for normal cellular function and therefore, a more sophisticated theory was required (Oberley & Buettner, 1979).

1.1.3 Oxidative Stress Theory

The Oxidative Stress Theory posits that there is a balance between ROS production and the removal of ROS by antioxidants within the cellular environment (Figure 1.4). Only when this balance is disrupted do ROS become capable of damaging crucial cellular constituents (Figure 1.4) (Cadenas & Sies, 1985). Consequently, developing therapeutic interventions aimed at preserving cellular homeostasis and preventing oxidative damage became the focus of many clinical trials. Initially, antioxidant compounds, sourced from plant or animal tissues, including vitamins C and E, found application in extending the shelf life of foods (Eskin & Przybylski R, 2001). Recognizing the inhibitory role of these antioxidants sparked significant interest in exploring their potential benefits for human health (Mousa et al., 2019). This shift

in perspective has since driven extensive research into the broader implications of antioxidants, transcending their initial use in food preservation (Eskin & Przybylski R, 2001).

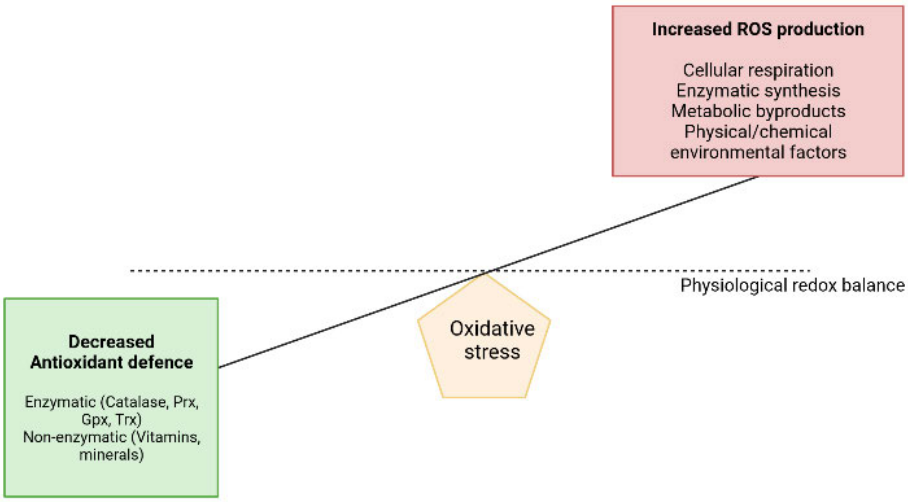

Figure 1.4: Typical representation of the oxidative stress theory.
The physiological redox balance is disturbed when there is an increase in the production or exposure to ROS simultaneously combined with a decrease in antioxidant capabilities, usually through a decrease in the availability of antioxidant enzymes. These factors combined constitute the Oxidative Stress Theory. This image was recreated based on Poljsak et al, (2013)

Antioxidants can be broadly divided into two classes, enzymatic and non-enzymatic, according to their mode of activity (Flieger et al., 2021; Mamta et al., 2014). Non-enzymatic antioxidants can be further divided into endogenous and exogenous antioxidants and primarily work by terminating free radical chain reactions (Flieger et al., 2021). Exogenous non-enzymatic antioxidants like vitamins A, C, and E, along with flavonoids, carotenoids, and phenolic acids, work by donating electrons to ROS leading to neutralisation (Mamta et al., 2014; Mousa et al., 2019). However, upon oxidation these compounds are seldom recycled (Mousa et al., 2019).

Enzymatic antioxidants consist of thiol-based and non-thiol-based antioxidants that detoxify the cellular environment from ROS. One of the oldest enzymatic antioxidants identified was catalase in 1818 by Louis Thenard, who, along with Joseph Louis Gay-Lussac, also contributed to the discovery of hydrogen peroxide. The enzymatic activity of catalase rapidly degrades hydrogen peroxide to water through a heme or manganese group at its active site (Fita & Rossmann, 1985; Whittaker, 2012). The first mechanistic insight into how thiol-

based antioxidants detoxify oxidants emerged from the characterisation of glutathione extracted from yeast lysates in 1932 by Willstätter (Willstatter, 1932). Here, cysteine residues on glutathione were shown to be oxidised by hydrogen peroxide, resulting in intermolecular disulfide bridge formation. Understanding the conformational changes of proteins after oxidant addition led to the discovery of additional thiol-based antioxidant proteins, which were later revealed to be part of complex signalling networks (Birben et al., 2012). An array of methods, ranging from genetic screens, biochemical assays, PCR-based methodologies, DNA sequencing, kinetic assays, and immunoblotting, were employed in discovering and characterising the three major thiol-based redox systems in cells: thioredoxin, glutaredoxin, and peroxiredoxin systems (Hanschmann et al., 2013). These systems play essential roles in cellular defence against oxidative stress and will be further described in the following sections.

1.1.3.1 The thioredoxin system

In a 1964 study, thioredoxin was first characterised in *Escherichia coli* when its role in the synthesis of deoxyribonucleotides was uncovered (Laurent et al., 1964). In this *in vitro* study, thioredoxin reductase reduced the oxidised form of thioredoxin which in turn provided reducing equivalents to ribonucleotide reductase for the synthesis of deoxyribonucleotides (Laurent et al., 1964). In a subsequent study, the secondary structure of thioredoxin was characterised using chromatography, which identified two critical cysteines essential for disulfide bridge formation (Reichard, 1968). Additionally, fluorescence spectroscopy was used to identify the oxidised and reduced forms of thioredoxin, which enabled subsequent studies to explore the role of thioredoxin in response to various stimuli (Reichard, 1968). The sequencing of this protein revealed an active site motif (Cys-Gly-Pro-Cys) which was later found to be conserved across most kingdoms (Lee et al., 2013).

The thioredoxin system works through thiol-disulfide exchange, where thioredoxin undergoes nucleophilic exchange with the disulfide bond of a substrate protein (Figure 1.5) (Dyson et al., 1991; Roos et al., 2009). This results in the oxidised form of thioredoxin while the substrate protein becomes reduced. The oxidised form of thioredoxin is recycled by thioredoxin reductase utilising NADPH as an electron donor (Figure 1.5) (Roos et al., 2009). Several studies have employed gene knockout technologies to delete or disrupt genes associated with the thioredoxin system. Yeast and bacterial cells subjected to these genetic modifications exhibit heightened sensitivity to oxidative stress, leading to a notable reduction

in viability (Lee et al., 2019; Raninga et al., 2015; Stancill et al., 2022). In mammals, mutations in this system are lethal for embryonic development (Matsui et al., 1996).

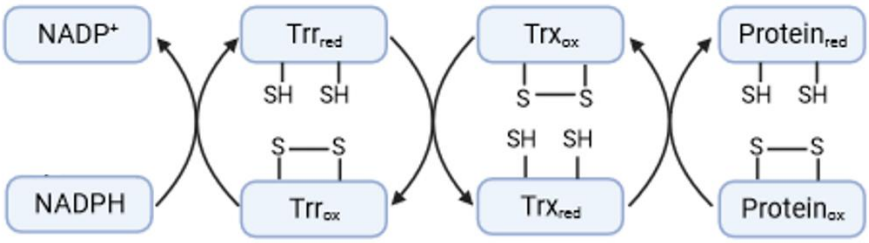

Figure 1.5: The thioredoxin system regulates cellular processes and maintains the cellular redox balance.

The cysteine residues (SH) on reduced thioredoxin undergo oxidation leading to the formation of an intramolecular disulfide bridge. Thioredoxin reductase facilitates its reduction, utilizing reducing equivalents derived from NADPH. Subsequently, the reduced thioredoxin becomes available for interactions with oxidized target proteins. Figure adapted from Karlenius & Tonissen, (2010)

1.1.3.2 The glutaredoxin system

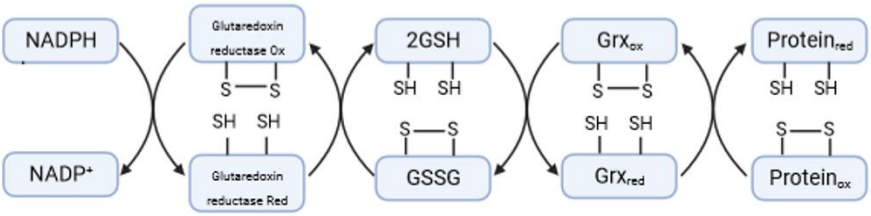

The glutaredoxin (Grx) system was initially discovered in 1976 by Holmgren and colleagues when an *E. coli* strain deleted for thioredoxin still showed reduction of ribonucleotide reductase (Holmgren, 1976). *In vitro* assays further characterised the stability, molecular size, catalytic properties, and thiol specificity of glutaredoxins (Holmgren, 1985).There are two classes of glutaredoxins. The first, known as monothiol glutaredoxins, typically feature a CGFS motif with one active cysteine residue in the active site (Herrero & De La Torre-Ruiz, 2007). These glutaredoxins play critical roles in iron-sulfur cluster biogenesis (Talib & Outten, 2021).

Figure 1.6: The glutaredoxin system maintains thiol-disulfide homeostasis.
In the glutaredoxin system, GSSG becomes oxidised and forms two glutathione molecules which then oxidises glutaredoxin, reducing target proteins. Oxidised GSSG is recycled into the system using glutathione reductase and reducing equivalents from NADPH. Figure adapted from Ren et al., (2017).

The second class of glutaredoxins (dithiol) functions similarly to thioredoxins. These low molecular weight (~12 kDa) proteins generally feature a redox-regulated disulfide motif (CXXC) (Lillig & Berndt, 2013; Netto & Antunes, 2016a). The electron flow in this system is similar to the thioredoxin system (Figure 1.6). Electrons from NADPH are used by glutaredoxin reductase, to reduce glutathione disulfide (GSSG) into two glutathione (GSH) molecules (Miller & Schmidt, 2019). Glutathione then reduces oxidised glutaredoxin, which, in turn, reduces oxidised proteins (Fernandes & Holmgren, 2004). The glutaredoxin system, in contrast to thioredoxin system, is also responsible for deglutathionylation. Under oxidative stress or even under normoxic conditions, free thiol or sulfenic acid residues form mixed disulfide bonds with glutathione molecule(s), in a process known as glutathionylation. These thiol residues are protected from hyperoxidation but the activity of these proteins can be disrupted (Fernandes & Holmgren, 2004; Gallogly & Mieyal, 2007). Glutathionylation is reversed by the glutaredoxin system (Fernandes & Holmgren, 2004; Gallogly & Mieyal, 2007).

1.1.3.3 The peroxiredoxin system

Initially, peroxiredoxins were purified from *Saccharomyces cerevisiae* using polyethylene glycol precipitation, chromatography, and gel filtration (Kim et al., 1988). The antioxidant activity of the then unidentified protein did not show catalase, superoxide dismutase, or glutathione peroxidase activity (Kim et al., 1988) and was found to require thiol reduction and was called thiol-specific antioxidant (TSA) (Kim et al., 1988). The unidentified protein was later renamed to 'peroxiredoxin', and six subtypes have been identified to date (Poole & Nelson, 2016; Wood et al., 2003).

All peroxiredoxins contain a conserved peroxidatic cysteine found in the protein's *N*-terminal region (Rhee et al., 2001; Toledano & Huang, 2016). Crystallographic studies have revealed that peroxiredoxins belonging to subtypes one through four exhibit an additional

cysteine residue in the C-terminal region, serving as a resolving component in the protein's structure. When the peroxidatic cysteine is oxidised by a peroxide, it forms sulfenic acid (SOH), leading to an intermolecular disulfide bridge with the resolving cysteine residue and this disulfide is reduced by the thioredoxin system, recycling the peroxiredoxin (Figure 1.7; Sue et al., 2005). The oxidised form of the peroxiredoxin is also able to oxidise other proteins and can therefore act a redox signalling relay (Sobotta et al., 2015).

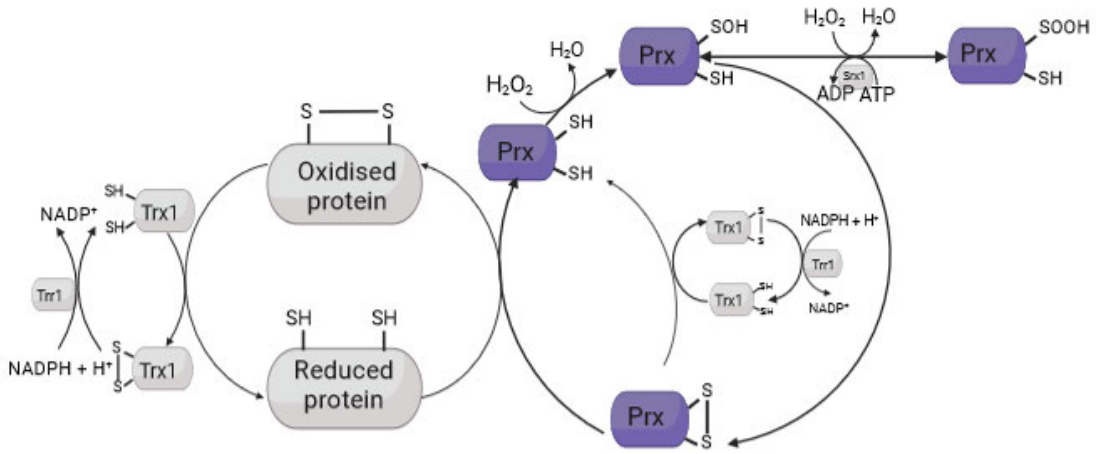

Figure 1.7: The peroxiredoxin system has a complex role in antioxidant defence and redox signalling.

Peroxiredoxins are directly oxidized by hydrogen peroxide, and this oxidation is subsequently reduced by the thioredoxin system. Additionally, peroxiredoxins have the capability to undergo hyperoxidation, forming sulfinic acid, a state that can be reduced by sulfiredoxin and ATP. The figure was adapted from Rhee (2016).

In most cells, peroxiredoxins are be reduced by the thioredoxin system (Figure 1.7). Kinetic studies revealed that peroxiredoxins are highly efficient in reducing hydrogen peroxide and alkyl hydroperoxides ($k_2 \sim 10^5$-10^8 M^{-1} s^{-1}) (Ogusucu et al., 2007) at rates comparable to catalase ($k_2 \sim 10^7$-10^8 M^{-1} s^{-1}) (Davies et al., 2008) and glutathione peroxidase ($k_2 \sim 10^5$–10^8 $M^{-1}s^{-1}$) (Ferrer-Sueta et al., 2011). However, as peroxiredoxins are present at higher concentrations (10-100 µM) within cells (Cox et al., 2010), they are considered the primary reducers of peroxides in most cell types.

In eukaryotes, under high hydrogen peroxide concentrations, the peroxidatic sulfenic acid can be further oxidized to sulfinic acid (SOOH) (Figure 1.7). Initially, this hyperoxidised isoform was considered catalytically dead, but work by Biteau and colleagues showed that

hyperoxidised peroxiredoxins could be reduced by a protein called sulfiredoxin along with ATP (Figure 1.7) (Biteau et al., 2003). The precise role(s) of peroxiredoxin hyperoxidation remains unclear (Veal et al., 2014). In the floodgate mechanism of redox signalling, hyperoxidation presumably inhibits peroxiredoxins, and hydrogen peroxide can go on to oxidise other peroxide-sensitive target proteins, allowing for peroxide-dependent signalling events to occur (Wood et al., 2003b). However, it is unclear how this mechanism operates in the presence of other hyperoxidation-resistant peroxiredoxins, catalases and non-thiol peroxidases (Forman et al., 2014). Alternatively, it has been demonstrated that peroxiredoxin hyperoxidation inhibits the thioredoxin-dependent reduction of peroxiredoxins, leading to increased levels of reduced thioredoxin which can support the repair of oxidised proteins by methionine sulfoxide reductases (Day et al., 2012). Lastly, hyperoxidised peroxiredoxins form decamer structures that show little peroxidase activity (Wood et al., 2002) but act as chaperones to refold damaged proteins (Jang et al., 2004).

1.1.3.4 Oxidative stress theory and clinical trials

The Free Radical Theory of Disease and Aging, and advances in our understanding of cellular antioxidants paved the way for clinical trials with the goal of mitigating excess ROS or enhancing intracellular antioxidant enzyme production. According to the Cochrane database (https://www.cochranelibrary.com/, accessed January 2024), more than 16,000 studies investigating the use of antioxidant supplementation for disease treatment have been conducted, with varied results.

Some trials indicate potential benefits, while others report no improvements or adverse effects. *N*-Acetylcysteine (NAC) supplementation in infertile men appeared to enhance the activity of the NRF2 pathway, resulting in increased sperm production (Jannatifar et al., 2020). Limited to no support has been observed for antioxidant use in preventing chronic diseases, as exemplified by large-scale trials investigating vitamin E and selenium in prostate cancer, which did not demonstrate clear preventative effects (Eidelman et al., 2004; Robinson et al., 2012). Interestingly, evidence suggests that obtaining antioxidants through a well-balanced diet, rather than supplements, may be more beneficial for overall health (Valko et al., 2007). Rather than exerting an antioxidant effect, consumption of redox active compounds within the diet may induce a mild oxidative stress and concomitant antioxidant response (Rahal et al., 2014). This effect has been well documented for mild exercise where oxidative stress in skeletal muscle induces an antioxidant response and the repair of damaged tissues (Thirupathi et al., 2020).

Ongoing research aims to explore more targeted and effective antioxidant therapies (Deledda et al., 2021). However, it is crucial to note that the use of antioxidant supplements for general health and disease prevention is not universally endorsed, and caution is advised, particularly against high-dose supplementation (Firuzi et al., 2011).

Recognizing the faster reactivity of enzymatic antioxidants compared to non-enzymatic counterparts, attention has shifted towards targeting these enzymes to alter signalling pathways to restore redox imbalances (Poljsak et al., 2013). For instance, mimics for catalase and superoxide dismutases (SODs) were proposed to remove superoxide and hydrogen peroxide (Table 1.1) (Anderson et al., 2018). However, these enzyme-based therapies were primarily effective in the extracellular space, and SOD mimics, being non-specific, may act as pro-oxidants, potentially impacting redox signalling pathways (Sotler et al., 2019). Glutathione peroxidase mimics have shown efficacy in eliminating hydrogen peroxide, small organic hydroperoxides, and cholesterol hydroperoxides. These compounds have been investigated in clinical trials involving patients with complete occlusion of the middle cerebral artery. Their application resulted in reduced oxidative stress damage to both gray and white matter in the brain. (Table 1.1) (Imai et al., 2002; Singh et al., 2017). Strategies involving the inhibition of NADPH oxidases or maintaining/replenishing glutathione (GSH) levels have also been explored with some success in replenishing depleted glutathione (Antoniades et al., 2010; Panda et al., 2022). While some clinical trials have reported positive outcomes, such as in the case of male and female fertility (Zavras et al., 2016), achieving effective antioxidant therapies for chronic diseases remains elusive, possibly due to the need for a deeper understanding of redox signalling processes (Margaritelis et al., 2022).

Table 1.1: Antioxidant clinical trials to intervene in chronic illness.

Meta-analysis of clinical trials from the Cochrane database examined the efficacy of antioxidants as an intervention to chronic illnesses such as cancer, heart disease, and other lifestyle-related conditions. Overall, antioxidant supplementation, demonstrated no effect in improving patient outcomes across various chronic illnesses.

Antioxidant		**Clinical trial objective (Clinical trial phase-Result)**	**Reference**
Non-enzymatic antioxidants	Vitamin E	Ageing, oxidative stress, cancers (Phase I; II -No effect)	Buettner et al., 1993; Bruno et al., 2016
	Vitamin C	Cardiovascular diseases (Phase I; II- No effect)	Hill et al., 2003; Fangelak, 2002
	N-acetylcysteine (NAC)	Liver paracetamol, cystic fibrosis (Phase I; II- No effect)	Smilkstein et al., 1998; Xu et al., 2016
	β-carotene	Lung cancer (Phase I, No effect)	
		Cardiovascular disease (Phase I – No effect)	Pryor et al., 2000
	Selenium	Lung cancer (Phase I – No effect)	Rees et al., 2013
	Zinc	ALS/motor neuron disease/MS (Phase I – No effect)	Cartes-Jofre et al., 2020, Parks et al., 2020
	Coenzyme Q10		Orrell et al., 2007. Saadi et al., 2021
	Alpha-lipoic acid (ALA)	Heart failure (Phase 1- No effect)	Baicus et al., 2024
		Diabetic peripheral neuropathy (Phase I-No effect)	
Enzymatic antioxidant mimics	SOD (Mn porphyrin)	Amyotrophic lateral sclerosis (ALS) (Phase I)	Benatar, 2007
	SOD (GC4419)	Oral mucositis of oropharyngeal cancer (Phase I)	Anderson et al., 2018

	Salens (EUK-8, EUK-134, EUK-189)	Sepsis, heart ischaemia-reperfusion, ALS (Pre-clinical)	Chatterjee et al., 2004; Langan et al., 2006; Zhang et al., 2006
	GPX (Ebselen)	Meniere disease (Phase III-No result); Bipolar disorder, acute ischaemic stroke, middle cerebral artery disease (Phase I- Some benefits)	Singh et al., 2016; Imai et al., 2003
	GSH esters	Aim to increase GSH in organs (Pre-clinical -No result)	Levy et al., 1993
	NRF2 activators (sulforaphane)	Bladder cancer, diabetes mellitus (Phase II, III- No result); Dilated cardiomyopathy (Phase III- No result)	Wise et al., 2016; Ungvari et al., 2010

1.1.4 Oxidative Eustress and Distress Theory

Accumulating evidence of the critical role played by hydrogen peroxide in cellular signalling processes, together with the failure of antioxidant clinical trials, challenged the concepts posited by the Oxidative Stress Theory (Gough & Cotter, 2011). To readdress the current limitations with the prevailing theories of oxidative stress, Sies and Jones suggested that the oxidative stress theory should be broadened to include oxidative eustress and oxidative distress (Figure 1.8) (Sies, 2017; Sies & Jones, 2020). This revised perspective suggested that hydrogen peroxide is necessary at low concentrations, but beyond a certain threshold, becomes detrimental (Sies & Jones, 2020).

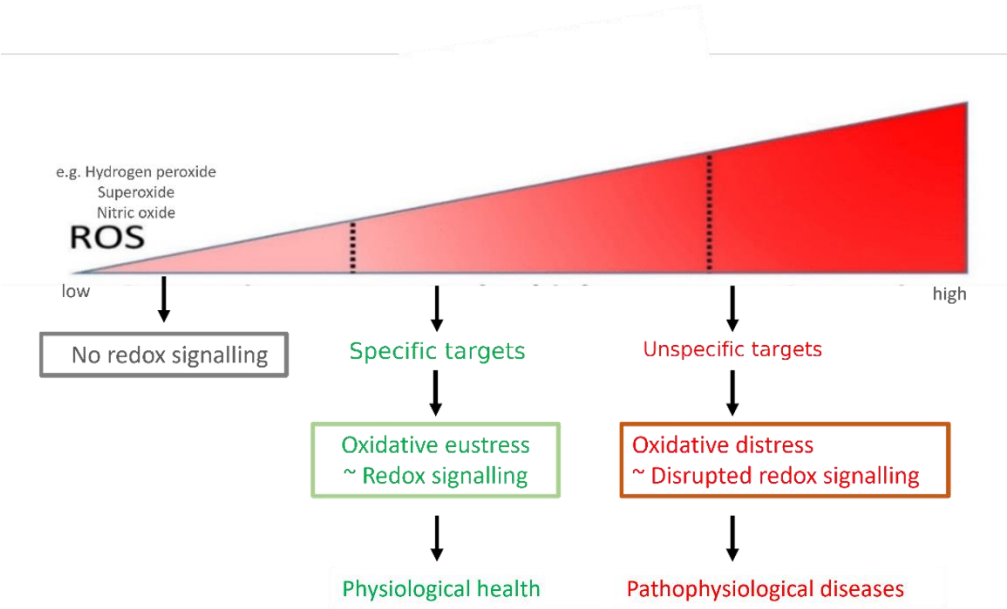

Figure 1.8: Oxidative eustress and distress theory.

The eustress/distress theory states that when hydrogen peroxide concentrations are too low, normal cellular function will be impaired. But at a suitable concentration, positive signalling processes will occur to ensure physiological function. However, as the hydrogen peroxide concentration increases, the cell will become stressed and need to mount an antioxidant defence response. This image was adapted from Fitzpatrick, (2020) and Sies, (2020).

The theory emphasized the dual nature of hydrogen peroxide recognizing its damaging effects and crucial roles in redox signalling and cellular adaptation to oxidative challenges (Sies

& Jones, 2020). For instance, investigations into the development of neurons utilising fluorescent-based sensors revealed that axodendritic cells failed to develop or regenerate when the concentration of internal hydrogen peroxide was below 0.1 nM (Ledo et al., 2022; Wilson et al., 2017). Conversely, in the range of 1-10 nM, neuron growth was normal and showed better regeneration efficiency at the upper limit of this range (Wilson et al., 2017). However, axonal growth would collapse at hydrogen peroxide concentrations greater than 100 nM. These studies revealed that important signalling events occur in the presence of mid-range hydrogen peroxide concentrations (Gough & Cotter, 2011). In the following section, we will define redox signalling, explore three mechanisms of redox signalling, and examine how cells adapt to oxidative stress.

1.1.4.1 Redox signalling

Defining redox signalling is nuanced and may encompass several definitions. For the purpose of this study, we define redox signalling as a kinetic process involving coordinated changes in the oxidation state of redox transduction machinery leading to specific outputs in response to hydrogen peroxide and other oxidants (Pillay et al., 2016). Redox-active molecules such as hydrogen peroxide, superoxide, or nitric oxide play a pivotal role in this process, leading to the formation of disulfide bridges that, in turn, induce structural alterations in proteins (Go et al., 2015; Klomsiri et al., 2011). Alternatively, the sulfinic acid form of a protein (SOH) may also contribute to redox signalling by oxidising cysteine residues of other proteins. Nevertheless, these proteins modified by oxidants activate or inhibit specific signalling cascades or transcription factors (Go et al., 2015; Klomsiri et al., 2011).

Hydrogen peroxide's role as an intracellular secondary messenger is attributed to its unique chemical properties, enabling it to participate in various cellular signalling pathways (Rhee, 2016). For example, hydrogen peroxide can diffuse from the site of its production or across the cell membrane with a relatively stable half-life of 1 ms (Reth, 2002). Additionally, hydrogen peroxide appears to have selective reactivity towards specific thiols (e.g.) hydrogen peroxide reacts with GSH with a second order rate constant of only 0.9 $M^{-1}s^{-1}$ and this rate constant increases dramatically for peroxiredoxins and glutathione peroxidases at around ~10^5-10^8 $M^{-1}s^{-1}$. Interestingly, mammalian plasma contains a bicarbonate/CO_2 buffer, which, upon interaction with hydrogen peroxide, generates the peroxymonocarbonate anion. When compared to hydrogen peroxide (Bakhmutova-Albert et al., 2010) this species can more readily

hyperoxidize peroxiredoxins allowing for oxidation of phosphatases in signalling pathways (Peskin et al., 2019).

In an immunoblot time-course study, it was found that protein kinase C (PKC) pathways, traditionally thought to be activated solely by diacylglycerol through calcium, can also be activated by hydrogen peroxide, indicating its role as a secondary signalling molecule (Kaul et al., 2003; Singh et al., 2022). Likewise, protein tyrosine phosphatases (PTPs), pivotal for numerous fundamental physiological processes, can be inactivated by hydrogen peroxide (Östman et al., 2011). Research has demonstrated that these enzymes harbour a crucial cysteine residue (His-Cys-X-X-Gly-X-X-Arg-Ser/Thr) essential for the inactivation of this signalling cascade, a process that can be subsequently reversed by glutathione (Östman et al., 2011). Another example, is the selective inactivation of GAPDH by hydrogen peroxide where the protein is first sulfenylated by hydrogen peroxide then glutathionylated ultimately inhibiting GAPDH glycolytic activity (Zaffagnini et al., 2019).

The specificity of hydrogen peroxide signalling can be seen from the selective oxidation of key redox-regulated transcription factors. Transcription factors play a crucial role in enabling the adaptive response to external stressors. For instance, in *S. cerevisiae*, the transcription factor Yap1 is essential for inducing the expression of key antioxidant genes in response to oxidative stress. Deletion of Yap1 in *S. cerevisiae* cells increased sensitivity to oxidative stress (Kuge & Jones, 1994). Across various species, there appear to be three types of signalling, direct signalling, sensor-mediated signalling, and indirect signalling (Pillay et al., 2016).

1.1.4.2 Direct redox signalling

A classic example of direct sensing by a transcription factor would be OxyR in *E coli*. OxyR reacts directly with hydrogen peroxide and has four critical cysteines that are oxidised to disulfide bridges (Figure 1.9) (Aslund et al., 1999). OxyR is extremely sensitive to low concentrations of hydrogen peroxide (1–200 nM) and has a switch-like activation profile (Zhang et al., 2019). The expression of over 56 genes, including catalase (*katG*), alkyl hydroperoxidase (*ahpCF*), and cytochrome c peroxidase (*ccpA*), is regulated by oxidized OxyR (Wan et al., 2019). The glutathione system reduces and inactivates oxidised OxyR *in vivo*, although the thioredoxin system can reduce OxyR *in vitro* (Aslund et al., 1999). The sensitivity of OxyR has been harnessed to create highly specific hydrogen peroxide redox sensors

(Belousov et al., 2006). These sensors, coupled with fluorescent proteins, enable targeted detection of hydrogen peroxide in specific locations within a cell (Belousov et al., 2006).

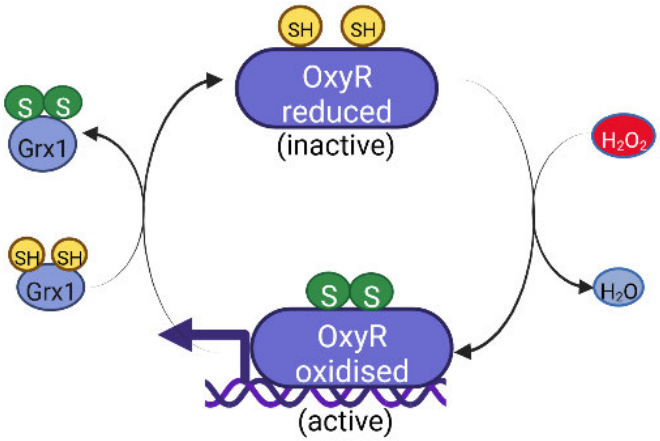

Figure 1.9: Direct hydrogen peroxide signalling.

The E. coli transcription factor, OxyR, is directly activated by hydrogen peroxide and then reduced by the glutathione/glutaredoxin system. This figure was adapted from Aslund et al, (1999).

1.1.4.3 Sensor-mediated redox signalling

Sensor-mediated hydrogen peroxide signalling includes examples of AP-1-like transcription factors (Xanthoudakis et al., 1992), p53/ HIF-1α (Zhang et al., 2014), FOXO/ IGF-1 (Essers et al., 2004), NRF2/Keap1 (Fourquet et al., 2010) and NF-κB/ IκB (Schmidt et al., 1995) homologs. Many of these transcription factors play an important role in regulating stress responses along with essential physiological processes, and their aberrant signalling may contribute to disease (Forman & Zhang, 2021). Sensor-mediated signalling commonly occurs when hydrogen peroxide oxidises a sensor molecule, usually a peroxiredoxin. This molecule will proceed to oxidise other targets including transcription factors which initiate a gene regulatory response. For example, in the fission yeast *Schizosaccharomyces pombe*, hydrogen peroxide oxidises the peroxiredoxin, Tpx1 which then oxidises Pap1 (Figure 1.10). In a *S. pombe Δtpx1* strain, exposure to hydrogen peroxide fails to activate Pap1 showing that Pap1 activation relies specifically on Tpx1 (Calvo et al., 2013). The nuclear export signal (NES) region of Pap1 is altered by oxidised Tpx1 resulting in a conformational change of the protein which can be transported into the nucleus and induces gene transcription including antioxidant genes like *trx1*, *trr1* and *srx1* (Jara et al., 2007; Vivancos et al., 2004). Both Tpx1 and Pap1 are

reduced by the thioredoxin system using reducing equivalents from NADPH (Morgan & Veal, 2007).

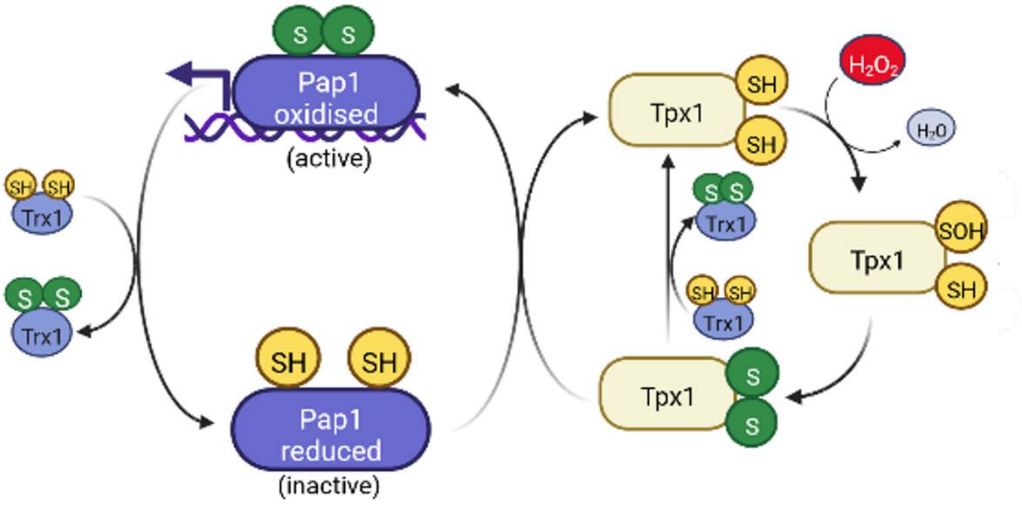

Figure 1.10: Sensor-mediated hydrogen peroxide signalling.

In S. pombe, consensus is that the peroxiredoxin, Tpx1, is oxidised by hydrogen peroxide which then oxidises the transcription factor, Pap1. Both Tpx1 and Pap1 are reduced by Trx1. This figure was adapted from Vivancos et al, (2005).

An example of a redox-regulated transcription factor in mammalian cells is nuclear factor in B cells (NF-κB) (Flohe et al., 1997). NF-κB is redox-regulated through the modulation of an inhibitory protein called IκB (inhibitor of κB) (Flohé et al., 1997). Under normal conditions, IκB keeps NF-κB in an inactive state in the cytoplasm (Flohé et al., 1997). Oxidative stressors such as hydrogen peroxide trigger the phosphorylation and degradation of IkB, allowing NF-κB to translocate into the nucleus and activate target genes (Flohé et al., 1997). Analogously, the NRF2 transcription factor is activated when the attached KEAP1 protein is oxidised (Fourquet et al., 2010). In the presence of oxidative or electrophilic stress, particular cysteine residues on Keap1, notably Cys151, undergo alterations. These modifications result in the dismantling of the Keap1/CUL3 ubiquitin ligase complex, leading to the stabilization of NRF2. Following this, NRF2 migrates to the nucleus, initiating an antioxidant response by activating diverse genes, such as those responsible for catalase, superoxide dismutases, and sulfiredoxin (Morgan & Liu, 2011; Oliveira-Marques et al., 2009).

1.1.4.4 Indirect redox signalling

Indirect redox signalling occurs when the thioredoxin or glutaredoxin systems become oxidised by normal cellular processes (Figure 1.11; Forman et al., 2014). In mammalian cells, under normal cellular conditions, the apoptosis signal-regulating kinase 1 (ASK1) is inactive when thioredoxin is bound in its reduced form (Saitoh et al., 1998). However, once thioredoxin becomes oxidised, it releases ASK1, initiating the activation of this pathway (Saitoh et al., 1998).

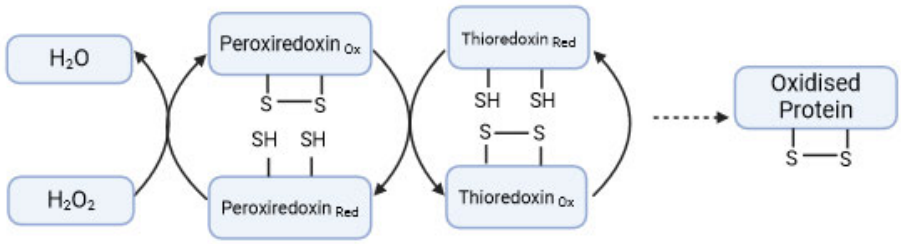

Figure 1.11: Indirect hydrogen peroxide signalling.

The peroxiredoxin system results in the oxidation of the thioredoxin system. The decreased availability of thioredoxin to reduce other oxidised proteins allows for continuous signal transduction processes. This figure was adapted from Pillay et al, (2016).

1.1.5 A method to quantify dynamic redox signals

Conceptual advances such as the oxidative eustress and distress theory, together with improved analytical tools clarified the terminology used to describe oxidative stress, reactive oxygen species and redox signalling. For example, the term oxidative stress has evolved from just ‘good antioxidant’ and ‘bad oxidants’ to a more nuanced understanding of the complex molecular mechanisms that balance redox homeostasis. Sies and Jones iterate that ROS should not be used as an umbrella term for molecules causing oxidative stress. Instead, specific species should be referenced individually, as certain molecules like hydrogen peroxide and nitric oxide have distinct signalling roles (Sies & Jones., 2020). Another example includes how ROS are defined, where molecules like hydrogen peroxide or superoxide should be referred specifically rather than bracketed under umbrella term ‘ROS’ (Margaritelis et al., 2022). Nonetheless, the precise characterisation of redox signalling processes needs further investigation. For example, can healthy redox signalling processes result in aberrant signalling? At which point does

oxidative eustress becomes oxidative distress? What are the critical limits of the eustress/distress signalling processes? How can these signals be measured?

Despite the progress in understanding redox signalling, there remains a measurement gap in quantifying redox signal transduction (Figure 1.12). A generic signalling pathway is defined by a signal input, its computation by the cell and eventual output (Figure 1.12). When defining redox signalling, hydrogen peroxide and other peroxides have been considered as input signals. Genetically encoded redox sensors have been used to determine the internal hydrogen peroxide production (Figure 1.12). The proteins involved in redox signalling events in response to hydrogen peroxide exposure have been identified and measured using genetic knockouts and western blotting experiments respectively (Figure 1.12). Additionally, kinetic studies have revealed the various reaction rates of these protein responses. Nonetheless, current methodological tools do not allow for the measurement of dynamic signalling responses to environmental stimuli. While signal outputs in terms of gene expression in response to hydrogen peroxide have been characterised (Figure 1.12), linking these outputs to the signalling response of redox-sensitive transcription factor activation remained obscure. Precise measurement tools to track signal changes in response to diverse stimuli will enable insights into the oxidative eustress/distress states of the cellular environment.

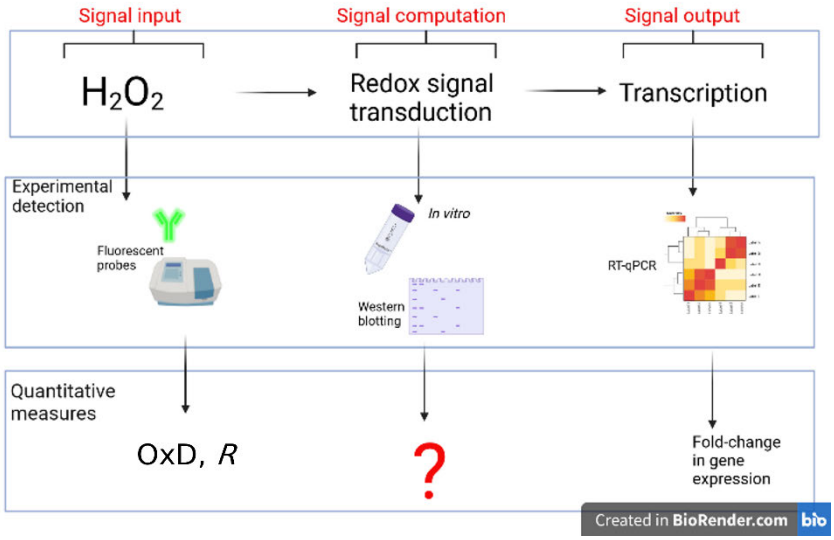

Figure 1.12: The measurement gap in redox-signalling processes.

A redox signal is constituted by a signal input, its computation and subsequent output. Quantitative measures for hydrogen peroxide detection and transcriptomic analysis are well defined. However, measuring the redox signal transduction process quantitatively is currently lacking.

A mathematical model was developed to quantify a generic protein kinase signalling profile by Heinrich and co-workers (Heinrich et al., 2002). In this description three signalling parameters were defined: signalling amplitude, time and duration. Signalling amplitude describes the average concentration of the active form of a protein over a signal interval. The signalling time is the average time to activate a protein, and signal duration is the average time the signalling protein is active for. The description will be further detailed in Chapter 2.1. In this thesis, I attempted to close this measurement gap in quantifying redox signalling dynamics using these parameters. Three applications will be evaluated. First, the activation dynamics of Tpx1/Pap1 will be quantified using the model organism *S. pombe*, with experimental optimisations for this quantification further assessed in Chapter 5. Second, data from genetically encoded redox sensors will be quantified. Third, signalling data generated from the NRF2/Keap1 pathway in response to oxidative stress scenarios will be analysed.

Chapter 2
Quantifying redox transcription factor dynamics as a tool to investigate redox signalling.

2.1 Abstract

A critical feature of the cellular antioxidant response is the induction of gene expression by redox-sensitive transcription factors. In many cells, activating these transcription factors is a dynamic process involving multiple redox steps, but it is unclear how these dynamics should be measured. Here, we show how the dynamic profile of the *Schizosaccharomyces pombe* Pap1 transcription factor is quantifiable by three parameters: signal amplitude, signal time and signal duration. In response to increasing hydrogen peroxide concentrations, the Pap1 amplitude decreased while the signal time and duration showed saturable increases. In co-response plots, these parameters showed a complex, non-linear relationship to the mRNA levels of four Pap1-regulated genes. We also demonstrate that hydrogen peroxide and *tert*-butyl hydroperoxide trigger quantifiably distinct Pap1 activation profiles and transcriptional responses. Based on these findings, we propose that different oxidants and oxidant concentrations modulate the Pap1 dynamic profile, leading to specific transcriptional responses. We further show how the effect of combination and pre-exposure stresses on Pap1 activation dynamics can be quantified using this approach. This method is therefore a valuable addition to the redox signalling toolbox that may illuminate the role of dynamics in determining appropriate responses to oxidative stress.

2.2 Introduction

An unavoidable consequence of aerobic metabolism is the exposure of cells to reactive oxygen species (ROS), such as hydrogen peroxide (Halliwell & Gutteridge, 2015). Hydrogen peroxide signals are essential for regulating an array of physiological responses, but excessive hydrogen peroxide loads result in oxidative stress and cell death (Sies, 2017; Sies & Jones, 2020; Sikes, 2017). The cellular response to hydrogen peroxide insult is multifaceted, involving several regulatory mechanisms, including the induction of specific transcriptional programs by redox-sensitive transcription factor pathways (He et al., 2017; Imlay, 2013). Significantly, cells lacking these transcription factors show increased peroxide sensitivity (Kuge & Jones, 1994; Kullik et al., 1995), but their constitutive activation can also be deleterious (Kudo et al., 1999; Sykiotis & Bohmann, 2010; Toone et al., 1998; Wakabayashi et al., 2003).

The fission yeast *Schizosaccharomyces pombe* is a valuable model for understanding oxidative stress and redox signalling in eukaryotes (Papadakis & Workman, 2015; Veal et al., 2014). Within these cells, the Pap1 transcription factor is activated by oxidation in response to low to intermediate (0.07-1 mM) hydrogen peroxide insults (Vivancos et al., 2004). The 2-Cys peroxiredoxin Tpx1 is likely the primary sensor of hydrogen peroxide and directly or indirectly oxidises several Pap1 cysteines to intramolecular disulfide bonds (Figure 2.1A) (Bozonet et al., 2005; Calvo et al., 2013; Vivancos et al., 2005). Oxidation masks the nuclear export sequence of Pap1 and increases its association with Prr1, leading to the enhanced transcription of several antioxidant and multidrug resistance genes (Calvo et al., 2012). Pap1 oxidation and activity are reversed by cytosolic (Trx1) and nuclear (Txl1) thioredoxins, and Pap1 is only activated under conditions where thioredoxin is oxidised (Bozonet et al., 2005; Brown et al., 2013; Calvo et al., 2013; Vivancos et al., 2005). Accordingly, Pap1 activation is abrogated at hydrogen peroxide concentrations (>1 mM) where the thioredoxin peroxidase activity of Tpx1 is inhibited by hyperoxidation (Jara et al., 2007). However, the Sty1 MAPK becomes increasingly activated in response to increasing concentrations of hydrogen peroxide (>0.2 mM) (Veal et al., 2014), leading to increased Atf1 activity and the enhanced transcription of a broad set of core stress response genes, including some regulated by Pap1 and/or Prr1 (Chen et al., 2008).

Additional evidence suggests that different oxidative inputs trigger quantitative differences in Pap1 activation dynamics (Domènech et al., 2018). For example, different hydrogen peroxide concentrations and different oxidants trigger differences in the Pap1

dynamic oxidation profile (Domènech et al., 2018) and the transcriptional dynamics of Pap1-regulated genes (Figure 2.1B-D) (Chen et al., 2008; Quinn et al., 2002). However, it is unclear how these dynamic profiles should be quantified. To close this quantification gap, we turned to the pioneering work of Heinrich and colleagues, who showed that three parameters, the signal time (τ), signal duration (ϑ) and signal amplitude (S), describe the dynamic profiles of phosphokinase signalling proteins (Heinrich et al., 2002).

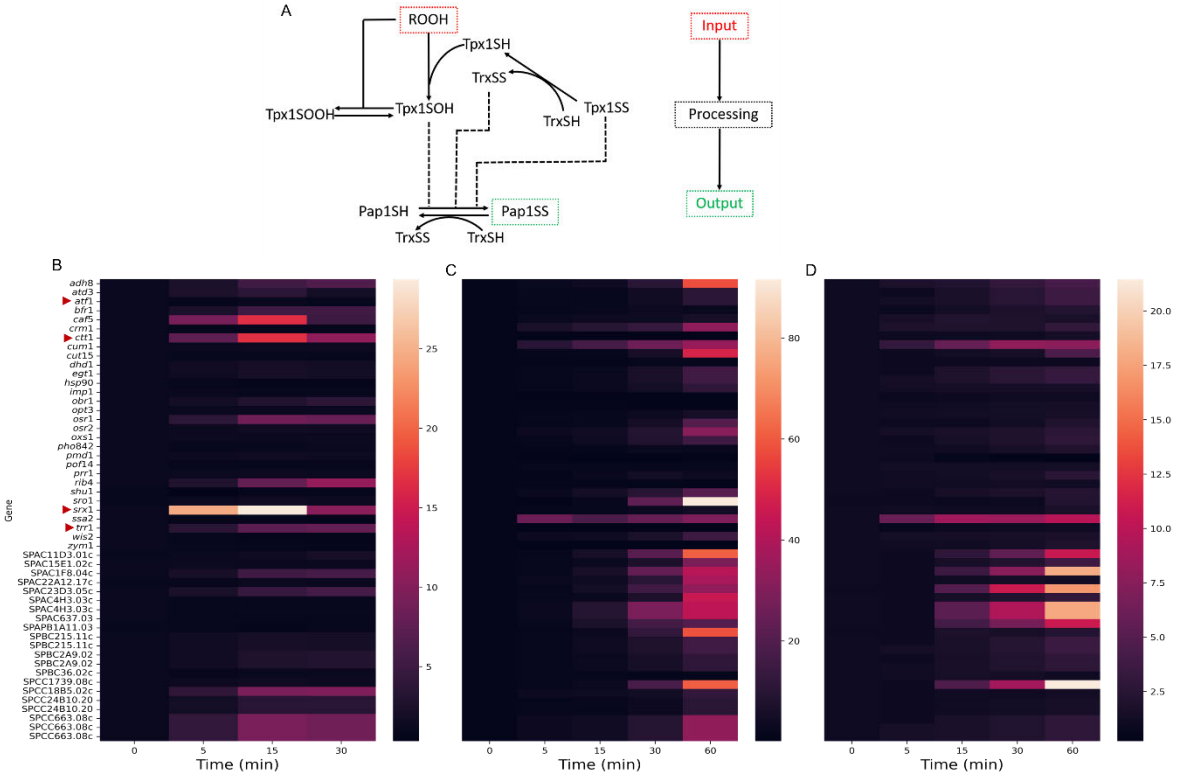

Figure 2.1: Redox signalling processing by the Pap1 system in fission yeast.

In S. pombe, hydrogen peroxide and other hydroperoxides oxidise the peroxiredoxin, Tpx1, which leads to the oxidation of the transcription factor, Pap1 (A). It is unclear whether Pap1 is oxidised by a Tpx1 sulfenic acid, a Tpx1 disulfide or oxidised thioredoxin. Tpx1 is fully hyperoxidised by high concentrations of hydrogen peroxide (> 1000 µM), preventing further Pap1 oxidation, but this hyperoxidised state is reversed by sulfiredoxin. Thioredoxin (Trx) reduces both Pap1 and Tpx1. In this system, the hydrogen peroxide concentration and kinetics of the peroxiredoxin and thioredoxin redox cycles determine the quantitative relationship between the hydroperoxide input and Pap1 output. The dynamics and transcript levels of Pap1-regulated genes show differences following exposure to 70 µM (B), 500 µM (C) and 6 mM (D) hydrogen peroxide bolus treatments (data taken from (Chen et al., 2008). *The genes, atf1, ctt1,*

srx1 and trr1, were analysed in this study and are indicated by a red arrow. Note that the scales for the fold-change in the heatmaps range from 0-30 (B), 0-90 (C) and 0-20 (D).

Briefly, the signal time measures the mean time of the activation signal:

$$\tau = \frac{\int_0^\infty t\mathrm{X}_i(t)dt}{\int_0^\infty \mathrm{X}_i(t)dt} \quad (1)$$

where X_i is the total concentration of activated signalling protein generated over the signalling interval (t). When comparing pathways, faster signalling processes have, on average, a shorter signal time than slower signalling processes. However, because signal time measures the mean time or midway point of a given dynamic profile, lower and higher doses of an input into the same pathway can yield correspondingly shorter and longer signal times (see Figure S.1 for a graphical description and explanation).

A related measure to the signal time is the signal duration (ϑ) which is the standard deviation around the signal time and approximates how long a given signalling protein remains active around the signal time:

$$\vartheta = \sqrt{\frac{\int_0^\infty t^2\mathrm{X}_i(t)dt}{\int_0^\infty \mathrm{X}_i(t)dt} - \tau_i^2} \quad (2)$$

Because the signal duration is defined as the standard deviation around the signal time, signalling processes with different signal times can still share equivalent signal durations (see Figure S.1). Finally, the signal amplitude (S) is not the maximum peak of the dynamic profile but the average concentration of the signalling protein over the signalling duration:

$$S_i = \frac{\int_0^\infty \mathrm{X}_i(t)dt}{2\vartheta} \quad (3)$$

As the amplitude is an average over the signalling duration, profiles with longer signal durations can have lower signal amplitudes than profiles with shorter signal durations (i.e.) a 'low and wide' profile will have a lower amplitude than a 'tall and narrow' profile for a similar concentration of activated signalling protein.

An advantage of this method is that these three parameters can describe any non-periodic dynamic profile allowing for quantitative comparisons between different inputs, different perturbations or even between different redox-regulated pathways (Pillay et al., 2016). This method has largely been used for theoretical and computational studies of phosphokinase systems, although it was shown that kinases control signal amplitude while phosphatases

control amplitude and duration for EGF-induced ERK phosphorylation *in vitro* (Hornberg et al., 2005). In this contribution, we tested whether this method could be used to quantify Pap1 dynamic profiles and whether different oxidants and oxidant concentrations led to distinct signal outputs in this pathway.

2.3 Results

2.3.1 Quantifying the effects of different hydrogen peroxide concentrations on the Pap1 oxidation profile.

Fission yeast cells were exposed to a range of bolus hydrogen peroxide concentrations (100-1000 µM), and dynamic changes in the fractional Pap1 oxidation ratio (oxidised Pap1/total Pap1) were determined by redox western blotting (Figure 2.2A-D). We confirmed that Pap1 oxidation was dependent on Tpx1 (Figure S.2), and following a 100 µM hydrogen peroxide dose, Pap1 showed a single oxidation peak, while at 200 µM hydrogen peroxide, a bimodal dynamic profile was obtained (Figure 2.2E). At higher hydrogen peroxide concentrations, Pap1 activation also showed an initial rapid oxidative peak followed by sustained activation in agreement with other studies (Domènech et al., 2018). The sustained activation of Pap1 at higher hydrogen peroxide concentrations (>500 µM) is absent in Δ*srx1* cells showing that Srx1-dependent reduction of hyper-oxidised Tpx1 drives further rounds of Pap1 activation within the system (Figure S.3) (Bozonet et al., 2005; Vivancos et al., 2005).

The apparent differences in these dynamic profiles obtained with different hydrogen peroxide concentrations were quantified by determining the Pap1 signal amplitude, time and duration over the signalling interval (equations 1-3). We found that signal amplitude decreased significantly as the hydrogen peroxide concentration increased from 100 to 200 µM, with no other significant differences noted at higher hydrogen peroxide concentrations (Figure 2.2F). By contrast, there were significant, dose-dependent increases in the Pap1 signalling time and duration as the hydrogen peroxide concentration increased from 100 to 500 µM (Figure 2.2G-H), matching the corresponding changes to the Pap1 oxidation profiles (Figure 2.2E). However, this effect appeared to be saturable as no further significant changes in the signal parameters were observed as the hydrogen peroxide concentration was increased to 1000 µM.

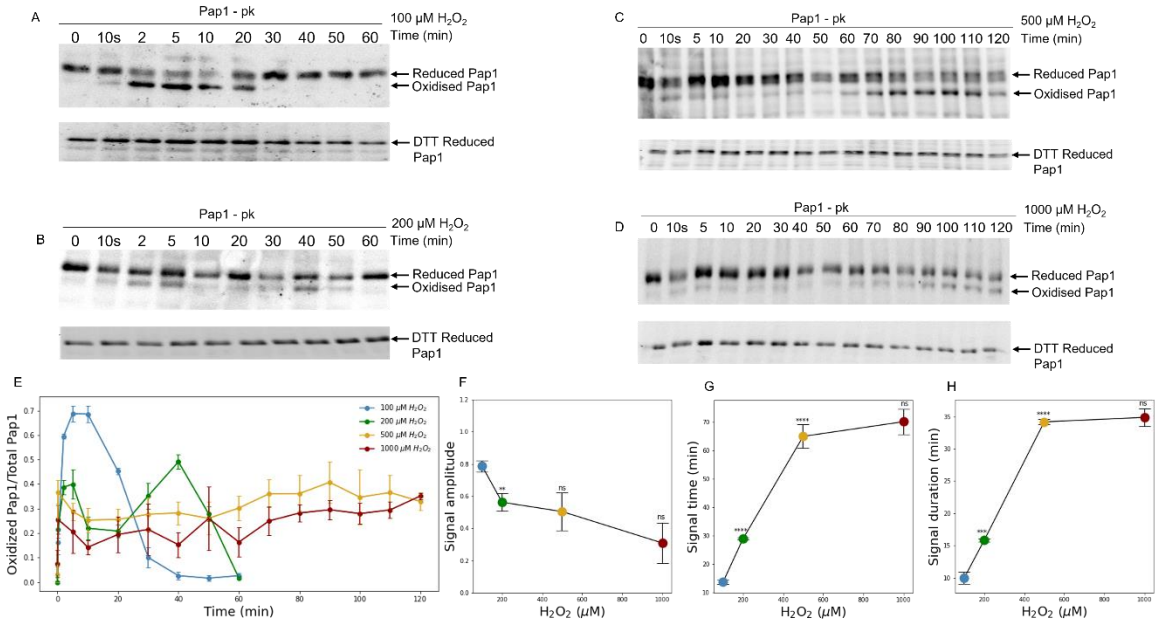

Figure 2.2: The Tpx1/Pap1 pathway in fission yeast exhibits dose-dependent quantitative effects in response to increasing levels of hydrogen peroxide.

*S. pombe cells were exposed to 100-1000 µM hydrogen peroxide, and Pap1 oxidation was determined by redox western blotting (A-D). Densitometric analysis of Pap1 oxidised and reduced bands were used to generate Pap1 signalling profiles (E), which were analysed to obtain the Pap1 signal amplitude (F), signal time (G) and signal duration (H). To determine whether increases in hydrogen peroxide lead to a significant change in a given signal parameter, each parameter value was compared to the preceding value by a two-tailed t-test with statistical significance denoted as **p<0.01, ***p<0.001, ****p<0.0001 and ns is not significant. All blots are representative of at least three independent experiments.*

We next sought to establish if the Pap1 signal parameters could be related to changes in the induction of gene expression by the transcription factor. RT-qPCR was used to monitor dynamic changes in the mRNA levels of four Pap1 target genes, *trr1*, *ctt1*, *srx1*, and *atf1*, which are all regulated differently. The induction of *trr1* transcription is independent of Atf1 (Toone et al., 1998; Veal et al., 2014), while Pap1 together with Prr1, as well as Atf1, activate *srx1*, *atf1* and *ctt1* transcription, with Pap1 playing a more substantial role at lower hydrogen peroxide levels (Chen et al., 2008; Quinn et al., 2002; Vivancos et al., 2004). Sty1 (Day & Veal, 2010) and Csx1 (Rodríguez-Gabriel et al., 2003) also regulate *atf1* mRNA stability post-transcription. Despite these differences, in transcriptomic experiments, all four genes showed weak or no induction in Δ*pap1* cells after 70 and 500 µM hydrogen peroxide bolus stresses,

confirming that Pap1 is essential for their induction across this range of hydrogen peroxide concentrations (Figure 5.20, (Chen et al., 2008).

We observed differences in the dynamics of relative mRNA levels in response to different hydrogen peroxide concentrations (Figure 2.3A). The *trr1* and *ctt1* mRNA levels increased at 15 min in response to the 100 µM hydrogen peroxide treatment and at 30 and 60 min respectively in response to the 200 µM hydrogen peroxide treatment. The *atf1* and *srx1* mRNA levels also increased at 15 and 30 min respectively for the 100 µM hydrogen peroxide treatment and shared similar dynamics following the 200 µM treatment. The mRNA levels of all these genes were elevated following the 500 and 1000 µM hydrogen peroxide treatments, with differences in timing likely reflecting the increased involvement of the Sty1/Atf1 pathway in the induction of *ctt1*, *srx1*, and *atf1* as hydrogen peroxide concentrations increased (Chen et al., 2003; Quinn et al., 2002). However, despite differences in their transcriptional regulation, the mRNA levels for all four genes shared similar bimodal kinetics at higher hydrogen peroxide concentrations.

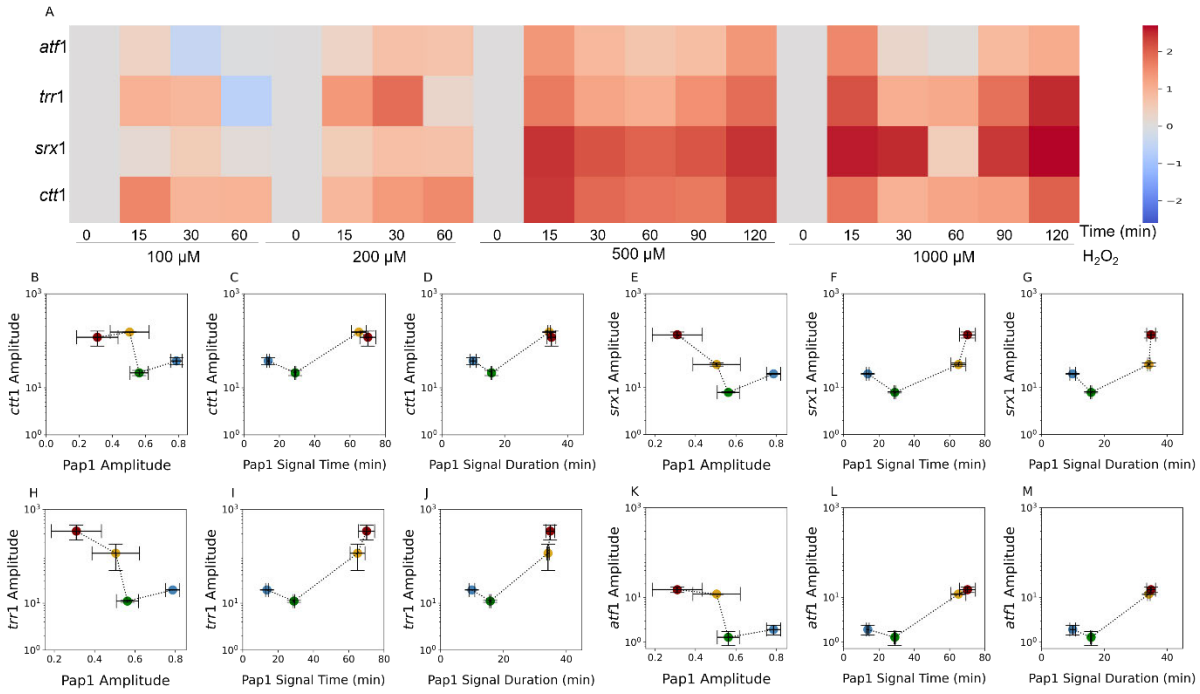

Figure 2.3: Dynamics of Pap1-dependent gene induction in response to hydrogen peroxide and correlation to Pap1 dynamic profiles.

The dynamic log10 fold-changes in the transcription of the Pap-1 regulated genes, ctt1, trr1, srx1 and atf1, were determined by RT-qPCR following bolus treatments with 100-1000 µM

hydrogen peroxide (A). The amplitude obtained from the dynamic gene expression profiles of ctt1, trr1, srx1 and atf1 were compared with the signal parameters obtained from the Pap1 oxidation profiles in co-response plots for 100 (blue), 200 (green), 500 (orange) and 1000 (red) μM hydrogen peroxide (B-M). The data represent the means and standard errors of at least three independent experiments.

We attempted to correlate Pap1 oxidation and gene induction by comparing Pap1 oxidation against the fold-change in these mRNA levels but the quantitative relationships between these outputs were unclear (Figure S.4). We therefore considered an alternate approach, and as the gene induction process was dynamic, we determined the average fold-change of these transcripts (i.e. amplitudes) from their transcriptional profiles (Figure 2.3A). These amplitudes were then compared to the Pap1 oxidation signal parameters in co-response plots (Figure 2.3B-M). The Pap1 activation and gene transcription processes for these genes are semi-independent; thus, the quantitative relationship between these processes was not expected to be linear. As the Pap1 amplitude increased, there was a decrease in fold-change mRNA amplitudes from 200 to 1000 μM hydrogen peroxide. By contrast, with increases in Pap1 signal time and duration, the fold-change in mRNA amplitudes increased exponentially between these hydrogen peroxide concentrations for all these genes (Figure 2.3F-G, I-J, L-M).

2.3.2 Quantifying the effects of different oxidants on the Pap1 oxidation profiles.

In addition to hydrogen peroxide, other peroxides are sensed by the Tpx1/Pap1 pathway, a property shared by other thiol-based signalling systems. For example, when compared to hydrogen peroxide, *tert*-butyl hydroperoxide (*t*-BOOH), a lipid hydroperoxide analogue, induced distinct transcriptional programs within *S. pombe* (Chen et al., 2008). We therefore asked whether these peroxides generated oxidant-specific Pap1 dynamic profiles. *S. pombe* cells were challenged with 100 or 200 μM *t*-BOOH, and the resultant Pap1 oxidation profiles were compared to the profiles generated in response to equivalent hydrogen peroxide concentrations (Figure 2.4A-C). Our experiments were limited to this *t*-BOOH concentration range because, as expected, higher concentrations, which do not activate Sty1/Atf1-dependent *srx1* expression (Vivancos et al., 2005), failed to induce Pap1 oxidation (Figure S.3).

The *t*–BOOH and hydrogen peroxide treatments resulted in distinct Pap1 dynamic profiles (Figure 2.4C), which could be quantified by determining the signal parameters for these plots. Using the 100 μM *t*-BOOH treatment as the standard condition, significant and

non-significant differences in the signal parameters between this treatment and the other treatments were observed (Figure 2.4D-F). We also noted that each individual *t*-BOOH or hydrogen peroxide treatment resulted in apparently distinct Pap1 dynamic profiles which were reflected in the signal parameters for these treatments. For example, the 100 µM *t*-BOOH treatment led to a Pap1 profile with a signal amplitude, time and duration of 0.45, 25.02 min and 15.97 min, respectively. In contrast, the 100 µM hydrogen peroxide treatment led to a Pap1 profile with values of 0.79, 13.70 min and 9.95 min for these parameters, respectively (Figure 2.4D-F). To visualise the differences in these Pap1 dynamic profiles, we compared the signal parameters obtained across all our treatments and found that each treatment resulted in specific combinations of signal parameters (Figure 2.4G). Significantly, these treatments were associated with distinct transcriptional induction dynamics (Figure S5). Collectively, our data points to a model in which different oxidants or oxidant concentrations trigger quantifiable changes in the Pap1 dynamic profile, contributing to differences in the induction of Pap1-dependent gene transcription. In the next section, we demonstrate how this quantification method and model of Pap1 activation could be used to investigate redox signalling in these cells.

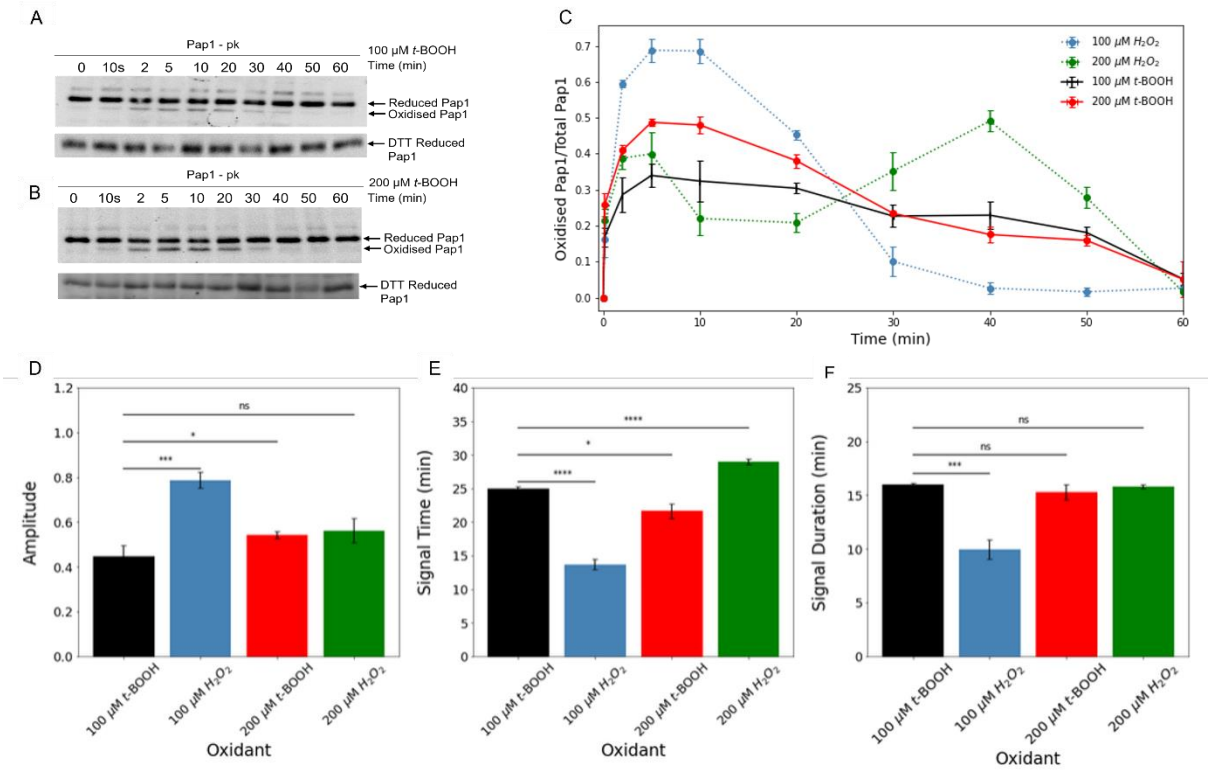

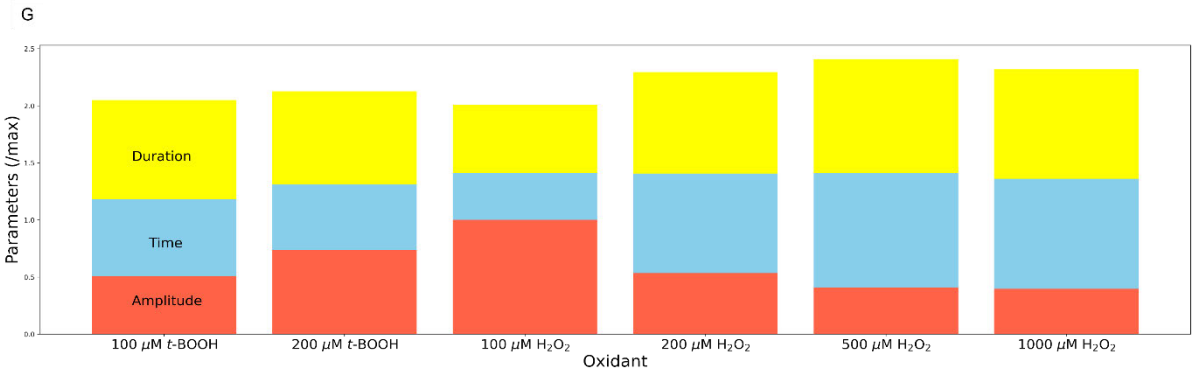

Figure 2.4: Differences in the Pap1 oxidation profiles following hydrogen peroxide and *t*-BOOH treatments can be quantified by signalling parameters.

*The oxidation state of Pap1 in S. pombe cells exposed to 100 and 200 µM t-BOOH was determined by redox western blotting (A-B). The Pap1 oxidation profiles (C) for t-BOOH were compared to the profiles obtained for cells exposed to equivalent hydrogen peroxide concentrations (dashed lines) over the same time interval. The signal amplitude (D), time (E) and duration (F) for these profiles were compared to the 100 µM t-BOOH treatment using a two-tailed t-test with statistical significance is indicated as follows: *p<0.05, **p<0.01, ***p<0.001, ****p<0.0001 and ns is not significant (n=3 independent experiments). The signal amplitude (red), time (blue) and duration (yellow) parameters for all the t-BOOH and hydrogen peroxide treatments were compared in a stacked bar plot (G). Here, the signal amplitude, time and duration parameters obtained for each treatment were scaled against the corresponding signal amplitude, time and duration maxima from the respective treatment datasets.*

2.3.3 Quantifying signal processing can lead to insights into redox signalling.

As redox signalling may play a role in redox dysregulation associated with disease (Berndt et al., 2022), we wanted to investigate whether differences in redox signal profiles resulted in distinct cell outcomes. Our previous experiments found that the only difference between the signal parameters obtained for the 100 µM *t*-BOOH and 200 µM hydrogen peroxide treatments was a significantly increased signal time for the hydrogen peroxide treatment (Figure 2.4D-F). This result allowed us to estimate this parameter's importance between these treatments. As Srx1 protein levels are expected to be minimal under non-stress conditions (Bozonet et al., 2005; Vivancos et al., 2005), we chose to monitor protein production as a readout of Pap1 transcriptional activity.

To enable Srx1 protein detection, we engineered yeast to express FLAG epitope-tagged Srx1 from its chromosomal locus. This allowed us to compare the production of FLAG-tagged Srx1 in cells treated with 200 µM hydrogen peroxide or 100 µM *t*-BOOH. Our investigation revealed that the overall Srx1 production was 2-fold higher in cells exposed to the hydrogen peroxide treatment compared to the *t*-BOOH treatment (Figure 2.5A-B). Interestingly, Srx1 production showed a similar dynamic pattern to that observed for Pap1 oxidation (Figure 2.4C). Notably, there were two peaks in Srx1 production at 30- and 50-min post-exposure to 200 µM hydrogen peroxide (Figure 2.5B), mirroring the dual peaks observed in the Pap1 oxidation profile at 5 and 40 min respectively (Figure 2.4C). Similarly, exposure to 100 µM *t*-BOOH resulted in a gradual increase in Srx1 production (Figure 2.5B) which also aligned with the Pap1 oxidation profile (Figure 2.4C). Thus, our data suggest that the difference in Pap1 dynamics between these treatments, as represented by the signalling time parameter, contributed to the distinct outcomes for Srx1 production in these cells. However, as this parameter is a measure of the overall profile, it did not describe all the intricacies of the Pap1 oxidation and Srx1 production dynamics.

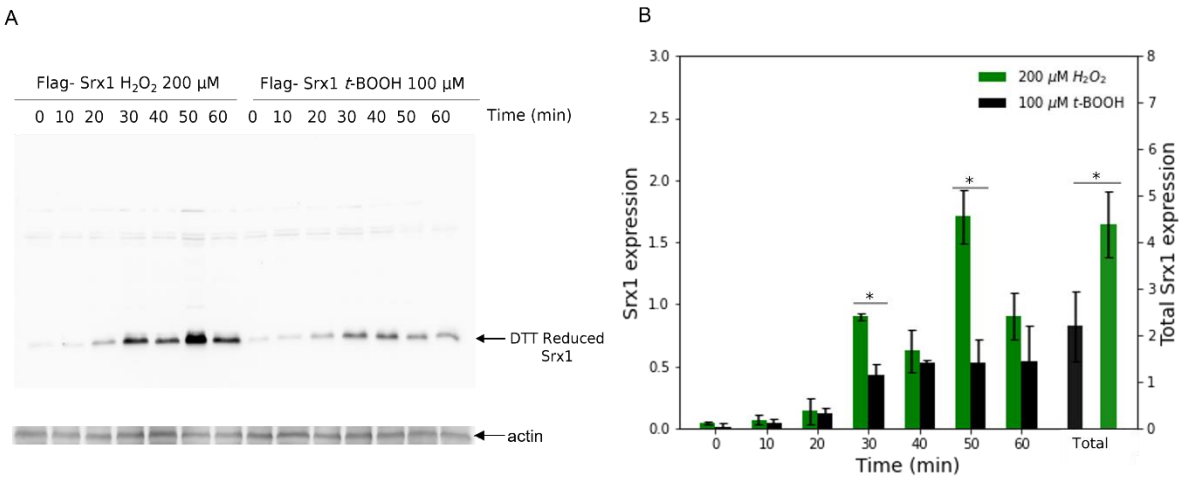

Figure 2.5: Srx1 production in *S. pombe* cells treated with 200 µM hydrogen peroxide or 100 µM *t*-BOOH.

FLAG-Srx1 levels were quantified by immunoblotting of cell lysate before and after bolus addition of 200 µM hydrogen peroxide or 100 µM t-BOOH using anti-Flag antibodies with actin as a loading control (A). The samples were treated with DTT and the FlagSrx1 levels determined by densitometry analysis of immunoblots normalised against the actin control to give the relative Srx1 expression at each time point. The total production of Srx1 across the time course is shown on the far right and has its own scale (B). Two-tailed t-tests were used to

*compare the difference in expression of Srx1 over the 60 minute time course and significant differences were noted as * representing $p<0.05$. The data represents the means and standard errors of duplicate experiments.*

Given that the Pap1 dynamic profile was sensitive to different oxidants (Figure 2.4), we next asked what effect a *t*-BOOH/hydrogen peroxide combination stress would have on the Pap1 dynamic profile. *S. pombe* cells were treated with 100 µM *t*-BOOH and hydrogen peroxide simultaneously, and Pap1 oxidation was monitored by western blotting (Figure 2.6A). Intriguingly, the combined effect of these two oxidants resulted in a profile dissimilar to each oxidant but instead resembled a single high dose (1000 µM) hydrogen peroxide treatment (Figure 2.6B). Quantifying these dynamic profiles showed that the signal parameters for the combination stress were indeed significantly different to the individual 100 µM *t*-BOOH and 100 µM hydrogen peroxide treatments (Figure 2.6C-E). On the other hand, the combination stress signal amplitude and duration were similar to the 1000 µM hydrogen peroxide treatment, although the signal time was significantly different between these treatments. These results are consistent with work in *Candida* and other yeast species showing that combination stressors are more potent at killing these cells than individual treatments (Kaloriti et al., 2014). Our work extends these findings as we were able to precisely quantify and compare the effects of these combination stresses on the activation of this redox-sensitive transcription factor.

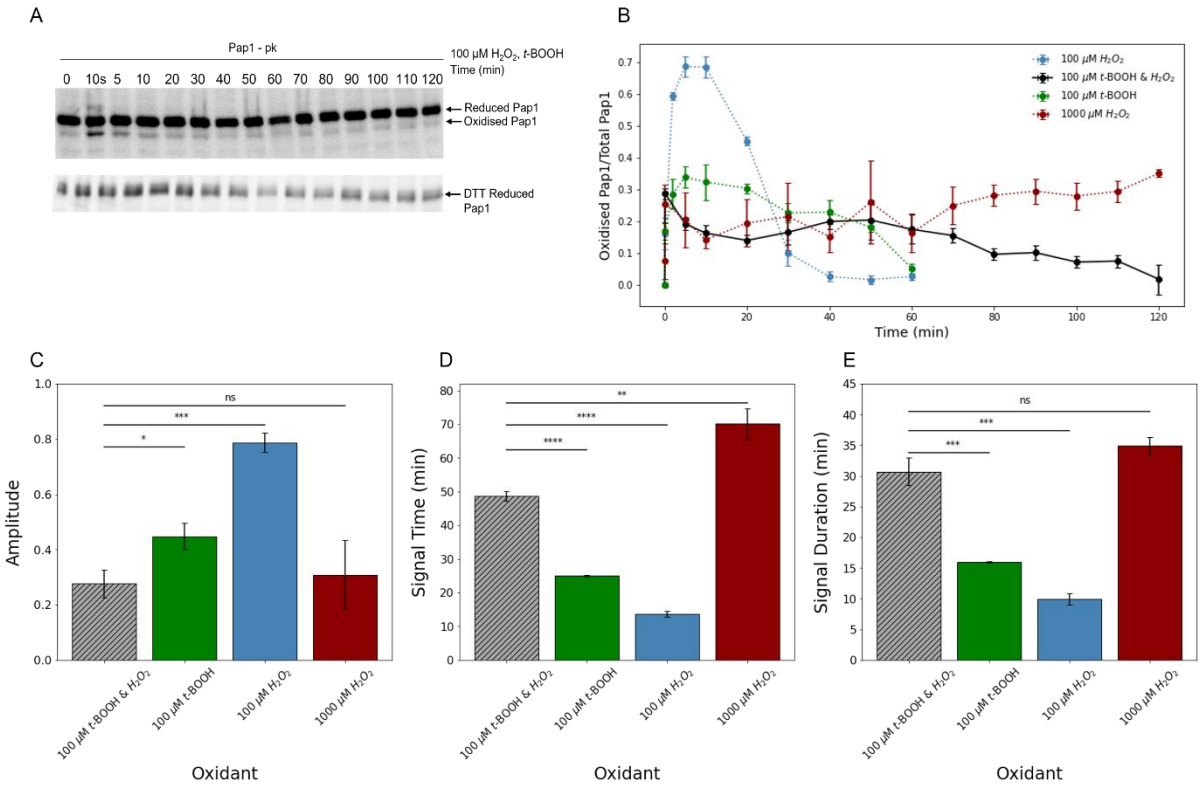

Figure 2.6: Combinations of *t*-BOOH and hydrogen peroxide at low doses yield similar Pap1 responses compared to a single high-dose concentration of hydrogen peroxide.

*Pap1 oxidation was tracked using western blotting following exposure of fission yeast cells to a 100 µM t-BOOH and 100 µM hydrogen peroxide combination stress (A). The combination stress dynamic profile was compared to the profiles obtained from single doses of 100 µM t-BOOH along with 100 µM and 1000 µM hydrogen peroxide (B). The signalling profiles were then analysed to determine the signal amplitude, time and duration (C-E). Statistical significance was tested by a two-tailed t-test with significance indicated as follows: *p<0.05, **p<0.01, ***p<0.001, ****p<0.0001 and ns is not significant. The experiments were undertaken in triplicate.*

It is well established that pre-exposure to a low dose stressor can protect cells against a subsequent higher dose of the stressor (Crawford & Davies, 1994; Pickering et al., 2013; Pomatto & Davies, 2017a). We next investigated how pre-exposure would affect the activation dynamics of Pap1. Cells (OD_{595}~0.2) were pre-exposed to a 100 µM hydrogen peroxide dose, allowed to recover (OD_{595}~0.5), and then exposed to a further 500 µM hydrogen peroxide stress (Quinn et al., 2002). The resulting Pap1 activation profile differed from the single dose of 500 µM hydrogen peroxide treatment and resembled the activation profile for cells treated with

200 µM (Figure 2.7A-B). These profiles could be compared and quantified using the signalling parameters, which revealed that pre-exposure with 100 µM hydrogen peroxide resulted in a Pap1 profile that had a significantly different signal time and duration to cells treated with a 500 µM hydrogen peroxide dose only. On the other hand, there were no significant differences in the signal parameters between these pre-exposed cells and cells treated with 200 µM hydrogen peroxide (Figure 2.7C-E). Thus, pre-exposure modified the Pap1 activation dynamics to match a lower dose of hydrogen peroxide showing how pre-exposure can lead to compensatory changes to the Pap1 signalling pathway.

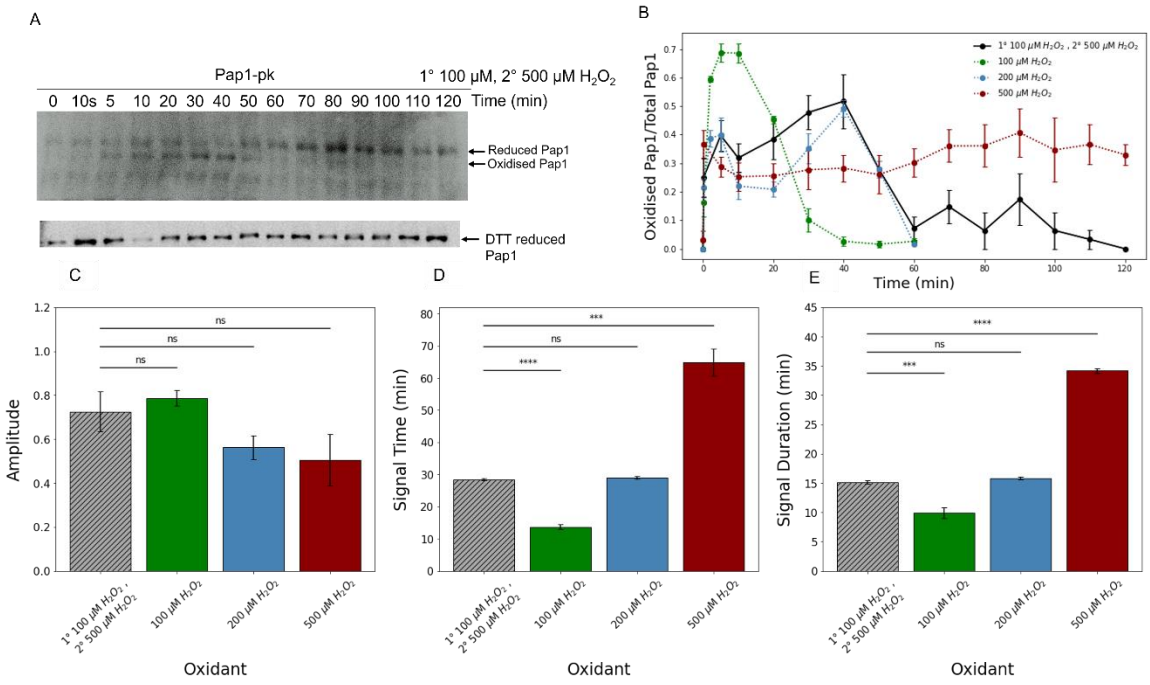

Figure 2.7: Quantifying the effect of pre-exposure on Pap1 activation dynamics in response to hydrogen peroxide.

*Cells were grown to an OD_{595}~0.2 and pre-treated with 100 µM (1°) hydrogen peroxide. At an OD_{595}~0.5 the cells were exposed to a further 500 µM (2°) hydrogen peroxide dose and Pap1 oxidation in these cells was analysed by western blotting (A). The pre-treatment Pap1 dynamic profile was compared to the profiles obtained from single doses of 100, 200 and 1000 µM hydrogen peroxide (B). The signalling parameters were then calculated to determine the signal amplitude, time and duration (C-E). Statistical significance was tested by a two-tailed t-test with significance indicated as follows: *p<0.05, **p<0.01, ***p<0.001, ****p<0.0001 and ns is not significant. The experiments were undertaken in triplicate.*

2.4 Discussion

In aerobic cells, redox-sensitive transcription factor pathways play critical roles in the adaptive response to oxidants (Espinosa-Diez et al., 2015). Clarifying the quantitative relationships between the signal input, transcription factor activation, and gene expression phases is crucial to understanding the role/s of adaptive antioxidant responses in conditions associated with redox dysregulation (Pillay et al., 2016; Sies & Jones, 2020). However, the transcription factor activation process is dynamic, and it has been unclear how the dynamic profiles of these redox transcription factors should be quantified.

To address this measurement gap, we investigated whether the dynamic profiles of *S. pombe* Pap1 could be quantified by three parameters: signal amplitude, time, and duration. Previous work showed that Pap1 could be activated by different hydrogen peroxide concentrations (~70-1000 μM) (Jara et al., 2007; Vivancos et al., 2006) and by *t*-BOOH, with specific oxidative inputs linked to particular transcriptional outputs (Chen et al., 2008). In this work, we showed how different hydrogen peroxide and *t*-BOOH concentrations led to quantifiably distinct Pap1 dynamic profiles which were associated with specific transcriptional outputs. These data support a model in which the Pap1 dynamic profile, and not just oxidised Pap1 itself, is the key output of this system key output of this system allowing these cells to mount a graded transcriptional response to different oxidants and oxidant concentrations. This model is consistent with other studies showing how different inputs affect the signal dynamics, and consequently, the activities and transcriptional programs. This model is consistent with other studies showing how different inputs affect the signal dynamics, and consequently, the activities and transcriptional programs (Hansen et al., 2015; Hao & O'Shea, 2012) of NF-κB (T. K. Lee et al., 2009; Tay et al., 2010), ERK (Arkun & Yasemi, 2018; Hornberg et al., 2005), p53 (Lahav et al., 2004), FOXO1 (Lasick et al., 2023), and baker's yeast Msn2 (Hansen & O'Shea, 2016; Hao & O'Shea, 2012; Purvis & Lahav, 2013).

Some aspects of this Pap1 dynamic activation model and quantification method require further investigation. The dynamic profiles, and therefore signal parameters, obtained for different oxidant and oxidant concentrations are likely a function of the thioredoxin and peroxiredoxin redox cycles (Chen et al., 2008; Domènech et al., 2018; Tomalin et al., 2016), as well as sulfiredoxin activity (Figure S2, (Bozonet et al., 2005; Vivancos et al., 2005)) and expression (Chen et al., 2008). However, the quantitative relationships between these signal parameters and the underlying molecular activities within the system remain to be determined.

It is also unclear whether this quantification method can be applied to other redox-regulatory mechanisms and different redox-regulated transcription factors. Redox transcription factors can have activation modes independent of their oxidation dynamics by the formation of complexes with different co-activating partners or other post-translational modifications (Calvo et al., 2012; Gulshan et al., 2011). For instance, the activation of the AP1-like transcription factors, Yap1 in *S. cerevisiae* (Gulshan et al., 2011) and Cap1 in *C. albicans* (Kos et al., 2016), depends on Ybp1 which acts as a sulfenic acid chaperone (Bersweiler et al., 2017). Moreover, both Pap1 and baker's yeast Yap1 can be also directly activated by electrophiles and heavy metal ions that promote intramolecular disulphide formation independently of the peroxiredoxin and thioredoxin systems (Azevedo et al., 2003; Kudo et al., 1999; Zuin et al., 2005). Similarly, differences in the oxidation state of Cys^{199} in *E. coli* OxyR are thought to be responsible for oxidant-specific transcriptional responses by this transcription factor (S. O. Kim et al., 2002). The quantification method described in this work can be used analyse and compare these different modes of transcription factor activation.

To test the utility of this quantification method, we undertook three further experiments to show how it can facilitate quantitative insights into redox signalling. First, we showed how a difference in Pap1 signal time between a *t*-BOOH and a hydrogen peroxide treatment affected Srx1 expression. It remains to be seen whether differences in the signal parameters for other redox transcription factors can be linked to specific aspects of cell physiology, particularly in disease. Second, given the oxidant-specific responses of the Pap1 system, we exposed fission yeast cells to a 100 μM hydrogen peroxide/*t*-BOOH combination stress. The resulting Pap1 dynamic profile resembled neither of these low doses but was similar to a 1000 μM hydrogen peroxide stress. These results are consistent with survival assays showing that combination stressors can kill yeast cells more efficiently than single dose stresses (Kaloriti et al., 2014; Quinn et al., 2002). Here, our results showed that Pap1 pathway itself is responsive to combination stresses from these oxidants. Third, we could use this method to quantify the effect of pre-exposure on the dynamics of Pap1 activation and found that pre-exposure leads to Pap1 activation dynamics similar to a lower dose of hydrogen peroxide. This result was expected given the increased expression of thioredoxin, thioredoxin reductase and catalase following pre-exposure to hydrogen peroxide (Pickering et al., 2013; Quinn et al., 2002), but demonstrates how this method could be applied to studies that aim to quantify the effects of chronic exposure on redox transcription factor activation (Crawford & Davies, 1994; Love et al., 1986; Pomatto & Davies, 2017b) .

There are some technical limitations with the experiments described in this work. For example, we used bolus hydroperoxide stresses which mimic the adaptation or survival response following acute exposure. It is possible that the Pap1 activation dynamics and signal parameters will respond differently to steady-state hydrogen peroxide inputs (Sobotta et al., 2013) or sub-cellular hydrogen peroxide production (Kritsiligkou et al., 2023). In addition, this method used a bulk-culture approach to study the activation of the Pap1 transcription factor. However, single-cell analyses may be required to reveal cell-specific behaviour and Pap1 signal parameter variations within a population exposed to oxidative stress (Hansen et al., 2015). Despite these limitations, our study provides evidence that the ability to quantify redox dynamic profiles is a valuable addition to the toolbox of redox signalling methods. While we focussed on the Pap1 system in fission yeast, we note that the thioredoxin/peroxiredoxin/hydrogen peroxide axis regulates a wide range of cellular targets across multiple cell types (Day et al., 2012; Netto & Antunes, 2016b; Peralta et al., 2015; Sobotta et al., 2015). Understanding the effect of dynamic, rather than binary (on/off) or steady-state, changes to these targets may better inform our understanding of redox regulation and the oxidative stress response.

2.5 Materials and Methods

2.5.1 Materials

Amino acids and reagents for general cultivation of *S. pombe* were purchased from Merck/Sigma. Alkaline phosphatase, BCA protein assay kits and Aminolink kits were obtained from ThermoFisher Scientific (Johannesburg, South Africa). YeaStar^{TM} RNA isolation kits, qPCR primers, New England Biolabs cDNA synthesis kit and qPCR master mix were purchased from Inqaba Biotech (Pretoria, South Africa). Analytical-grade hydrogen peroxide was purchased from Labcare supplies (Durban, South Africa). Primary anti-V5 Pk antibody (Lot #065M480IV, CAT: V4014-100UG), FLAG-tag antibody (Lot #SLBQ7119V, CAT: F3165-2MG), clarity ECL substrate, and ammonium persulphate were obtained from Bio-Rad (Durban, South Africa). Anti-mouse (rabbit) IgG peroxidase antibody (Lot #106M4870V, CAT: A9044-2ML), iodoacetamide and PEG-maleimide were from Sigma. The α-β actin-HRP conjugated antibody (CAT: A3854) produced in mice was obtained from Merck. All other reagents for buffers and solutions were purchased from Merck/Sigma.

2.5.2 Fission yeast strains

The *S. pombe* strains used in this study were SB3 *(h^{-}ade6-M216 leu1-32 ura4-D18 pap1.3Pk:ura4^{+} his7-366)*, SB4 *(h^{+} ade6 leu1-32 ura4-D18 pap1.3Pk:ura4^{+} tpx1::ura4^{+} his7-366)*, SB6 (*h^{-} ade6-M216 leu1-32 ura4-D18 his7-366 srx1::ura4^{+}*) and SB8 *(h^{-} ade6 leu1-32 ura4-D18 srx1::ura4^{+} pap1.3Pk:ura4^{+} his7-366)* (Bozonet et al., 2005) and LT1 (*h^{-} ade6-M216 leu1-32 ura4-D18 his7-366 srx1::ura4^{+} Flag-srx1:LEU2*) expressing N-terminally FLAG epitope-tagged Srx1 from its native promoter and genomic locus. These strains were maintained on solid Edinburgh minimal medium plates and patched every three days. To construct LT1 1kb upstream of the *srx1* open reading frame was amplified by PCR from *S. pombe* genomic DNA and ligated into the Nco1 and Pst1 sites of pRep41 FLAG (Bozonet et al., 2005) to generate pRep41promFLAGsrx1. This plasmid was digested with Pst1 and BamH1 and the promFLAGsrx1 fragment ligated into the Pst1 and BamH1 sites of pRip1 to generate the non- replicating pRip1 promFLAGsrx1. pRip1 promFLAGsrx1 was linearised by digestion with HindIII, then transformed into SB6 (*h^{-} ade6-M216 leu1-32 ura4-D18 his7-366 srx1::ura4^{+}*) cells which were plated on solid Edinburgh minimal medium 2 (EMM2) containing 225 mg/l histidine and 225 mg/l adenine. Integration of the promFLAG-srx1 fragment at the correct chromosomal loci was confirmed by PCR and sequencing of genomic DNA extracts from transformed colonies. Growth assays on medium containing hydrogen

peroxide were used to confirm that FLAG-Srx1 expression restored wild-type levels of peroxide-resistance.

2.5.3 S. pombe cell culture and challenge to oxidants

S. pombe cells were cultivated in EMM2, supplemented with adenine (225 mg/L), histidine (225 mg/L), uracil (225 mg/L), lysine (225 mg/L) and leucine (250 mg/L) (Nurse, 2001; Petersen & Russell, 2022). Cells were grown to mid-log phase (OD_{595}~0.4-0.5) at 30°C and 180 rpm (Nurse, 2001) and exposed to 100–1000 µM hydrogen peroxide or 100-200 µM *tert*-butyl hydroperoxide (*t*-BOOH). 1-5 x 10^7 cells were harvested at different time points over a 60-120 min time course (Bozonet et al., 2005; Vivancos et al., 2004) and added to 1 volume of ice-cold 20% (w/v) trichloroacetic acid (TCA). As expected from the hydrogen peroxide concentrations used in this study (Bozonet et al., 2005; Vivancos et al., 2004), the cells recovered following their treatments with the doubling time of the cultures treated with 500 and 1000 µM increasing significantly compared to the control cells (Figure S.6). The cells were pelleted (3000 x *g*, 5 min, 4°C), snap-frozen in liquid nitrogen and stored at -80°C.

2.5.4 Protein isolation and alkylation of Pap1 and Srx1

Cell pellets were thawed on ice, resuspended in 10% TCA and transferred to screw-cap tubes containing 0.5 mm glass beads (Roth). The cells were lysed (bead-beating) for 15 seconds, placed on ice for one minute and the process repeated. Additional 10% TCA (500 µl) was added and the tubes vortexed. The lysate was separated from the beads by piercing the tube with a hot needle and transferring to a new microfuge tube. Both tubes were then centrifuged in a 50 ml Falcon tube (2,000 x g, 30 seconds, 21°C). For Pap1 quantification, the protein was pelleted by centrifugation (13,000 x *g*, 10 min, 4°C), the supernatant removed, and the pellet washed three times with acetone, air dried, resuspended in freshly prepared IAA buffer (75 mM iodoacetamide, 1% (w/v) SDS, 100 mM Tris-HCl pH 8.0) and incubated (25°C, 20 min). The Flag-Srx1 samples were prepared similarly but resuspended in protein buffer (1% (w/v) SDS, 100 mM Tris-HCl pH 8.0) and treated with DTT. The protein concentration was determined using a Pierce BCA protein assay kit, and Pap1 samples were then treated with alkaline phosphatase (1 U/µl) for one hr at 37°C.

2.5.5 Western blot analysis of Pap1 oxidation and Srx1

Equal protein amounts (30 µg) were loaded onto 8% Tris-glycine SDS-PAGE gels and separated by electrophoresis (200 V, 45 min). Protein was then transferred to the nitrocellulose

membrane (0.2 µm) for three hrs in an ice-cold transfer buffer (Tris 25 mM (pH 8.0), 200 mM glycine, 10% methanol, 0.8% SDS). Subsequently, the membrane was blocked with 10% bovine serum albumin (BSA) in TBST (Tris 20 mM (pH 8.0), 137 mM $NaCl_2$, 0.1% (v/v) Tween 20) and incubated with primary monoclonal pk-antibody (1 µg/ml) overnight at 4°C to detect Pap1 bands while Srx1 was detected with primary monoclonal FLAG-antibody (1 µg/ml). The membranes were then washed four times with TBST for five min and incubated with diluted Horse radish peroxidase (HRP) conjugated anti-mouse IgG secondary antibody (1:20,000) for one hr, then washed again with TBST for five min. The bands were then visualised with ECL reagent (Bio-Rad) on the G-BOX Chemi-XR5 Gene*Sys* imaging system, and bands were sized according to Precision Plus Protein™ WesternC™ standard. The antibody concentrations were chosen to ensure that bands were imaged in the linear range for quantitative western blot detection. Protein normalisation was carried out using Ponceau S (0.1%) staining (Sander et al., 2019) and DTT (0.1 M) controls (Tomalin et al., 2016). FLAG-Srx1 levels were normalised against an actin control using diluted α-β actin-HRP conjugated antibody (1:10,000). Uncropped blot images are presented in the Supplementary Information.

2.5.6 Quantification of Pap1 regulated gene expression

A transcriptomic dataset from the Bahler lab (Chen et al., 2008) was analysed to select Pap1-regulated genes that showed at least a two-fold increase in transcription with *ctt1, srx1, trr1* and *atf1* selected for RT-qPCR. These genes have also been routinely to assess the transcriptional response to oxidative stress as their products play critical roles in the antioxidant response in the fission yeast (Quinn et al., 2002; Vivancos et al., 2004). Briefly, *S. pombe* SB3 cells were cultured and challenged as previously described and samples (2 ml) were taken, immediately snap-frozen in liquid nitrogen and stored at -80°C. Samples were then thawed on ice, pelleted (500 x *g*, 3 min, 21°C), and RNA was extracted using the YeaStar™ RNA Kit. The quantity of RNA was measured by spectrometry at 260 and 230 nm, and purity was assessed on a 1% denaturing agarose gel (200 mM 3-(*N*-morpholino) propanesulfonic acid (MOPS), 50 mM sodium acetate, 10 mM EDTA, 37% formaldehyde). Isolated RNA was then converted to cDNA using ProtoScript II first strand cDNA synthesis Kit using 1 µg of the RNA template with an oligo d(T)23 primer mix. Quantification of cDNA was analysed by real-time qPCR on Quantstudio™ 5 real-time PCR system with Luna universal qPCR master mix and the fold-change in expression was calculated using the $2^{-\Delta\Delta C_T}$ method. For these experiments, both *gpd3* and *act1* were tested as reference genes as analysis of a transcriptomic dataset showed that transcription of both these genes remained constant over a range of oxidative

stresses (Chen et al., 2008) (Figure 5.20). In the main paper, we have shown the heat maps generated using *gpd3* as a reference gene and all primers are listed in Table S1 (Supplementary Information).

2.5.7 Computational and statistical methods

The reduced and oxidised band intensity from western blots was quantified using ImageJ (https://imagej.nih.gov/ij). The fractional Pap1 oxidation profiles (oxidised/total) were plotted over time (Domènech et al., 2018; Padayachee et al., 2020), and the signalling parameters were calculated using equations 1-3. Total Srx1 production was quantified using ImageJ and normalised against the band intensity obtained from the actin control. All computational analyses and statistical tests were carried out in Python (https://www.python.org/) using Jupyter notebooks with SciPy (https://scipy.org), Pandas (https://pandas.pydata.org) and Matplotlib (https://matplotlib.org/). Deming regression was used to compare the Pap1 signalling parameters to the signalling parameters obtained for *ctt1*, *trr1*, *srx1* and *atf1* (Figure S7). Unless otherwise stated, all data are representative of at least three independent biological experiments. Uncropped images and a link to the relevant code and the raw data for reproducing the figures are available in the Supplementary Information and https://github.com/djl94/Chapter2_supp.git.

Chapter 3

Quantifying the signalling profiles of genetically encoded redox sensors

Abstract

Genetically encoded redox sensors, such as the Hyper and roGFP sensor families, are powerful tools for enumerating the real-time dynamics of hydrogen peroxide in cells. In typical experiments, a dynamic profile of sensor oxidation and reduction is obtained following an external hydrogen peroxide perturbation. Using these profiles to characterise the quantitative relationship between the hydrogen peroxide concentration and sensor outputs is challenging as non-linearity in sensor responses to hydrogen peroxide may not be evident. Further, it is unclear how different sensors could be compared. We tested whether these profiles could be characterised by the area under the curve (AUC), signal amplitude, signal time and signal duration parameters. In baker's yeast, the Hyper7 AUC and amplitude showed a strong linear correlation (r>0.9) to a wide range of hydrogen peroxide concentrations (1-1000 μM). These responses were higher than roGFP2-Tsa2ΔC$_R$ parameters at hydrogen peroxide concentrations greater than 100 μM. By contrast, the roGFP2-Tsa2ΔC$_R$ AUC and amplitude plots presented distinct linear correlation equations for lower (<100 μM) and higher hydrogen peroxide (>100 μM) concentrations establishing that this sensor's output is range specific. The signal time and duration for HyPer7 were lower than roGFP2-Tsa2ΔC$_R$ at higher hydrogen peroxide concentrations (>100 μM), showing that its activation/deactivation cycle was faster. By contrast, in the fission yeast, the AUC and amplitude for HyPer7 and roGFP2-Tpx1.C169S both showed distinct linear correlations for lower (<50 μM) and higher (>50 μM) concentrations, and the signal time and duration were constant in this background. These results show that any purported correlation between hydrogen peroxide input and sensor output depends on the sensor, cell type and the hydrogen peroxide concentration range chosen. In summary, this method facilitates the characterisation signalling data generated by redox sensors.

3.1 Introduction

Reactive oxygen species (ROS) are central to oxidative stress, a phenomenon implicated in various diseases such as cancer and neurodegenerative disorders (Checa & Aran, 2020). Besides their role in oxidative damage, ROS, such as hydrogen peroxide, are also essential for signalling, metabolism, and proliferation processes (Checa & Aran, 202). Several techniques have been used to detect intracellular hydrogen peroxide levels, including fluorogenic approaches (Rhee et al., 2010), electron spin resonance (Gulaboski et al., 2019), and enzymatic assays (Carter et al., 1994). However, many of these techniques produce artefacts, or are indirect measurements of intracellular hydrogen peroxide levels (Lukyanov & Belousov, 2014). For instance, a popular fluorogenic sensor, 2',7'-dichlorodihydrofluorescein (DCFH), can yield fluorescent signals due to non-specific reactions with nitric oxide and peroxynitrite, and is sensitive to factors like local oxygen levels, pH, and light, potentially leading to inaccurate hydrogen peroxide estimations (Murphy et al., 2022).

To address these challenges, genetically encoded redox sensors were developed to better detect intracellular hydrogen peroxide generation (Pak et al., 2020; Smolyarova et al., 2022). These sensors used hydrogen peroxide sensing machinery found within biological systems (Belousov et al., 2006) (e.g.) OxyR, a transcriptional factor in *Escherichia coli*, is extremely sensitive to hydrogen peroxide (>100 nM) (Belousov et al., 2006; Storz et al., 1990). By integrating circular permutated yellow fluorescent protein (cpYFP), into the OxyR conformational region, the HyPer1 sensor was created (Figure 3.1A) (Belousov et al., 2006). HyPer1 exhibits distinct excitation peaks at 420 nm and 500 nm, with an emission peak at 516 nm from which a ratiometric output is calculated (Bilan & Belousov, 2016; Markvicheva et al., 2011; Smolyarova et al., 2022). However, the original HyPer1 sensor exhibited a limited dynamic range and saturated at higher hydrogen peroxide concentrations (>100 µM) (Belousov et al., 2006). Subsequent mutations, and the integration of a more sensitive OxyR domain from *Neisseria meningitidis* generated the HyPer7 sensor, which had an expanded dynamic range while maintaining sensitivity and stability over a wider pH range (Bilan et al., 2013; Markvicheva et al., 2011).

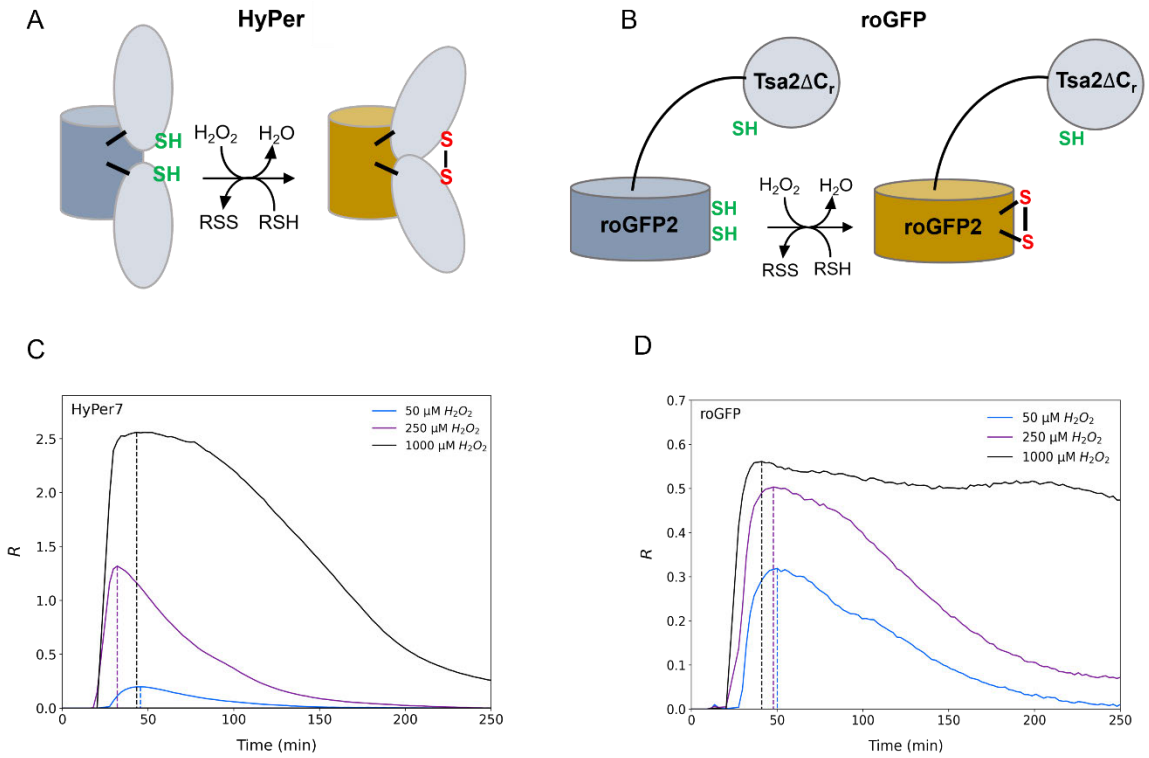

Figure 3.1: Interpretation of signalling data generated by genetically encoded redox sensors.

The HyPer7 sensor is oxidised by hydrogen peroxide and has two excitation peaks at 405 and 488 nm and one emission at a peak at 516 nm, from which the ratiometric signal (R) is calculated (A). The roGFP2 sensors are coupled to a highly sensitive peroxidase protein like Tsa2. The peroxidatic cysteine residue in Tsa2 is oxidised by hydrogen peroxide, which then oxidises the GFP structure and has excitation peaks at 405 and 408 nm and an emission peak at 511 nm (B). These sensors typically generate dynamic signalling profiles following a bolus hydrogen peroxide stress. Note the maximal peak activation time (dashed vertical lines) is concentration and sensor dependent (C-D).

Another class of hydrogen peroxide sensors, the redox-sensitive GFP-based proteins (roGFPs), were engineered by introducing cysteine residues into the surface of the GFP's β-barrel structure (Morgan et al., 2016; Gutscher et al., 2009). Hydrogen peroxide oxidises the cysteine residues within the GFP β-barrel and which can be detected by the distinct excitation (405 nm and 488 nm) and emission (511 nm) peaks of the sensor. To achieve a dynamic range and sensitivity comparable to HyPer7, roGFPs were fused with yeast thiol-peroxidases, such as Orp1 and Tsa2, from *Saccharomyces cerevisiae* (Figure 3.2B) (Morgan et al., 2016). These fusions allowed for better hydrogen peroxide detection while tolerating pH changes (Gutscher

et al., 2009). A limitation of these sensors is that the fused peroxiredoxin can become hyperoxidised, and therefore, the sensor output may be limited (Morgan et al., 2016). Both the HyPer7 and roGFP sensors are reduced by the internal antioxidant systems, such as glutaredoxins or thioredoxins (BilanDmitry et al., 2018).

Two methods are commonly used to quantify the ratiometric fluorescence intensities from these sensors. The degree of oxidation (OxD) measures the fractional oxidation of the sensor and is calculated from the emission fluorescence following excitation at 405, and 488 nm. Excess DTT or hydrogen peroxide/diamide are used to determine the fully reduced and oxidized fluorescence outputs, respectively.

$$OxD = \frac{I405 \cdot I488_{red} - I405_{red} \cdot I488}{I405 \cdot I488_{red} - I405 \cdot I488_{ox} + I405_{ox} \cdot I488 - I405_{red} \cdot I488} \quad (1)$$

Alternatively, the ratio (R) of fluorescence intensities involves calculating the ratio of fluorescence excitation from the two emission wavelengths (equation 2). Unlike OxD which is bounded between zero and one, R has no upper or lower bounds.

$$R = \frac{I405}{I488} \quad (2)$$

The correlation between the ratiometric signal from sensors, and the hydrogen peroxide concentration is purportedly quasi-linear from theoretical models, with non-linearity expected at both the lower and upper boundaries of the sensors dynamic range (Meyer & Dick, 2016). However, it is difficult to determine the linearity between sensor output and hydrogen peroxide input from inspection of signal profiles (cf. Figure 3.1C-D). Another concern is 'when' to measure signal output as the signal output peak can vary depending on the sensor and hydrogen peroxide concentrations as well as cell type (Figure 3.1C-D; de Cubas et al., 2021; Kritsiligkou et al., 2021). It is also unclear whether measuring just a single peak is sufficient to describe the complete dynamic profile. These limitations become concerning when quantitative data is required for kinetic fitting experiments, or for comparisons of the effect of different drugs or mutations on cellular hydrogen peroxide levels. To overcome these limitations, we tested whether dynamic profiles of these sensors could be quantified using area under the curve (AUC), signal amplitude, signal time and signal duration parameters (Chapter 2, Heinrich et al., 2002; Hornberg et al., 2005; Pillay et al., 2016).

3.2 Results

3.2.1 Evaluating the performance of genetically encoded redox sensors in response to external hydrogen peroxide concentrations.

The signalling profiles generated from the response of HyPer7 and roGFP2-Tsa2ΔC$_R$ to increasing bolus hydrogen peroxide concentrations (1-1000 µM) in *S. cerevisiae* were reported previously (Kritsiligkou et al., 2021). Both sensors were rapidly activated by hydrogen peroxide with HyPer7 showed an exponential decay in the signal (Figure 3.2A-B). By contrast, roGFP2-Tsa2ΔC$_R$ showing a more sustained activation profile particularly at higher hydrogen peroxide concentrations.

To determine whether there was indeed a linear correlation between sensor output and hydrogen peroxide concentration, we determined the linear correlations between the AUC and amplitude and hydrogen peroxide over the entire range (*y1*, 1-1000 µM), the upper range (*y2*, 100-1000 µM), and the lower range (*y3*, 1-100 µM) of hydrogen peroxide concentrations used in these experiments (Figure 3.2C-F). We found that the AUC and amplitude for HyPer7 was greater than roGFP2-Tsa2ΔC$_R$ over the upper range of hydrogen peroxide concentrations. The HyPer7 AUC (0.997 vs 0.807) and amplitude (0.957 vs 0.863) also showed a stronger linear correlation to the entire range of hydrogen peroxide concentrations than roGFP2-Tsa2ΔC$_R$. In particular, the HyPer7 AUC had a strong correlation (r>0.99) with hydrogen peroxide concentration over the upper range as well as the entire range of hydrogen peroxide concentrations. Over the lower hydrogen peroxide concentration range (1-100 µM), roGFP2-Tsa2ΔC$_R$ had a higher AUC and amplitude, with both sensors showing a strong linear correlation (r>0.99) between AUC and hydrogen peroxide concentration in contrast to the lower correlations obtained for their amplitudes (Figure 3.2E-F). Interestingly, the AUC and amplitude correlation equations for HyPer7 over the different hydrogen peroxide concentrations (*y1*, *y2* and *y3*) were more similar than the gradients obtained for Tsa2ΔC$_R$ (Figure 3.2C-F).

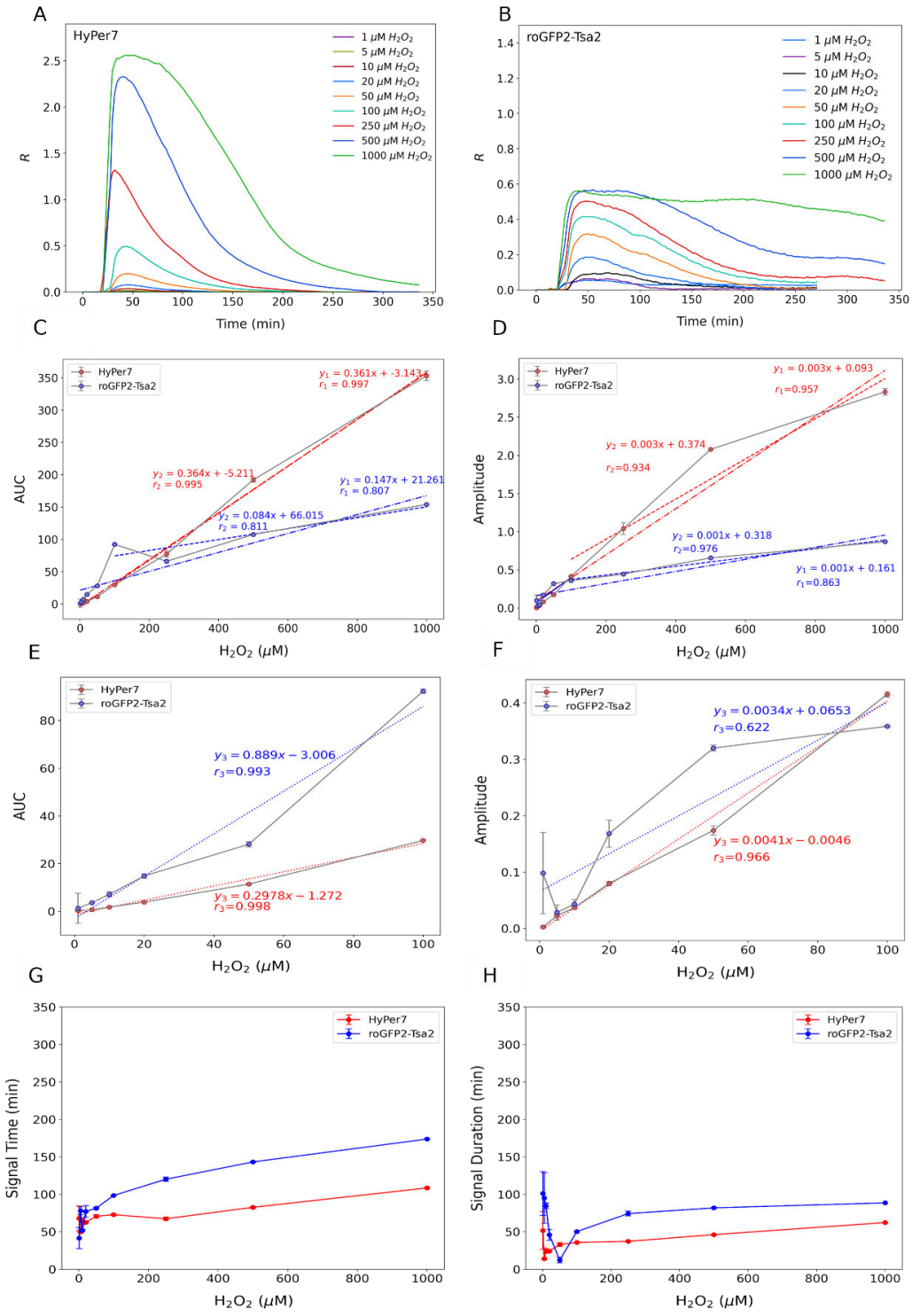

Figure 3.2: The signalling profiles and parameters for HyPer7 and roGFP2-Tsa2ΔCR generated in *S. cerevisiae* exposed to hydrogen peroxide.

S. cerevisiae cells were exposed to bolus hydrogen peroxide concentrations ranging from 1-1000 μM, and the ratiometric outputs were measured using the genetically encoded redox sensors, HyPer7 (red) and roGFP2-Tsa2ΔC$_R$ (blue) (A-B). From these profiles, the AUC (C,

E) and signal amplitude (D, F) were determined over the entire hydrogen peroxide range (1-1000 µM) or for a lower range (1-100 µM) (E-F). Linear regression equations and correlation coefficients were obtained for the regions 1-1000 (y_1), 100-1000 (y_2) and 1-100 µM (y3). The signal time (G) and duration (H) for both sensors were also determined. The data represent the means and standard errors of at least three independent experiments (Kritsiligkou et al., 2021).

We next sought to determine how the timing of the sensor outputs were related to hydrogen peroxide concentrations (Figure 3.3G-H). HyPer7 had a lower signal time and duration than roGFP2-Tsa2ΔC$_R$, showing that its activation/deactivation cycle was faster than the roGFP2 sensor. There was a gradual increase in signal time and duration, particularly for roGFP2-Tsa2ΔC$_R$, at higher concentrations of hydrogen peroxide, showing that there was a shift in the time and width of the curves as the hydrogen peroxide concentration increased. Collectively, these results showed that the dynamic profiles from these sensors can be analysed using the signal parameters AUC, amplitude, time and duration in order to select the most appropriate sensor based on the expected hydrogen peroxide concentration in an experiment. Moreover, our analysis showed that the output from these probes did not saturate at the higher hydrogen peroxide concentrations used in this experiment.

3.2.2 Quantifying HyPer7 and roGFP2-Tpx1 response in S. pombe

It was unclear whether the insights we obtained for HyPer7 and roGFP2 were specific for baker's yeast or would hold for different cells. Fission yeast cells, with either HyPer7 or roGFP2-Tpx1.C169S, were exposed to a hydrogen peroxide concentration range of 5-1000 µM and the OxD determined over 80 min (Figure 3.3; de Cubas et al., 2021). HyPer7 reached the maximal oxidation limit of the sensor (OxD=1) at 200 µM hydrogen peroxide (Figure 3.3A), showing that the sensor response had saturated by this concentration. The roGFP2-Tpx1.C169S sensor displayed less distinct peaks when compared with HyPer7 in both *S. pombe* and *S. cerevisiae* (Figure 3.3B). Moreover, the sensor appears to reach an oxidation limit at an OxD of 0.6, which may be due to sensor-specific Tpx1 hyperoxidation limiting the signal output of the sensor (Morgan et al., 2016).

As with baker's yeast, the linear correlation between the AUC and signal amplitude and hydrogen peroxide concentration was determined for different concentration ranges: the full range (*y1*, 5-1000 µM), and a lower range (*y2*, 5-50 µM). When compared to baker's yeast,

both sensors exhibited a weaker linear correlation (r<0.9) over the whole peroxide range as the OxD readings plateaued at >200 µM hydrogen peroxide (Figure 3.3C-D). However, when considering the lower hydrogen peroxide range (5-50 µM), the linear correlations for both sensors for AUC and signal amplitude showed strong correlations r>0.9 with similar regression equations (Figure 3.3E-F). Therefore, both HyPer7 and roGFP-Tpx1.C169S are suitable for analysis at lower hydrogen peroxide concentrations, but OxD signal responses for hydrogen peroxide concentrations above this level should be treated with caution.

The signal time remained relatively unchanged at approximately 30 minutes for HyPer7 and 32 minutes for roGFP-Tpx1.C169S after the bolus addition of 1-200 µM hydrogen peroxide and then increased to over 40 minutes for both sensors after the addition of 1000 µM hydrogen peroxide (Figure 3.3G). Similarly, signal duration was ~16 minutes for HyPer7 and 19 minutes for roGFP-Tpx1.C169S after exposure to 1-200 µM hydrogen peroxide and then increased to ~20 minutes at higher hydrogen peroxide concentrations (Figure 3.3H). The signal duration was ~20 minutes lower than the signal time whereas these parameters were similar in bakers yeast. This result was in contrast to the distinct peaks of HyPer7 and roGFP- Tsa2ΔC_R in bakers yeast.

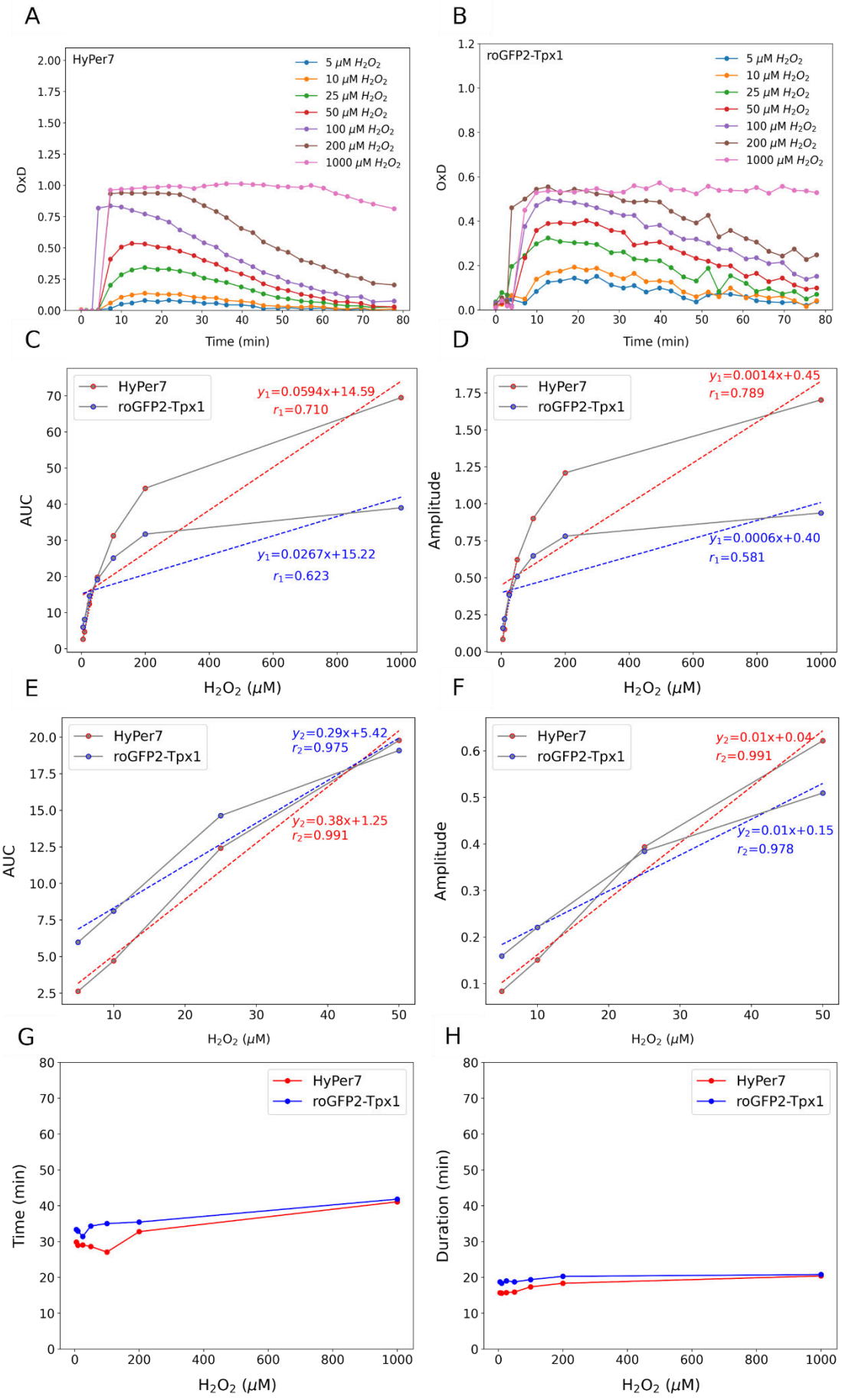
A
HyPer7
5 μM H2O2
10 μM H2O2
25 μM H2O2
50 μM H2O2
100 μM H2O2
200 μM H2O2
1000 μM H2O2
OxD
Time (min)
B
roGFP2-Tpx1
5 μM H2O2
10 μM H2O2
25 μM H2O2
50 μM H2O2
100 μM H2O2
200 μM H2O2
1000 μM H2O2
OxD
Time (min)
C
HyPer7
roGFP2-Tpx1
y1=0.0594x+14.59
r1=0.710
y1=0.0267x+15.22
r1=0.623
AUC
H2O2 (μM)
D
HyPer7
roGFP2-Tpx1
y1=0.0014x+0.45
r1=0.789
y1=0.0006x+0.40
r1=0.581
Amplitude
H2O2 (μM)
E
HyPer7
roGFP2-Tpx1
y2=0.29x+5.42
r2=0.975
y2=0.38x+1.25
r2=0.991
AUC
H2O2 (μM)
F
HyPer7
roGFP2-Tpx1
y2=0.01x+0.04
r2=0.991
y2=0.01x+0.15
r2=0.978
Amplitude
H2O2 (μM)
G
HyPer7
roGFP2-Tpx1
Time (min)
H2O2 (μM)
H
HyPer7
roGFP2-Tpx1
Duration (min)
H2O2 (μM)

Figure 3.3: The signalling profiles and parameters for HyPer7 and roGFP2-Tpx1.C169S generated in *S. pombe* exposed to hydrogen peroxide.

S. pombe cells were exposed to hydrogen peroxide ranging from 5-1000 µM, and the dynamic fluorescence was measured using the genetically encoded redox sensors HyPer7 (red) and roGFP2-Tpx1.C169S (blue) (A-B). We evaluated three linear regions, with associated correlation equations, for AUC and signal amplitude, which were 5-1000 (y_1) µM (C-D) the lower range, 5-50 µM (y2) (E-F) The linear regression and correlation coefficients (r^2) for these sensor OxD output and hydrogen peroxide concentration are shown on the figures (de Cubas et al., 2021).

3.2.3 Comparison of sensor performance of different genetic backgrounds.

The oxidation of redox sensors is a function of both the sensor oxidation and reduction dynamics (Zhuravlev et al., 2024). Here, the natural cytoplasmic redox systems will actively reduce the oxidised sensor resulting in decreased sensor signal. To this end, de Cubas et al., (2021) mutated components of the thioredoxin system from *S. pombe* and monitored the performance of HyPer7 across a hydrogen peroxide range of 5-1000 µM. When compared to the wildtype cells, the signalling profiles of the Δ*trx1* strain showed sustained activation of the HyPer7 sensor even at the lower hydrogen peroxide concentrations (Figure 3.4A). Comparatively, the Δ*trr1* strain showed rapid activation of the HyPer7 sensor that was sustained for the duration of the time course and then gradually decreased in signal but did not return to base signal after hydrogen peroxide concentrations greater than 100 µM (Figure 3.4B) compared to the activation/deactivation dynamics of the wildtype cells (Figure 3.3A).

We then determined how deleting the thioredoxin system impacted the signalling parameters. Here, the Δ*trx1* strain showed that the AUC and signal amplitude were higher compared to the wildtype and Δ*trr1* strains (Figure 3.4C-D). These results for AUC and signal amplitude suggest that thioredoxin is the main HyPer7 reductant (de Cubas et al., 2021).

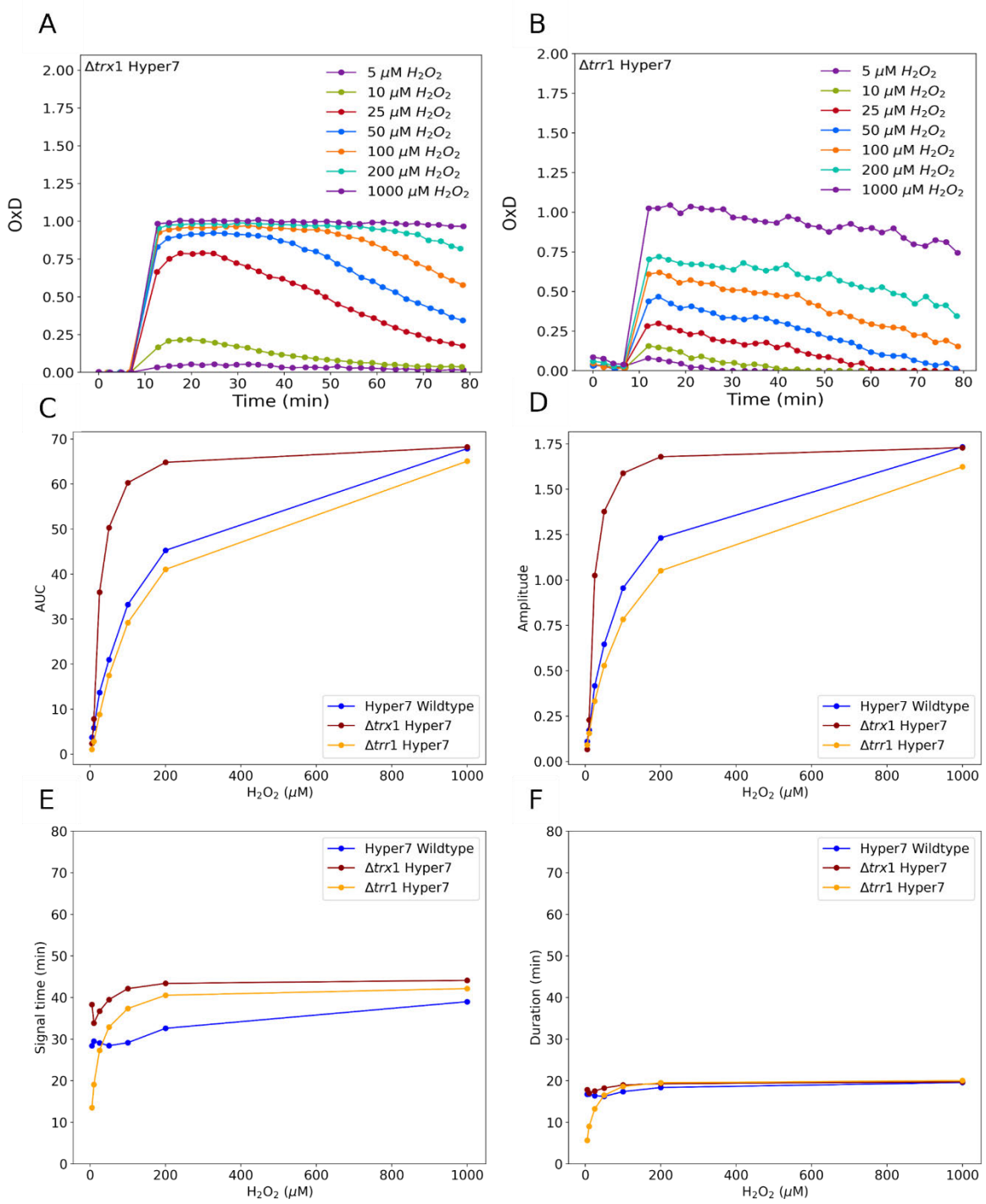

Figure 3.4: The signal parameters for HyPer7 in *S. pombe* strains lacking thioredoxin and thioredoxin reductase.

S. pombe Δtrx1 (red) and Δtrr1 (orange) strains were exposed to hydrogen peroxide ranging from 1-1000 µM and the fluorescence of HyPer7 activity was measured (A-B). The area under the curve was measured (C), and subsequently, the signalling amplitude (D), time (E) and duration (F) were calculated for each strain and compared to the wildtype cell.

The signal time remained relatively consistent for the wildtype strain (~ 30 minutes) and the Δ*trx1* (~42 minutes) while the Δ*trr1* strain displayed a linear increase in signal time that saturated at 100 µM hydrogen peroxide at ~38 minutes (Figure 3.4E). A similar pattern was observed for the signal duration where the wildtype and Δ*trx1* strains had signal durations of ~17 minutes, and the Δ*trr1* strains signal duration increased quasi-linearly to a hydrogen peroxide range of 100 µM and then saturated at ~18 minutes (Figure 3.4F). In the Δ*trr1* strain, the signal time and duration are lower when compared to the wildtype and Δ*trx1* strains at lower hydrogen peroxide concentrations confirming their role in probe reduction.

3.3 Discussion

Genetically encoded redox sensors have significantly advanced the quantification of biomolecular redox states within cells (Murphy et al., 2022) and have facilitated key discoveries in various settings, including the monitoring of hydrogen peroxide gradients during wound healing (Niethammer et al., 2009), insights into developmental processes (Knoefler et al., 2012), and age-related alterations in ROS generation (Lennicke & Cochemé, 2020). The increasing diversity of redox sensors has prompted interest in comparing and characterising them (Palmer et al., 2011). However, quantifying the temporal dynamic response of different sensors is challenging (Hung et al., 2014).

In our analysis, we determined the AUC alongside Heinrich signalling parameters of signal amplitude, time, and duration, to characterise the dynamic profiles of redox sensor data. Using this approach, we compared the responses of HyPer7 and roGFP-Tsa2ΔC$_R$ in *S. cerevisiae* as well as the response of HyPer7 and roGFP-Tpx1.C169S to hydrogen peroxide in fission yeast. Quantitative analysis revealed that linear increases in AUC and signal amplitude were observed for HyPer7 and roGFP sensors in both yeast backgrounds. These data showed linearity in response to specific hydrogen peroxide concentrations and, therefore, serves as a crucial control when evaluating redox sensors. Further, calibration curves based off the AUC and signal amplitude may be useful for other applications (Figure 3.2C-D). For instance, the linear segment of the graph for signal amplitude or AUC can be used to relate the oxidative effect of various drugs to (external) hydrogen peroxide concentrations. The signal parameters of time and duration indicate when and for how long a sensor is active, and high-quality sensors

should ideally demonstrate low variation in these parameters, a consistency observed in HyPer7 but less so for roGFP-based redox sensors (Figure 3.3E-F).

Lastly, a quantitative approach allowed us to measure the impact of antioxidant proteins on redox sensor oxidation/reduction dynamics through the genetic manipulation of the cell. The Hyper7 sensor, coupled with quantitative analysis, revealed an increase in all signalling parameters in Δ*trx1* cells (Figure 3.4C-F). On the other hand, Δ*trr1* cells had reduced AUC and signal amplitude, revealing decreased oxidation of HyPer7, which could result from Trx1 oxidation of the sensor. Indeed, in Δ*trr1* cells, Pap1 becomes constitutively active, which corresponds to increased oxidation of the sensor (Brown et al., 2013; Day et al., 2012). By quantifying the temporal dynamics of redox sensors, we provide an analytical tool to assess sensor data quantitatively. This approach offers a quantitative comparison of different sensors, and their utility in various cellular backgrounds can be evaluated.

3.4 Methods

All computational analysis was carried out in a Jupyter notebook using Python (https://www.python.org/) programming languages with the following most represent packages of NumPy, SciPy (https://scipy.org), matplotlib (https://matplotlib.org/) and sklearn. The datasets for HyPer7 and roGFP-TSA2 was kindly provided by Pari Kritsiligkou and Tobias Dick (Kritsiligkou et al, 2021) and sensor data from HyPer7 in fission yeast were digitised from plotdigitizer (de Cubas et al., 2021). The baseline values were correct by subtracting the oxygen consumption by the yeast culture (Kritsiligkou et al., 2021). All subsequent quantification using the signalling parameters of signal amplitude, time and duration are readily available as a Jupyter notebook uploaded to Github https://github.com/djl94/Chapter3_supp.git.

Chapter 4

Quantifying pretreatment effects in the NRF2/Keap1 pathway for assessing cellular adaptation to oxidative stress.

Abstract

In human cells, the NRF2-Keap1 pathway plays a central role in the cellular antioxidant response and is activated by several oxidants. Dysregulation of the pathway may contribute to, or is a consequence of, a range of conditions, including drug-induced liver disorders and ageing. Because the NRF2 activation is dynamic, quantitative comparisons between oxidants, oxidant concentrations and dosage schedules have been challenging. Using published data, we show how, in response to diethyl maleate or *tert*-butylhydroquinone (0-200 μM), NRF2 dynamic profiles can be characterised by their signal amplitude, signal time and signal duration parameters. Pre-exposure to these oxidants 8 hr before a second dose (0-200 μM) decreased the NRF2 signal time and duration from ~6 hrs to ~4 hrs, with the 200 μM pre-exposure concentrations leading to higher NRF2 signal amplitudes across the range of second dose concentrations. By contrast, oxidant pre-exposure 24 hrs before a second dose led to a lower signal amplitude when compared to naïve cells, or cells pre-exposed to these oxidants for 8 hr. Srxn1 expression was used as an output of NRF2 activity and was also reduced in these 24 hr pre-exposed cells for different oxidant concentrations. These data show that both oxidant concentration and the timing of repeat exposure affect NRF2 activation and the induction of Srxn1 expression. Thus, studies aiming to understand NRF2 signalling in disease or to modulate NRF2 pharmacologically must consider the dynamics of NRF2 activation, particularly in conditions where the pathway is expected to be repeatedly activated.

4.1 Introduction

All living organisms, including yeast, bacteria, and mammals, possess an innate ability to adapt to harmful substances without suffering permanent damage (Crawford & Davies, 1994; Pomatto & Davies, 2017b). This phenomenon is commonly referred to as the "adaptive response" and enables organisms to withstand seemingly lethal toxicity doses when exposed to an initial mild dose (Crawford & Davies, 1994). Several studies have highlighted that genes related to antioxidant defence are upregulated when cells are pre-adapted, establishing a resilient reservoir within organisms to cope with lethal toxic doses (Salo et al., 1996). For example, in *Drosophila melanogaster*, an initial 1 mM hydrogen peroxide exposure protected the flies against a subsequent, usually lethal, 50 mM hydrogen peroxide dose (Pickering et al., 2013, Love et al., 1986). Pre-exposure induced heat shock proteins that allowed for apparent protection from the toxic hydrogen peroxide dose (Pickering et al., 2013; Love et al., 1986). These adaptive responses are generally controlled by transcription factors but understanding the dynamic behaviour of these processes and the effectiveness of pretreatment strategies is not clear (Pomatto & Davies, 2017b).

To better understand the dynamic behaviour of pre-exposure on a key transcription factor, Bischoff and colleagues monitored the NRF2/Keap1 pathway in human G2 cell lines (Bischoff et al., 2019a). This pathway has been shown to be integral in responding to oxidative and electrophile stress and its dysregulation has been associated with diabetes, inflammation, and cancer (Yamamoto et al., 2018). Under normal, non-stressed conditions, NRF2 is tagged for rapid degradation within the proteasome due to the formation of a ubiquitin E3 ligase complex involving Keap1 and CUL3 (Figure 4.1) (Zhao et al., 2021; Suzuki et al., 2016). However, when an oxidative or electrophilic stressor is present, specific cysteine residues on Keap1undergo modifications that result in the disassembly of the Keap1/CUL3 ubiquitin ligase complex, stabilising NRF2 (Figure 4.1) (Zhao et al., 2021; Suzuki et al., 2016). Subsequently, NRF2 translocates into the nucleus, where it initiates an antioxidant response by transcribing genes, including those encoding catalase, superoxide dismutases, and sulfiredoxin (Figure 4.1) (Zhao et al., 2021; Suzuki et al., 2016).

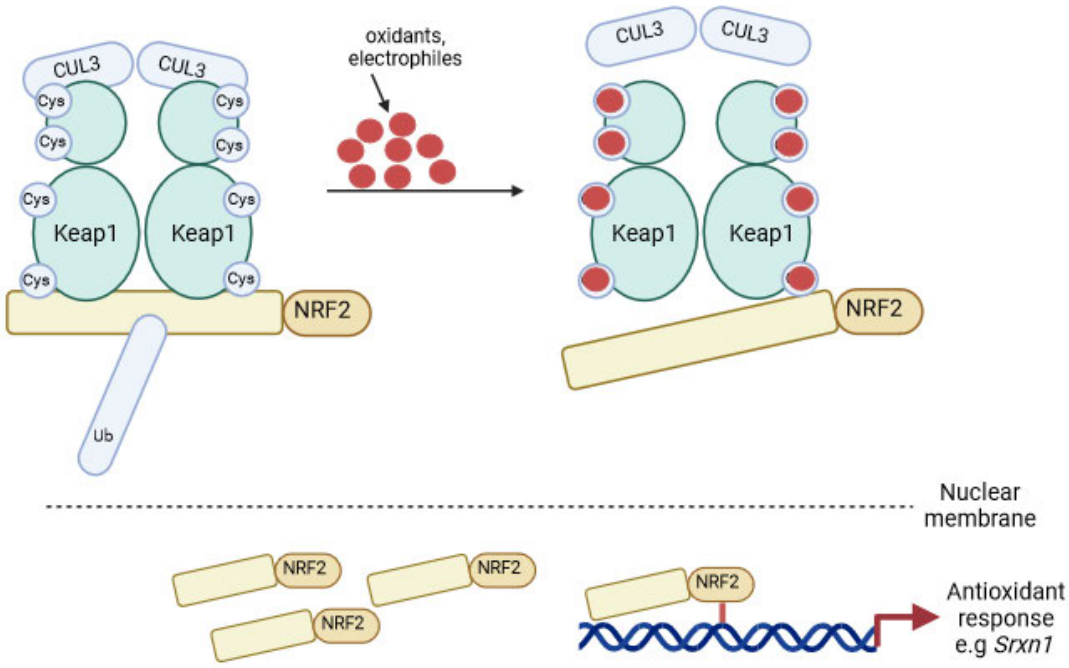

Figure 4.1: The NRF2/Keap1 pathway induces antioxidant responses to oxidative and electrophilic stress.

Under normal conditions, NRF2 undergoes rapid degradation as it is ubiquitinated by CUL3. However, upon the introduction of oxidants like DEM or tBHQ, the cysteine residues on Keap1 are modified resulting in the dissociation of Keap1/CUL3 from NRF2. The NRF2 molecule is translocated to the nucleus to induce an antioxidant response (Modified from Yamamoto et al., 2018).

Through its activity, NRF2 may contribute to the prevention of age-related diseases, the delay of cell senescence (Rajasekaran et al., 2011) and preventing drug–induced liver damage (Bischoff et al., 2019b) by potentiating the antioxidant response. While this hypothesis may seem plausible, it has also been demonstrated that NRF2 overexpression in cancer cells leads to resistance to therapeutic drugs, effectively shielding tumour cells from treatment (Hu et al., 2013). Furthermore, prolonged NRF2 activation in mice has been linked to the onset of cardiomyopathy due to reductive stress (Rajasekaran et al., 2011). As a result, whether the NRF2 pathway should be constitutively activated or inhibited as a therapeutic strategy is unclear. To understand how the NRF2 pathway responds to oxidative stress, several studies have considered the dynamic signalling response through western blotting, GFP tagging and

single-cell approaches, which have given insights into the regulatory mechanisms of the pathway (Hiemstra et al., 2022; Baird et al., 2014; Bischoff et al., 2019; Johansson et al., 2017). However, quantifying the dynamic profiles of NRF2 could provide insight into how pre-adaptation and repeat exposures affects the activation of the pathway.

4.2 Results

4.2.1 Quantifying the response of the NRF2 pathway to increasing concentrations of DEM and tBHQ

Before assessing the ability of the NRF2 pathway to respond to pre-adaption, the timing of when the pathway has become fully adapted or partially adapted was first assessed. These times were established by monitoring the dynamic response of NRF2 in HepG2-reporter cells containing GFP-tagged NRF2 (Bischoff et al., 2019b; ter Braak et al., 2022). Cells were exposed to a single-dose dose (0-200 µM) of diethyl maleate (DEM) or *tert*-butylhydroquinone (tBHQ) which activate the NRF2 pathway through distinct mechanisms. DEM functions by depleting glutathione levels, indirectly leading to NRF2 activation (Baird et al., 2014; Bischoff et al., 2019b), while tBHQ directly oxidises cysteine residues on Keap1 (Baird et al., 2011; Bischoff et al., 2019).

The dynamic response of the NRF2 pathway to exposure to DEM and tBHQ showed that NRF2 had reached its maximal activation ~5 hrs after initial exposure and started to decline ~8 hrs after the initial exposure; the authors selected 8 hrs as a partial adaption time point (Figure 4.2A-B). The second adaption point was when the maximal NRF2 activation had returned to baseline activation ~24 hrs after the initial exposure (Figure 4.2A-B). Once the adaptation time points were determined, pre-exposure experiments were conducted. This involved monitoring NRF2 dynamic responses to different initial combinations of DEM and tBHQ, followed by administering second doses after 8 or 24 hrs from the initial exposure. The

effect of these treatments on the cellular antioxidant response was assessed by monitoring the expression of sulfiredoxin (Srxn1), a protein regulated by NRF2 (Wu et al., 2021).

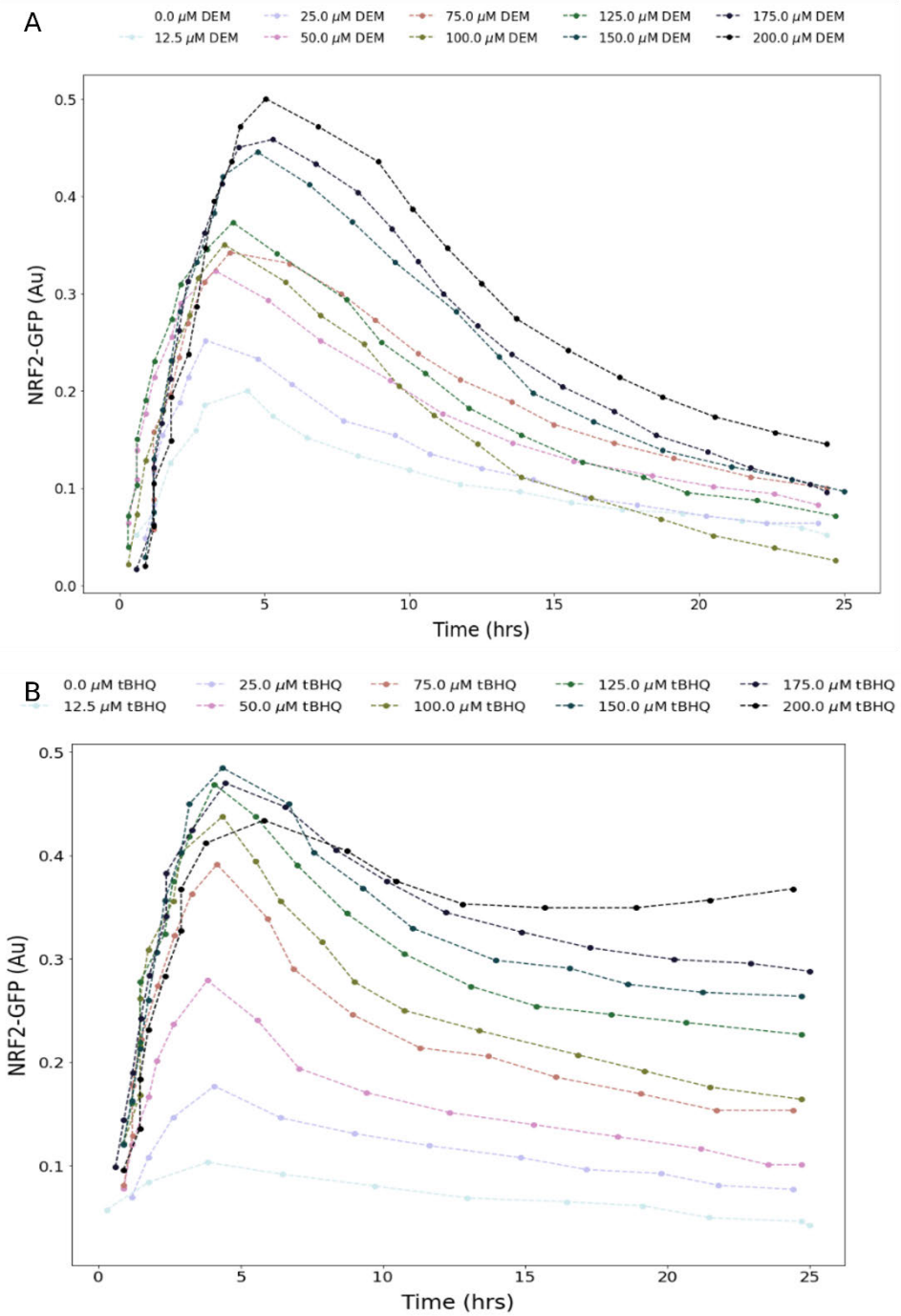

Figure 4.2: The response of the NRF2 pathway to increasing oxidant levels of DEM and tBHQ.

The fluorescence intensity of the NRF2 was measured in HepG2-reporter cells exposed to a single dose of DEM (A) and tBHQ (B) in the concentration range of 0-200 µM. The NRF2 protein levels were monitored by fluorescence through live imaging confocal microscopy (A-B).

For the next set of experiments, initial DEM concentrations of 0-200 µM were applied to HepG2 cells which were then exposed to further doses of DEM after 8 hrs (Figure 4.3A-D) or after 24 hrs (Figure 4.4A-D). In this context, a second dose of DEM after 8 hrs does appear to strongly induce NRF2, particularly at 200 µM (Figure 4.3).

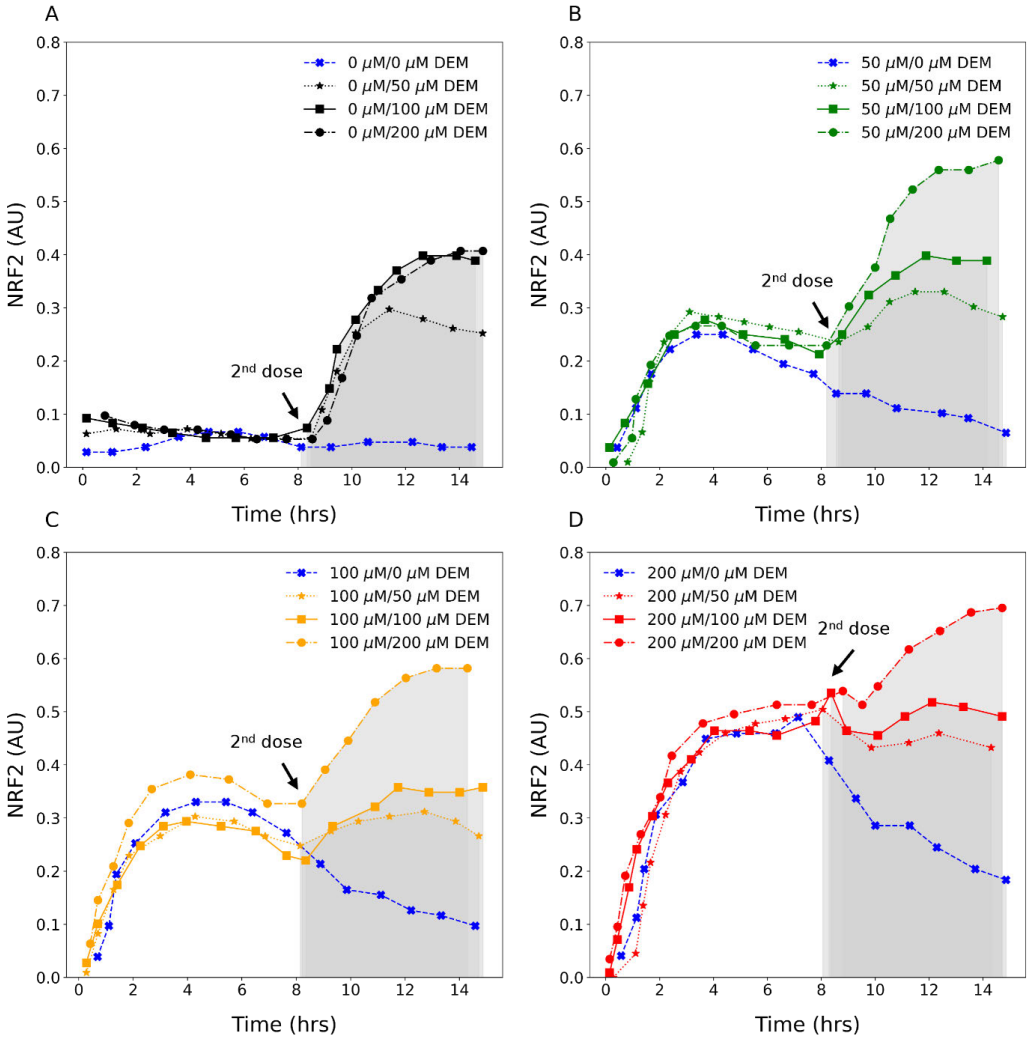

Figure 4.3: The activation dynamics of NRF2 following treatment with DEM after a second dose at 8 hrs.

HepG2-reporter cells were GFP tagged to monitor the activation dynamics of NRF2 using live cell confocal imaging. The average intensity of NRF2 in the nucleus was monitored after initially exposing cells to 0 µM (A) (black), 50 µM (B) (green), 100 µM (C) (orange), and 200 µM (D) (red) DEM 8 hrs and compared to cells treated with a single dose (represented by the blue curves in each plot). Subsequently, a second dose of DEM was administered ranging from 0 µM (cross), 50 µM (star), 100 µM (square), and 200 µM (circle), resulting in four

combinations of repeat exposure conditions. The signal parameters calculated based on the shaded region of each curve.

When there is no second dose applied the NRF2 signal returns to baseline (Figure 4.3A-D). For all cells, a second dose of DEM increases the availability of NRF2 compared to cells without a second dose, with the 200 μM treatment having the largest effect. In cells with no pre-exposure (Figure 4.3A), the response of cells exposed to 100-200 μM DEM was similar. By contrast, in cells pre-exposed to DEM (50-200 μM), there were noticeable differences in the NRF2 signal obtained for these cells. In some of the experiments, the NRF2 signal following an initial dose appeared to match the signal for the second dose if concentrations were equal to or less than the initial dose. For example, the 100 μM first dose and 100 μM second dose as well as the 50 and 100 μM treatments appeared to have similar NRF2 responses (Figure 4.3C). A second dose of 200 μM appears to greatly increase the overall NRF2 response when compared to the initial dose of any concentration (Figure 4.3A-D).

The profiles of NRF2 fluorescence intensity after the initial and second dose after 24 hrs were different when compared to the 8 hr adaption period (Figure 4.4A-D). Here, distinct peaks for all concentration combinations were observed in the initial dose, with the signal returning to baseline in most scenarios. Interestingly, after the addition of the second dose between 50-200 μM, the NRF2 signal intensity appears to decrease. In contrast to the 8 hr data, there were no differences in the NRF2 responses following a second dose of DEM (Figure 4.4A-D). Thus, by 24 hrs, the cellular environment appears to reset, returning to a pre-stress state and resulting in a response similar to that of unexposed cells.

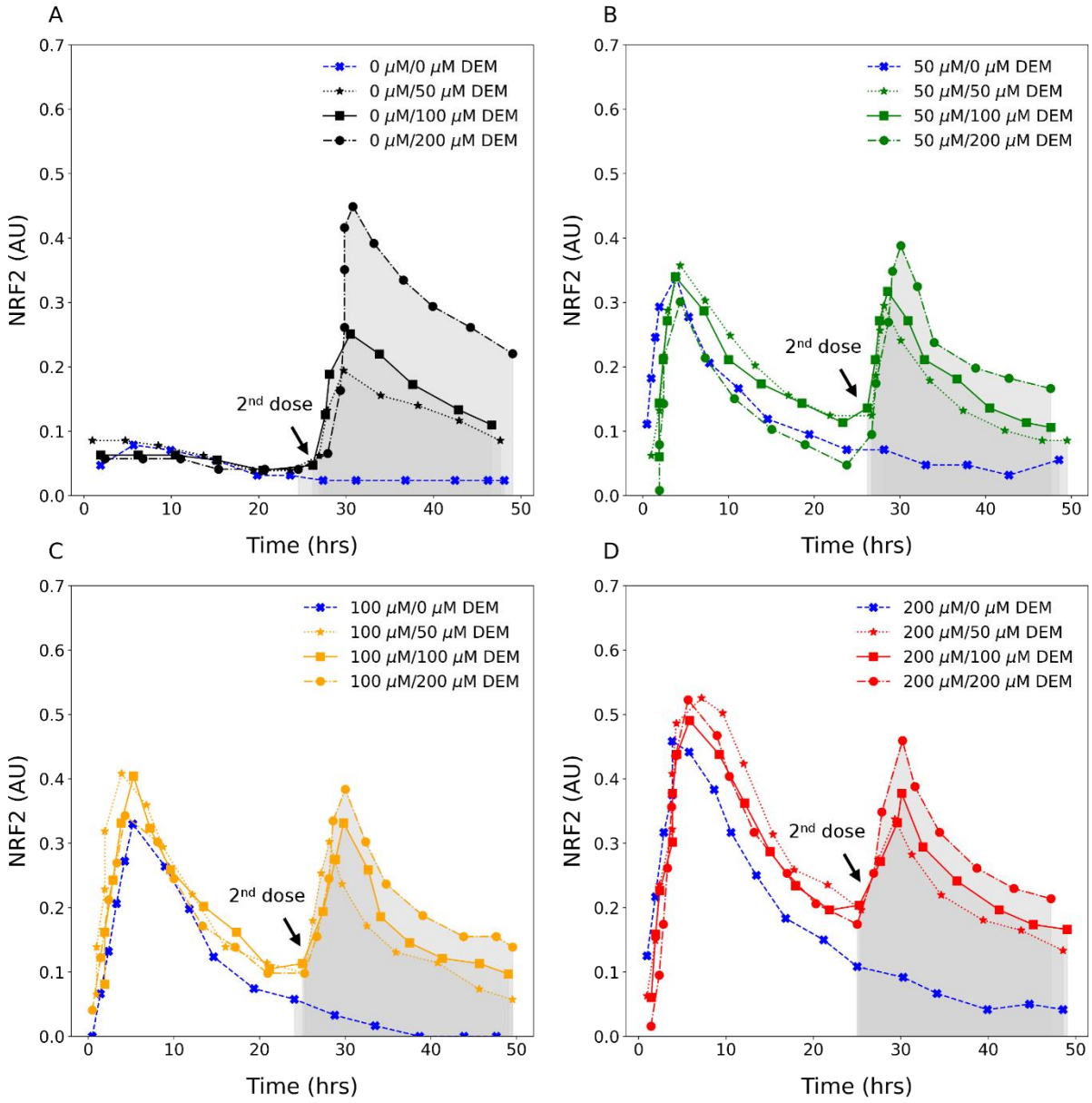

Figure 4.4: The activation dynamics of NRF2 following treatment with DEM after a second dose at 24 hrs.

HepG2-reporter cells were GFP tagged to monitor the activation dynamics of NRF2 using live cell confocal imaging. The average intensity of NRF2 in the nucleus was monitored after initially exposing cells to 0 μM (A) (black), 50 μM (B) (green), 100 μM (C) (orange), and 200 μM (D) (red) DEM 24 hrs after the initial seeding (represented by the blue curves in each plot). Subsequently, a second dose of DEM was administered ranging from 0 μM (cross), 50 μM (star), 100 μM (square), and 200 μM (circle), resulting in four combinations of repeat exposure conditions. The signal parameters were calculated based on the shaded region of each curve.

Next the HepG2 cells were exposed to varying combinations of initial and secondary dose concentrations of tBHQ. Here, we also observed that the 8 hr pre-exposure period resulted in higher NRF2 fluorescence intensities compared to the initial dose (Figure 4.5A-D). However, the 24-hour adaption was different compared to DEM exposure, where the only lower tBHQ combinations resulted in NRF2 intensities returning to zero, while initial and secondary exposure to 200 µM tBHQ resulted in sustained increasing signal intensities (Figure 4.6A-D). Overall, these cells appeared to have a broader signal response compared to the two distinct peaks observed for cells pre-exposed to DEM.

These data raised two key questions. First, how do various oxidants compare in activating the NRF2 pathway? Second, what impact does pre-exposure have on the NRF2 pathway? However, drawing meaningful conclusions based solely on the profiles is challenging due to the complexity of these data. To answer these questions, we therefore determined the signal parameters of these profiles (shown in grey on the graphs, adjusted for 8 hr and 24 hr exposure times).

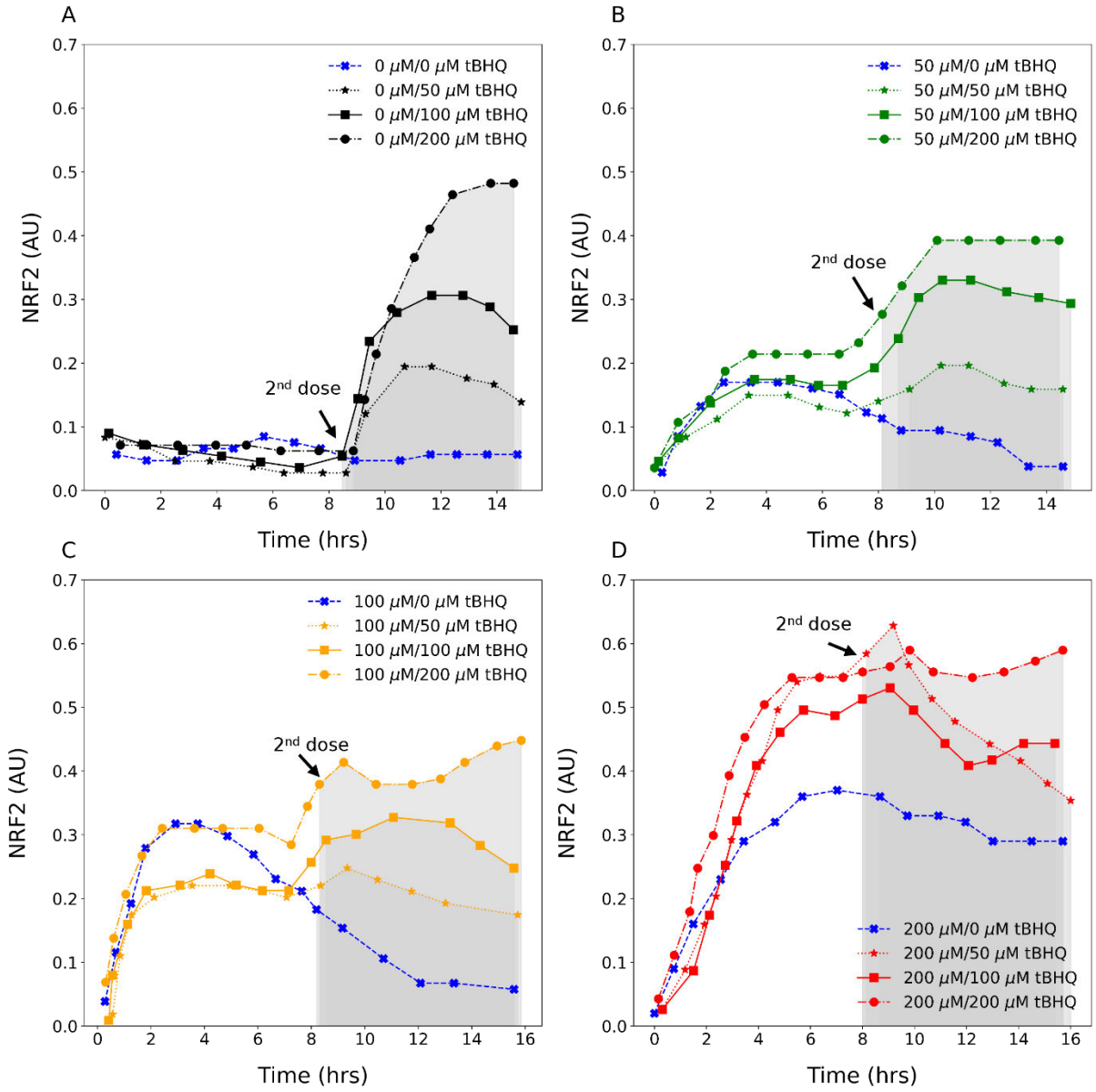

Figure 4.5:The activation dynamics of NRF2 following treatment with tBHQ after a second dose at 8 hrs and the associated signalling parameters.

HepG2-reporter cells were GFP tagged to monitor the activation dynamics of NRF2 using live cell confocal imaging. The average intensity of NRF2 in the nucleus was monitored after initially exposing cells to 0 μM (A) (black), 50 μM (B) (green), 100 μM (C) (orange), and 200 μM (D) (red) tBHQ 8 hrs after the initial seeding (represented by the blue curves in each plot). Subsequently, a second dose of tBHQ was administered, ranging from 0 μM (cross), 50 μM (star), 100 μM (square), and 200 μM (circle), resulting in four combinations of repeat exposure conditions. The signal parameters were calculated based on the shaded region of each curve.

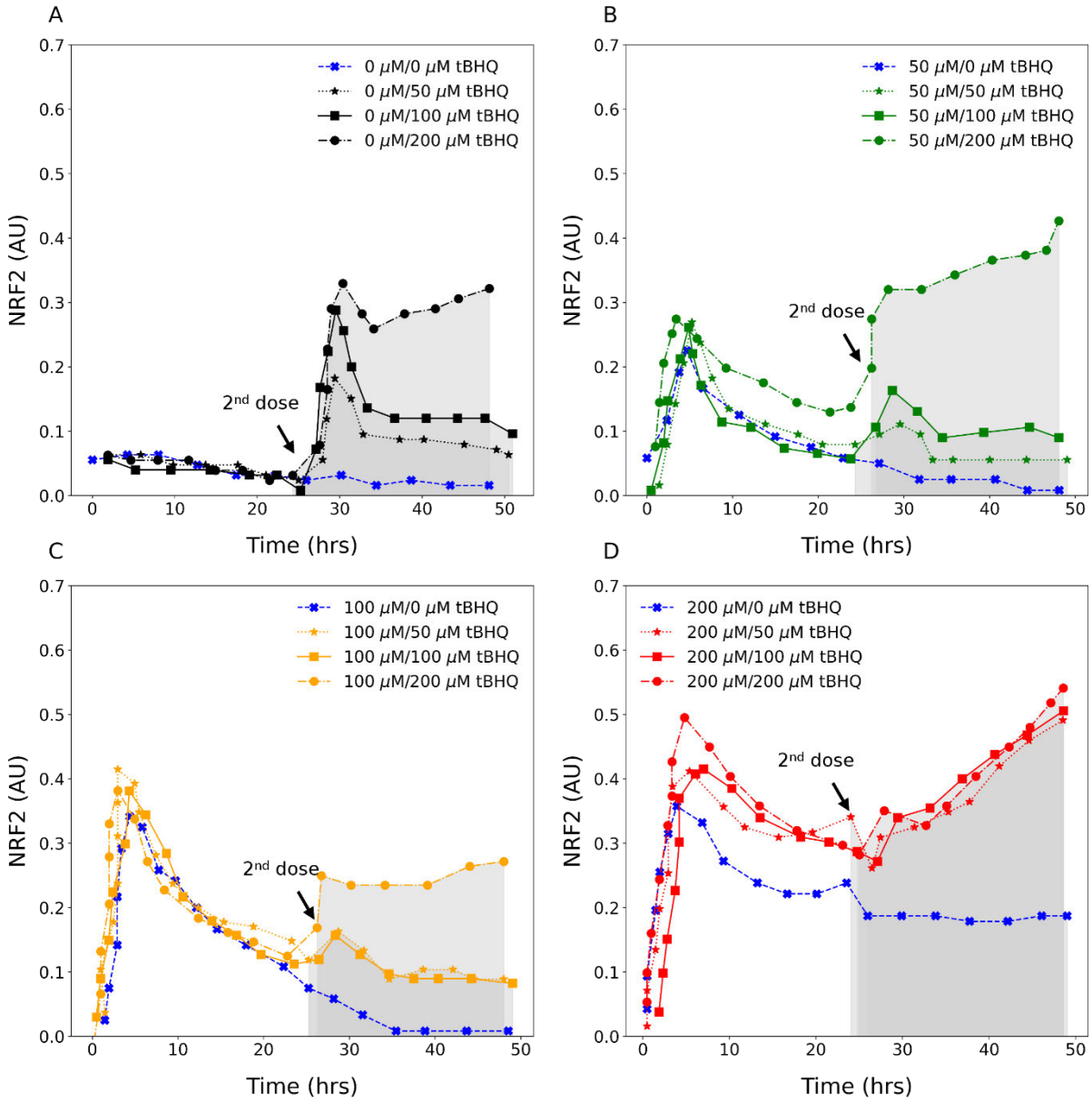

Figure 4.6: The activation dynamics of NRF2 following treatment with tBHQ after a second dose at 24 hrs.

HepG2-reporter cells were GFP tagged to monitor the activation dynamics of NRF2 using live cell confocal imaging. The average intensity of NRF2 in the nucleus was monitored after initially exposing cells to 0 µM (A) (black), 50 µM (B) (green), 100 µM (C) (orange), and 200 µM (D) (red) tBHQ 24 hrs after the initial seeding (represented by the blue curves in each plot). Subsequently, a second dose of DEM was administered ranging from 0 µM (cross), 50 µM (star), 100 µM (square), and 200 µM (circle), resulting in four combinations of repeat exposure conditions. The signal parameters were calculated based on the shaded region of each curve.

4.2.2 Comparison of the oxidants DEM and tBHQ using signal parameter quantification

DEM and tBHQ have different modes of NRF2 activation and we tested whether these oxidants resulted in different NRF2 signal dynamics. DEM and tBHQ triggered similar NRF2 activation responses in amplitude when naïve cells were treated with these oxidants (blue lines, Figure 4.7A), and after cells were treated with the oxidants following an 8 hr exposure step. The 200 μM initial dose of these oxidants resulted substantial increases in signal amplitude (Figure 4.7A). The signal time and duration for both oxidants remained relatively constant and was not affected the oxidant concentration (Figure 4.7B-C). Thus, NRF2 response to these two oxidants was similar despite their different modes of action. On the other hand, when we quantified the response of NRF2 after a 24 hr pre-exposure to DEM and tBHQ, we obtained differences between these oxidant amplitudes. Unlike the 8hr exposure, cells pre-treated with 200 μM tBHQ showed closer responses to cells treated with a lower dose of this oxidant (Figure 4.7D). By contrast, cells pre-treated with 200 μM DEM showed a higher NRF2 activation response than cells treated with a lower concentration of this oxidant. The signal time and duration following a 24 hr pre-treatment regime (Figure 4.7E-F) were higher than cells treated for 8 hrs showing the dynamics of these responses was dependent on the timing of the oxidative stress.

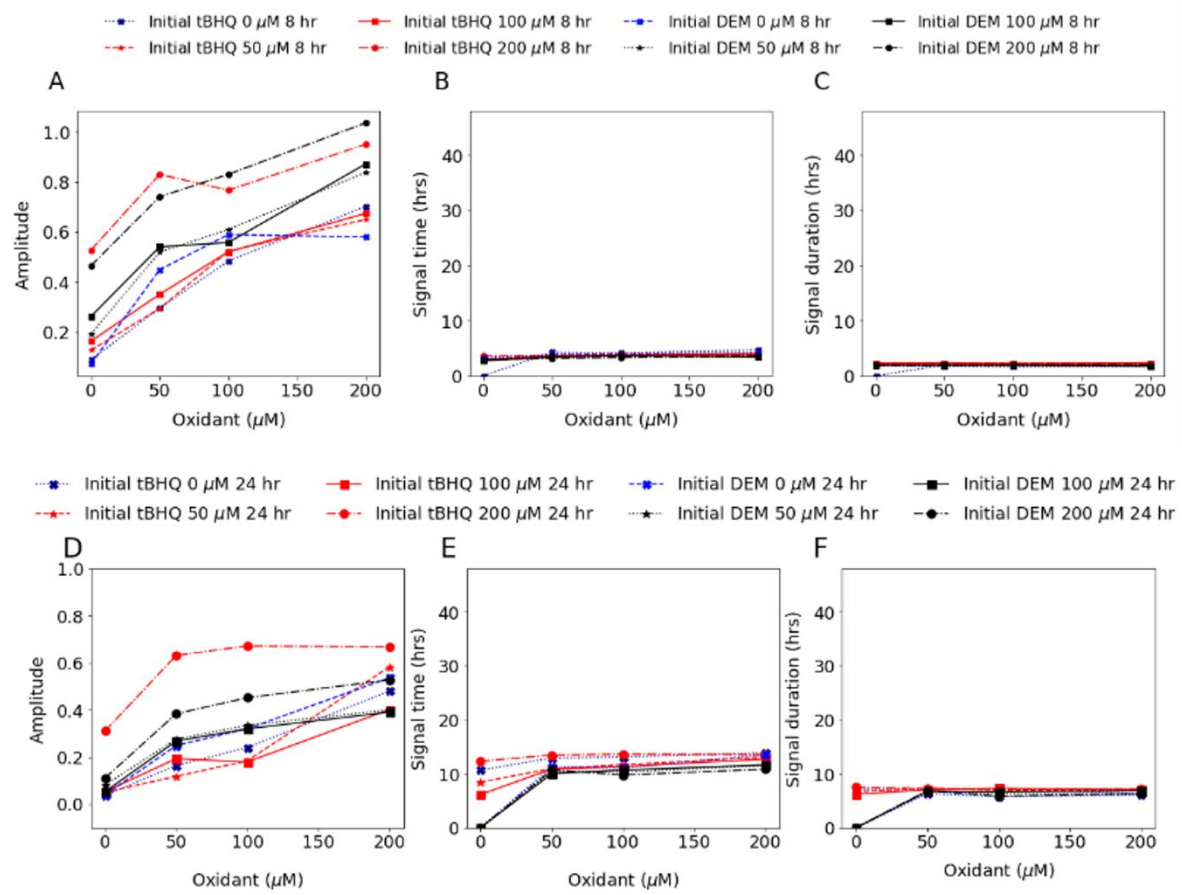

Figure 4.7: The associated signalling parameters of NRF2 following treatment with tBHQ and DEM after a second dose at 8 hrs and 24 hrs.

The area under the curve was calculated from the shaded portion of each signal profile. From these profiles, the signalling parameters of amplitude (A-D), time (C-E) and duration (D-F) were determined and plotted together for each exposure condition with an initial 8 hr and 24 hr exposure, respectively. To establish a baseline for each parameter, the black or red dotted line represents the initial 8-hr and 24-hr exposure to 0 μM (cross) tBHQ and DEM. This baseline was then compared to the subsequent doses of 50 μM (star), 100 μM (square), and 200 μM (circle) tBHQ and DEM, respectively.

.

4.2.3 Quantifying the effects of pre-exposure to 8 hrs and 24 hrs on the NRF2 pathway by different oxidants

We next wanted to determine the effect of the different pre-exposure times on the signalling parameters and compared the effect of pre-exposure to DEM for 8 hrs and then 24 hrs (Figure 4.8). Interestingly, the signal amplitude was greater for NRF2 activation when cells were pre-adapted for 8 hrs. However, pre-exposure for 24 hrs showed some increase in the signal

amplitude but an initial dose of 100 µM and a second dose of 200 µM resulted in a signal amplitude that was less than un-exposed cells (Figure 4.8A). When comparing the signal times and durations the 8 hr adaption period did show reduced times compared the 24 hr pre-exposure period (Figure 4.8B-C). These data suggest that the 24 hr adaption period dampens the response of NRF2 to DEM compared to a shorter 8 hr exposure period.

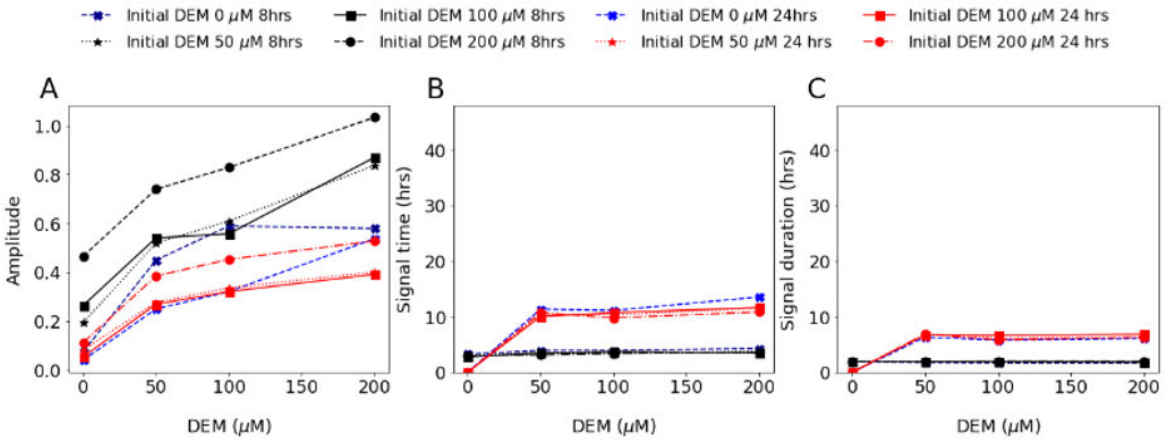

Figure 4.8: The associated signalling parameters of NRF2 following treatment with DEM after a second dose at 8 hrs and 24 hrs.

The area under the curve was calculated from the shaded portion of each signal profile . From these profiles, the signalling parameters of amplitude (A), time (B) and duration (C) were determined and plotted together for each exposure condition. To establish a baseline for each parameter, the black or red dotted line represents the initial 8 hrs and 24-hour exposure to 0 µM (cross) DEM. This baseline was then compared to the subsequent doses of 50 µM (star), 100 µM (square), and 200 µM (circle) DEM, respectively.

Another way to determine how the pre-exposure period affected NRF activity was to measure the production of an antioxidant protein, Srxn1, whose production is regulated by NRF2 (Soriano et al., 2008). Similar to NRF2, the production of Srxn1 was measured through live confocal fluorescence imaging following the same treatments and adaption periods with DEM and tBHQ, respectively. The 8 hr pre-exposure to DEM doubled Srxn1 production compared to naïve cells, and did not return to baseline when compared to lower Srxn1 production for the 24 hr pre-exposure period. A 24-hour adaption period only slightly increased Srxn1 production when compared to naïve cells (Figure 4.9A-D). Furthermore, these data suggested that regardless of the initial to secondary dosage of DEM, the amount of Srxn1 produced will be similar given the same adaption period.

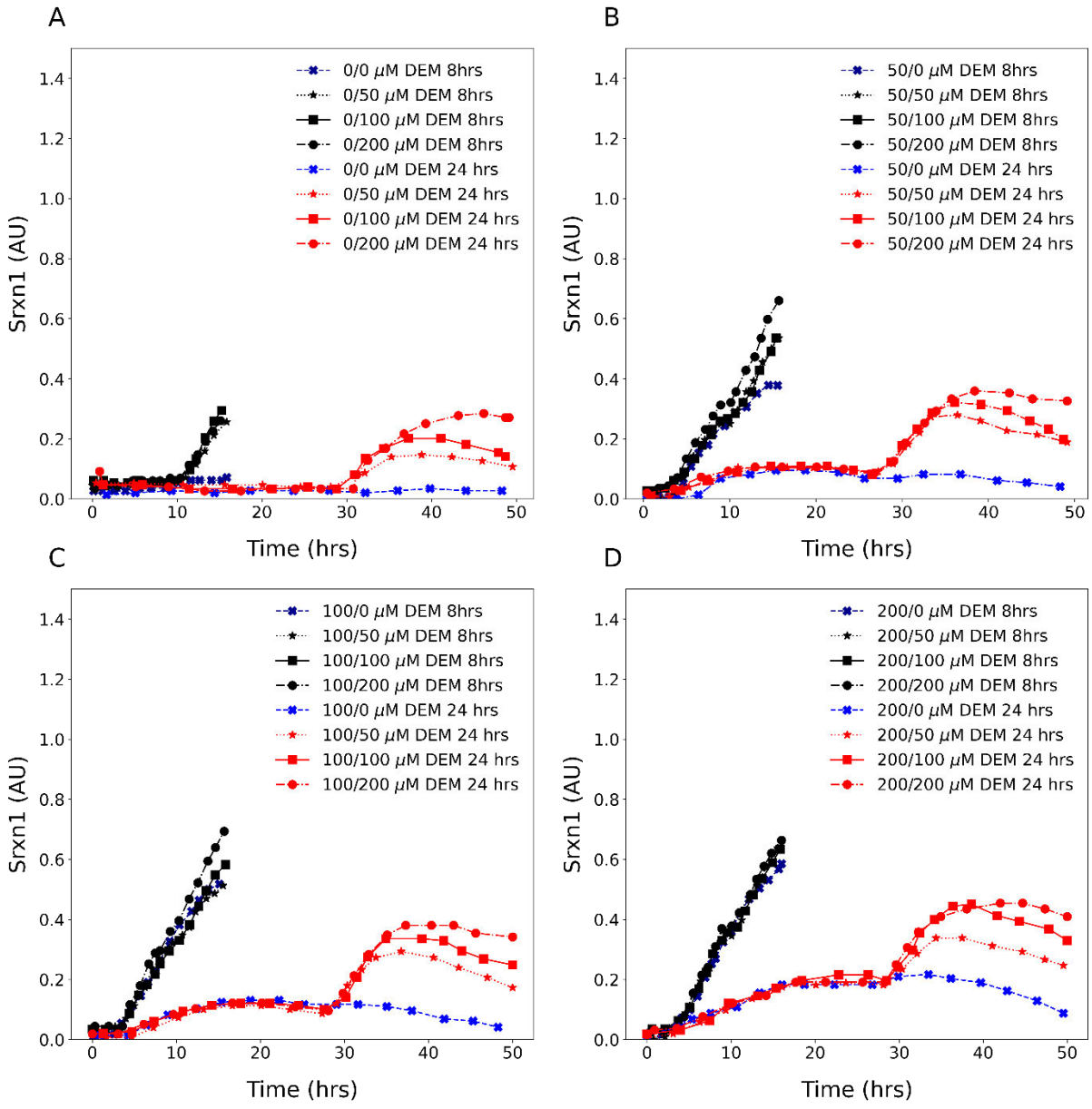

Figure 4.9: The associated signalling profiles of Srxn1 production following treatment with DEM after a second dose at 8 hrs and 24 hrs.

HepG2-reporter cells were GFP tagged at the Srx locus to monitor the expression dynamics of Srxn1 using live cell confocal imaging. The average intensity of Srxn1 in the cytoplasm was monitored after initially exposing cells to 0 μM (A) (cross), 50 μM (B) (star), 100 μM (C) (square), and 200 μM (circle) DEM 8 hrs (black) and 24 hrs (red) after the initial seeding (represented by the blue curves in each plot). Subsequently, a second dose of DEM was administered ranging from 0 μM (cross), 50 μM (star), 100 μM (square), and 200 μM (circle), resulting in four combinations of repeat exposure conditions. The AUC was calculated based on the shaded region of each curve.

To assess the effect of the pre-exposure periods to tBHQ, we compared the signalling parameters for 8 and 24 hrs. We also found that the resulting signal amplitudes were similar to naïve cells and only the 200 µM exposure for the 24 hr adaption, increased compared to naïve cells (Figure 4.10A). The signal times and durations for the 24 hr adaption period were longer than the 8 hr adaption period, which corresponded to the wider signalling profiles, similar to treatment with DEM (Figure 4.10C-D). We also assessed the effect of the pre-exposure periods on Srxn1 production. Here, an 8 hr pre-exposure period with tBHQ resulted in dose-increased production of Srxn1 The 24 hr adaption period also resulted in increased Srxn1 production when compared to naive cells (Figure 4.11A-C). Interestingly, the 200 µM initial and secondary 24 hr exposure did not increase the overall amount of Srxn1 produced (Figure 4.11D).

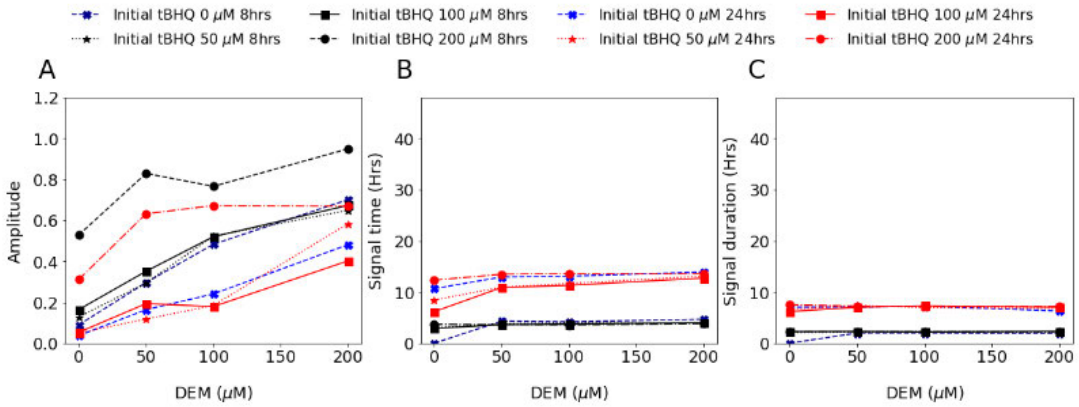

Figure 4.10: The associated signalling parameters of NRF2 following treatment with tBHQ after a second dose at 8 hrs and 24 hrs.

The area under the curve was calculated from the shaded portion of each signal profile (A). From these profiles, the signalling parameters of amplitude (B), time (C) and duration (D) were determined and plotted together for each exposure condition. To establish a baseline for each parameter, the black or red dotted line represents the initial 8 hrs and 24-hour exposure to 0 µM (cross) tBHQ. This baseline was then compared to the subsequent doses of 50 µM (star), 100 µM (square), and 200 µM (circle) tBHQ, respectively.

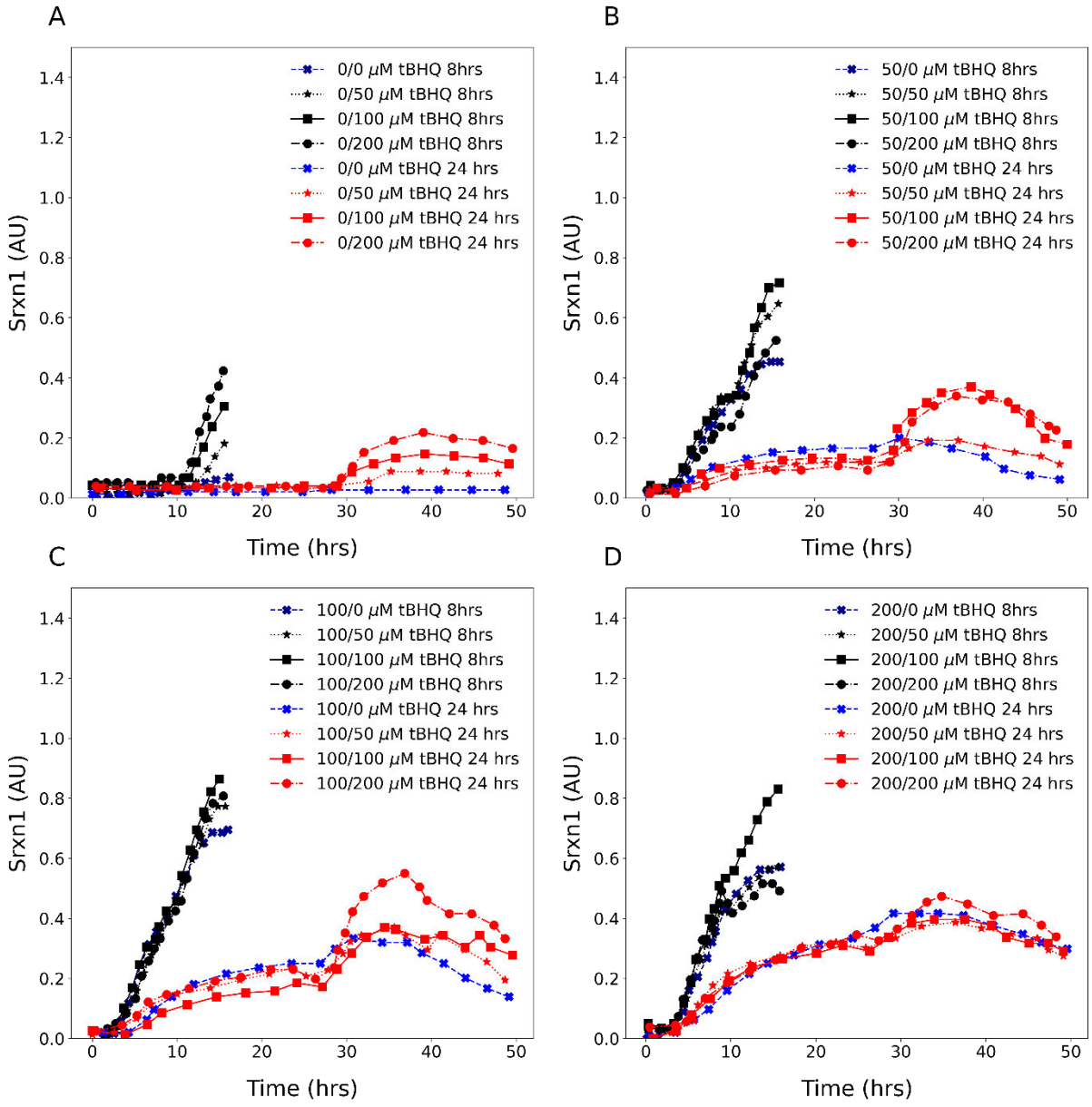

Figure 4.11: The associated signalling profiles of Srxn1 production following treatment with tBHQ after a second dose at 8 hrs and 24 hrs.

HepG2-reporter cells were GFP tagged on the Srx locus to monitor the expression dynamics of Srxn1 using live cell confocal imaging. The average intensity of Srxn1 in the cytoplasm was monitored after initially exposing cells to 0 μM (A) (cross), 50 μM (B) (star), 100 μM (C) (square), and 200 μM (D) (circle) DEM 8 hrs (black) and 24 hrs (red) after the initial seeding (represented by the blue curves in each plot. Subsequently, a second dose of DEM was administered ranging from 0 μM (cross), 50 μM (star), 100 μM (square), 200 μM (circle) resulting in four combinations of repeat exposure conditions. The AUC was calculated based on the shaded region of each curve.

4.3 Discussion

Cells experience constant exposure to environmental stressors, xenobiotics, and oxidative stress, leading to the development of cellular adaptive mechanisms (Davies, 1999). The NRF2/Keap1 pathway in mammalian cells plays a central role in the response to oxidative stress and dysregulation of the pathway associated with disease (Yamamoto et al., 2018). One survival strategy against toxic oxidative stress levels involves pre-exposing cells to a low dose of a toxin followed by a higher dose of a toxin, resulting in a priming effect (Davies, 1999). Similarly, cells pre-adapted to oxidative stress through hydrogen peroxide exposure show upregulated antioxidant proteins, enabling them to withstand higher oxidative stress levels . Assessing the efficacy of adaptation by utilising signal quantification parameters can enumerate this information from complex datasets.

Overall, repeated exposure to the different types of oxidants, DEM and tBHQ, did induce different responses to the NRF2 pathway. We observed that the pathway activation was concentration-dependent, where a 200 µM dose resulted in a larger difference in signal amplitude compared to naïve cells. The lower dosages of DEM and tBHQ had similar effects on the activation of NRF2. These data suggest that the NRF2 pathway responds to different oxidants in a similar way, unlike the fission yeast where different oxidants yielded unique signal outputs in the transcription factor Pap1 (Lind et al., 2024). Furthermore, priming the cells with DEM and tBHQ resulted similar Srxn1 production (Figure 4.9; Figure 4.11) while *S. pombe* cells had reduced transcriptional responses to pre-exposure to hydrogen peroxide (Spitz et al., 1987).

Another key consideration is the timing of repeated exposure to oxidative stress scenarios (Bischoff et al., 2019). The timing of the dosage is important for clinical drug administration to determine the effectiveness of treatment regimens (Tyson et al., 2020). To test this effect, the NRF2 pathway was dosed 8 hrs and 24 hrs after an initial dosage of DEM and tBHQ. Interestingly, the signal amplitude showed that an 8 hr adaption period elicited a stronger pathway response than a 24 hr. This result is consistent with the response of mammalian fibroblasts where a shorter initial exposure to hydrogen peroxide (~18 hrs) displayed maximal protection to oxidative stress compared to a 36 hr initial exposure (Davies, 1999).

In summary, these findings suggest that pre-adaptation to oxidative stress conditions does not always result in alterations to this signalling pathway and a saturation point at higher oxidant concentration will be reached. Moreover, shorter adaptation periods appear to increase the NRF2 pathway response while longer adaptions led to a dampened signal output.

4.4 Material and methods

4.4.1 Computational and statistical methods

Data obtained from Biscoff et al 2019 was digitised using plotdigitiser (https://plotdigitizer.com) and the signalling parameters calculated (Chapter 2.1). All computational analyses and statistical tests were carried out in Python (https://www.python.org/) using Jupyter notebooks with SciPy (https://scipy.org), Pandas (https://pandas.pydata.org) and Matplotlib (https://matplotlib.org/). All the relevant code and raw data for reproducing the figures are available in the github folder https://github.com/djl94/Chapter4_supp.git

Chapter 5

Optimising Experimental Approaches to Study Redox Signalling Dynamics

5.1 Introduction

In the previous chapters, the method optimisation and control experiments were omitted for brevity. These methods are described in greater detail so that the data can be replicated by other labs. We focused on several optimisation phases to quantify the Pap1 signalling pathway in fission yeast cells indicated by the tool icons in Figure 5.1.

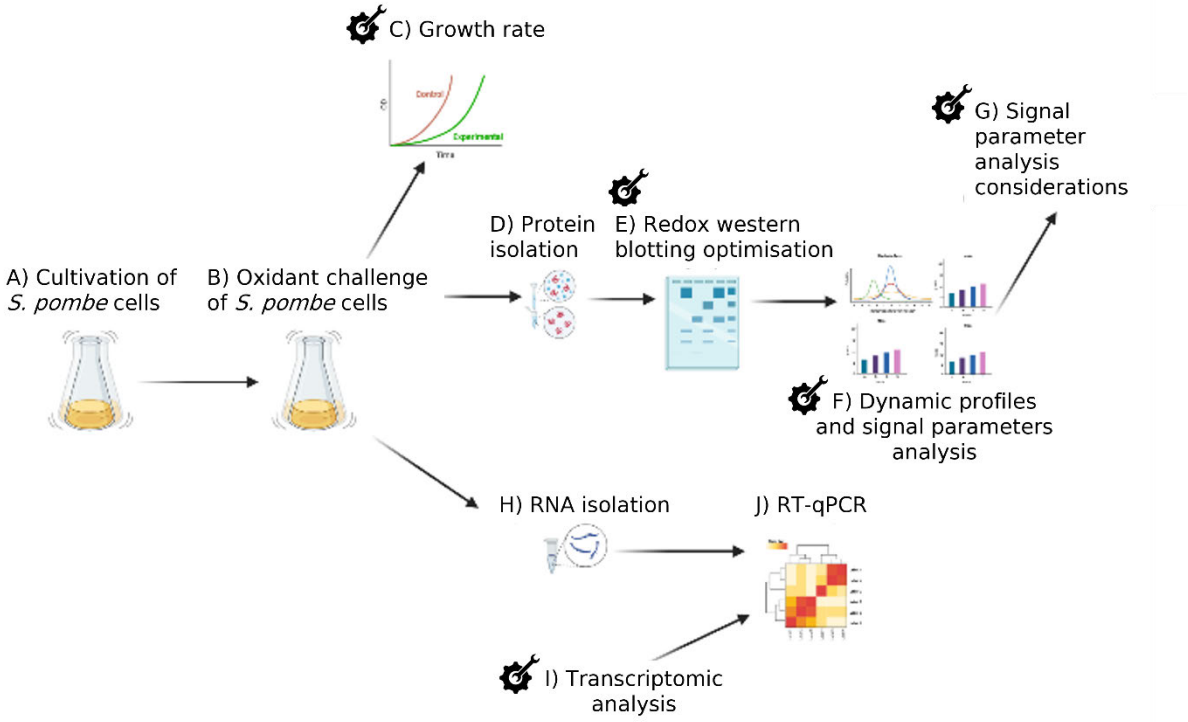

Figure 5.1: The optimisation of standard methodologies used to quantify redox signals. *S. pombe cells were cultured to early exponential phase and then exposed to different concentrations of hydrogen peroxide and tert-butylhydroperoxide (A, B). The effect of hydrogen peroxide on cell growth rates was also evaluated (C). To quantify redox signals, protein was extracted from the cells under different oxidative stress conditions (D). Redox western blotting was used to separate and quantify the oxidised and reduced isoforms of Pap1 (E). The dynamic changes in the oxidised and reduced isoforms of Pap1 were used to generate signal profiles from which the signal amplitude, time and duration could be calculated (F).*

Computational methods and different normalisation methods were used to analyse these dynamics profiles (G). Total mRNA was isolated from the cells to measure the effect of oxidants on Pap1-dependent gene expression (H). These genes were chosen from a transcriptomic dataset of S. pombe cells exposed to bolus concentrations of hydrogen peroxide (Chen et al. 2008) (I). RT-qPCR was then carried out on the selected genes (J) to investigate the relationship between the oxidant stimuli and redox signalling dynamics. The optimisation steps are indicated by the tool icon.

Initially, *S. pombe* cells were cultivated to early exponential phase and challenged with a range of hydrogen peroxide or tert-butyl hydroperoxide concentrations (Figure 5.1A-B) (Lee et al., 2008; Hu et al., 2022; Quinn et al., 2002). During our preliminary investigations, exposure to high concentrations of hydrogen peroxide resulted in sustained Pap1 oxidation beyond a 2-hr threshold following initial exposure. However, whether this sustained effect is influenced by the cell's doubling time is unclear. To address this, we considered the impact of these oxidants on the doubling time of *S. pombe* cells over a 2-hr time-course (Figure 5.1C). The cells were then harvested to collect protein or total mRNA and the oxidation state of Pap1 was determined by redox western blotting (Figure 5.1D, H). While western blotting is semi-quantitative certain considerations can be implemented to ensure the accuracy of the data (Ghosh et al., 2014; Pillai-Kastoori et al., 2020). These include maintaining a consistent protein concentration throughout the experiments and optimising the primary antibody-to-secondary antibody ratios to ensure that the protein of interest (Pap1) was detected within the linear fluorescence range (Figure 5.1E) (Murphy et al., 2013; Ghosh et al., 2014).

Once reliable data was obtained, the western blots could be analysed and plotted into dynamic curves from which the area under the curve and signalling parameters were calculated. It is worth noting that there were multiple ways to generate the dynamic profile. For instance, we could plot oxidised Pap1 over total Pap1 (which consists of Pap1 in its reduced form plus oxidised Pap1). Alternatively, we could divide oxidised Pap1 by DTT-reduced Pap1 to account for any complexes with Pap1 or divide oxidised Pap1 by the total protein for a specific sample (Figure 5.1F). Therefore, we systematically assessed whether the utilisation of these different normalization methods resulted in significant changes in the signal parameter values (Figure 5.1G).

An important feature of this study was to investigate the relationship between gene expression and signalling parameters in response to varying input stimuli. To achieve this, we identified genes regulated by Pap1. Microarray analysis of the fission yeast at different concentrations of hydrogen peroxide was previously undertaken by Chen et al. (2008), including analysis on mutant strains lacking *pap1*. This dataset consisted of >5000 genes of which over 700 genes displayed at least a 2-fold increase in gene expression. These genes were then categorised for further analysis to ultimately select a subset of genes associated to Pap1-regulation (Figure 5.1I-J). This chapter aims to provide detailed information on optimising western blotting methodologies for Pap1 dynamic profile quantification and the design and optimisation of an RT-qPCR assay. We aim to provide an accurate framework for quantifying any redox signal and highlight key experimental optimisations so that this work can be readily extended to other signalling systems.

5.2 Materials

Amino acids and reagents for general cultivation of *S. pombe* or *E. coli* were purchased from Merck/Sigma. PCR reagent, DreamTaq DNA polymerase, alkaline phosphatase, BCA protein assay kits, and Aminolink kits were obtained from Thermo Fisher Scientific (Johannesburg, South Africa). YeaStarTM RNA isolation kits, qPCR primers, the New England Biolabs cDNA synthesis kit, and qPCR master mixes were purchased from Inqaba Biotech (Pretoria, South Africa). Analytical-grade hydrogen peroxide was purchased from Labcare Supplies (Durban, South Africa) used within one month of opening. Primary anti-V5 Pk antibody (Lot #065M480IV, catalogue number V4014-100UG), Clarity^{TM} ECL substrate, TEMED, and ammonium persulfate were obtained from Bio-Rad (Durban, South Africa). FLAG-tag antibody (catalogue number F3165-2MG), anti-mouse (rabbit) IgG peroxidase antibody (Lot #106M4870V, catalogue number A9044-2ML), iodoacetamide, kanamycin, and Freund's adjuvant were products of Sigma. β-actin-HRP conjugated antibodies (catalogue number A3854) were obtained from Merck. The Pap1-pET28a(+) plasmid construct was produced by Genescript LTD (Hong Kong, China) and codon-optimized for protein expression in *E. coli*. Nickel affinity purification columns were purchased from Qiagen (Johannesburg, South Africa).

All other reagents for buffers and solutions were purchased from Merck/Sigma. The *S. pombe* strains used in this study were a gift from Elizabeth Veal (Newcastle University), while *E. coli* BL21 cells were lab stocks.

5.2.1 Preparation of culture medium

5.2.1.1 General yeast cultivation medium with amino acid supplements (YE5S)

YE5S contained yeast extract (0.5%), glucose (3%) and, depending on the genetic background of the *S. pombe* strains (Table 5.1) adenine, lysine, uracil and histidine, all to a final concentration of 225 mg/L and leucine to 250 mg/L if required (Nurse, 2001). Agar (2%) was added to YE5S for solid growth. All components were combined, autoclaved, and stored at 4°C.

Table 5.1: *S. pombe* strains and genotypes used in this study.

Strain name	Genotype	Source Reference
972	h-	Gift from Dr EA Veal
SB3	H–ade6-M216 pap1+(3Pk)::ura4+his7-366	Bozonet et al, 2005
SB4	H+ade6 pap1+(3Pk)::ura4+tpx1::ura4+his7-366	Bozonet et al, 2005
SB8	h–ade6 srx1::ura4+pap1+(3Pk)::ura4+his7-366	Bozonet et al, 2005
LT1	h-ade6-M216 leu1-32 ura4-D18 his7-366 srx1::ura4+ Flag-srx1:leu2+	This study

5.2.1.2 Edinburgh minimal medium (EMM) with supplements

Edinburgh minimal medium was made with the following reagents, potassium hydrogen phthalate (14.7 mM), di-sodium hydrogen orthophosphate (15.5 mM), ammonium chloride (93 mM), glucose (2%), in addition to amino acids at the final concentration of 225 mg/L, adenine, histidine, uracil, lysine, and leucine (250 mg/L). If required, agar (2%) for solid growth was added (Nurse, 2001). All components were combined to the desired volume and autoclaved then sterile salts, minerals and vitamin stocks were added. The salts stock contained magnesium chloride (0.26 M), calcium chloride (4.99 mM), potassium chloride (0.67 M), and di-sodium sulphate (14.1 mM). These chemicals were combined, autoclaved, and stored at 4°C. The mineral stock contained boric acid (80.9 mM), manganese sulphate (23.7 mM), zinc sulphate (13.9 mM), ferric chloride (7.4 mM), molybdic acid (2.47 mM), potassium iodide (6.02 mM), copper sulphate (1.6 mM), citric acid (47.6 mM). Chemicals were dissolved, filter sterilised (0.2 µm filter) and stored at 4°C (Nurse, 2001). The vitamin stock contained nicotinic

acid (81.2 mM), myo-inositol (55.5 mM), biotin (40.8 mM), and panthothenic acid (4.2 mM). These reagents were combined, filter sterilised (0.2 µm filter) and stored at 4°C (Nurse, 2001).

5.2.1.3 Luria Bertani (LB) medium (with kanamycin)

LB medium consisted of yeast extract (0.5%), tryptone powder (1%), sodium chloride (0.5%) and supplemented with kanamycin (50 µg/ml) if required. Agar (2%) was added for solid growth if needed (Lurias & Delbrock, 1943).

5.2.1.4 Nutrient-rich culture medium (SOC)

SOC medium was made with the following reagents: yeast extract (0.5%), tryptone powder (2%), glucose (20 mM), sodium chloride (10 mM), potassium chloride (2.5 mM) and magnesium chloride (10 mM).

5.2.2 Preparation of buffers and solutions

5.2.2.1 Ammonium persulfate solution (APS) (10%)

For SDS-PAGE electrophoresis, a fresh 10% APS solution was required and made by dissolving APS crystals into distilled water.

5.2.2.2 Acrylamide solution (30%)

A 30% acrylamide solution was prepared by mixing 29% acrylamide with 1% N, N' methylene-bisacrylamide in distilled water. The solution was filtered through Whatman filter paper (0.5 mm) and stored in an amber bottle at 4°C.

5.2.2.3 Bovine serum albumin (10%) solution for blocking nitrocellulose membranes

A BSA solution (10%) was made by dissolving BSA crystals (5 g) into 50 ml 1 x TBST buffer (Section 2.4.24) and stored at 4°C.

5.2.2.4 CTAB buffer

CTAB buffer was prepared by dissolving hexadecyltrimethylammonium bromide (2%) and polyvinylpyrrolidene (1%) in distilled water with Tris-HCl (100 mM, pH 8.0), EDTA (20 mM, pH 8.0) and sodium chloride (1.4 M).

5.2.2.5 Coomassie blue dye

Brilliant blue R-250 (0.125%) was dissolved in distilled water with methanol (50%) and acetic acid (10%).

5.2.2.6 Destain solution 1

Destain solution 1 was made by diluting methanol (50%) and acetic acid (10%) in distilled water.

5.2.2.7 Destain solution 2

Destain solution 2 was prepared by diluting methanol (5%) and acetic acid (7%) in distilled water.

5.2.2.8 Dithiothreitol (DTT) stock solution

DTT powder was dissolved into distilled water to a final concentration of 1 M. This solution was made fresh before use.

5.2.2.9 Extraction buffer

For DNA isolations, extraction buffer was made by combining Tris-HCl (200 mM, pH 8.0), EDTA (25 mM, pH 8.0) and sodium chloride (200 mM) with 0.2% SDS in distilled water.

5.2.2.10 Equilibration buffer for protein purification

Equilibration buffer consisted of imidazole (20 mM), sodium chloride (0.5 M), Tris (20 mM) and β-mercaptoethanol (1 mM).

5.2.2.11 Elution buffer for protein isolation from Ni-NTA columns

To a 1X PBS solution, an imidazole concentration gradient (20, 40, 60, 80, 100, 120, 150, 180 and 250 mM) was added together with 20% glycerol for storage at -20°C.

5.2.2.12 IAA buffer

Fresh IAA buffer was made before use by dissolving iodoacetamide (75 mM) in distilled water with Tris-HCl (100 mM, pH 8.0) and 1% SDS.

5.2.2.13 Isopropyl ß-D-1-thiogalactopyranoside (IPTG) stock solution

An IPTG stock solution (100 mM) was prepared by dissolving IPTG powder in distilled water, which was then filter sterilised (0.2 µm filter), aliquoted and stored at -20°C.

5.2.2.14 Kanamycin stock solution

A kanamycin stock (50 mg/ml) was made by dissolving kanamycin sulphate into distilled water which was filtered sterilised (0.2 µm filter) and stored at 4°C.

5.2.2.15 Loading buffer for DNA electrophoresis

Bromophenol blue (0.25%) was dissolved in distilled water with 30% glycerol, aliquoted and stored at -20°C.

5.2.2.16 3-(N-morpholino) propanesulfonic acid (MOPS) buffer for RNA electrophoresis

A 10X MOPS buffer solution was prepared by dissolving MOPS free acid (0.2 M), sodium acetate (0.05 M) and EDTA (0.01 M) in distilled water and adjusting the pH to 7.0. A 1X MOPS buffer was prepared by diluting 100 ml of 10X buffer into 900 ml of distilled water.

5.2.2.17 Phosphate buffered saline (PBS)

A 10 X PBS solution was prepared by dissolving sodium chloride (1.37 M), potassium chloride (27 mM), disodium phosphate (100 mM) and potassium dihydrogen phosphate (18 mM) in distilled water.

5.2.2.18 TE buffer

TE buffer was prepared by combining Tris-HCl (1 M) and EDTA (0.5 M) in distilled water and adjusting the pH to 8.0.

5.2.2.19 TAE buffer for DNA electrophoresis

A 50 X TAE buffer was prepared by dissolving Tris (2M) and EDTA (50 mM) in distilled water in combination with glacial acetic acid (1 M). The pH was then adjusted to 8.0. A 1X TAE solution was prepared by adding 10 ml of the 50X TAE to 990 ml of distilled water.

5.2.2.20 Tris lower buffer (SDS-PAGE resolving)

A resolving Tris buffer was prepared by dissolving Tris (3 M) in distilled water and adjusting the pH to 8.8 with the subsequent addition of SDS (0.8%).

5.2.2.21 Tris upper buffer (SDS-PAGE stacking)

The stacking Tris buffer consisted of Tris-HCl (0.5 M) adjusted to pH 6.8 with SDS (0.4%)

5.2.2.22 Transfer buffer

Transfer buffer was made by dissolving Tris (25 mM) and glycine (200 mM) in distilled water with methanol (10%) and SDS (0.8%).

5.2.2.23 Tris-buffered saline (TBS)

A 10X TBS solution was prepared by dissolving Tris (200 mM) with sodium chloride (1.5 M) in distilled water and adjusting the pH to 7.6.

5.2.2.24 Tris-buffered saline with Tween (TBST)

A TBST solution was prepared by diluting 100 ml of 10X TBS into 899 ml distilled water with 1 ml of Tween 20.

5.2.2.25 SDS loading dye (non-reducing)

A non-reducing SDS loading dye was prepared by dissolving bromophenol blue (0.005%), glycerol (10 %), and SDS (0.8 %) with Tris (500 mM) in distilled water and adjusting the pH to 6.7. The loading dye was stored at 4°C.

5.2.2.26 SDS-PAGE electrophoresis buffer

A 10X SDS-PAGE running buffer consisted of dissolving Tris (250 mM), glycine (192 mM) and SDS (1%) in distilled water. A 1X SDS-PAGE running solution was prepared by diluting 100 ml of the 10X stock into 900 ml of distilled water.

5.3 Methods

5.3.1 Cultivation and general husbandry of S. pombe

For long-term storage *S. pombe* strains (Table 5.1) were stored in 50% (v/v) glycerol at -80°C. Strains were then patched from the frozen stock onto YE5S plates and incubated at 30°C for three days. *S. pombe* cells were streaked to yield single colonies which were then patched weekly onto fresh YE5S plates. Unless stated otherwise, all experiments were carried out in Edinburgh minimal medium (EMM) by inoculating 10 ml of medium with patched cells and grown overnight (180 rpm, 30°C). The optical density (OD_{595}) of the overnight culture was measured by spectrometry and diluted to an OD_{595} of ~0.15 in fresh medium (Nurse, 2001; Petersen & Russell, 2022).

5.3.2 Challenging S. pombe cells to oxidants

For these experiments the protocol of Day et al (2012) was used to culture *S. pombe* cells to mid-log phase/OD~0.5 (50 ml) and the cells were exposed to 0.1–1 mM hydrogen peroxide. The culture (2 ml) was harvested at different time points over a 60–120-minute time course and added to ice-cold trichloroacetic acid (20%). Similarly, *S. pombe* cells were exposed

to 100 and 200 µM *tert*-butyl hydroperoxide (*t*-BOOH) and/or a combination of 70 and 100 µM hydrogen peroxide. For pre-treatment experiments, *S. pombe* cells were inoculated to OD_{595}~0.15 and cultured for 1 hr before the addition of 100 µM hydrogen peroxide. Then at OD_{595}~0.5, an additional 500 µM hydrogen peroxide was added and 2 ml of cultured collected over a 120-minute time period (Quinn et al., 2002). The cells were pelleted (2 500 x *g*, 5 min, 4°C) snap frozen in liquid nitrogen and stored at -80°C.

5.3.3 Determining the doubling rate and cell number sensitivity of S. pombe to hydrogen peroxide

S. pombe cells were cultured to an OD_{595} (0.4–0.5), and hydrogen peroxide ranging from 0.1-1 mM was added to the culture. OD_{595} readings were taken every 30 min for the first 3 hrs, and then at 3-hr intervals thereafter (Peterson & Russell., 2022). The following formula (1) was used to calculate the doubling time:

$$(1)\ \mu = \frac{\ln(2)}{k} \text{ where } k = \frac{\ln(OD_{T2} - OD_{T1})}{(T2 - T1)}$$

the final OD_{595} reading (OD_{T2}) was subtracted from the initial OD_{595} reading (OD_{T1}) and divided by the time elapsed (*T2* and *T1*) (Petersen & Russell, 2022). The cell number was determined by taking 1 ml of cell culture, which was serially diluted 10 000-fold over in PBS [137 mM NaCl, 2.7 mM KCl, 10 mM Na_2HPO_4, 1.8 mM KH_2PO_4] and 0.1 ml was then plated on EMM medium and incubated at 30°C until the formation of single colonies.

5.3.4 Genomic DNA isolation

S. pombe strains were cultured overnight in YE5S medium, and 1 ml of cells were harvested by pelleting (14 000 x *g*, 5 min, 21°C). The pellet was resuspended in extraction buffer (400 µL), and the cells were lysed by bead-beating (0.5 mm glass beads) at (13 000 x *g*, 15 sec, 21°C), then placed on ice for 1 minute. This step was repeated. RNase A (10 µg/ml) was added to the lysate, which was incubated at 80°C for 2 min. CTAB buffer (400 µL) and chloroform: isoamyl alcohol (24:1) with 5% phenol was added to the lysate and mixed gently. The DNA containing the aqueous layer was separated by centrifugation (14 000 x *g*, 10 min, 21°C) and transferred to a fresh microfuge tube containing ice-cold propan-2-ol (600 µl). The DNA was allowed to precipitate overnight at -20°C and then pelleted by centrifugation (13 000 x *g*, 10 min, 4°C). The pellet was washed twice with 70% ethanol (500 µl), dried for 30 min, and resuspended in 50 µl of TE buffer (Kang et al., 1998). DNA purity and concentration were determined by spectrometry at (A_{260}/A_{280} and A_{260}/A_{230}). The quality of DNA was assessed by

agarose gel electrophoresis (80 V, 1 hr) and visualised with ethidium bromide (5 µg/ml) under UV light.

5.3.5 Collection of S. pombe samples for RNA isolation

After exposure to hydrogen peroxide concentrations (0.1-1 mM) *S. pombe* cells (2 ml) were harvested and pelleted (500 x *g*, 3 min, 21°C), immediately frozen in liquid nitrogen and stored at –20°C. Total RNA was isolated using a YeaStar^{TM} RNA kit. RNA purity and concentration was determined by spectrometry at (A_{260}/A_{280} and A_{260}/A_{230}). The quality of RNA was assessed by denaturing 1% agarose electrophoresis (80 V, 1 hr) using 1X MOPS buffer (200 mM MOPS, 50 mM sodium acetate, 10 mM EDTA, 37% formaldehyde) and visualised with ethidium bromide (5 µg/ml).

5.3.6 cDNA synthesis and qPCR of Pap1 regulated genes

Isolated RNA was then converted to cDNA by a ProtoScript II first strand cDNA synthesis Kit using 1 µg of RNA template with an oligo d(T)23 primer mix. Quantification of cDNA was analysed by real-time qPCR on Quantstudio^{TM} 5 real-time PCR system with a Luna universal qPCR master mix and the fold-change in expression was calculated using the $\Delta\Delta C_t$ method (Rao *et al*., 2013; Bustin *et al*., 2009). The primers for RT-qPCR were designed using IDT software (https://eu.idtdna.com) to check for primer internal structures, annealing temperatures and gene product specificity. Primers used in this study are listed in Table 5.2 where all primers used an annealing temperature of 60°C. The qPCR products were checked by agarose gel (2%) electrophoresis.

Table 5.2: List of primers used for RT-qPCR assay.

The annealing temperature for all primers was 60°C.

Primer	Sequence	Expected product size (bp)
ctt1 forward	AGAAACCTGGACAGCAAGATAA	80
ctt1 reverse	GCGTTCACGTACAGGAGATATAG	
srx1 forward	GACTACGTGCTCACGATGAA	86
srx1 reverse	CAGATACAGGCGTAGAGTGTTAG	
trr1 forward	CCATACTGCAGCCATCTATCTC	91
trr1 reverse	CTGACCACCAGCAGCAATA	
atf1 forward	GGTAAACCGCCTGTTGTAAATG	97
atf1 reverse	GAACCTGGGAGAGTAAGCATAAC	
gpd3 forward	GTGTCATCATCTCTGCTCCTTC	105
gpd3 reverse	GCAAGAGGCGTTGGAGATAA	
act1 forward	ACGTCGCTTTGGACTTTGA	109
act1 reverse	CGCTCGTTTCCGATAGTGATAA	

5.3.7 Protein isolation for Western blot analysis

Total protein lysate was prepared according to the protocol of Day et al., (2014). Cell sample pellets were thawed on ice and resuspended in 10% TCA (200 µl), into screw-cap tubes and 0.5 mm glass beads (750 µl) was added. The cells were lysed by bead-beating for 15 seconds, placed on ice for 1 minute, and the process was repeated. An additional 10% TCA (500 µl) was added and the tubes vortexed briefly. The lysate was separated from the beads by piercing the screw-cap tubes with a heated needle, and the tube was secured into a sterile 1.5 ml tube. The screw-cap tube containing the beads and lysate was placed into a 1.5 ml tube and together were secured into a 50 ml Falcon tube and centrifuged (2 000 x g, 30 seconds, 21°C) to separate the lysate from the beads. The protein was pelleted by centrifugation (10 000 x *g*, 10 min, 4°C), the supernatant was removed, and the pellet was washed three times with acetone. Pellets were air-dried and then resuspended in freshly prepared IAA buffer (1.4% iodoacetamide, 100 mM Tris-HCl, 1% SDS, pH 8.0) and incubated at 25°C for 20 min for alkylation. The samples were centrifuged (13 000 x *g*, 3 min, 21°C), and the supernatant was pipetted into a fresh microfuge tube. The protein concentration was measured using a Pierce BCA protein assay kit, following the manufacturer's instructions. The protein samples were treated with alkaline phosphatase (1 U/µl) for 1 hr at 37°C for Pap1 dephosphorylation. A total

of 30 µg of protein was loaded onto each gel lane across all western blotting experiments to ensure equal protein loading.

5.3.8 SDS-PAGE electrophoresis

For SDS-PAGE electrophoresis a resolving gel was prepared by combining 30% acrylamide, with Tris lower buffer, 10% APS and TEMED and a stacking gel was prepared with 30% acrylamide with Tris upper buffer, 10% APS and TEMED. Gels for Pap1 and Srx1 separation were made to 8% and 15% (Table 5.3) respectively.

Table 5.3: Preparation of resolving and stacking solution for an 8% and 15% SDS-PAGE gel.

Reagent	8%		15%	
	Resolving (ml)	**Stacking (ml)**	**Resolving (ml)**	**Stacking (ml)**
30% acrylamide	4	0.65	8	0.65
Tris lower buffer	3.75	-	4	-
Tris upper buffer	-	1.25	-	1.25
Distilled water	7.25	3.05	3.7	3.05
APS (10%)	0.1	0.05	0.16	0.05
TEMED	0.03	0.001	0.016	0.001

Protein samples were prepared by adding 4X SDS loading dye (10 µl) and boiled at 100°C for 5 min cooled to 4°C before electrophoresis at (200 V, 45 min) in 1X SDS tank buffer. For a reduced Pap1 control, DTT (2 µl) was added to the samples and run on a separate gel under the same electrophoresis conditions.

5.3.9 Protein transfer to nitrocellulose membrane

After SDS-PAGE electrophoresis, the gel was placed underneath a nitrocellulose membrane (0.2 µm) and sandwiched between transfer stacks (Bio-Rad). The protein was allowed to transfer for 3 hrs (200 V) in an ice-cold transfer buffer with an icepack that was changed after 1.5 hrs to keep the buffer cold. Alternatively, a semi-dry transfer was also done according to the 30-minute standard protocol of Bio-Rad Trans-Blot Semi-Dry Transfer Cell. Transfer efficiency to nitrocellulose was checked by staining with Ponceau S (0.1%). Additionally, effective gel transfer was checked by staining the gel post-transfer with Coomassie blue (50 ml) overnight (21°C, overnight) followed by destaining with Destain solution 1 (50 ml) followed by Destain solution 2 (50 ml).

5.3.10 Optimising the primary-to-secondary antibody ratio for Pap1 antibodies.

We developed a dot blot assay to ensure that Pap1 bands obtained from our assays were within the linear range of our imaging system. Three protein concentrations were dotted onto nitrocellulose membrane (0.2 µm) in the range of (20-40 µg). The membrane was then blocked with 10% BSA and incubated with anti-v5-pk antibodies (0.25-1 µg/ml) overnight at 4°C with gentle agitation. The membranes were washed with TBST four times and then incubated with an anti-mouse secondary antibody with dilutions ranging from 1:25 000–1:120 000. The blots were washed with TBST four times, developed using ECL substrate (Bio-Rad) and then imaged using the G-BOX Chemi-XR Gene*Sys* imaging system. Densitometry (ImageJ) was used to quantify the blots which were then plotted to determine the linear detection range and oxidation pattern of Pap1 and Srx1 expression.

5.3.11 Western blot development for Pap1 and Srx1

Following protein transfer, the nitrocellulose membrane was blocked with 10% BSA (21°C, 30 min, 50 rpm) and then incubated overnight with primary anti-v5-pk antibodies (0.5 µg/ml) (4°C, overnight, 50 rpm) for Pap1 and with anti-FLAG antibodies for Srx1. The membrane was washed with TBST four times with 5-minute incubations and then incubated with anti-mouse secondary antibody (1:20 000) (21°C, 1 h, 50 rpm). The membrane was washed with TSBT four times, incubated with ECL substrate (Bio-Rad) and imaged using the G-BOX Chemi-XR Gene*Sys* imaging system.

5.3.12 ImageJ analysis and signal quantification of redox western blots

Using the ImageJ analysis software (https://imagej.nih.gov/ij), the band intensity of the reduced and oxidised bands was measured separately to give $Pap1_{red}$ and $Pap1_{ox}$ and then added together for $Pap1_{total}$. To calculate the fractional Pap1 activation, $Pap1_{ox}$ was divided by $Pap1_{total,}$ which could be plotted against time (t) to generate dynamic signalling profiles. Alternatively, fractional Pap1 activation was determined by dividing Pap1 by DTT-reduced Pap1 by (total Pap1 protein). From these profiles, the area under the curve (X_i), and the signalling parameters could be calculated. Signalling time (τ), duration (θ) and amplitude (S_i) were calculated as described by relevant equations described in chapter 2.

5.3.13 Computational and statistical methods

All computational analyses and *t*-tests were carried out in Python (https://www.python.org/) using Jupyter notebooks with SciPy (https://scipy.org), Pandas (https://pandas.pydata.org), and matplotlib (https://matplotlib.org/). The relevant code, raw data files can be found on GitHub (https://github.com/djl94/Chapter5_supp.git). The *S. pombe* transcriptomic datasets from (Chen et al., 2008) was represented by heatmaps using python seaborn packages. RT-qPCR primers were designed using IDT primer design software (https://eu.idtdna.com). Figure images were generated in Biorender (https://www.biorender.com/).

5.3.14 Competent cell preparation of E. coli BL21 cells for transformation with Pap1-pET28a(+)

E. coli BL21 cells were inoculated overnight into LB medium (200 rpm, 37°C) and an aliquot of these cells was diluted into fresh medium to an OD_{600}~0.1 and allowed to grow until OD_{600}~0.4 (150 rpm, 37°C). The cells were placed on ice for 10 min pelleted, (4 500 x *g*, 10 min, 4°C) and the pellet was resuspended in 10 ml ice-cold calcium chloride (0.1 M) and subsequently centrifuged (4 500 x g, 10 min, 4°C). The pellet was resuspended in 2 ml of ice-cold calcium chloride and left of ice for at least 30 min before transformation with Pap1-pET28a(+).

The Pap1-pET28a(+) clones were made to 0.04 µg/µl in distilled water. Competent cells (20 µl) were combined with pET28a clones (2.5 µl) to a final concentration of 100 ng plasmid DNA and incubated on ice (30 min, 4°C). The mixture was heat shocked (42°C, 90 seconds) and quickly cooled on ice (4°C, 2 min). Pre-warmed SOC medium (80 µl) was added to the transformation mixture and the mixture was incubated (37°C, 1 h, 150 rpm). The transformation mixture (50 µl) was spread plated onto LB plates containing kanamycin (50 µg/ml) and grown until the formation of single colonies at 37°C. A single colony was selected and cultured in LB medium containing kanamycin (50 µg/ml) (37°C, 200 rpm, overnight) and 1 ml samples were collected to make 15% glycerol stock solutions for long-term storage at -80°C. As controls, the viability of competent cells was checked by plating onto LB agar without kanamycin, and the activity of kanamycin was checked by plating competent cells without the plasmid on kanamycin plates. Plasmid DNA was isolated using a GeneJET Plasmid Miniprep Kit (ThermoFisher) and the Pap1 insert was amplified using T7 promoter sequencing primers.

5.3.15 Expression of Pap1 in E. coli BL21 cells

E. coli cells containing Pap1-pET28a(+) were cultured in LB medium (37°C, overnight, 200 rpm) with kanamycin (50 µg/ml) from a single colony on an LB agar plate. The following morning the cells were pelleted (1 500 x g, 5 min, 21°C) and resuspended in LB medium (50 ml) and grown (37°C, 1 h, 150 rpm) before the addition of IPTG (0.5 M) to begin protein induction. The cells were then pelleted (12 000 x *g*, 10 min, 4°C) and stored at –20°C for further use. Samples at 1 h intervals were taken to determine the optimum induction time for Pap1.

5.3.16 Nickle affinity purification

After induction the pellets were resuspended in 10 volumes of cold 1X PBS with AEBSF (0.2 mM) and PMSF (1 mM). The cells were sonicated for 1 minute with 30 second intervals on ice using a VirSonic 60 Ultrasonic Cell Disrupter (8 W) and this was repeated five times. The cell suspension was centrifuged (12 000 x *g*, 10 min, 4°C) and the supernatant transferred to a prepared Ni-NTA purification column (Bio-Rad).

The Ni-NTA column was loaded with Ni-NTA resin (2 ml) and equilibration buffer (section 5.2.2.10) and allowed to flow-through the column. The crude cell suspension was incubated on the column overnight at 4°C on a Revolver TM 360 sample mixer. The unbound faction was collected as flow-through, and the column was washed with two columns (3 ml) of 1X PBS buffer. To determine the optimal concentration of imidazole required to elute Pap1, the column was washed with a concentration gradient of imidazole ranging from 20 mM to 250 mM. Samples of (1 ml) were collected and analysed on SDS-PAGE to visualise the elution of Pap1. The resin was cleaned with 0.5 M sodium hydroxide (30 min, 21°C), and stored in 30% ethanol (2 ml) at 4°C.

5.3.17 Protein concentration and buffer exchange

The pooled Pap1 samples were buffer exchanged into PBS using dialysis tubing to remove imidazole and concentrated using PEG 20 000. The concentration of purified Pap1 protein was determined using a BCA assay with a standard curve generated using bovine serum albumin (BSA) in PBS buffer.

5.3.18 Preparation of native Pap1 antibodies

5.3.18.1 Chicken immunization

Two hens were immunised with purified Pap1 protein (50 µg/ml, 1 ml) mixed with an equal volume of Freund's complete adjuvant and received booster shots with Freund's incomplete adjuvant at 2, 4, and 6 weeks. Eggs were collected from the hens before immunisation and for 16 weeks after the first immunisation and stored at 4°C. Ethics permission was obtained from the UKZN animal ethics committee (ethics number: 037/15/Animal).

5.3.18.2 IgY isolation

Isolation of IgY from the egg yolks was carried out according to Goldring and Coetzer (2003). In brief, the egg yolk was rinsed under gentle running water to remove albumin, and the yolk sac was punctured to collect the yolk in a measuring cylinder. Two volumes of 1X PBS buffer with 0.002% sodium azide were added and mixed thoroughly. The solution was transferred to a glass beaker, and PEG 6 000 (3.5%) was added until completely dissolved. The solution was filtered through Whatman filter paper (0.5 mm) into a fresh measuring cylinder and transferred to a clean glass beaker. Additional PEG 6 000 (12%) was added, dissolved, and centrifuged (12 000 x *g*, 10 min, 21°C). The pellet was resuspended in the initial yolk volume with 1X PBS, and PEG 6 000 (12%) was added, dissolved, and centrifuged (12 000 x *g*, 10 min, 21°C). The pellet was resuspended in 1/6 of the yolk volume in 1X PBS containing 0.1% sodium azide. Isolated IgY was stored at 4°C.

5.3.19 Purification of polyclonal anti-Pap1 antibodies

Before the isolation of polyclonal antibodies, purified Pap1 protein (5 mg) was coupled to an AminoLink^{TM} column (ThermoFisher) according to manufactures instructions. The column was then washed with 6 volumes of 1X PBS buffer. Next, the isolated IgY was diluted with an equal volume of 1X PBS and circulated over the prepared column (overnight, 21°C). The crude IgY was removed, and the column washed with 10 volumes of 1X PBS and the bound IgY, specific to Pap1, was eluted by lowering the pH to 3.0 and collected as 950 µl fractions in microfuge tubes containing neutralisation buffer (1M Tris-HCl, pH 9.0). The concentration of IgY was determined at A_{280} and calculated according to the IgY extinction coefficient ($\varepsilon_{280nm}^{1\ mg/ml} = 1.25$) (Goldring & Coetzer., 2003).

5.4 Results

5.4.1 The growth rate and CFU/ml of S. pombe cells are altered following treatment with hydrogen peroxide.

At low hydrogen peroxide concentrations (<200 µM) the Pap1 activation/deactivation cycle is complete in 60 min; therefore, most studies use this time course (Nakamura et al., 2005; Toone et al., 1998). However, few studies track the full oxidation cycle of Pap1 at higher doses of hydrogen peroxide (Domènech et al., 2018). In our pilot experiments, we observed that Pap1 oxidation was complete by 60 min when the cells were exposed to low concentrations of hydrogen peroxide but sustained for longer in cells exposed to higher concentrations of hydrogen peroxide. However, tracking Pap1 oxidation beyond 60 min may have introduced a confounding factor because *S. pombe* cells have a doubling time of 2 hrs in rich medium and 3 hrs in minimal medium.

To determine the doubling time of *S. pombe* cells we obtained growth curve profiles following hydrogen peroxide treatment in the range of 0.1-1 mM (Figure 5.2A). Our results showed that adding 100 and 200 µM hydrogen peroxide did significantly increase the doubling time of *S. pombe* cells, making a time course longer than 60 min unsuitable for analysis at lower hydrogen peroxide concentrations (Figure 5.2B). However, exposing the cells to higher concentrations (500 µM and 1000 µM) significantly increased the doubling time to over 7 hrs compared to 3 hrs in untreated cells (Figure 5.2B). Therefore, a two-hr tracking period was well within the doubling time of *S. pombe* cells and was suitable for tracking Pap1 oxidation. We also tested whether there was a significant increase in colony-forming units (CFU/ml) within two hrs after hydrogen peroxide treatment, but the cell number only substantially increased after 5 hrs (Figure 5.2), and it was within the normal range of 1-5 x 10^7 cells.

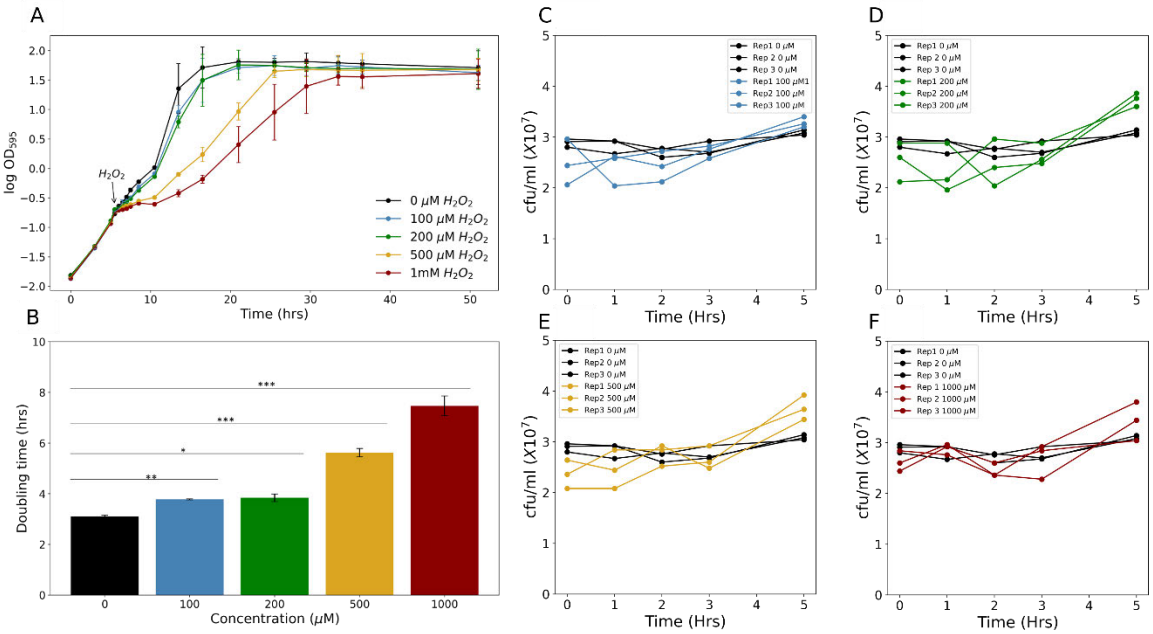

Figure 5.2: The growth curves, doubling time and survival of *S. pombe* cells after bolus addition of hydrogen peroxide (0.1-1 mM).

*The log increase in OD_{595} of S. pombe cells after adding bolus concentrations of hydrogen peroxide was determined over 52 hrs in minimal medium (A) (n=3). The doubling times of the cells were then calculated and compared to the untreated cells (B). The effect of hydrogen peroxide on the doubling time was assessed using a two-tailed t-test with statistical significance denoted as *p<0.01, **p<0.001, ***p<0.0001 (n=3). Cells were treated with 0, 100 (C), 200 (D), 500 (E) or 1000 (F) μM hydrogen peroxide and the CFU/ml was determined by collecting cell samples every hour over a five hour period and plating onto YE5S medium. The independent replications for each experiment is shown on the plots for the 100 (blue lines), 200 (green lines), 500 (yellow lines) and 1000 (red lines) μM hydrogen treatments together with the no-hydrogen peroxide control (black lines).*

5.4.2 Optimisation of western blotting technique for redox quantification

Previous studies have shown that inappropriate quantification can skew western blot analysis (Mishra et al., 2017; Pillai-Kastoori et al., 2020). However, there were several ways in which we attempted to overcome these limitations. First, ensuring that equal protein concentrations were loaded in each lane across all blots gave us confidence that we were comparing the same protein levels across our experiments (standard curve Figure S.24). Second, we adjusted the primary antibody and secondary antibody combinations was as well as at different protein quantities to determine the linear detection range for the assay. The linear

range of *S. pombe* protein lysate detection was determined by densitometric analysis of dot blots (Figure 5.3A-E) with 20-30 µg/ml of total protein visualised with a primary antibody concentration of 0.5-0.75 µg/ml to a secondary antibody dilution of 1:50, 000-1:80, 000 (Figure 5.3F-J). We selected 30 µg/ml of total protein for our experiments, 0.5 µg/ml primary pk antibody and a 1:50 000 dilution of secondary antibody.

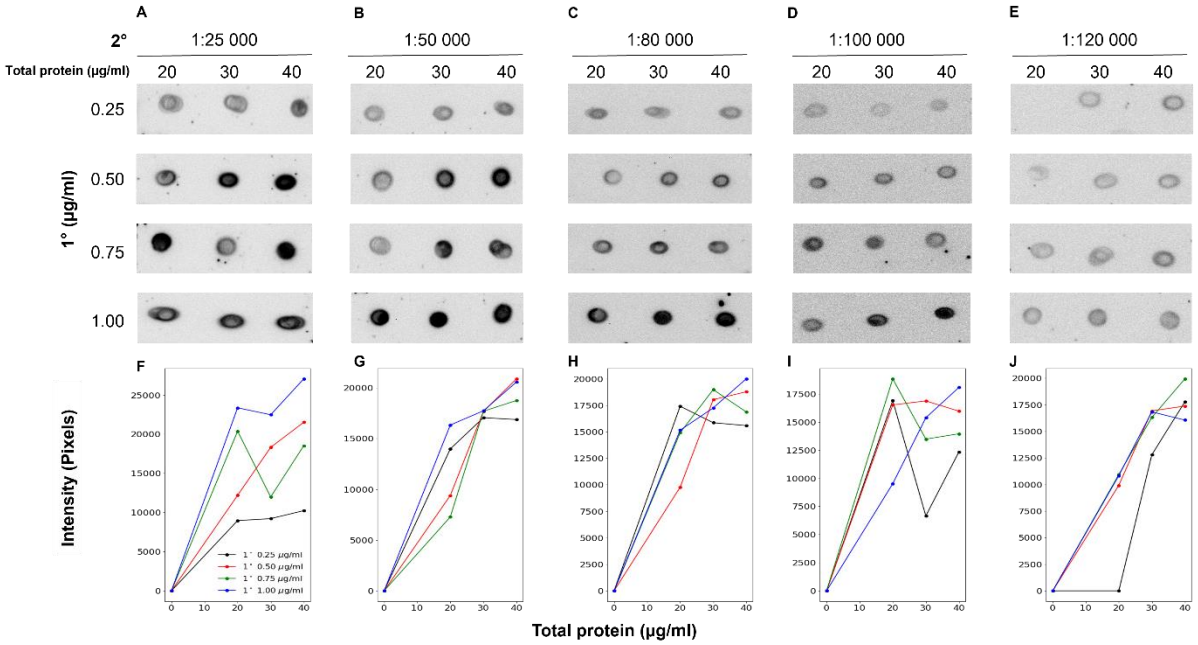

Figure 5.3: Enhancing the α-pk antibody to secondary antibody against *S. pombe* strain SB3 cell lysate to determine the linear detection range for western blotting experiments. *Protein lysate (20-40 µg/ml) was dotted onto nitrocellulose membrane and incubated with various concentrations of (1°) α-pk antibody (0.25-1 µg/ml) against several dilutions of secondary (2°) anti-mouse IgG peroxidase antibody (1:25 000-1:120 000). The blots were visualized using ECL on a G-BOX Chemi-XR5 GeneSys imaging system (A-E). Densitometry was used to quantify the blots to determine the linear range of protein detection (F-J).*

5.4.3 Analytical and practical considerations for signal parameter quantification

The signalling parameters of amplitude, time and duration were calculated from Western blotting data. Specific equations used for these calculations are detailed in the introduction of (Chapter 2.2). The signalling parameters offer insights into the characteristics of signal profiles and are elaborated in the introductions of Chapter 2.2, with additional information available in Supplementary Figure S.1. (Heinrich et al., 2002; Pillay et al., 2016).

We previously outlined experimental optimisations for our western blots including protein loading optimisation and primary to secondary antibody ratio optimisations (section 5.4.2). In addition to these considerations, several analytical factors were considered to effectively generate signalling profiles from western blotting data. First, while dynamic datasets have been published, we aimed to assess whether signalling parameters could be influenced by experiments that lacked careful optimisation. Second, in cases where blots were saturated, we examined whether this saturation effect would impact signal quantification. Third, various methods for data normalization, including the use of a total protein control or a DTT-reduced control, were also explored in this section.

To evaluate the benefits of optimising these parameters on Pap1 signal quantification, we compared the optimised conditions to detect Pap1 with a preliminary Pap1 oxidation dataset. This initial dataset lacked optimisation for consistent protein concentrations across the experiments, as well as for primary and secondary antibody concentrations and combinations. Our findings revealed significant differences in most of the signalling parameters between the two datasets. Specifically, the non-optimized dataset tended to overestimate signal amplitude (Figure 5.4A), while signal time and duration were underestimated compared to the optimised dataset (Figure 5.4B-C). These results show that optimising western blots for signal quantification processes does yield significant differences to the signalling parameters and these experimental conditions should be considered before quantifying redox signalling profiles.

A

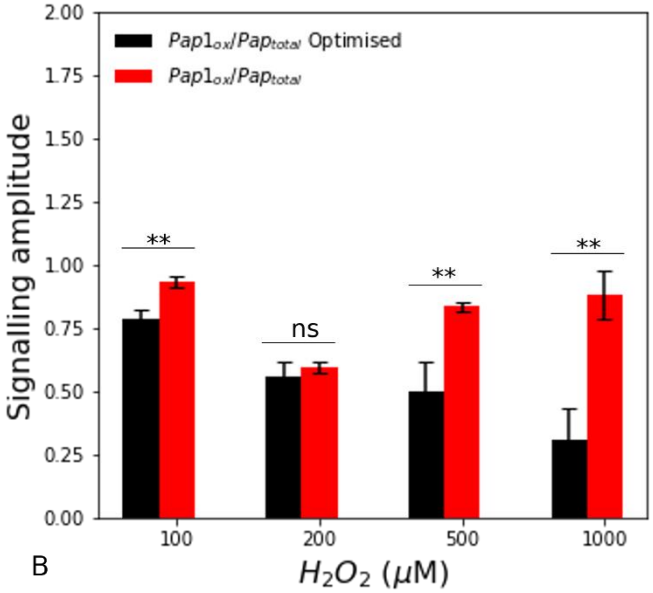
Pap1ox/Paptotal Optimised
Pap1ox/Paptotal
Signalling amplitude
2.00
1.75
1.50
1.25
1.00
0.75
0.50
0.25
0.00
**
ns
**
**
100
200
500
1000
H2O2 (μM)

B

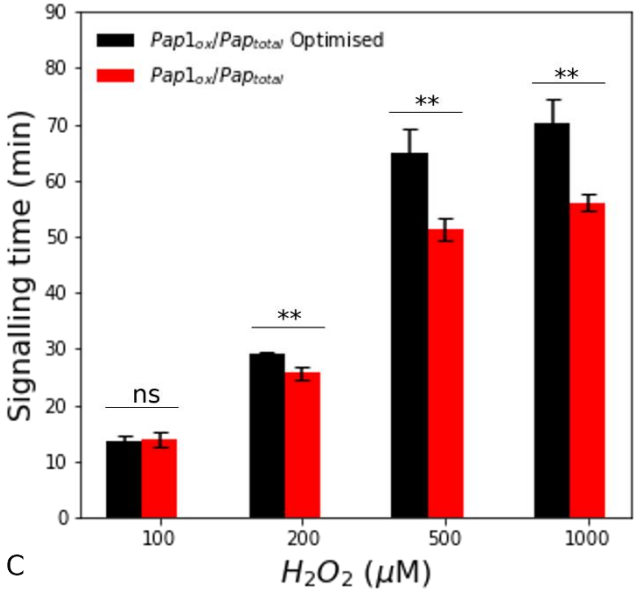
Pap1ox/Paptotal Optimised
Pap1ox/Paptotal
Signalling time (min)
90
80
70
60
50
40
30
20
10
0
ns
**
**
**
100
200
500
1000
H2O2 (μM)

C

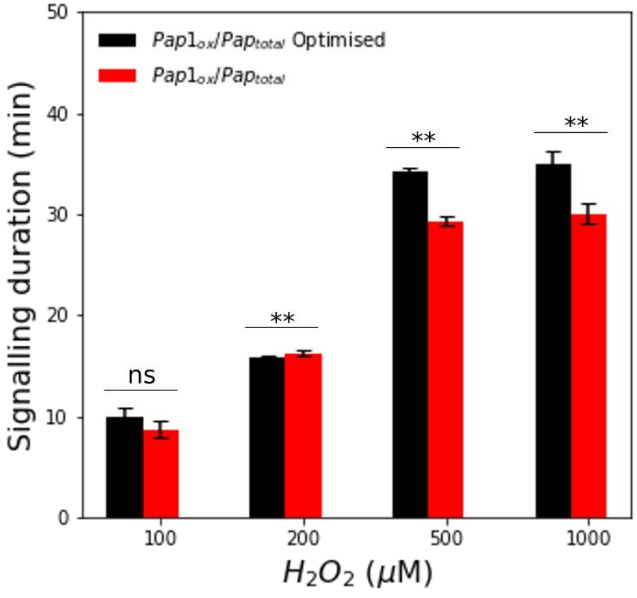
Pap1ox/Paptotal Optimised
Pap1ox/Paptotal
Signalling duration (min)
50
40
30
20
10
0
ns
**
**
**
100
200
500
1000
H2O2 (μM)

Figure 5.4: Effect of western blot optimisation on signalling parameters.
Fission yeast cells were exposed to 0.1-1 mM hydrogen peroxide stress and protein extracted. The same amount of protein loaded onto each gel (30 µg) using our optimized assay conditions (black) (0.5 µg/ml primary pk antibody and a 1:50 000 dilution of secondary antibody). The signalling amplitude, time and durations were calculated and compared to the fractional Pap1 oxidation of western blots that were not optimised for these conditions (red) (A-C). A two-tailed t-test was used to compare these effects, and the data represents the mean of three independent replicates.

Next, we investigated whether saturation of the Pap1 bands on the western blots had an impact on the signalling parameters. To determine this the blotting images were contrasted to display the maximum pixilation on ImageJ. The signalling profiles across the hydrogen peroxide range (0.1-1 mM) revealed a similar pattern for the oversaturated to optimised western blots for Pap1 oxidation (Figure 5.5A-D). However, saturation does appear to reduce the amount of signal detection as the average area under the curve was less than the optimised version of the analysis. We found that for the majority of the signalling parameters analysed, there were no significant differences observed between the saturated and non-saturated version of analysis (Figure 5.6A-C). Apart from a significant difference in signal amplitude after the

addition of 100 µM hydrogen peroxide. This suggests that published data that appear to be saturated can still be used for signal quantification.

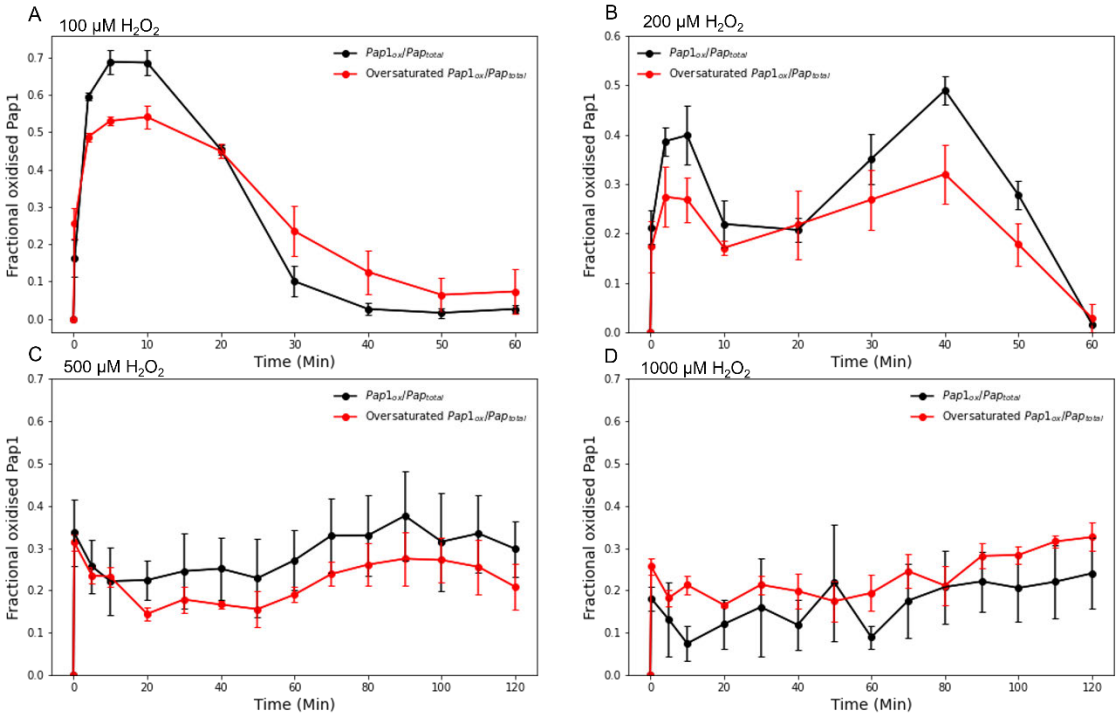

Figure 5.5: Comparing the effect of optimised assay conditions of Pap1 to oversaturated Pap1 data on dynamic signal profiles.

Western blotting experiments were optimised for protein concentration, primary to secondary ratios and detection in the linear range (black). These same blots were oversaturated (red), removing the linear range of detection, and plotted together with optimised profiles for Pap1 oxidation after exposure to 100-1000 µM hydrogen peroxide (n=3).

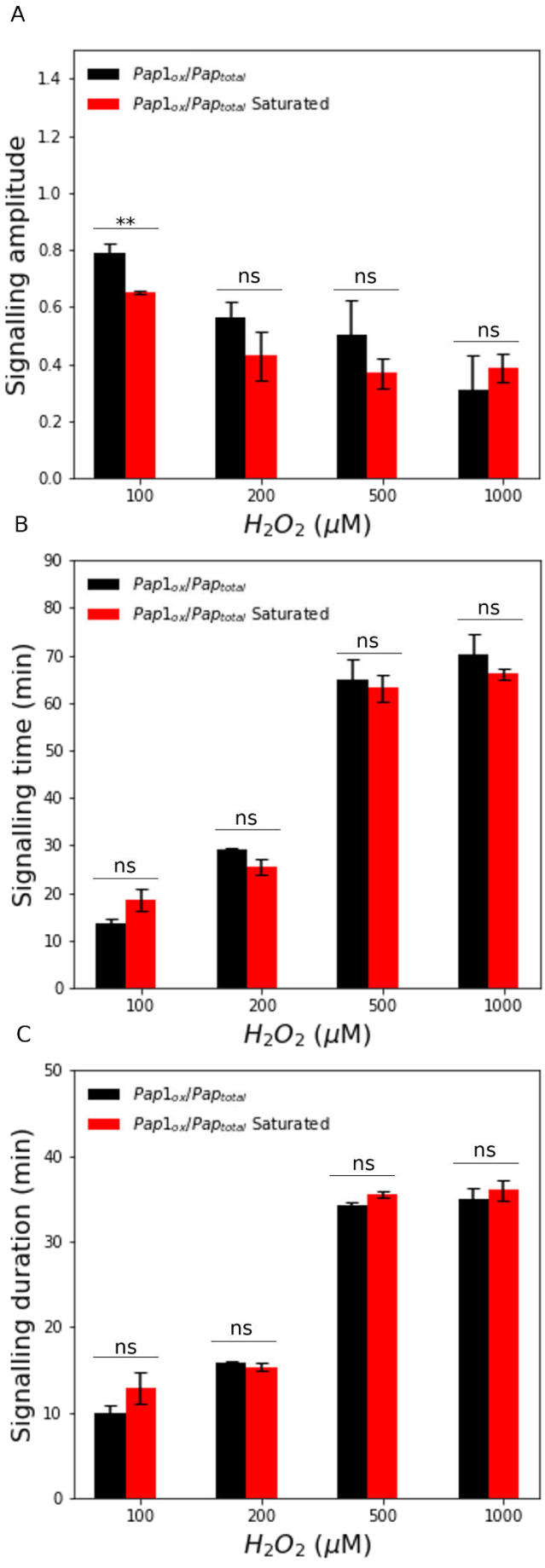
A
$Pap1_{ox}/Pap_{total}$
$Pap1_{ox}/Pap_{total}$ Saturated
Signalling amplitude
1.4
1.2
1.0
0.8
0.6
0.4
0.2
0.0
**
ns
ns
ns
100
200
500
1000
H_2O_2 (μM)
B
$Pap1_{ox}/Pap_{total}$
$Pap1_{ox}/Pap_{total}$ Saturated
Signalling time (min)
90
80
70
60
50
40
30
20
10
0
ns
ns
ns
ns
100
200
500
1000
H_2O_2 (μM)
C
$Pap1_{ox}/Pap_{total}$
$Pap1_{ox}/Pap_{total}$ Saturated
Signalling duration (min)
50
40
30
20
10
0
ns
ns
ns
ns
100
200
500
1000
H_2O_2 (μM)

Figure 5.6: Comparison of signal parameters for Pap1 dynamics for optimised blotting experiments to saturated western blots.

The signalling profiles for Pap1 oxidation were quantified for signal amplitude, time and duration from western blotting experiments that were in the linear detection range of ImageJ software. These blots were saturated (red) out of the dynamic detection range, and the signalling parameters of Pap1 oxidation were calculated and statistically compared to unsaturated blots (black) using t-tests (n=3).

There are several methods to determine the fractional Pap1 oxidation and in our analysis, we assessed three different approaches. First, the reduced and oxidised bands of Pap1 were added to obtain 'Pap1 total' from which the fractional oxidation was calculated as the ratio of Pap1 oxidised divided by the total. The second approach was to divide oxidised Pap1 over a DTT-reduced Pap1 band. This method takes into consideration any molecular complexes formed with Pap1. However, the saturation point (upper limit of the linear detection range) for one reduced band would be reached sooner. The third option was to calculate the ratio of Pap1 oxidised protein to the total protein content in each sample lane. However, the ratio of oxidised Pap1 across the whole proteome was expected to be a small value in comparison to the other two methods. Therefore, we represented the total protein profiles on different axis compared to Pap1 total and DTT control methods. We evaluated these approaches to determine the best analysis technique for quantifying Pap1 signalling profiles.

The signalling profiles at lower hydrogen peroxide treatments (<200 µM) showed similar patterns across all three methods (Figure 5.8A-B) indeed when correlated the r^2 values are >0.9 (Figure S.9A-F). At higher hydrogen peroxide concentrations, different oxidation patterns emerged based on the chosen approach. In both the DTT and total protein control, a second oxidation peak was observed around 100 min after hydrogen peroxide exposure. Surprisingly, a peak greater than one was observed suggesting that the amount of reduced Pap1 was greater than the total concentration of Pap1 (Figure 5.7C-D). Additionally, the correlation between the three methods was lost at higher concentrations with r^2 <0.6 suggesting that the Pap1 ratio method should be used at these concentrations (Figure S.25G-L). We next checked how the choice of each of these methods affected the signal parameters.

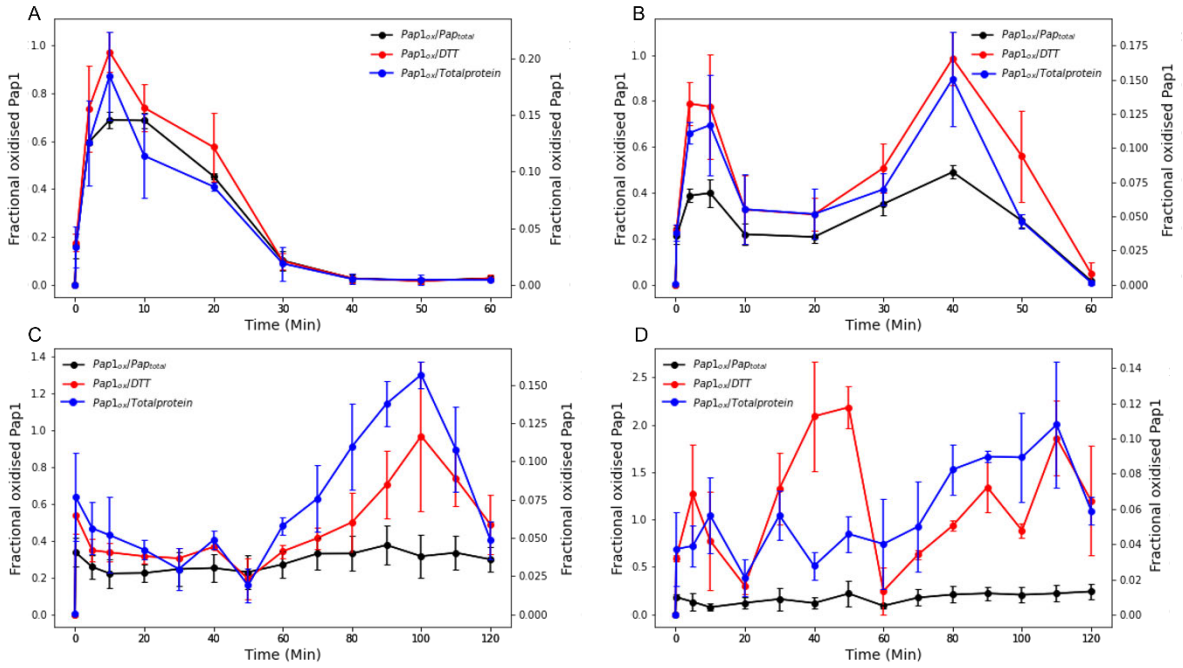

Figure 5.7: Comparative normalisation of fractional Pap1 oxidation against reduced Pap1 (DTT control) and total protein control.

S. pombe cells were exposed to 100-1000 µM hydrogen peroxide and samples collected and processed using western blotting. Densitometric analysis was used to quantify oxidised Pap1. To determine the fractional Pap1 oxidation, oxidised Pap1 was divided against Pap1 total (black), Pap1 reduced (DTT control) (red) and total protein(A-D) (blue) (n=3).

The signal amplitude showed significant differences between the methods used for Pap1 quantification. Notably, the amplitudes for the DTT control was greater than the amplitudes for Pap1 total while the total protein amplitudes were significantly less compared to the other two normalisation methods (Figure 5.8A). Interestingly, no significant differences were observed among the different methods when calculating the signal time and duration suggesting that these two parameters are not affected the approach to obtain a Pap1 oxidation ratio (Figure 5.8C-D).

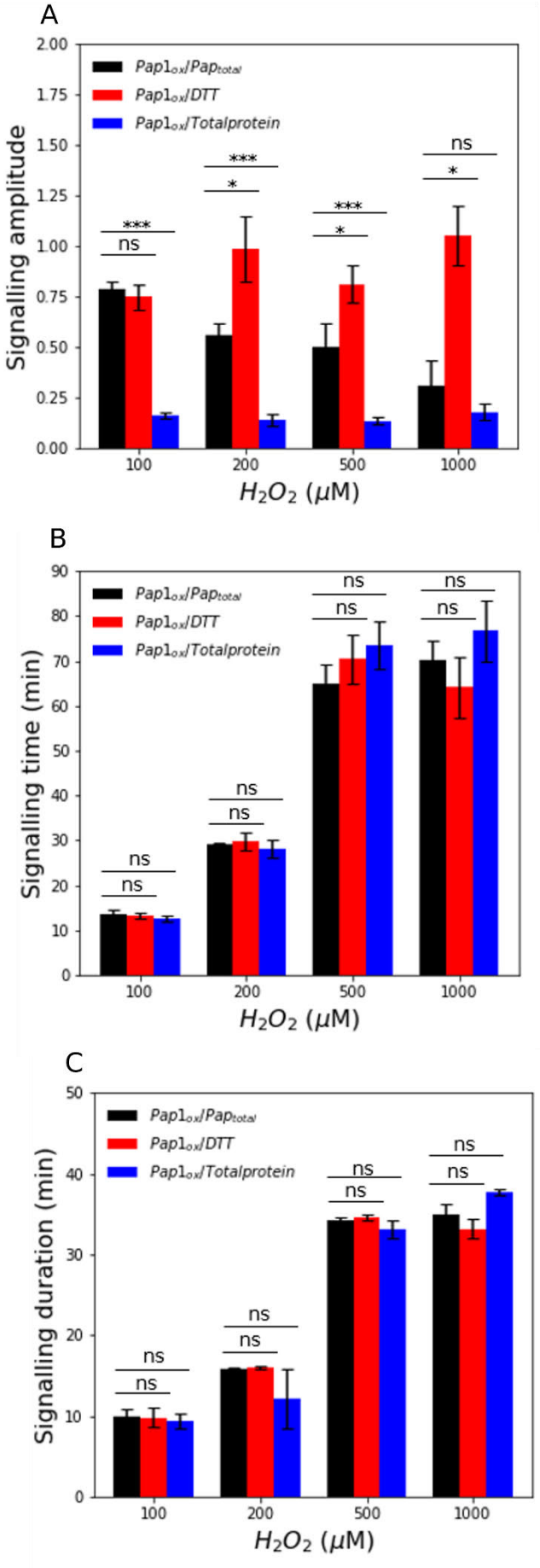
A
Signalling amplitude
Pap1ox/Paptotal
Pap1ox/DTT
Pap1ox/Totalprotein
H2O2 (μM)
B
Signalling time (min)
C
Signalling duration (min)

Figure 5.8: Determination of the signaling parameters for fractional Pap1 oxidation using different normalization methods.

The signal amplitude, time and duration were calculated from the signal profiles of Pap1 oxidation normalised against total Pap1, total reduced Pap1 (DTT control) and total protein controls. The parameters were statistically compared using two-tailed t-tests (n=3).

In summary, there are several factors to consider when quantifying dynamic oxidation profiles. To accurately compare the different experiments equal protein concentrations optimised to the linear range of primary and secondary antibody concentrations must be used as this has a significant effect on the signalling parameters. However, computational analysis of the blotting data when saturated does not have a significant effect on signal parameter calculations and therefore, contrasting blots does not impact the overall analysis. Lastly, the use of normalisation methods to generate the Pap1 ratio only affects the signalling amplitude and not signal time and duration. However, given the suitability of analysis to these applications DTT and total protein control methods for Pap1 oxidation calculations are not recommended.

5.4.4 Primer design and assessment for RT-qPCR experiments

Genes for RT-qPCR were selected by analysing published transcriptomic data which revealed that 700 genes had at least a two-fold upregulation in expression after the bolus addition of 70 µM, 500 µM, and 6 mM hydrogen peroxide to *S. pombe* cells (Chen et al., 2008). For the qPCR experiments in this study (Chapter 2) we determined which genes were regulated by Pap1. Each category was represented as heatmaps (supplementary information) with the last 6 columns showing gene induction in Δ*pap1* cells exposed to 70 µM and 500 µM hydrogen peroxide. We then selected genes that were downregulated more than 10-fold in the Δ*pap1* cells and the change in expression over time was plotted in the following figures below.

In addition, genes induced in these transcriptomic datasets were further analysed according to their Gene ontology function category (GO) on PomBase. The upregulated genes were found in the following GO categories: oxidoreductase activity, DNA regulation, ubiquitination, cell cycle regulation, mRNA processes, mitochondrial function, transmembrane transport, protein transport into the nucleus, signal transduction, autophagy, lipid regulation, iron regulation, vitamin biosynthesis, retrotransposons as well as genes with unknown function.

Oxidoreductases encompass a wide range of enzymes including, oxidases, peroxidases and dehydrogenases (Rustici et al., 2007). These enzymes catalyse various biochemical processes including detoxification and the metabolism of exogenous molecules, such as xenobiotics, ROS and metabolic byproducts (Rustici et al., 2007). The effect of hydrogen peroxide on the transcription of 105 oxidoreductase genes were combined into heatmaps (Figure S.28) and we observed that 70 µM hydrogen peroxide treatment reduced the overall oxidoreductase response when compared to a 500 µM hydrogen peroxide treatment. Interestingly, 6mM hydrogen peroxide treatment had lower induction in these genes compared to the 500 µM hydrogen peroxide dose.

In total, 28 genes associated to oxidoreductase activity were found to be Pap1 regulated and were *zym1, yhb1, osr1, adh8, dhd1, atd3, zta1, orb1, plr1, ctt1, srx1, gst2,* SPAPB1A11.03, SPBC2A9.02, SPAPB24D3.08C, SPCC1739.08C, SPBC23G7.10C, SPCC6630.08C, SPAC1F8.04C, SPCC24B10.20. Of these genes *zym1* and *adh8* has a fold increase over 60 when *S. pombe* cells were exposed to 500 µM hydrogen peroxide (Figure 5.9). Additionally, *ctt1* and *srx1* had a 30-fold increase in expression and *trr1* increased 15-fold in expression after exposure to 500 µM hydrogen peroxide (Figure 5.10), and therefore these three genes were selected for our RT-qPCR assay. Catalase (*ctt1*), sulfiredoxin (*srx1*) and thioredoxin reductase (*trr1*) have been independently shown to be regulated by Pap1 (Nakagawa et al., 2000; Calvo et al., 2012).

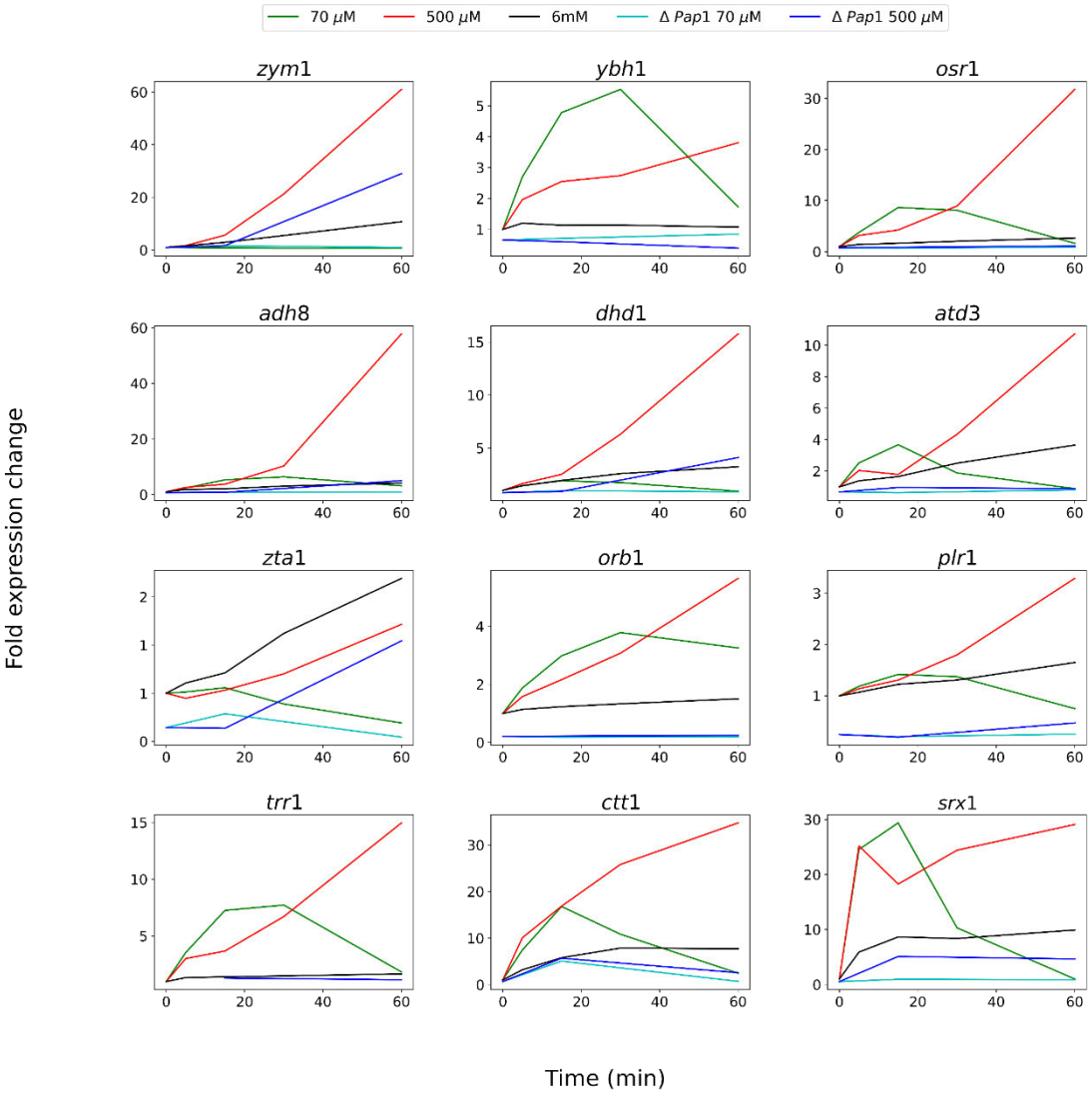
70 μM
500 μM
6mM
Δ Pap1 70 μM
Δ Pap1 500 μM
zym1
ybh1
osr1
adh8
dhd1
atd3
zta1
orb1
plr1
trr1
ctt1
srx1
Fold expression change
Time (min)

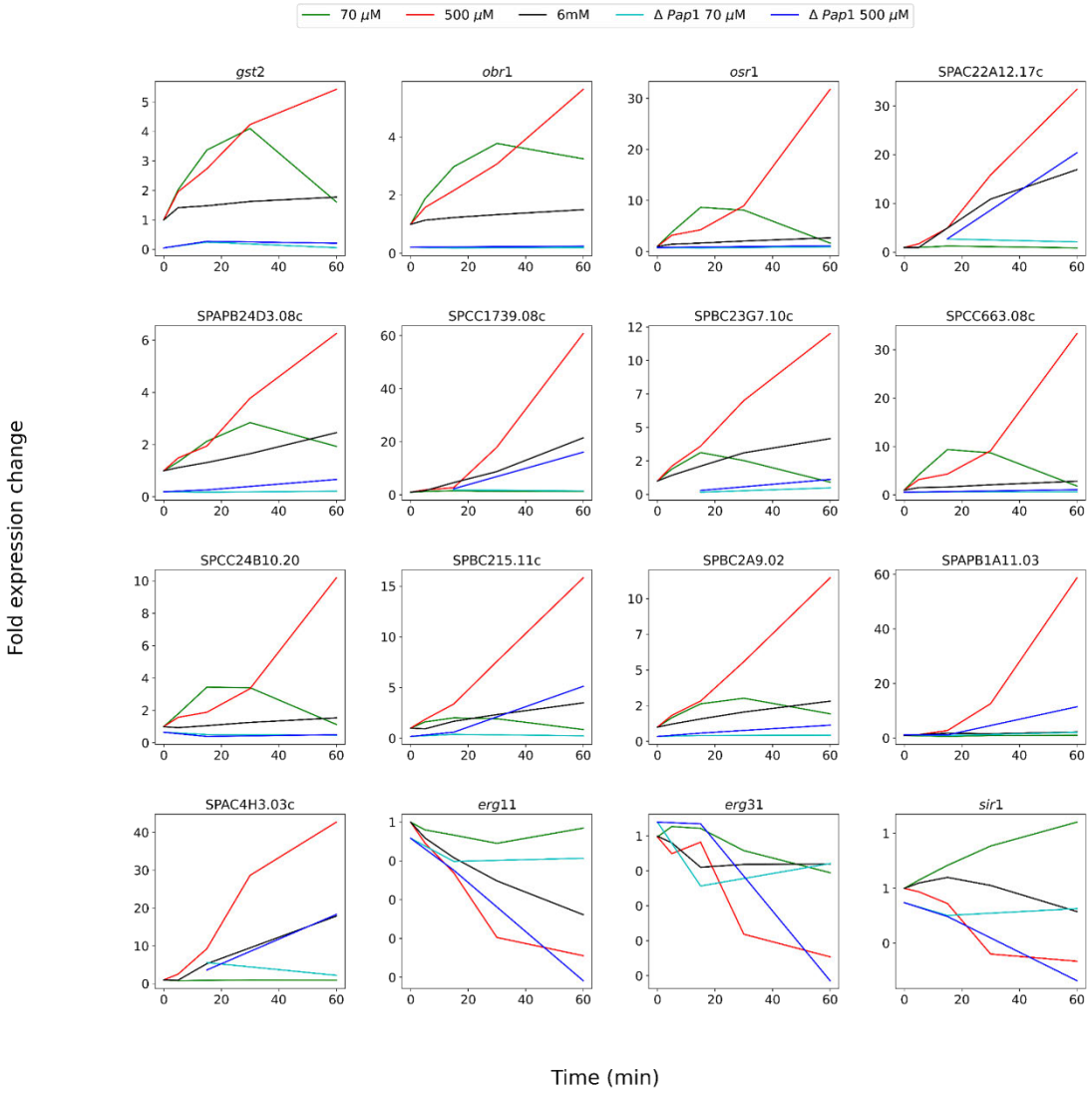

Figure 5.9: Pap1- regulated genes associated with oxidoreductase activity.

The dynamic mRNA transcript levels of S. pombe cells exposed to 70 µM (green), 500 µM (red), and 6 mM (black) hydrogen peroxide were obtained from Chen et al., 2008. In total 104 of genes linked to oxidoreductase activity displayed at least a two-fold increase in expression when compared to untreated samples. To determine which subset of genes was Pap1-regulated, the expression linked ΔPap1 was also plotted after exposure to 70 µM hydrogen peroxide (light blue) and 500 µM hydrogen peroxide (dark blue) resulting in 28 genes.

The next subset of genes considered were genes associated with DNA regulation and repair and include the following functions: chromatin remodelling, repairing double or single stranded DNA breaks, amino acid mispairing, DNA loop binding as well as the repressing or activation of transcription of genes hubs and, includes histone methylation or demethylation.

The relative changes in expression for this gene category was observed on heatmaps (Figure S.28:) for 55 genes; it should be noted that DNA damage-response protein (Ddr48) had a large increase in expression from 0.9 to 96 after 30 min of exposure to 500 µM hydrogen peroxide. Furthermore, in the Δ*pap1* mutant strain this gene showed an expression of 182-fold when compared to 82-fold in the wildtype and was removed from the analysis as it skewed the dataset.

The general trend showed that at 70 µM hydrogen peroxide there is no significant increase in expression for these genes and expression only begins to increase substantially after exposure to 500 µM and 6 mM hydrogen peroxide (Figure S.28:). Furthermore, this is also exemplified in the Δ*pap1* mutant after exposure to 500 µM hydrogen peroxide. However, no genes were found to be significantly downregulated in the Δ*pap1* cells. Despite this, *oxs1* has been showed to be regulated by Pap1 in other studies and does show a small reduction in expression (Figure 5.10) (Chen et al., 2018). Additionally, *oxs1* in turn has been shown to regulate a host of other genes including *gal10*, *gut5*, *hsp90*, *pho842*, *sro1*, *ssa2*, *wis2*, SPBC1347.14c and SPBC36.02c. Another gene, *prr1*, which also plays a role in transcriptional regulation, did not show a significant upregulation when exposed to hydrogen peroxide but is known to be regulated by Pap1(Figure 5.10) (Ohmiya et al., 200).

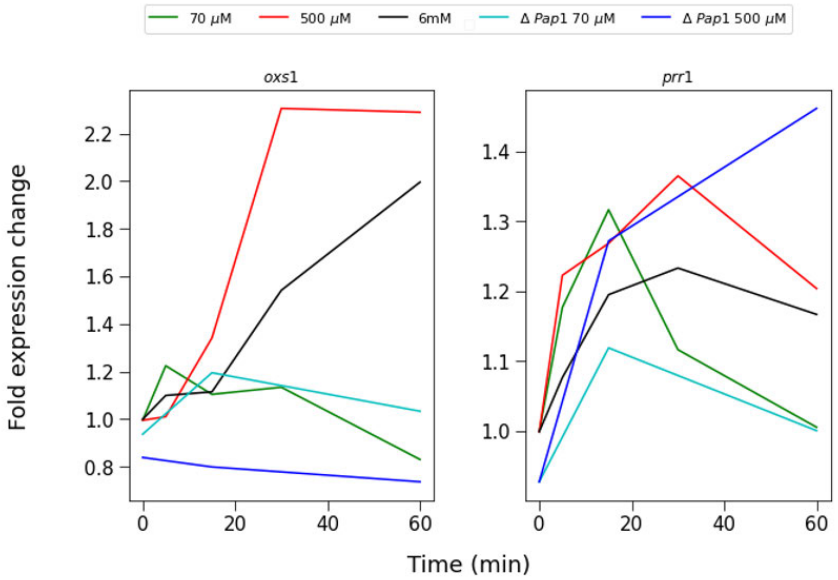

Figure 5.10: Pap1- regulated genes associated with DNA repair and regulation.

The dynamic mRNA transcript levels of S. pombe cells exposed to 70 µM (green), 500 µM (red), and 6 mM (black) were obtained from Chen et al., 2006. In total 55 of the genes linked

to DNA repair and regulation displayed at least a two-fold increase in expression when compared to untreated samples. To determine which subset of genes was Pap1-regulated, the expression linked ΔPap1 was also plotted after exposure to 70 µM hydrogen peroxide (light blue) and 500 µM hydrogen peroxide (dark blue) resulting in two genes regulated by Pap1.

This next subset of 38 genes primarily regulates mRNA, including splicing regulation, metabolic activities related to mRNA, and both negative and positive regulation of nuclear-transcribed mRNA (Heatmap as Figure S29). The collective response within this subset of genes did not exhibit a significant upregulation at 70 µM hydrogen peroxide. However, an overall increase in expression was noted after exposure to 500 µM and 6 mM hydrogen peroxide. (Figure S11). Notably, only the genes *puf5* and *dpb2* appear to be Pap1 regulated as there is a decrease in transcription within a *pap1* mutant cell after exposure to hydrogen peroxide.

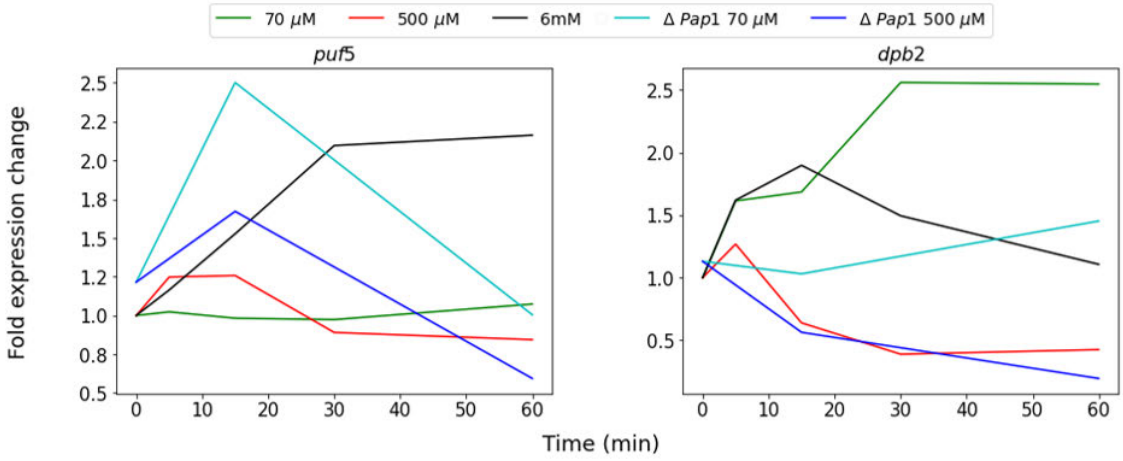

Figure 5.11: Pap1- regulated genes associated with mRNA regulation.
The dynamic mRNA transcript levels of S. pombe cells exposed to 70 µM (green), 500 µM (red), and 6 mM (black) were obtained from Chen et al., 2006. In total 38 of the genes linked to mRNA regulation displayed at least a two-fold increase in expression when compared to untreated samples. To determine which subset of genes was Pap1-regulated, the expression linked ΔPap1 was also plotted after exposure to 70 µM hydrogen peroxide (light blue) and 500 µM hydrogen peroxide (dark blue) resulting in two genes regulated by Pap1.

The gene subset involved in signal transduction is linked to diverse kinase signalling pathways with a moderate increase in induction after the addition of 70 µM hydrogen peroxide but substantial increases in expression of these genes was found for exposure at 500 µM and

6 mM hydrogen peroxide (Figure S.30). Interestingly, *pyp2* exerts a unique role by directly inhibiting Sty1 which is key in the negative regulation of the stress-activated protein kinase signalling cascade. The Sty1 pathway is activated once the Pap1 pathway encounters elevated hydrogen peroxide concentrations. Of the 95 genes associated with signal transduction four exhibited a downregulation in a Δ*pap1* strain delete and were SPAC1039.02, *hsp90*, *ssa2*, and *wis2* are associated to Pap1 but also undergoes regulation by *oxs1* (Figure 5.12).

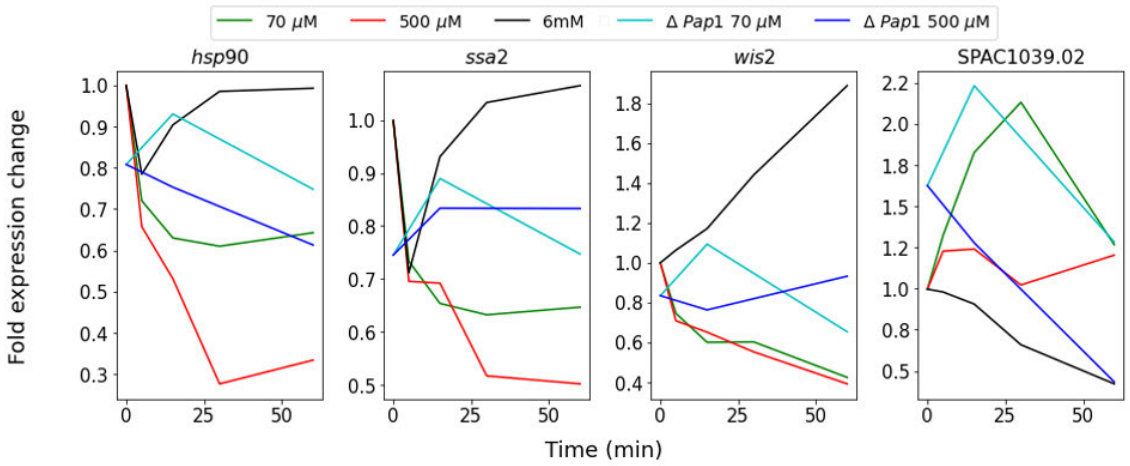

Figure 5.12: Pap1- regulated genes associated with signal transduction.
The dynamic mRNA transcript levels of S. pombe cells exposed to 70 µM (green), 500 µM (red), and 6 mM (black) were obtained from Chen et al., 2006. In total 95 of the genes linked to signal transduction displayed at least a two-fold increase in expression when compared to untreated samples. To determine which subset of genes was Pap1-regulated, the expression linked ΔPap1 was also plotted after exposure to 70 µM hydrogen peroxide (light blue) and 500 µM hydrogen peroxide (dark blue) resulting in four genes regulated by Pap1.

The next subset of genes analysed were genes associated with cell cycle regulation. In total there were 78 genes associated with cell cycle regulation that showed a two-fold increase in expression after exposure to hydrogen peroxide. The increase was primarily at the lower hydrogen peroxide concentration (70 µM) whereas at higher concentrations we noticed these genes were in-fact downregulated (Heatmap Figure S. 31). However, three genes that showed at least a two fold increase in expression and were regulated by Pap1 viz. *sro1*, *atf1* and *cum1* (Figure 5.13).

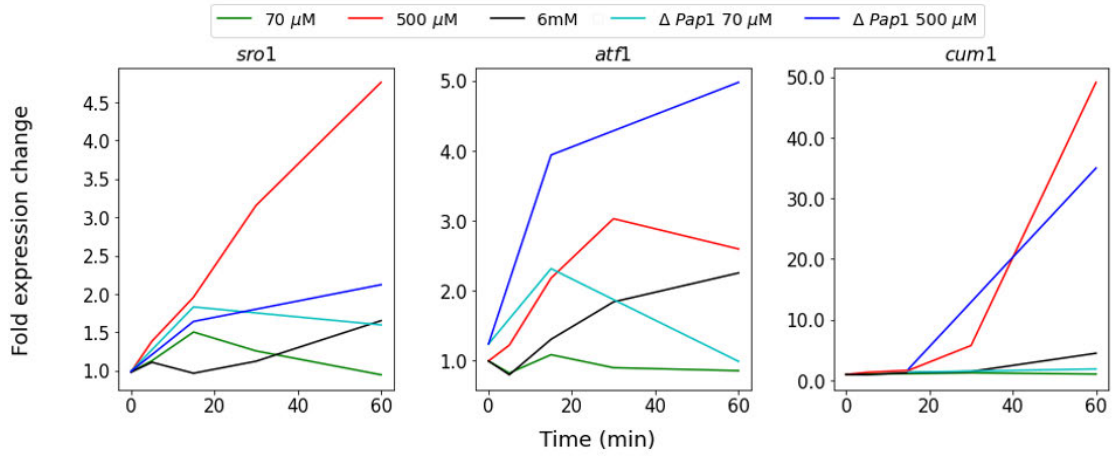

Figure 5.13: Pap1- regulated genes associated with cell cycle regulation.

The dynamic mRNA transcript levels of S. pombe cells exposed to 70 µM (green), 500 µM (red), and 6 mM (black) were obtained from Chen et al., 2006. In total 78 of the genes linked to cell cycle regulation displayed at least a two-fold increase in expression when compared to untreated samples. To determine which subset of genes was Pap1-regulated, the expression linked ΔPap1 was also plotted after exposure to 70 µM hydrogen peroxide (light blue) and 500 µM hydrogen peroxide (dark blue) resulting in three genes regulated by Pap1.

The genes associated with vitamin biosynthesis are important for cell growth, maintenance, and energy functions. Notably, the 28 genes associated with vitamin biosynthesis exhibited a substantial upregulation following exposure to 500 µM hydrogen peroxide. Notably, there was a general increase in expression at 70 µM hydrogen peroxide in comparison to 500 µM, with 6 mM hydrogen peroxide exposure showing the lowest expression among

these concentrations. (Heatmap Figure S. 32). Among these genes, *rib4* and *alr2* displayed downregulation in the *Δpap1* cell and therefore may be Pap1 regulated (Figure 5.14).

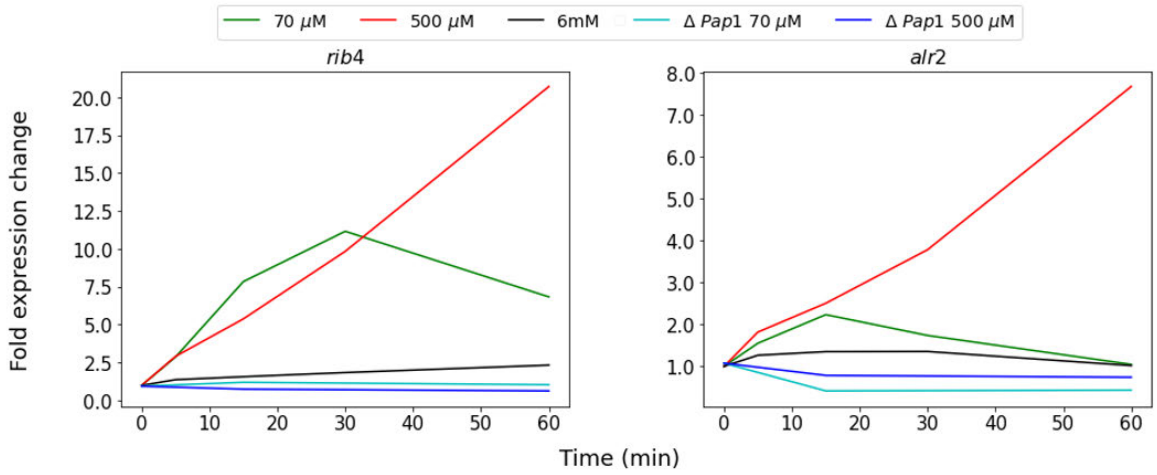

Figure 5.14: Pap1- regulated genes associated with vitamin biosynthesis.

The dynamic mRNA transcript levels of S. pombe cells exposed to 70 µM (green), 500 µM (red), and 6 mM (black) were obtained from Chen et al., 2006. In total 28 of the genes linked to vitamin regulation displayed at least a two-fold increase in expression when compared to untreated samples. To determine which subset of genes was Pap1-regulated, the expression linked ΔPap1 was also plotted after exposure to 70 µM hydrogen peroxide (light blue) and 500 µM hydrogen peroxide (dark blue) resulting in two genes regulated by Pap1.

Transmembrane transport in the context of oxidative stress will transport antioxidant proteins and metabolites in or out of the cell or within cellular structures (Sies, 1997). In total there was 68 genes that showed a two-fold increase in expression with the highest increases observed after the addition of 500 µM hydrogen peroxide. The genes *caf5*, *opt3*, and *osr2* showed a decrease in expression in the absence of Pap1, suggesting a potential role for Pap1 regulating some transmembrane transport activities (Figure 5.15). Additionally, other genes, *bfr1*, *pho842*, and SPBC36.02c (Figure 5.15) have been previously associated with Pap1 regulation in various studies and were also included in this analysis (He et al., 2017; Toone et al., 1998).

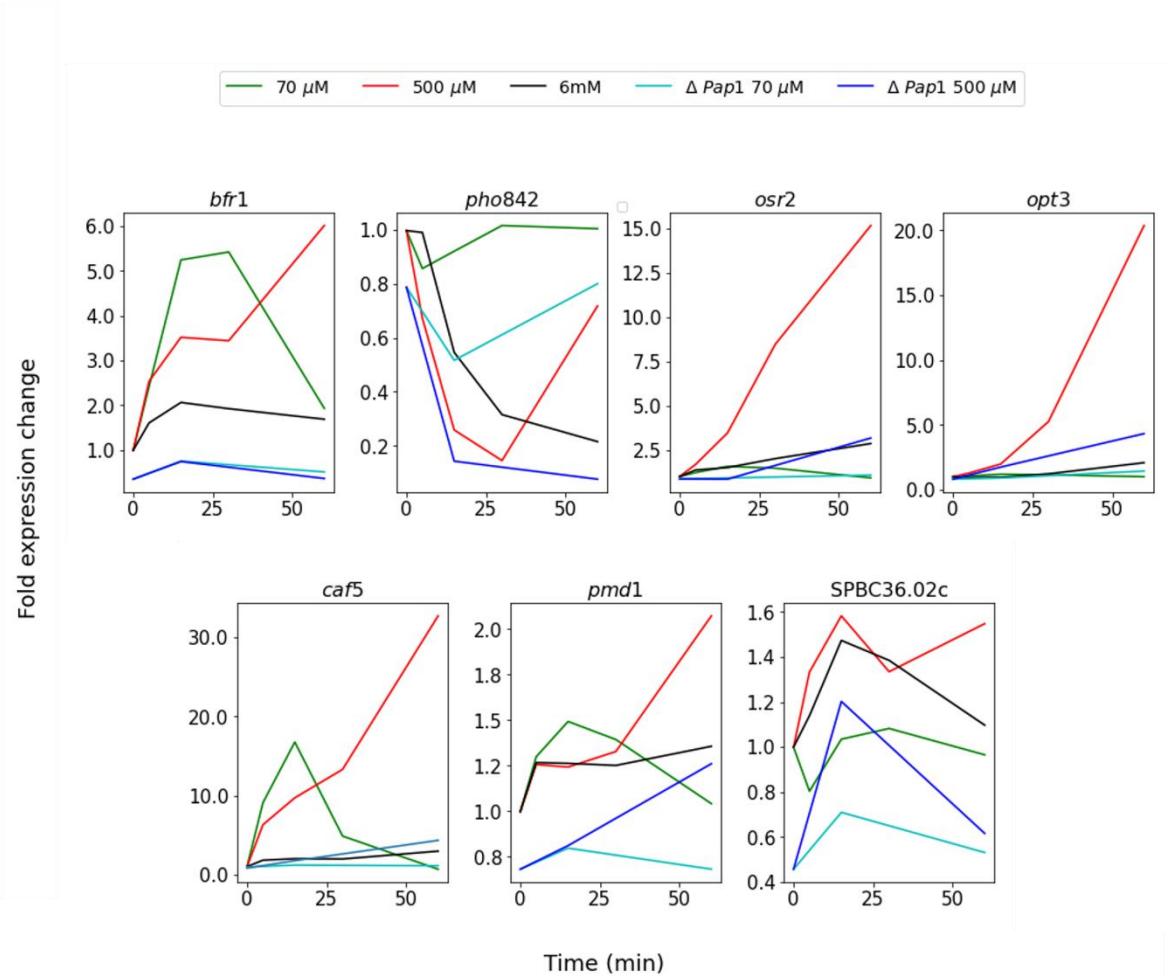

Figure 5.15: Pap1- regulated genes associated with transmembrane transport.

The dynamic mRNA transcript levels of S. pombe cells exposed to 70 µM (green), 500 µM (red), and 6 mM (black) were obtained from Chen et al., 2006. In total 68 of the genes linked to transmembrane transport displayed at least a two-fold increase in expression when compared to untreated samples. To determine which subset of genes was Pap1-regulated, the expression linked ΔPap1 was also plotted after exposure to 70 µM hydrogen peroxide (light blue) and 500 µM hydrogen peroxide (dark blue) resulting in seven genes regulated by Pap1.

We also observed a small subset of genes that showed upregulation to proteins associated with transmembrane transport into the nucleus. Of these genes *cut15, imp1* and *crm1* are linked to Pap1 regulation (Figure 5.16).

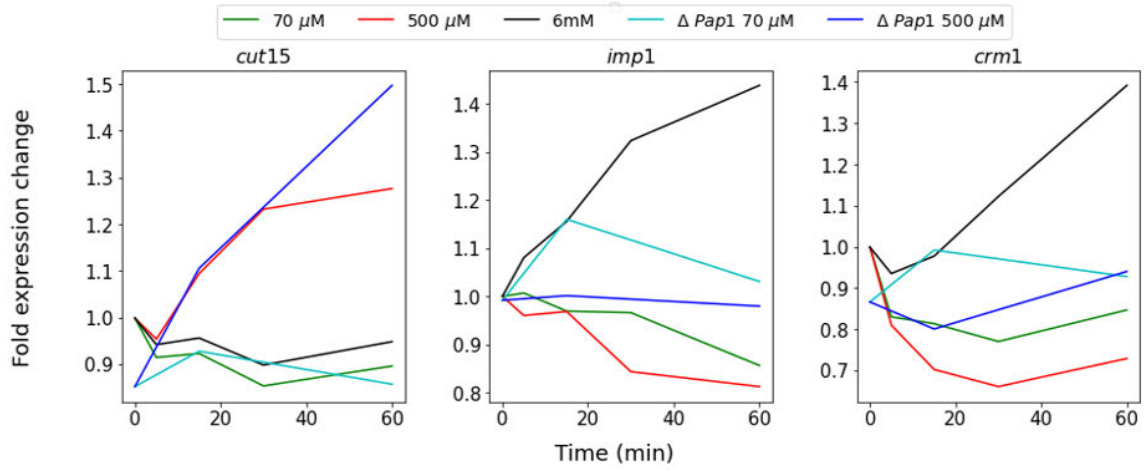

Figure 5.16: Pap1- regulated genes associated with protein transport into the nucleus. *The dynamic mRNA transcript levels of S. pombe cells exposed to 70 µM (green), 500 µM (red), and 6 mM (black) were obtained from Chen et al., 2006. In total only three genes linked to protein transport into the nucleus displayed at least a two-fold increase in expression when compared to untreated samples. To determine which subset of genes was Pap1-regulated, the expression linked ΔPap1 was also plotted after exposure to 70 µM hydrogen peroxide (light blue) and 500 µM hydrogen peroxide (dark blue) resulting in three genes regulated by Pap1.*

Lipid regulation plays a pivotal role in maintaining cellular functionality and promoting growth. Within the 33 genes listed (Heatmap Figure S. 34), *lsd90* exhibited a substantial increase in expression, from 0.9 to 123-fold after 60 min exposure to 500 µM hydrogen peroxide. Notably, in the Pap1 mutant, this upregulation intensified to 240. Despite its significant expression changes, *lsd90* has not been previously associated with Pap1 regulation.

In general, the majority of these genes did not display pronounced upregulation. Among them, *pof14* is the only gene linked to Pap1 regulation, yet it did not exhibit a significant decrease in regulation in the Pap1 mutant (Figure 5.17). *Pof14* is known for its involvement in protein binding with *cul1*, *erg9*, and *skp1*, all integral to lipid regulation (Tafforeau et al., 2006). Conversely, *egt1*, another gene associated with lipid regulation and linked to Pap1 regulation (Pluskal et al., 2014), did not demonstrate a two-fold increase in regulation and was excluded.

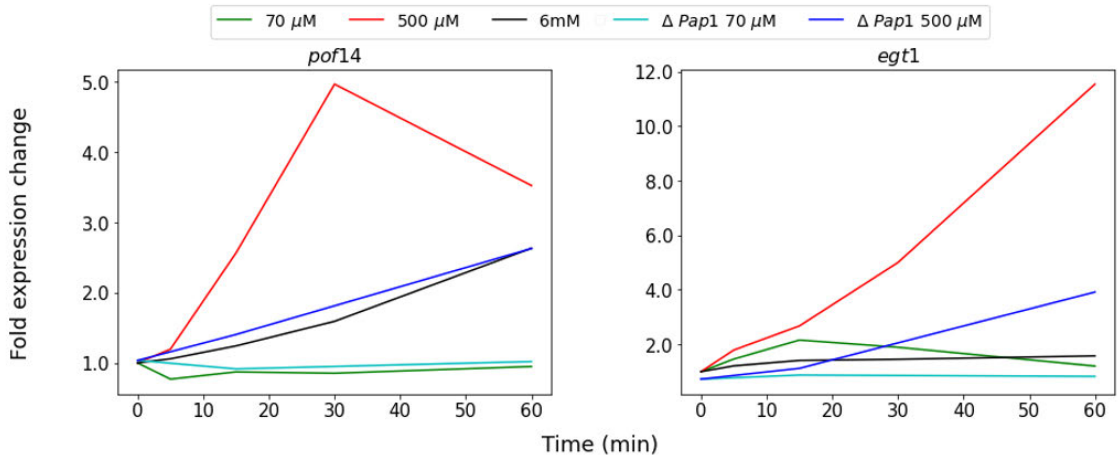

Figure 5.17: Pap1- regulated genes associated with lipid regulation.

The dynamic mRNA transcript levels of S. pombe cells exposed to 70 µM (green), 500 µM (red), and 6 mM (black) were obtained from Chen et al., 2006. In total 33 of genes linked to lipid regulation displayed at least a two-fold increase in expression when compared to untreated samples. To determine which subset of genes was Pap1-regulated, the expression linked ΔPap1 was also plotted after exposure to 70 µM hydrogen peroxide (light blue) and 500 µM hydrogen peroxide (dark blue) resulting in two genes regulated by Pap1.

Iron is required for the activity of iron-dependent enzymes which are essential to the functioning of cellular metabolism (Guha et al., 2011). Interestingly, *shu1* showed considerable upregulation from 0.9 to an 80-fold increase in expression when exposed to 500 µM hydrogen peroxide but was downregulated in a Δ*pap1* cell (Figure 5.18).

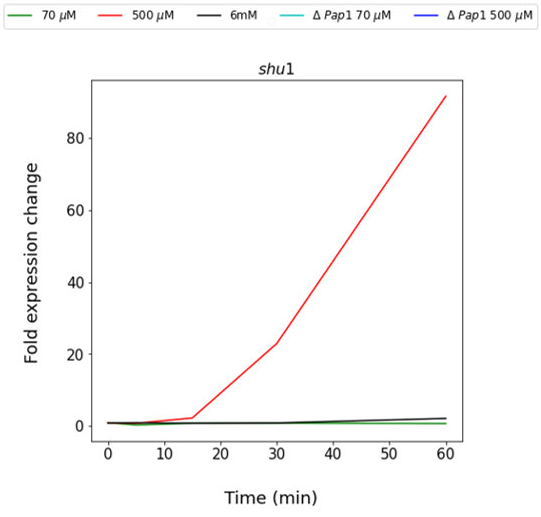

Figure 5.18: Pap1- regulated genes associated with iron regulation.

The dynamic mRNA transcript levels of S. pombe cells exposed to 70 µM (green), 500 µM (red), and 6 mM (black) were obtained from Chen et al., 2006. The shu1 gene linked to iron regulation displayed at least a two-fold increase in expression when compared to untreated samples. To determine which subset of genes was Pap1-regulated, the expression linked ΔPap1 was also plotted after exposure to 70 µM hydrogen peroxide (light blue) and 500 µM hydrogen peroxide (dark blue).

Several genes exhibited both upregulation and downregulation in their expression levels. However, the functions of these genes remain unknown (Figure 5.19). Notably, a few genes demonstrated downregulation in the Pap1 mutant.

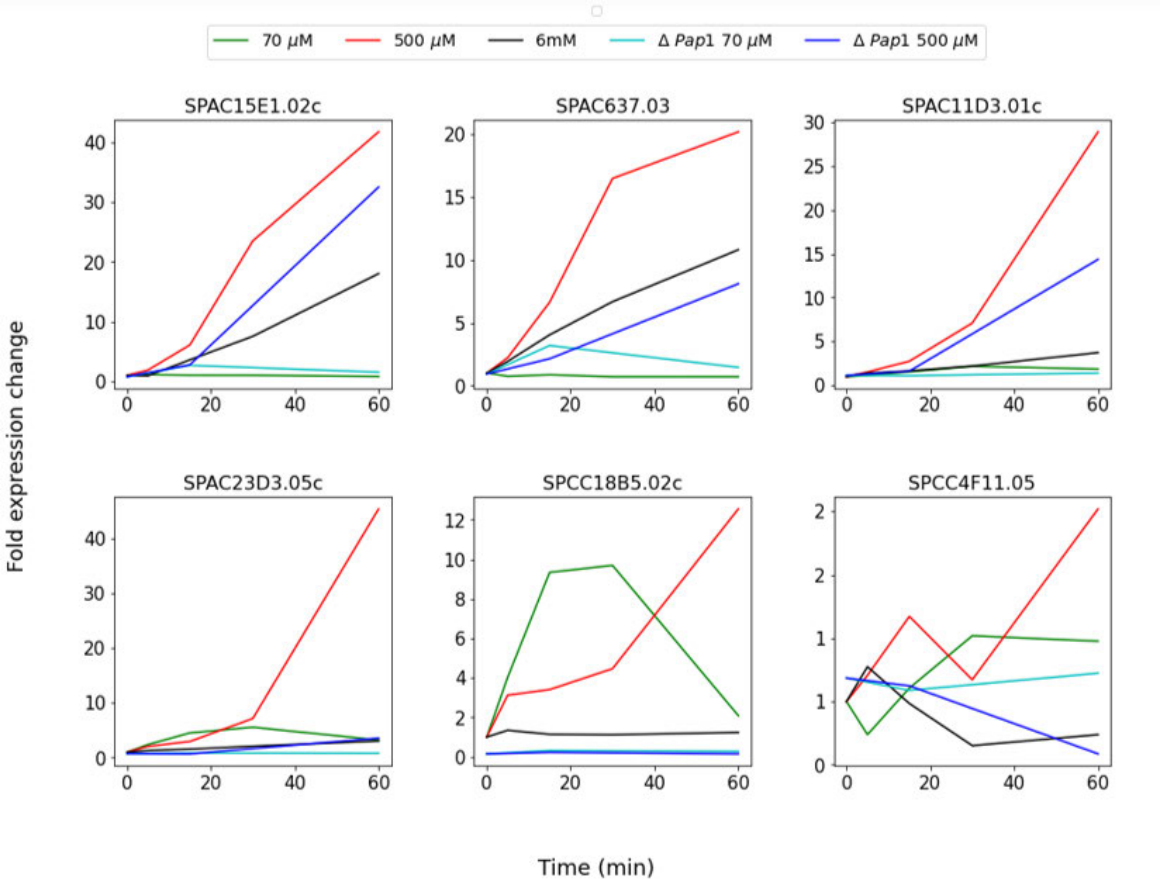

Figure 5.19: Pap1- regulated genes associated with unknown functions.

The dynamic mRNA transcript levels of S. pombe cells exposed to 70 µM (green), 500 µM (red), and 6 mM (black) were obtained from Chen et al., 2006. In total 65 of genes linked to

unknown functions displayed at least a two-fold increase in expression when compared to untreated samples. To determine which subset of genes was Pap1-regulated, the expression linked ΔPap1 was also plotted after exposure to 70 µM hydrogen peroxide (light blue) and 500 µM hydrogen peroxide (dark blue) resulting in six genes regulated by Pap1.

The last consideration before commencing with RT-qPCR analysis was to select relevant reference genes to be used as internal controls. To achieve this, no change in gene expression should be observed in *S. pombe* cells after exposure to hydrogen peroxide. In total 8 genes were identified and this data in combination with published reference genes we selected *gpd3* and *act1* as reference genes to use in our study (Figure 5.20).

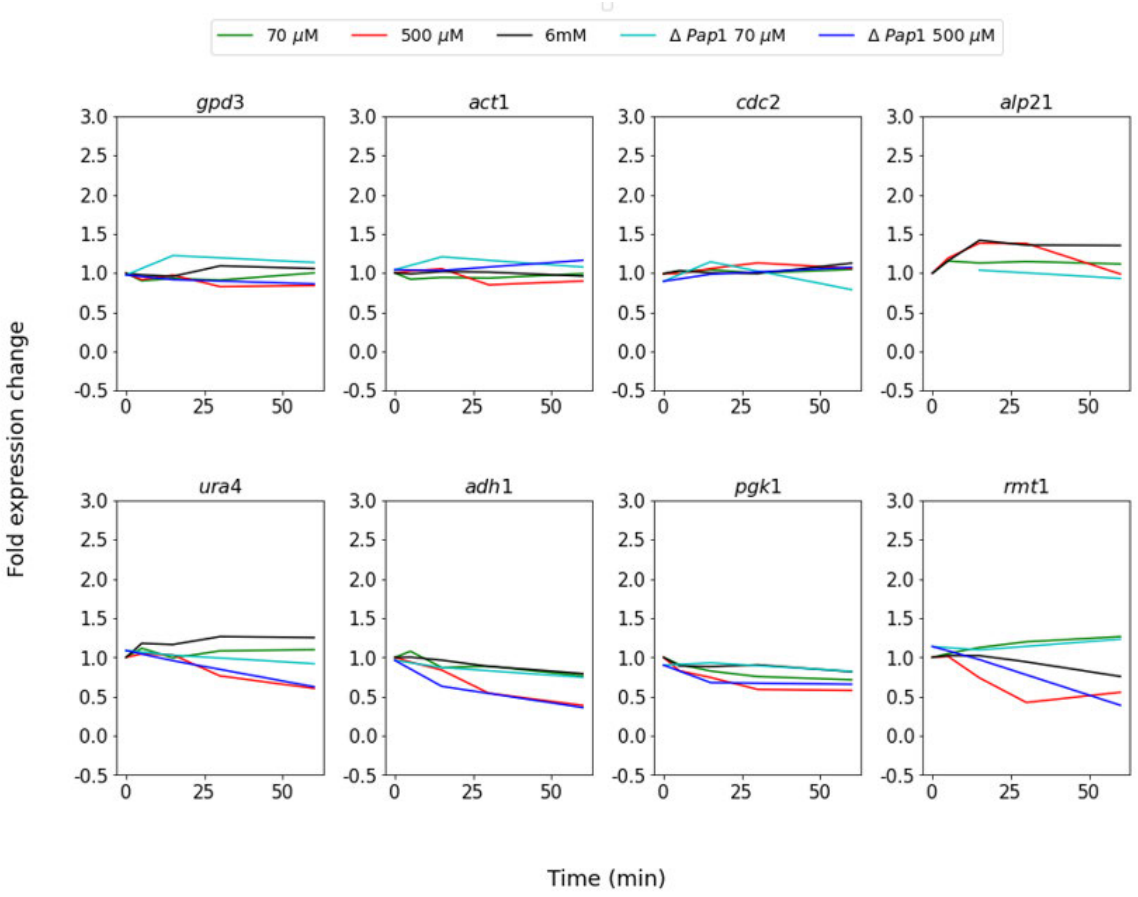

Figure 5.20: Possible reference genes to use for RT-qPCR experiments.

The dynamic mRNA transcript levels of S. pombe cells exposed to 70 µM (green), 500 µM (red), and 6 mM (black) were obtained from Chen et al., 2006. Genes that did not display any change in expression after exposure to all hydrogen peroxide concentrations (70 µM, 500 µM and 6mM) as well as no upregulation in the Δpap1 strain were evaluated for control genes for

further RT-qPCR assays these genes included gpd3, act1, cdc2, apl21, ura4, adh1, pgk1 and rmt1.

There were several gene categories that had no genes regulated by Pap1 but displayed at least a two-fold increase in expression these included genes associated to ubiquitination, mitochondrial function, autophagy, retrotransposons and ribosome biogenesis. In most of these gene subsets there was substantial upregulation after the wildtype cells and *Δpap1* cells were exposed to 500 µM hydrogen peroxide. The relevant heatmaps to this associated data can be found in the supplementary information (Figure S. 36, Figure S.37, Figure S.38, Figure S.39)

Based on the Pap1-regulated genes identified, a RT-qPCR assay was designed, and qPCR primers were developed. To confirm the specificity of these primers, end-point PCR was performed using *S. pombe* genomic DNA as the template (Figure 5.21A). The resulting PCR products were visualised on an agarose gel and compared to the expected product sizes based on the DNA standard curve (Figure 5.21B). The analysis indicated that the PCR products were of the expected sizes (Table 5.2), showing that the primers were specific to the target genes and did not produce any non-specific products. Our no template controls were also clear. This step validated the use of the primers in subsequent RT-qPCR experiments. However, it is important to note that this validation was conducted on genomic DNA and not on cDNA, which means the possibility of non-specific amplification in the RT-qPCR reactions had not been ruled out.

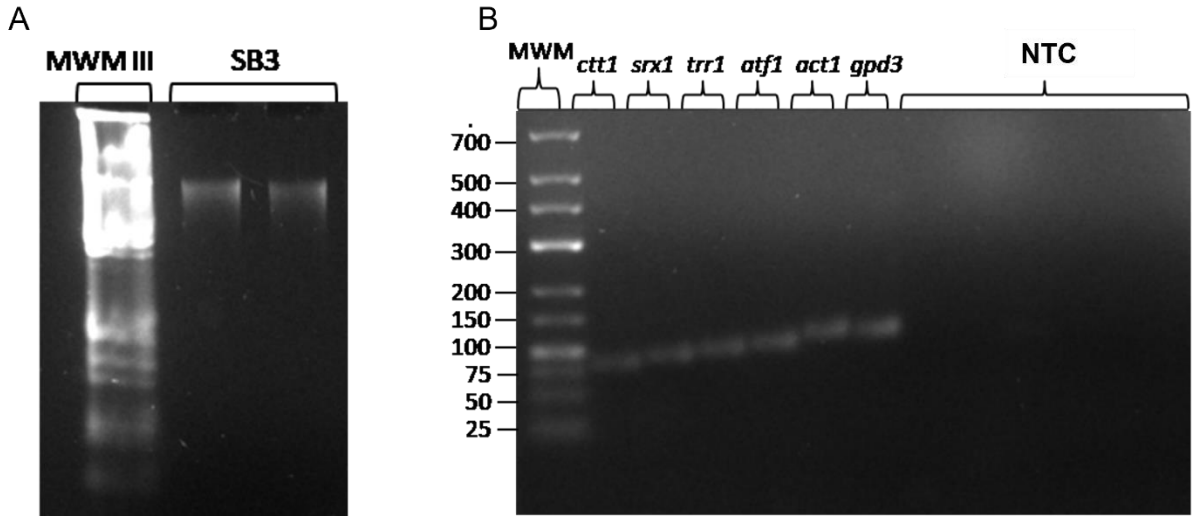

Figure 5.21:Assessment qPCR primer design for Pap1-reglated genes on *S. pombe* genomic DNA.

Genomic DNA from S. pombe cells (SB3) was chemically extracted, and the purity and quality of the DNA were assessed on a 1% agarose gel (A). The primers selected for qPCR amplification of ctt1, srx1, trr1, atf1, act1 and gpd3 were tested on genomic DNA to determine primer specificity, no template controls (NTC) (B). The products were assessed on a 2% agarose gel and sized (B).

After isolating total RNA from *S. pombe*, the quality and integrity of the RNA was assessed by denaturing gel electrophoresis. Clear and distinct 28S and 18S ribosomal RNA bands were obtained, showing that the RNA was of good quality and suitable for downstream applications (Figure 5.22A). Next, cDNA was synthesised from the isolated RNA using reverse transcription. To ensure the effectiveness and specificity of the primers used in subsequent qPCR experiments, a test experiment was carried out using primers for the target genes *ctt1*, *srx1*, *trr1*, *atf1*, *act1*, and *gpd3*. The qPCR products were then analysed on an agarose gel, which confirmed the expected sizes of the amplicons, indicating the primers were specific and effective for amplifying the target genes (Figure 5.22B). Overall, these steps showed that isolated RNA was high quality and the specificity of the primers used in the subsequent RT-qPCR experiments.

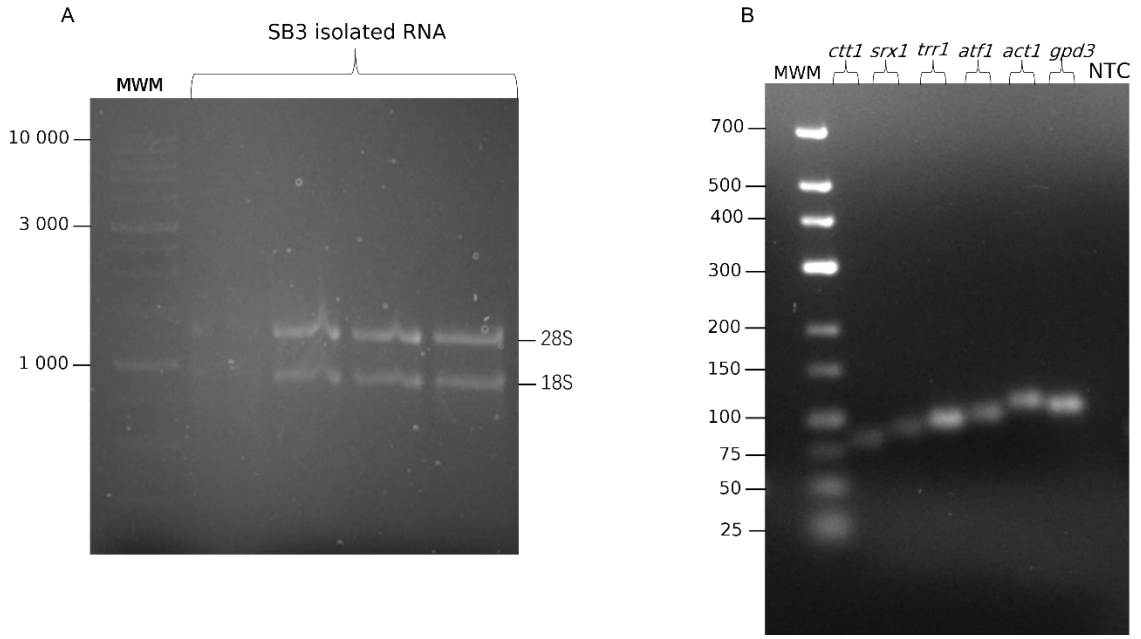

Figure 5.22: Isolated RNA from *S. pombe* cells and RT-qPCR of Pap1-regulated genes.
Total RNA was isolated, and the quality and purity were assessed on a 1% denaturing gel (A). cDNA was subsequently synthesised, and Pap1 target genes were amplified. The qPCR products were run on a 2% agarose gel (B) and the sizes were determined by the standard

curve (C). The products sizes were as follows, ctt1 (80 bp), srx1 (86 bp), trr1 (91 bp), atf1 (97 bp), act1 (109 bp) and gpd3 (105 bp).

5.4.5 Generation of native Pap1 antibodies

Epitope tagging offers several advantages to visualising proteins through immunofluorescence. This approach avoids the need for protein-specific antibodies which can save time and costs as there are many commercially available antibodies (Fritze and Anderson., 2000). Additionally, these tags often well engineered and generally highly specific as there is minimal cross-reactivity with other proteins. However, epitope tagging has been known to alter protein folding which can have impacts on the conclusions drawn from certain studies (Cao et al., 2017). In preliminary work and data shown by other groups, the introduction of a pk-tag to the Pap1 protein appears to affect the oxidation pattern of *S. pombe* cells exposed to hydrogen peroxide (Bozonet et al., 2005). One likely explanation is that the tag is preventing Pap1 from undergoing full oxidation in the presence of hydrogen peroxide this may further impact how we understand the dynamic responses of Pap1 to oxidative stress. To address this, we aimed to generate native Pap1 antibodies through chicken immunisation as there are no commercially available Pap1 antibodies.

The Pap1 protein was expressed in *E. coli* BL21 cells over a 24-hr period using IPTG induction (Figure 5.23A). The expression of Pap1 protein remained stable throughout the induction period. Subsequently, a three-hr induction period was selected, and larger samples were collected and purified using nickel affinity columns. The Pap1 protein eluted from the column at an imidazole concentration of 100 mM. However, at this concentration, additional lower molecular weight proteins also eluted. However, we observed a single Pap1 band eluted at an imidazole concentration of 150 mM. This concentration was used for purifying the Pap1 protein without the co-elution of contaminant bands. (Figure 5.23B). Unfortunately, the concentration of purified Pap1 protein was low and to overcome this limited protein yield we pooled samples together and concentrated Pap1 using PEG 20,000. We then assessed the concentrated protein on SDS-PAGE to ensure the quality of isolated Pap1 was maintained (Figure 5.23C). All protein concentrations were determined using a BSA standard curve (Figure S.23).

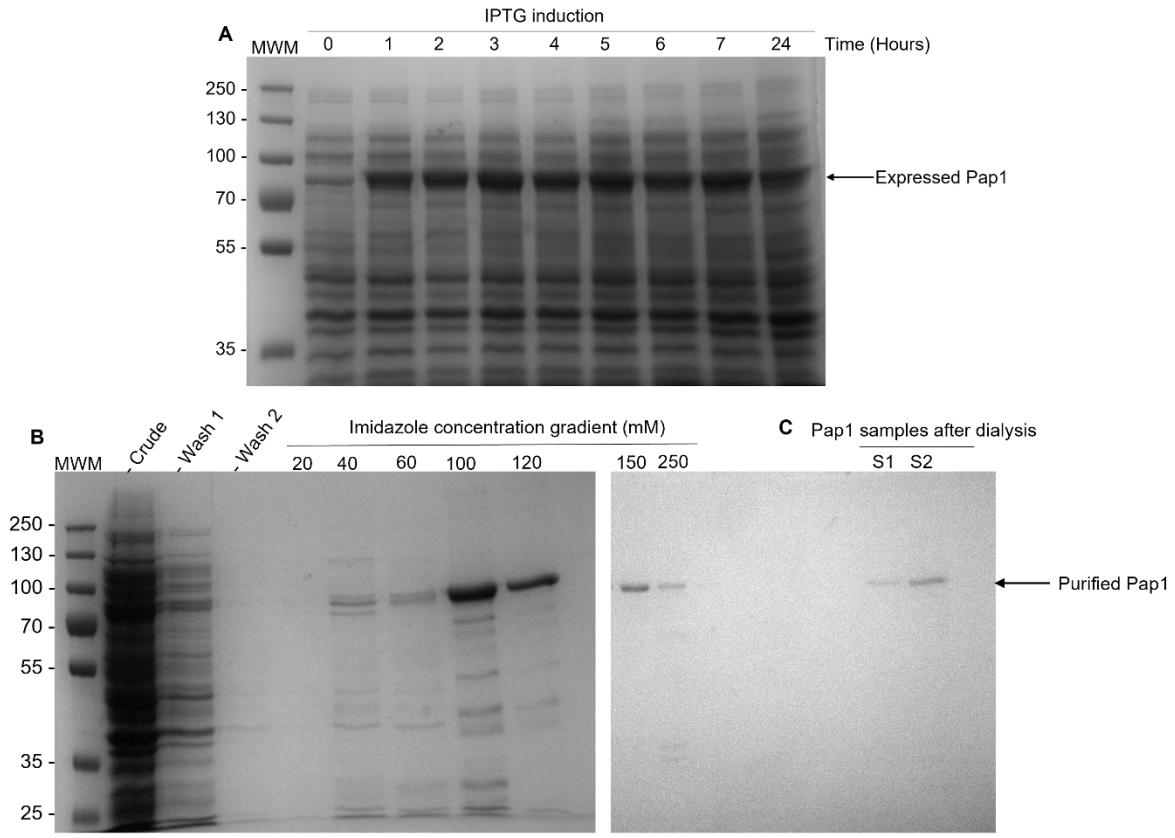

Figure 5.23: Optimal IPTG induction time for Pap1 expression, nickel affinity purification and concentration of Pap1 recombinant protein.

E. coli BL21 cells containing a pap1 insert were induced with IPTG over 24 hrs (A). An imidazole gradient (20-250 mM) was used to elute Pap1 (B). Purified Pap1 was pooled and concentrated using PEG 20 000 and checked by SDS-PAGE electrophoresis for purity (C).

To generate native Pap1 polyclonal antibodies, two hens (S1 and S2) were immunized with the purified Pap1 protein (Goldring & Coetzer, 2003). Total IgY was isolated from the egg yolks and stored at 4°C or further purified by AminoLink Coupling Resin to isolate polyclonal Pap1 antibodies (Figure 5.24A-B). The antibodies were obtained as different fractions eluted from the column. Preliminary tests were conducted to assess the antibodies' ability to detect Pap1 protein in a cell lysate or the purified Pap1 protein at two different dilutions, using four different antibody fractions.

The results indicated that the polyclonal antibodies had a stronger signal against the cell lysate compared to the purified antibody (Figure 5.24A-B). This suggests potential non-

specific binding, requiring further purification. Additionally, the antibodies would need validation through western blotting to confirm their specificity to Pap1.

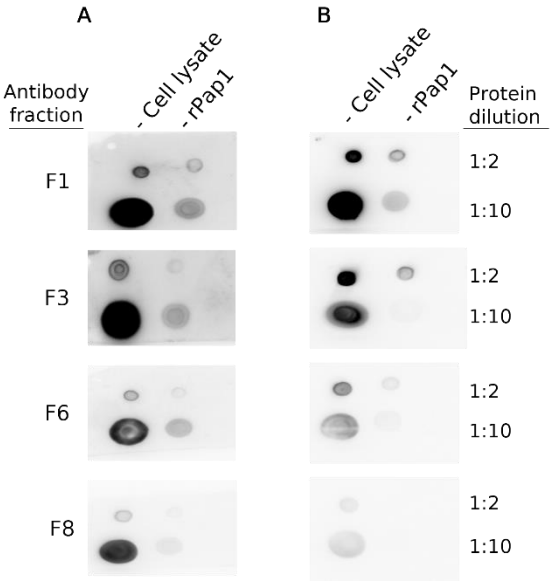

Figure 5.24: Assessment of polyclonal Pap1 antibodies against *S. pombe* cell lysate and purified Pap1 protein samples.

Native Pap1 antibodies were obtained by immunizing two hens (A-B). The cell lysate and purified Pap1 protein (rPap1) were diluted 1:2 and 1:10 and incubated with purified polyclonal Pap1 antibody fractions (F1, F3, F6, F8). The dot blots were visualized with HRP-conjugated anti-chicken secondary antibodies to a 1:10 000 dilution and visualized with chemiluminescence.

5.5 Discussion

In this chapter, we highlighted key experimental optimisations necessary for precise quantification of time-dependent redox signals. These optimisations involved determining the doubling rate of *S. pombe* cells for selecting an optimal sampling period, optimisation of western blotting protocols, ensuring robust quantification analysis of western blot data, exploring published transcriptomic data for insights into oxidative stress responses and how this is linked to signalling processes, and developing Pap1 polyclonal antibodies to better understand the oxidation pattern of Pap1.

To accurately capture the time-dependent parameters of redox signals, it was essential to monitor the dynamics of transcription factor activation. However, due to the known doubling rate of *S. pombe* in EMM medium (~3 hrs) (Petersen & Russell, 2022), time-course experiments with bolus amounts of hydrogen peroxide typically do not extend beyond 60 min. To assess these effects, we exposed fission yeast cells to 0.1-1 mM hydrogen peroxide and tracked the doubling time until stationary phase (Figure 5.2). Intriguingly, we observed an increase in the overall doubling time with hydrogen peroxide exposure. Notably, the cell number remained consistent for the first three hrs and only increased during the subsequent five hrs (Figure 5.2).

Previous studies in fission yeast have demonstrated that exposure to nitric oxide induces a stress response mechanistically linked to cell cycle stress (Guha Majumdar & Subramanian, 2019). Additionally, Pap1 has been implicated in the nitrosative stress response therefore, it is likely that oxidative stress would induce a similar response, inhibiting cellular replication. Indeed, even low levels of oxidative stress in cultured cells have been shown to inhibit key checkpoints during the cell cycle (Crawford & Davies, 1994; Pomatto & Davies, 2017a). Antioxidant proteins detoxify the cell during oxidative stress, potentially stalling cellular division. To this end normal cellular function shifts during oxidative stress responses and consequently longer sampling periods could enhance our understanding of dynamic cellular stress responses. We applied this to our western blotting experiments and selected a 2-hr time course for higher (>500 µM) hydrogen peroxide concentrations.

Western blotting, a widely employed technique for protein detection and semi-quantification (Rudyk & Eaton, 2014), comes with inherent limitations in terms of reproducibility, quantification, and specificity (Mishra et al., 2017). These challenges can be mitigated through careful optimization and the inclusion of appropriate controls (Rudyk & Eaton, 2014). In our study, to enhance reproducibility across experiments and biological replicates, we loaded 30 µg of total protein onto each gel lane, which was within the recommended range of 20-30 µg (Figure 5.3) (Mishra et al., 2017). Addressing challenges associated with quantifying protein levels on western blots, such as suboptimal primary-to-secondary antibody ratios and non-linear fluorescence or chemifluorescence detection ranges (Rudyk & Eaton, 2014), we optimized the primary antibody concentration to 1 µg/ml and the secondary antibody dilution to 1:50,000, resulting in reliable Pap1 detection (Figure 5.3).

One of our objectives was to assess the impact of these optimizations on signal quantification parameters. Our findings revealed that these optimizations significantly influenced signal quantification, emphasising the importance of considering such measures to obtain the most accurate dynamic signalling data (Figure 5.4, Figure 5.6). The importance of optimising western blotting was highlighted by a study using actin, a commonly found protein, where variations in densitometric values were observed between optimised and non-optimised western blots (Pillai-Kastoori et al., 2020).

Another consideration was determining the optimal method for deriving the signalling profile from the reduced and oxidized bands in the western blots and their effect on signalling parameters. Three methods were evaluated: the first involved calculating the Pap1 ratio by dividing oxidised Pap1 by the sum of oxidised and reduced Pap1. The second method involved dividing the oxidised Pap1 band by DTT-reduced Pap1 to account for Pap1 complexes at different molecular weights (Figure 5.8) (Mishra et al., 2017). However, this method could lead to an overestimation due to the higher intensity of oxidised bands compared to fully reduced DTT bands. The third method was to divide the oxidized protein by the total protein, but this resulted in a numerically small value which is challenging to validate (Figure 5.8) (Mishra et al., 2017). While these normalization options are valid, the DTT control served better as a loading control alongside total protein. However, the DTT and total protein controls were suboptimal for quantifying dynamic signalling data particularly for higher hydrogen peroxide concentrations.

Improving the specificity of western blotting often involves using protein-specific antibodies (Edfors et al., 2018), which are currently not commercially available for Pap1. Consequently, we generated Pap1 antibodies through recombinant protein expression and chicken immunization, enabling us to detect Pap1 in *S. pombe* cell lysates and against purified Pap1 protein (Figure 5.24). However, these antibodies require further testing to assess whether the pk-tag has any impact on the oxidation pattern of Pap1.

Oxidative stress response involves many cellular processes and can be observed as transcriptional changes (Chen et al., 2008). We conducted a transcriptomic analysis of *S. pombe* cells exposed to hydrogen peroxide and identified a coordinated response involving the upregulation and downregulation of more than 700 genes (Chen et al., 2008). This analysis provided insights into the overall dynamic stress response to hydrogen peroxide, offering starting points for exploring gene categories influenced in oxidative stress responses to varying doses of hydrogen peroxide (Figure 5.10-5.20). From this analysis we designed a RT-qPCR assay to determine if there was a link between the signalling profiles and gene expression.

In conclusion, implementing time-dependent quantification of the Tpx1/Pap1 signal necessitated careful consideration of growth conditions and optimisation of the western blotting protocol for reliable data collection. For studies investigating the effects of high doses of stress-inducing agents, we propose extending the sampling times. Moreover, optimising western blotting assays has a substantial impact on signal quantification, particularly when utilising reducing and total protein controls to generate signal profiles. Lastly, our observations indicate that the overall effect of oxidative stress on the transcriptome is complex, involving many pathways, and subcategorising genes into functions aids in selecting relevant genes for further analysis to elucidate the relationship between signal parameters and gene expression.

Chapter 6
Final Discussion

"When you can measure what you are speaking about, and express it in numbers, you know something about it; but when you cannot measure it, when you cannot express it in numbers, your knowledge is of a meagre and unsatisfactory kind" ~ Lord Calvin

The discovery that oxygen generates harmful by-products known as reactive oxygen species (ROS) and their association with aerobic respiration laid the foundation for the field of redox biology (Halliwell & Gutteridge, 2015). The implication that ROS led to the formation of free radicals that damaged cellular components culminated in the Free Radical Theory of Disease and Ageing (Harman, 1956). This theory evolved into the Oxidative Stress Theory when antioxidant molecules that detoxify the cellular environment from ROS were discovered. The foundation of the Oxidative Stress Theory is that an imbalance between antioxidants and ROS can lead to oxidative stress, resulting in disease progression (Cadenas & Sies, 1985). Further research revealed that ROS, including hydrogen peroxide, play integral roles in vital signalling processes such as cell proliferation, growth, and immune function. With the recognition of hydrogen peroxide's dual role in metabolism, lower peroxide concentrations are now understood to serve as positive signalling molecules associated with oxidative eustress, while higher peroxide concentrations are linked to oxidative distress (Sies & Jones, 2020). This understanding forms the basis of the Eustress/Distress Theory (Sies & Jones, 2020). An emerging area of interest within this theory is in dynamic signalling processes where information is transmitted through signalling molecules.

Although not generally appreciated within the redox biology field, the shape of the signalling profile captures a wealth of information such as the molecule activity, concentration and localisation over-time. Studying dynamics offers an opportunity to better understand a system in time rather than measuring static time-points (Purvis & Lahav, 2013). However, quantifying and comparing dynamic signalling profiles remains challenging due to a lack of standardised measures. In this study, we proposed a quantitative approach to quantify dynamic profiles in terms of area under the curve, signal amplitude, time, and duration. We explored the applicability of these measures in three experimental contexts.

Our first application was to quantify the Tpx1/Pap1 pathway in fission yeast in response to a number of oxidative stress scenarios. Here, we found that quantifying the dynamic profile, rather than just the oxidised Pap1 protein, demonstrated distinct responses to increasing doses of hydrogen peroxide. We then evaluated whether these responses in signal amplitude, time, and duration corresponded to unique gene expression patterns. We found that changes in signalling profiles encode information that triggers specific time-dependent transcriptional responses. The Pap1 pathway responded to the oxidant *t*-BOOH at a distinct signal time compared to the signal time for hydrogen peroxide response. These data suggest that the shape of the signalling profile encodes specific information, and the timing of the signal has distinct implications for the gene/protein expression outputs. We also found that these dynamics were shifted when the pathway was placed under combinatory stress or when pre-exposed to hydrogen peroxide. These measures allow for the quantitative assessment of these various stressors rather than a qualitative approach.

We then focused on quantifying the dynamics of genetically encoded redox sensors. There are several limitations associated with evaluating redox probes and the corresponding signalling data. First, being able to distinguish between different probes has been limited with current quantification methods. Second, establishing calibration curves for the upper and lower limits to external hydrogen peroxide concentrations is also challenging. We evaluated the redox probes HyPer7 and roGFP-Tsa2 in baker's yeast and obtained linear correlation curve responses to hydrogen peroxide for area under the curve and signal amplitude. These data could assess whether there was a proportional increase of the signal to increasing hydrogen peroxide concentrations and at what concentration points there is a weak signal, or a saturation effect of the signal. We were also able to assess the effect of gene deletions on the oxidation/reduction capacity of the cell.

In our third application we assessed the signalling dynamics of the NRF2/Keap1 pathway, in response to the oxidants DEM and tBHQ, which has been shown to be upregulated in cancer cells (Yamamoto et al., 2018). Two main effects were quantitatively evaluated, the effect of pre-exposure to different oxidant concentrations, and the timing of the pre-exposure scenarios to the NRF2 response. Quantifying the signalling profiles reduced the complexity of the data and signal analysis revealed that higher oxidant concentrations increased the signal amplitude, but longer pre-exposure periods resulted in a dampened NRF2 response. There was a decrease in signal time and duration with a 24 hr pre-exposure period when compared to naïve or an 8

hr adaption period. These data highlighted that pathway dynamics are important when attempting to modulate this pathway.

There were some limitations associated to quantifying dynamic signalling data. The first challenge was in generating these datasets as we used western blotting which is costly and time-consuming. Here, an attractive alternative involves using genetically encoded redox sensors to generate dynamic signalling data in a high throughput manner. Automating data analysis through the development of a software package to rapidly calculate signalling parameters could be facilitated with the assistance of AI (Hiroshima et al., 2020). These improvements could facilitate the generation of dynamic signalling databases, offering a platform to evaluate large signalling datasets to study emergent properties of signalling molecules over time.

To conclude, we successfully assessed dynamic redox signaling profiles across several applications within fission yeast, a novel undertaking in this field. This quantitative analytical approach represents a significant conceptual advance, enabling precise comparisons of oxidative stress effects. By simplifying the analysis of complex datasets, this method provided new insights into redox sensor data and the NRF2 signaling pathway. We believe this approach marks an important step toward understanding the role of dynamics in regulating the oxidative stress response in cell physiology and disease.

References

Alper, T. (1956). The Modification of Damage Caused by Primary Ionization of Biological Targets. In *Source: Radiation Research, 5(6),* 573–586. https://doi.org/10.2307/3570579

Anderson, C. M., Sonis, S. T., Lee, C. M., Adkins, D., Allen, B. G., Sun, W., Agarwala, S. S., Venigalla, M. L., Chen, Y., Zhen, W., Mould, D. R., Holmlund, J. T., Brill, J. M., & Buatti, J. M. (2018). Phase 1b/2a Trial of the Superoxide Dismutase Mimetic GC4419 to Reduce Chemoradiotherapy-Induced Oral Mucositis in Patients With Oral Cavity or Oropharyngeal Carcinoma. *International Journal of Radiation Oncology Biology Physics*, *100*(2), 427–435. https://doi.org/10.1016/j.ijrobp.2017.10.019

Antoniades, C., Bakogiannis, C., Tousoulis, D., Reilly, S., Zhang, M. H., Paschalis, A., Antonopoulos, A. S., Demosthenous, M., Miliou, A., Psarros, C., Marinou, K., Sfyras, N., Economopoulos, G., Casadei, B., Channon, K. M., & Stefanadis, C. (2010). Preoperative atorvastatin treatment in CABG patients rapidly improves vein graft redox state by inhibition of Rac1 and NADPH-oxidase activity. *Circulation*, *122*(11), 1–15. https://doi.org/10.1161/CIRCULATIONAHA.109.927376

Arkun, Y., & Yasemi, M. (2018). Dynamics and control of the ERK signaling pathway: Sensitivity, bistability, and oscillations. *PLoS ONE*, *13*(4), 1–24. https://doi.org/10.1371/journal.pone.0195513

Aslund, F., Zheng, M., Beckwith, J., & Storz, G. (1999). Regulation of the OxyR transcription factor by hydrogen peroxide and the cellular thiol--disulfide status. *Proceedings of the National Academy of Sciences*, *96*(11), 6161–6165. https://doi.org/10.1073/pnas.96.11.6161

Azevedo, D., Tacnet, F., Delaunay, A., Rodrigues-Pousada, C., & Toledano, M. B. (2003). Two redox centers within Yap1 for H_2O_2 and thiol-reactive chemicals signaling. *Free Radical Biology and Medicine*, *35*(8), 889–900. https://doi.org/10.1016/S0891-5849(03)00434-9

Bacq, Z. M., & Herve, A. (1951). Protection of mice against a lethal dose of x rays by cyanide, azide and malononitrile. *British Institude of Radiology*, *26*(287), 617–621. https://doi.org/10.1259/0007-1285-24-287-617

Baird, L., Swift, S., Llères, D., & Dinkova-Kostova, A. T. (2014). Monitoring Keap1-Nrf2 interactions in single live cells. In *Biotechnology Advances*, *32*(6), 1133–1144. https://doi.org/10.1016/j.biotechadv.2014.03.004

Bakhmutova-Albert, E. V., Yao, H., Denevan, D. E., & Richardson, D. E. (2010). Kinetics and mechanism of peroxymonocarbonate formation. *Inorganic Chemistry*, *49*(24), 11287–11296. https://doi.org/10.1021/ic1007389

Bardaweel, S. K., Gul, M., Alzweiri, M., Ishaqat, A., Alsalamat, H. A., & Bashatwah, R. M. (2018). Reactive oxygen species: The dual role in physiological and pathological conditions of the human body. *Eurasian Journal of Medicine*, *50*(3), 193–201. https://doi.org/10.5152/eurasianjmed.2018.17397

Baumgart, E., Fahimi, H. D., Stich, A., & Völkl, A. (1996). L-lactate dehydrogenase A4- and A3B isoforms are bona fide peroxisomal enzymes in rat liver: Evidence for involvement in intraperoxisomal NADH reoxidation. *Journal of Biological Chemistry*, *271*(7), 3846–3855. https://doi.org/10.1074/jbc.271.7.3846

Belousov, V. V., Fradkov, A. F., Lukyanov, K. A., Staroverov, D. B., Shakhbazov, K. S., Terskikh, A. V., & Lukyanov, S. (2006). Genetically encoded fluorescent indicator for intracellular hydrogen peroxide. *Nature Methods*, *3*(4), 281–286. https://doi.org/10.1038/nmeth866

Berndt, C., Buchanan, Bob. B., Lillig, C. H., & Sies, H. (2022). *Redox regulation of differentiation and de-differentiation* (C. Berndt & H. C. Lillig, Eds.; 1st ed.). Taylor and Francis Group. www.crcpress.com/Oxidative-Stress-and-Disease/book-series/CRCOXISTRDIS

Bersweiler, A., D'Autréaux, B., Mazon, H., Kriznik, A., Belli, G., Delaunay-Moisan, A., Toledano, M. B., & Rahuel-Clermont, S. (2017). A scaffold protein that chaperones a cysteine-sulfenic acid in H_2O_2 signaling. *Nature Chemical Biology*, *13*(8), 909–915. https://doi.org/10.1038/nchembio.2412

Bilan, D. S., & Belousov, V. V. (2016). HyPer Family Probes: State of the Art. *Antioxidants and Redox Signaling*, *24*(13), 731–751. https://doi.org/10.1089/ars.2015.6586

Bilan, D. S., Pase, L., Joosen, L., Gorokhovatsky, A. Y., Ermakova, Y. G., Gadella, T. W. J., Grabher, C., Schultz, C., Lukyanov, S., & Belousov, V. V. (2013). HyPer-3: A genetically

encoded H_2O_2 probe with improved performance for ratiometric and fluorescence lifetime imaging. *ACS Chemical Biology*, *8*(3), 535–542. https://doi.org/10.1021/cb300625g

Birben, E., Sahiner, U. M., Sackesen, C., Erzurum, S., & Kalayci, O. (2012). Oxidative Stress and Antioxidant Defense- review article. *World Allergy Organization Journal*, *5*, 9–19. https://doi.org/10.1097/WOX.0b013e3182439613

Bischoff, L. J. M., Kuijper, I. A., Schimming, J. P., Wolters, L., Braak, B. ter, Langenberg, J. P., Noort, D., Beltman, J. B., & van de Water, B. (2019a). A systematic analysis of Nrf2 pathway activation dynamics during repeated xenobiotic exposure. *Archives of Toxicology*, *93*(2), 435–451. https://doi.org/10.1007/s00204-018-2353-2

Biteau, B., Labarre, J., & Toledano, M. B. (2003). ATP-dependent reduction of cysteine-sulphinic acid by *S. cerevisiae* sulphiredoxin. *Nature*, *425*(6961), 977–980. https://doi.org/10.1038/nature02079

Boyland, E., & Sargent, S. (1951). The local greying of hair in mice treated with x rays and radiomimetic drugs. *British Journal of Cancer*, *5*(4), 433–440. https:// doi: 10.1038/bjc.1951.49

Bozonet, S. M., Findlay, V. J., Day, A. M., Cameron, J., Veal, E. A., & Morgan, B. A. (2005). Oxidation of a eukaryotic 2-Cys peroxiredoxin is a molecular switch controlling the transcriptional response to increasing levels of hydrogen peroxide. *Journal of Biological Chemistry*, *280*(24), 23319–23327. https://doi.org/10.1074/jbc.M502757200

Brieger, K., Schiavone, S., Miller, F. J., & Krause, K. H. (2012). Reactive oxygen species: From health to disease. *Swiss Medical Weekly*, *142*(1), w13659-w13659. https://doi.org/10.4414/smw.2012.13659

Brown, J. D., Day, A. M., Taylor, S. R., Tomalin, L. E., Morgan, B. A., & Veal, E. A. (2013). A peroxiredoxin promotes H_2O_2 signaling and oxidative stress resistance by oxidizing a thioredoxin family protein. *Cell Reports*, *5*(5), 1425–1435. https://doi.org/10.1016/j.celrep.2013.10.036

Cadenas, E., & Sies, H. (1985). Oxidative stress: excited oxygen species and enzyme activity. *Oxidative Stress*, *23*, 217–237. https://doi.org/https://doi.org/10.1016/0065-2571(85)90049-4

Calvo, I. A., Ayte, J., & Hidalgo, E. (2013). Reversible thiol oxidation in the H_2O_2-dependent activation of the transcription factor Pap1. *Journal of Cell Science*, *126*(10), 2279–2284. https://doi.org/10.1242/jcs.124370

Calvo, I. A., García, P., Ayté, J., & Hidalgo, E. (2012). The transcription factors Pap1 and Prr1 collaborate to activate antioxidant, but not drug tolerance, genes in response to H_2O_2. *Nucleic Acids Research*, *40*(11), 4816–4824. https://doi.org/10.1093/nar/gks141

Carter, W. O., Naryanan, P. K., & Robinson, J. P. (1994). Intracellular hydrogen peroxide and superoxide anion detection in endothelial cells. *Journal of Leukocyte Biology*, *55*(2), 253–258. https://doi.org/10.1002/jlb.55.2.253

Checa, J., & Aran, J. M. (2020). Reactive oxygen species: Drivers of physiological and pathological processes. *Journal of Inflammation Research*, *13*, 1057–1073. https://doi.org/10.2147/JIR.S275595

Chen, D., Toone, W. M., Mata, J., Lyne, R., Burns, G., Kivinen, K., Brazma, A., Jones, N., & Bähler, J. (2003). Global Transcriptional Responses of Fission Yeast to Environmental Stress. *Molecular Biology of the Cell*, *14*, 214–229. https://doi.org/10.1091/mbc.E02-08

Chen, D., Wilkinson, C. R., Watt, S., Penkett, C. J., Mark Toone, W., Jones, N., & Bähler, J. (2008). Multiple Pathways Differentially Regulate Global Oxidative Stress Responses in Fission Yeast. *Molecular Biology of the Cell*, *19*, 308–317. https://doi.org/10.1091/mbc.E07-08

Cox, A. G., Winterbourn, C. C., & Hampton, M. B. (2010). Mitochondrial peroxiredoxin involvement in antioxidant defence and redox signalling. In *Biochemical Journal*, *425*(2), 313–325. https://doi.org/10.1042/BJ20091541

Crawford, D. R., & Davies, K. J. A. (1994). Adaptive Response and Oxidative Stress. *Environmental Health Perspectives*, *102*, 25–28. https://doi.org/10.1289/ehp.94102s1025

Davies, M. J., Hawkins, C. L., Pattison, D. I., & Rees, M. D. (2008). Mammalian heme peroxidases: From molecular mechanisms to health implications. *Antioxidants and Redox Signaling*, *10*(7), 1199–1234. https://doi.org/10.1089/ars.2007.1927

Day, A. M., Brown, J. D., Taylor, S. R., Rand, J. D., Morgan, B. A., & Veal, E. A. (2012). Inactivation of a Peroxiredoxin by Hydrogen Peroxide Is Critical for Thioredoxin-Mediated

Repair of Oxidized Proteins and Cell Survival. *Molecular Cell*, *45*(3), 398–408. https://doi.org/10.1016/j.molcel.2011.11.027

Day, A. M., & Veal, E. A. (2010). Hydrogen peroxide-sensitive cysteines in the Sty1 MAPK regulate the transcriptional response to oxidative stress. *Journal of Biological Chemistry*, *285*(10), 7505–7516. https://doi.org/10.1074/jbc.M109.040840

de Cubas, L., Pak, V. V., Belousov, V. V., Ayté, J., & Hidalgo, E. (2021). The mitochondria-to-cytosol H_2O_2 gradient is caused by peroxiredoxin-dependent cytosolic scavenging. *Antioxidants*, *10*(5), 731. https://doi.org/10.3390/antiox10050731

Deledda, A., Annunziata, G., Tenore, G. C., Palmas, V., Manzin, A., & Velluzzi, F. (2021). Diet-derived antioxidants and their role in inflammation, obesity and gut microbiota modulation. *Antioxidants*, *10*(5), 708. https://doi.org/10.3390/antiox10050708

Domènech, A., Ayté, J., Antunes, F., & Hidalgo, E. (2018). Using in vivo oxidation status of one- and two-component redox relays to determine H_2O_2 levels linked to signaling and toxicity. *BMC Biology*, *16*(1), 1–15. https://doi.org/10.1186/s12915-018-0523-6

Dyson, H. J., Tennant, L. L., & Holmgrens, A. (1991). Proton-Transfer Effects in the Active-Site Region of *Escherichia coli* Thioredoxin Using Two-Dimensional H NMR. *Biochemistry*, *30*(17), 4262–4268. https://doi.org/https://doi.org/10.1021/bi00231a023

Edfors, F., Hober, A., Linderbäck, K., Maddalo, G., Azimi, A., Sivertsson, Å., Tegel, H., Hober, S., Szigyarto, C. A. K., Fagerberg, L., von Feilitzen, K., Oksvold, P., Lindskog, C., Forsström, B., & Uhlen, M. (2018). Enhanced validation of antibodies for research applications. *Nature Communications*, *9*(1), 4130. https://doi.org/10.1038/s41467-018-06642-y

Eidelman, R. S., Hollar, D., Hebert, P. R., Lamas, G. A., & Hennekens, C. H. (2004). Randomized trials of vitamin E in the treatment and prevention of cardiovascular disease. *Archives of Internal Medicine*, *164*(14), 1552–1556. https://doi.org/10.1001/archinte.164.14.1552

Eskin, N. A. M., & Przybylski R. (2001). *Antioxidants and shelf life of foods*. CRC press.

Espinosa-Diez, C., Miguel, V., Mennerich, D., Kietzmann, T., Sánchez-Pérez, P., Cadenas, S., & Lamas, S. (2015). Antioxidant responses and cellular adjustments to oxidative stress. *Redox Biology*, *6*, 183–197. https://doi.org/10.1016/j.redox.2015.07.008

Fenton, M. A. (1894). Oxidation of tartaric acid in presence of iron. *Journal of the Chemical Society*, *65*, 899-910

Fernandes, A. P., & Holmgren, A. (2004). Glutaredoxins: Glutathione-Dependent Redox Enzymes with Functions Far Beyond a Simple Thioredoxin Backup System. *Antioxidants and Redox Signalling*, *6*(1), 63–74. https://doi.org/https://doi.org/10.1089/152308604771978354

Ferrer-Sueta, G., Manta, B., Botti, H., Radi, R., Trujillo, M., & Denicola, A. (2011). Factors affecting protein thiol reactivity and specificity in peroxide reduction. *Chemical Research in Toxicology*, *24*(4), 434–450. https://doi.org/10.1021/tx100413v

Finikova, O. S., Troxler, T., Senes, A., DeGrado, W. F., Hochstrasser, R. M., & Vinogradov, S. A. (2007). Energy and electron transfer in enhanced two-photon-absorbing systems with triplet cores. *Journal of Physical Chemistry*, *111*(30), 6977–6990. https://doi.org/10.1021/jp071586f

Firuzi, O., Miri, R., Tavakkoli, M., & Saso, L. (2011). Antioxidant Therapy: Current Status and Future Prospects. *Current Medicinal Chemistry*, *18*(25), 3871–3888. https://doi.org/10.2174/092986711803414368

Fita, I., & Rossmann, M. G. (1985). The Active Center of Catalase. *Journal of molecular biology*, *185*(1), 21-37. https://doi.org/10.1016/0022-2836(85)90180-9

Flieger, J., Flieger, W., Baj, J., & Maciejewski, R. (2021). Antioxidants: Classification, natural sources, activity/capacity measurements, and usefulness for the synthesis of nanoparticles. *Materials*, *14*(15), 4135. https://doi.org/10.3390/ma14154135

Flohé, L. (2020). Looking back at the early stages of redox biology. *Antioxidants*, *9*(12), 1–39. https://doi.org/10.3390/antiox9121254

Flohé, L., Brigelius-Flohé, R., Saliou, C., Traber, M. G., & Packer, L. (1997). Redox regulation of NF-KAPPA B activation. *Free Radical Biology and Medicine*, *22*(6), 1115–1126. https://doi.org/10.1016/S0891-5849(96)00501-1

Forman, H. J., Ursini, F., & Maiorino, M. (2014). An overview of mechanisms of redox signaling. *Journal of Molecular and Cellular Cardiology*, *73*, 2–9. https://doi.org/10.1016/j.yjmcc.2014.01.018

Forman, H. J., & Zhang, H. (2021). Targeting oxidative stress in disease: promise and limitations of antioxidant therapy. *Nature Reviews Drug Discovery*, *20*(9), 689–709. https://doi.org/10.1038/s41573-021-00233-1

Fourquet, S., Guerois, R., Biard, D., & Toledano, M. B. (2010). Activation of NRF2 by nitrosative agents and H_2O_2 involves KEAP1 disulfide formation. *Journal of Biological Chemistry*, *285*(11), 8463–8471. https://doi.org/10.1074/jbc.M109.051714

Gallogly, M. M., & Mieyal, J. J. (2007). Mechanisms of reversible protein glutathionylation in redox signaling and oxidative stress. *Current Opinion in Pharmacology*, *7*(4), 381–391. https://doi.org/10.1016/j.coph.2007.06.003

George, P., & Irivine, D. H. (1954). Free radical production in oxidation-reduction reactions of peroxidase, catalase and methyoglobin. *The Chemistry of Biological After-Effects of Ultraviolet and Ionizing Radiations*, *27*(314), 131–137. https://doi.org/10.1259/0007-1285-27-314-131

Gerschman, R., Gilbert, D. L., Nye, S. W., Dwyer, P., & Fenna, W. 0. (1954). Oxygen Poisoning and X-irradiation: A Mechanism in Common1. *Science*, *119*(1), 1–4. https://DOI: 10.1126/science.119.3097.623

Gladyshev, V. N. (2014). The free radical theory of aging is dead. Long live the damage theory! *Antioxidants and Redox Signaling*, *20*(4), 727–731. https://doi.org/10.1089/ars.2013.5228

Go, Y. M., Chandler, J. D., & Jones, D. P. (2015). The cysteine proteome. *Free Radical Biology and Medicine*, *84*, 227–245. https://doi.org/10.1016/j.freeradbiomed.2015.03.022

Goldring, J. P. D., & Coetzer, T. H. T. (2003). Isolation of chicken immunoglobulins (IgY) from egg yolk. *Biochemistry and Molecular Biology Education*, *31*(3), 185–187. https://doi.org/10.1002/bmb.2003.494031030213

Gough, D. R., & Cotter, T. G. (2011). Hydrogen peroxide: A Jekyll and Hyde signalling molecule. *Cell Death and Disease*, *2*(10), e213-8. https://doi.org/10.1038/cddis.2011.96

Guha Majumdar, A., & Subramanian, M. (2019). Hydroxychavicol from Piper betle induces apoptosis, cell cycle arrest, and inhibits epithelial-mesenchymal transition in pancreatic cancer cells. *Biochemical Pharmacology*, *166*, 274–291. https://doi.org/10.1016/j.bcp.2019.05.025

Guha, S., López-Maury, L., Shaw, M., Bähler, J., Norbury, C. J., & Agashe, V. R. (2011). Transcriptional and cellular responses to defective mitochondrial proteolysis in fission yeast. *Journal of Molecular Biology*, *408*(2), 222–237. https://doi.org/10.1016/j.jmb.2011.02.044

Gulaboski, R., Mirčeski, V., Kappl, R., Hoth, M., & Bozem, M. (2019). Quantification of Hydrogen Peroxide by Electrochemical Methods and Electron Spin Resonance Spectroscopy. *Journal of The Electrochemical Society*, *166*(8), G82–G101. https://doi.org/10.1149/2.1061908jes

Gulshan, K., Lee, S. S., & Moye-Rowley, W. S. (2011). Differential oxidant tolerance determined by the key transcription factor Yap1 is controlled by levels of the Yap1-binding protein, Ybp1. *Journal of Biological Chemistry*, *286*(39), 34071–34081. https://doi.org/10.1074/jbc.M111.251298

Gutscher, M., Sobotta, M. C., Wabnitz, G. H., Ballikaya, S., Meyer, A. J., Samstag, Y., & Dick, T. P. (2009). Proximity-based protein thiol oxidation by H_2O_2 -scavenging peroxidases. *Journal of Biological Chemistry*, *284*(46), 31532–31540. https://doi.org/10.1074/jbc.M109.059246

Halliwell, B. A., & Gutteridge, J. M. C. (2015). *Free radicals in biology and medicine* (5th ed.). Oxford University Press.

Hanschmann, E.-M., Godoy, J. R., Berndt, C., Hudemann, C., & Lillig, C. H. (2013). Thioredoxins, Glutaredoxins, and Peroxiredoxins—Molecular Mechanisms and Health Significance: from Cofactors to Antioxidants to Redox Signaling. *Antioxidants & Redox Signaling*, *19*(13), 1539–1605. https://doi.org/10.1089/ars.2012.4599

Hansen, A. S., Hao, N., & O'shea, E. K. (2015). High-throughput microfluidics to control and measure signaling dynamics in single yeast cells. *Nat Protoc.*, *10*(8), 1181–1197. https://doi.org/10.1038/nprot.2015.079

Hansen, A. S., & O'Shea, E. K. (2016). Encoding four gene expression programs in the activation dynamics of a single transcription factor. *Current Biology*, *26*, 269–271. https://doi.org/10.1016/j

Hao, N., & O'Shea, E. K. (2012). Signal-dependent dynamics of transcription factor translocation controls gene expression. *Nature Structural and Molecular Biology*, *19*(1), 31–40. https://doi.org/10.1038/nsmb.2192

Harman, D. (1956). *Aging: A theory based on free radical and radiation chemistry*, *2*(1), 1-5. https://escholarship.org/uc/item/3w86c4g7

He, L., He, T., Farrar, S., Ji, L., Liu, T., & Ma, X. (2017). Antioxidants Maintain Cellular Redox Homeostasis by Elimination of Reactive Oxygen Species. *Cellular Physiology and Biochemistry*, *44*(2), 532–553. https://doi.org/10.1159/000485089

Heinrich, R., Neel, B. G., & Rapoport, T. A. (2002). Mathematical models of protein kinase signal transduction. *Molecular Cell*, *9*(5), 957–970. https://doi.org/10.1016/S1097-2765(02)00528-2

Herrero, E., & De La Torre-Ruiz, M. A. (2007). Monothiol glutaredoxins: A common domain for multiple functions. *Cellular and Molecular Life Sciences*, *64*(12), 1518–1530. https://doi.org/10.1007/s00018-007-6554-8

Hiroshima, M., Yasui, M., & Ueda, M. (2020). Large-scale single-molecule imaging aided by artificial intelligence. *Microscopy*, *69*(2), 69–78. https://doi.org/10.1093/jmicro/dfz116

Holmgren, A. (1976). Hydrogen donor system for Escherichia coli ribonucleoside-diphosphate reductase dependent upon glutathione. *Biochemistry*, *73*(7), 2275-2279. https://doi.org/10.1073/pnas.73.7.2275

Holmgren, A. (1985). Glutaredoxin from *Escherichia coli* and Calf Thymus. *Methods in Enzymology*, *113*, 525–540. https://doi.org/10.1016/S0076-6879(85)13071-5

Holmström, K. M., & Finkel, T. (2014). Cellular mechanisms and physiological consequences of redox-dependent signalling. *Nature Reviews Molecular Cell Biology*, *15*(6), 411–421. https://doi.org/10.1038/nrm3801

Hornberg, J. J., Bruggeman, F. J., Binder, B., Geest, C. R., Bij De Vaate, A. J. M., Lankelma, J., Heinrich, R., & Westerhoff, H. V. (2005). Principles behind the multifarious control of signal transduction: ERK phosphorylation and kinase/phosphatase control. *FEBS Journal*, *272*(1), 244–258. https://doi.org/10.1111/j.1432-1033.2004.04404.x

Imai, H., Graham, D. I., Masayasu, H., & Macrae, I. M. (2002). Antioxidant ebselen reduces oxidative damage in focal cerebral ischemia. *Free Radical Biology and Medicine*, *34*(1), 56–63. https://doi.org/10.1016/S0891-5849(02)01180-2

Imlay, J. A. (2013). The molecular mechanisms and physiological consequences of oxidative stress: Lessons from a model bacterium. *Nature Reviews Microbiology*, *11*(7), 443–454. https://doi.org/10.1038/nrmicro3032

Isenberg, I., & Szent-Gyorgyi. (1958). Free radical formation in riboflavin complexes. *Biochemistry*, *44*, 857–862. https://doi.org/10.1073/pnas.44.9.857

Ivanova, D. G., & Yankova, T. M. (2013). The free radical theory of aging in search of a strategy for increasing life span. *Folia Medica*, *55*(1), 33–41. https://doi.org/10.2478/folmed-2013-0003

Jang, H. H., Lee, K. O., Chi, Y. H., Jung, B. G., Park, S. K., Park, J. H., Lee, J. R., Lee, S. S., Moon, J. C., Yun, J. W., Choi, Y. O., Kim, Y. W., Kang, J. S., Cheong, G., Yun, D., Rhee, S. G., Cho, M. J., & Lee, S. Y. (2004). Two Enzymes in One: Two Yeast Peroxiredoxins Display Oxidative Stress-Dependent Switching from a Peroxidase to a Molecular Chaperone Function. *Cell*, *117*, 625–635. https://doi.org/10.1016/j.cell.2004.05.002

Jannatifar, R., Parivar, K., Roodbari, N. H., & Nasr-Esfahani, M. H. (2020). The effect of N-acetyl-cysteine on NRF 2 antioxidant gene expression in asthenoteratozoospermia men: A clinical trial study. *International Journal of Fertility and Sterility*, *14*(3), 171–175. https://doi.org/10.22074/ijfs.2020.44411

Jara, M., Vivancos, A. P., Calvo, I. A., Moldó, A., Sansó, M., & Hidalgo, E. (2007). The Peroxiredoxin Tpx1 Is Essential as a H_2O_2 Scavenger during Aerobic Growth in Fission Yeast. *Molecular Biology of the Cell*, *18*, 2288–2295. https://doi.org/10.1091/mbc.E06

Jensen, P. K. (1966). Antimycin-insensitive oxidation of succinate and reduced nicotinamide-adenine dinucleotide in electron-transport particles. *Biochimica et Biophysica Acta*, *122*, 157–166. https://doi.org/10.1016/0926-6593(66)90057-9

Kaloriti, D., Jacobsen, M., Yin, Z., Patterson, M., Tillmann, A., Smith, D. A., Cook, E., You, T., Grimm, M. J., Bohovych, I., Grebogi, C., Segal, B. H., Gow, N. A. R., Haynes, K., Quinn, J., & Brown, A. J. P. (2014). Mechanisms underlying the exquisite sensitivity of *Candida albicans* to combinatorial cationic and oxidative stress that enhances the potent

fungicidal activity of phagocytes. *MBio*, *5*(4), e01334-14. https://doi.org/10.1128/mbio.01334-14

Karlenius, T. C., & Tonissen, K. F. (2010). Thioredoxin and cancer: A role for thioredoxin in all states of tumor oxygenation. *Cancers*, *2*(2), 209–232. https://doi.org/10.3390/cancers2020209

Kaul, S., Kanthasamy, A., Kitazawa, M., Anantharam, V., & Kanthasamy, A. G. (2003). Caspase-3 dependent proteolytic activation of protein kinase Cδ mediates and regulates 1-methyl-4-phenylpyridinium (MPP+)-induced apoptotic cell death in dopaminergic cells: Relevance to oxidative stress in dopaminergic degeneration. *European Journal of Neuroscience*, *18*(6), 1387–1401. https://doi.org/10.1046/j.1460-9568.2003.02864.x

Kawagishi, H., & Finkel, T. (2014). ROS and disease: Finding the right balance. *Nature Medicine*, *20*(7), 711–713. https://doi.org/10.1038/nm.3625

Keilin, D., & Hartree, E. F. (1939). Cytochrome and cytochrome oxidase. *J. Chem. Soc. 127*(4), 167–191. https://doi.org/10.1098/rspb.1939.0016

Kim, K., Kim, I. H., Lee, K. Y., Rhee, S. G., & Stadtman, E. R. (1988). The isolation and purification of a specific 'protector' protein which inhibits enzyme inactivation by a Thiol/Fe(III)/O2 mixed-function oxidation system. *Journal of Biological Chemistry*, *263*(10), 4704–4711. https://doi.org/10.1016/s0021-9258(18)68840-4

Kim, S. O., Merchant, K., Nudelman, R., Beyer, W. F., Keng, T., Deangelo, J., Hausladen, A., & Stamler, J. S. (2002). OxyR: A Molecular Code for Redox-Related Signaling. *Cell*, *109*, 383–396. https://doi.org/10.1016/S0092-8674(02)00723-7

Klomsiri, C., Karplus, P. A., & Poole, L. B. (2011). Cysteine-Based Redox Switches in Enzymes. *Antioxidants and Redox Signals*, *14*, 1065–1077. www.liebertonline.com=ars

Knoefler, D., Thamsen, M., Koniczek, M., Niemuth, N. J., Diederich, A. K., & Jakob, U. (2012). Quantitative In Vivo Redox Sensors Uncover Oxidative Stress as an Early Event in Life. *Molecular Cell*, *47*(5), 767–776. https://doi.org/10.1016/j.molcel.2012.06.016

Kos, I., Patterson, M. J., Znaidi, S., Kaloriti, D., da Silva Dantas, A., Herrero-de-Dios, C. M., d'Enfert, C., Brown, A. J. P., & Quinn, J. (2016). Mechanisms underlying the delayed activation of the cap1 transcription factor in *Candida Albicans* following combinatorial

oxidative and cationic stress important for phagocytic potency. *MBio*, *7*(2), 1–15. https://doi.org/10.1128/mBio.00331-16

Kritsiligkou, P., Bosch, K., Shen, T. K., Meurer, M., Knop, M., & Dick, T. P. (2023). Proteome-wide tagging with an H_2O_2 biosensor reveals highly localized and dynamic redox microenvironments. *PNAS*, *120*(48), 1–9. https://doi.org/10.1073/pnas.2314043120

Kritsiligkou, P., Shen, T. K., & Dick, T. P. (2021). A comparison of Prx- And OxyR-based H_2O_2 probes expressed in *S. cerevisiae*. *Journal of Biological Chemistry*, *297*(1). https://doi.org/10.1016/j.jbc.2021.100866

Kudo, N., Taoka, H., Toda, T., Yoshida, M., & Horinouchi, S. (1999). A novel nuclear export signal sensitive to oxidative stress in the fission yeast transcription factor Pap1. *Journal of Biological Chemistry*, *274*(21), 15151–15158. https://doi.org/10.1074/jbc.274.21.15151

Kuge, S., & Jones, N. (1994). YAP1 dependent activation of TRX2 is essential for the response of *Saccharomyces cerevisiae* to oxidative stress by hydroperoxides. *EMBO Journal*, *13*(3), 655–664. https://doi.org/10.1002/j.1460-2075.1994.tb06304.x

Kullik, I., Stevens, J., Toledano, M. B., & Storz, G. (1995). Mutational Analysis of the Redox-Sensitive Transcriptional Regulator OxyR: Regions Important for DNA Binding and Multimerization. *Journal of Bacteriology*, *177*(5), 1285–1291. https://journals.asm.org/journal/jb

Lahav, G., Rosenfeld, N., Sigal, A., Geva-Zatorsky, N., Levine, A. J., Elowitz, M. B., & Alon, U. (2004). Dynamics of the p53-Mdm2 feedback loop in individual cells. *Nature Genetics*, *36*(2), 147–150. https://doi.org/10.1038/ng1293

Lasick, K. A., Jose, E., Samayoa, A. M., Shanks, L., Pond, K. W., Thorne, C. A., & Paek, A. L. (2023). FOXO nuclear shuttling dynamics are stimulus-dependent and correspond with cell fate. *Molecular Biology of the Cell*, *34*(3), 1–11. https://doi.org/10.1091/mbc.E22-05-0193

Laurent, T. C., Colleen, E., & Reichard~, P. (1964). Enzymatic Synthesis of Deoxyribonucleotides. *The Journal of Biological Chemistry*, *239*(10), 3436–3444. www.jbc.org

Leak, R. K., Li, P., Zhang, F., Sulaiman, H. H., Weng, Z., Wang, G., Anne Stetler, R., Shi, Y., Cao, G., Gao, Y., & Chen, J. (2015). Apurinic/apyrimidinic endonuclease 1 upregulation

reduces oxidative DNA damage and protects hippocampal neurons from ischemic injury. *Antioxidants and Redox Signaling*, *22*(2), 135–148. https://doi.org/10.1089/ars.2013.5511

Ledo, A., Fernandes, E., Salvador, A., Laranjinha, J., & Barbosa, R. M. (2022). In vivo hydrogen peroxide diffusivity in brain tissue supports volume signaling activity. *Redox Biology*, *50*, 102250. https://doi.org/10.1016/j.redox.2022.102250

Lee, D., Ming-Jing Xu, I., Kung-Chun Chiu, D., Leibold, J., Pui-Wah Tse, A., Hao-Ran Bao, M., Wai-Hin Yuen, V., Yuen-Ki Chan, C., Kit-Ho Lai, R., Wai-Ching Chin, D., For-Fan Chan, D., Cheung, T.-T., Chok, S.-H., Wong, C.-M., Lowe, S. W., Oi-Lin Ng, I., & Chak-Lui Wong, C. (2019). Induction of oxidative stress through inhibition of thioredoxin reductase, Is an effective therapeutic approach for Hepatocellular carcinoma. *Hepatology*, *69*(4), 1768–1786. https://doi.org/10.1002/hep.30467/suppinfo

Lee, S. Y., Lee, H. S., Kim, E. Y., Ko, J. J., Yoon, T. K., Lee, W. S., & Lee, K. A. (2013). Thioredoxin-interacting protein regulates glucose metabolism and affects cytoplasmic streaming in mouse oocytes. *PLoS ONE*, *8*(8), e70708. https://doi.org/10.1371/journal.pone.0070708

Lee, T. K., Denny, E. M., Sanghvi, J. C., Gaston, J. E., Maynard, N. D., Hughey, J. J., & Covert, M. W. (2009). A noisy paracrine signal determines the cellular NF-κB response to lipopolysaccharide. *Science Signaling*, *2*(93), 1–18. https://doi.org/10.1126/scisignal.2000599

Lennicke, C., & Cochemé, H. M. (2020). Redox signalling and ageing: Insights from Drosophila. *Biochemical Society Transactions*, *48*(2), 367–377. https://doi.org/10.1042/BST20190052

Lillig, C. H., & Berndt, C. (2013). Glutaredoxins in thiol/disulfide exchange. *Antioxidants and Redox Signaling*, *18*(13), 1654–1665. https://doi.org/10.1089/ars.2012.5007

Love, J. D., Vivino, A. A., & Minton', K. W. (1986). Hydrogen Peroxide Toxicity May Be Enhanced by Heat Shock Gene Induction in Drosophila. *Journal of Cellular Physiology*, *126*, 60–68.https://doi.org/10.1002/jcp.1041260109

Lukyanov, K. A., & Belousov, V. V. (2014). Genetically encoded fluorescent redox sensors. *Biochimica et Biophysica Acta - General Subjects*, *1840*(2), 745–756. https://doi.org/10.1016/j.bbagen.2013.05.030

Lurias, S. E., & Delbrock, M. (1943). Mutations of bacteria from virus sensitivity to virus resistance. *Genetics*, *28*, 491–511. https://doi: 10.1093/genetics/28.6.491

Mamta, M., Misra, K., Dhillon, G. S., Brar, S. K., & Verma, M. (2014). *Antioxidants*. Springer.

Margaritelis, N. V., Chatzinikolaou, P. N., Chatzinikolaou, A. N., Paschalis, V., Theodorou, A. A., Vrabas, I. S., Kyparos, A., & Nikolaidis, M. G. (2022). The redox signal: A physiological perspective. *IUBMB Life*, *74*(1), 29–40. https://doi.org/10.1002/iub.2550

Markvicheva, K. N., Bilan, D. S., Mishina, N. M., Gorokhovatsky, A. Y., Vinokurov, L. M., Lukyanov, S., & Belousov, V. V. (2011). A genetically encoded sensor for H_2O_2 with expanded dynamic range. *Bioorganic and Medicinal Chemistry*, *19*(3), 1079–1084. https://doi.org/10.1016/j.bmc.2010.07.014

Matsui, M., Oshima, M., Oshima, H., Takaku, K., Maruyama, T., Yodoi, J., & Taketo, M. M. (1996). Rapid communication Early Embryonic Lethality Caused by Targeted Disruption of the Mouse Thioredoxin Gene. *In developmental biology*, *178(*1), 179-185. https://doi.org/10.1006/dbio.1996.0208

Matsuzaki, S., Szweda, P. A., Szweda, L. I., & Humphries, K. M. (2009). Regulated production of free radicals by the mitochondrial electron transport chain: Cardiac ischemic preconditioning. *Advanced Drug Delivery Reviews*, *61*(14), 1324–1331. https://doi.org/10.1016/j.addr.2009.05.008

Maurel, A., Hernandez, C., Kunduzova, O., Bompart, G., Cambon, C., Parini, A., & Francé, B. (2003). Age-dependent increase in hydrogen peroxide production by cardiac monoamine oxidase A in rats. *Am J Physiol Heart Circ Physiol*, *284*, 1460–1467. https://doi.org/10.1152/ajpheart.00700.2002.-Oxidative

McCord, J. M., & Fridovich, I. (1969). Superoxide Dismutase an enzymic function for erythrocuprein (hemocuprein). *Journal of biological chemistry*, *244*(22), 6049-6055.

Mcgroarty, E., Hsieh, B., Wied, D. M., Gee, R., & Tolbert, N. E. (1974). Alpha Hydroxy Acid Oxidation by Peroxisomes. *Archives of Biochemistry and Biophysics*, *161*, 194–210. https://doi.org/10.1016/0003-9861(74)90251-3

Meyer, A. J., & Dick, T. P. (2016). Fluorescent Protein-Based Redox Probes. *Antioxidant and Redox Signaling*, *13*(5), 621-650. https://doi.org/10.1089/ars.2009.2948

Miller, C. G., & Schmidt, E. E. (2019). Disulfide reductase systems in liver. *British Journal of Pharmacology*, *176*, 532–543. https://doi.org/10.1111/bph.v176.4/issuetoc

Mishra, M., Tiwari, S., & Gomes, A. V. (2017). Protein purification and analysis: Next generation western blotting techniques. *Expert Review of Proteomics*, *14*(11), 1037–1053. Taylor and Francis Ltd. https://doi.org/10.1080/14789450.2017.1388167

Morgan, B. A., & Veal, E. A. (2007). Functions of Typical 2-Cys Peroxiredoxins in Yeast. *Peroxiredoxin system*, *44*, 253–265. https://doi.org/10.1007/978-1-4020-6051-9_12

Morgan, B., Van Laer, K., Owusu, T. N. E., Ezeriņa, D., Pastor-Flores, D., Amponsah, P. S., Tursch, A., & Dick, T. P. (2016). Real-time monitoring of basal H_2O_2 levels with peroxiredoxin-based probes. *Nature Chemical Biology*, *12*(6), 437–443. https://doi.org/10.1038/nchembio.2067

Morgan, M. J., & Liu, Z. G. (2011). Crosstalk of reactive oxygen species and NF-κB signaling. *Cell Research*, *21*(1), 103–115. https://doi.org/10.1038/cr.2010.178

Mousa, A. M., El-Sammad, N. M., Abdel-Halim, A. H., Anwar, N., Khalil, W. K. B., Nawwar, M., Hashim, A. N., Elsayed, E. A., & Hassan, S. K. (2019). Lagerstroemia speciosa (L.) pers leaf extract attenuates lung tumorigenesis via alleviating oxidative stress, inflammation and apoptosis. *Biomolecules*, *9*(12), 871. https://doi.org/10.3390/biom9120871

Murphy, M. P., Bayir, H., Belousov, V., Chang, C. J., Davies, K. J. A., Davies, M. J., Dick, T. P., Finkel, T., Forman, H. J., Janssen-Heininger, Y., Gems, D., Kagan, V. E., Kalyanaraman, B., Larsson, N. G., Milne, G. L., Nyström, T., Poulsen, H. E., Radi, R., Van Remmen, H., … Halliwell, B. (2022). Guidelines for measuring reactive oxygen species and oxidative damage in cells and in vivo. *Nature Metabolism*, *4*(6), 651–662. https://doi.org/10.1038/s42255-022-00591-z

Nakamura, T., Keep, R. F., Hua, Y., Hoff, J. T., & Xi, G. (2005). Oxidative DNA injury after experimental intracerebral hemorrhage. *Brain Research*, *1039*(1–2), 30–36. https://doi.org/10.1016/j.brainres.2005.01.036

Netto, L. E. S., & Antunes, F. (2016a). The Roles of peroxiredoxin and thioredoxin in hydrogen peroxide sensing and in signal transduction. *Molecules and Cells*, *39*(1), 65–71. https://doi.org/10.14348/molcells.2016.2349

Netto, L. E. S., & Antunes, F. (2016b). The Roles of Peroxiredoxin and Thioredoxin in Hydrogen Peroxide Sensing and in Signal Transduction. *Molecules and Cells*, *39*(1), 65–71. https://doi.org/10.14348/molcells.2016.2349

Niethammer, P., Grabher, C., Look, A. T., & Mitchison, T. J. (2009). A tissue-scale gradient of hydrogen peroxide mediates rapid wound detection in zebrafish. *Nature*, *459*(7249), 996–999. https://doi.org/10.1038/nature08119

Nurse, P. (2001). Fission Yeast handbook. *Genetics*, *365*(1544), 238102. https://doi.org/10.1103/PhysRevLett.87.238102

Oberley, L. W., & Bueftner, G. R. (1979). Role of Superoxide Dismutase in Cancer: A Review. *Cancer Research*, *39*, 1141–1149. http://aacrjournals.org/cancerres/article-pdf/39/4/1141/2404071/cr0390041141.pdf

Ogusucu, R., Rettori, D., Munhoz, D. C., Soares Netto, L. E., & Augusto, O. (2007). Reactions of yeast thioredoxin peroxidases I and II with hydrogen peroxide and peroxynitrite: Rate constants by competitive kinetics. *Free Radical Biology and Medicine*, *42*(3), 326–334. https://doi.org/10.1016/j.freeradbiomed.2006.10.042

Oliveira-Marques, V., Marinho, H. S., Cyrne, L., & Antunes, F. (2009). Role of Hydrogen Peroxide in NF-kB Activation: From Inducer to Modulator. *Antioxidants and Redox Signalling*, 2223–2243. https://doi.org/10.1089/ars.2009.2601

Oshino, N., Jamieson, D., Sugano, T., & Chance, B. (1975). Optical Measurement of the Catalase-Hydrogen Peroxide Intermediate (Compound I) in the Liver of Anaesthetized Rats and its Implication to Hydrogen Peroxide Production in situ. *Biochem. J*, *146*, 67–77. https://doi.org/10.1042/bj1460067

Östman, A., Frijhoff, J., Sandin, Å., & Böhmer, F. D. (2011). Regulation of protein tyrosine phosphatases by reversible oxidation. *Journal of Biochemistry*, *150*(4), 345–356. https://doi.org/10.1093/jb/mvr104

Padayachee, L., Rohwer, J. M., & Pillay, C. S. (2020). The thioredoxin redox potential and redox charge are surrogate measures for flux in the thioredoxin system: Thioredoxin redox charge and flux. *Archives of Biochemistry and Biophysics*, *680*(108231), 1–12. https://doi.org/10.1016/j.abb.2019.108231

Panda, P., Verma, H. K., Lakkakula, S., Merchant, N., Kadir, F., Rahman, S., Jeffree, M. S., Lakkakula, B. V. K. S., & Rao, P. V. (2022). Biomarkers of Oxidative Stress Tethered to Cardiovascular Diseases. *Oxidative Medicine and Cellular Longevity, 2022*(1), 9154295 https://doi.org/10.1155/2022/9154295

Papadakis, M. A., & Workman, C. T. (2015). Oxidative stress response pathways: Fission yeast as archetype. *Critical Reviews in Microbiology*, *41*(4), 520–535. https://doi.org/10.3109/1040841X.2013.870968

Peralta, D., Bronowska, A. K., Morgan, B., Dóka, É., Van Laer, K., Nagy, P., Gräter, F., & Dick, T. P. (2015). A proton relay enhances H_2O_2 sensitivity of GAPDH to facilitate metabolic adaptation. *Nature Chemical Biology*, *11*(2), 156–163. https://doi.org/10.1038/nchembio.1720

Peskin, A. V., Pace, P. E., & Winterbourn, C. C. (2019). Enhanced hyperoxidation of peroxiredoxin 2 and peroxiredoxin 3 in the presence of bicarbonate/CO2. *Free Radical Biology and Medicine, 145*, 1–7. https://doi.org/10.1016/j.freeradbiomed.2019.09.010

Petersen, J., & Russell, P. (2022). Growth and the environment of *Schizosaccharomyces pombe*. *Cold Spring Harbor Protocols*, *2016*(3), 210–226. https://doi.org/10.1101/pdb.top079764

Pickering, A. M., Vojtovich, L., Tower, J., & Davies, K. J. A. (2013). Oxidative stress adaptation with acute, chronic, and repeated stress. *Free Radical Biology and Medicine, 55*, 109–118. https://doi.org/10.1016/j.freeradbiomed.2012.11.001

Pillai-Kastoori, L., Schutz-Geschwender, A. R., & Harford, J. A. (2020). A systematic approach to quantitative Western blot analysis. *Analytical Biochemistry, 593*(1), 113608. https://doi.org/10.1016/j.ab.2020.113608

Pillay, C. S., Eagling, B. D., Driscoll, S. R. E., & Rohwer, J. M. (2016). Quantitative measures for redox signaling. *Free Radical Biology and Medicine, 96*, 290–303. https://doi.org/10.1016/j.freeradbiomed.2016.04.199

Pluquet, O., Pourtier, A., & Abbadie, C. (2015). The unfolded protein response and cellular senescence. A review in the theme: Cellular mechanisms of endoplasmic reticulum stress signaling in health and disease. *American Journal of Physiology - Cell Physiology*, *308*(6), 415–425. https://doi.org/10.1152/ajpcell.00334.2014

Pluskal, T., Ueno, M., & Yanagida, M. (2014). Genetic and metabolomic dissection of the ergothioneine and selenoneine biosynthetic pathway in the fission yeast, *S. pombe*, and Construction of an overproduction system. *PLoS ONE*, *9*(5), e97774. https://doi.org/10.1371/journal.pone.0097774

Pohjoismäki, J. L., & Goffart, S. (2017). The role of mitochondria in cardiac development and protection. *Free Radical Biology and Medicine*, *106*, 345–354. https://doi.org/10.1016/j.freeradbiomed.2017.02.032

Poljsak, B., Šuput, D., & Milisav, I. (2013). Achieving the balance between ROS and antioxidants: When to use the synthetic antioxidants. *Oxidative Medicine and Cellular Longevity*, *2013*(1), 956792. https://doi.org/10.1155/2013/956792

Pomatto, L. C. D., & Davies, K. J. A. (2017). The role of declining adaptive homeostasis in ageing. *Journal of Physiology*, *595*(24), 7275–7309. https://doi.org/10.1113/JP275072

Poole, L. B., & Nelson, K. J. (2016). Distribution and features of the six classes of peroxiredoxins. *Molecules and Cells*, *39*(1), 53–59. https://doi.org/10.14348/molcells.2016.2330

Purvis, J. E., & Lahav, G. (2013). Encoding and decoding cellular information through signaling dynamics. *Cell*, *152*(5), 945–956. https://doi.org/10.1016/j.cell.2013.02.005

Quinn, J., Findlay, V. J., Dawson, K., Millar, J. B. A., Jones, N., Morgan, B. A., & Toone, W. M. (2002). Distinct Regulatory Proteins Control the Graded Transcriptional Response to Increasing H_2O_2 Levels in Fission Yeast *Schizosaccharomyces pombe*. *Molecular Biology of the Cell*, *13*, 805–816. https://doi.org/10.1091/mbc.01-06

Rahal, A., Kumar, A., Singh, V., Yadav, B., Tiwari, R., Chakraborty, S., & Dhama, K. (2014). Oxidative stress, prooxidants, and antioxidants: The interplay. *BioMed Research International*, *2014*(1), 761264. https://doi.org/10.1155/2014/761264

Rajasekaran, N. S., Varadharaj, S., Khanderao, G. D., Davidson, C. J., Kannan, S., Firpo, M. A., Zweier, J. L., & Benjamin, I. J. (2011). Sustained Activation of Nuclear Erythroid 2-Related Factor 2=Antioxidant Response Element Signaling Promotes Reductive Stress in the Human Mutant Protein Aggregation Cardiomyopathy in Mice. *Antioxidants and Redox Signaling*, *14*(6), 957–971. https://doi.org/10.1089/ars.2010.3587

Raninga, P. V, Trapani, G. Di, Vuckovic, S., Bhatia, M., & Tonissen, K. F. (2015). Inhibition of thioredoxin 1 leads to apoptosis in drug-resistant multiple myeloma. *Oncotarget*, *6*(17), 15410. https:// doi: 10.18632/oncotarget.3795

Rawat, D., Alzoubi, A., Gupte, R., Chettimada, S., Watanabe, M., Kahn, A. G., Okada, T., McMurtry, I. F., & Gupte, S. A. (2014). Increased Reactive Oxygen Species, Metabolic Maladaptation, and Autophagy Contribute to Pulmonary Arterial Hypertension-Induced Ventricular Hypertrophy and Diastolic Heart Failure Pulmonary Hypertension. *Hypertension*, 1266–1274. https://doi.org/10.1161/HYPERTENSIONAHA

Reichard, P. (1968). *The Biosynthesis of Deoxyribose*. John Wiley and Sons.

Ren, X., Zou, L., Zhang, X., Branco, V., Wang, J., Carvalho, C., Holmgren, A., & Lu, J. (2017). Redox Signaling Mediated by Thioredoxin and Glutathione Systems in the Central Nervous System. In *Antioxidants and Redox Signaling* , *27*(13), 989–1010. Mary Ann Liebert Inc. https://doi.org/10.1089/ars.2016.6925

Reth, M. (2002). Hydrogen peroxide as second messenger in lymphocyte activation. *Nature Immunology*, *3*(12), 1129–1134. https://doi.org/10.1038/ni1202-1129

Rhee, S. G. (2016). Overview on Peroxiredoxin. *Molecules and Cells*, *39*(1), 1–5. https://doi.org/10.14348/molcells.2016.2368

Rhee, S. G., Chang, T. S., Jeong, W., & Kang, D. (2010). Methods for detection and measurement of hydrogen peroxide inside and outside of cells. *Molecules and Cells*, *29*(6), 539–549. https://doi.org/10.1007/s10059-010-0082-3

Rhee, S. G., Kang, S. W., Chang, T. S., Jeong, W., & Kim, K. (2001). Peroxiredoxin, a novel family of peroxidases. *IUBMB Life*, *52*(1–2), 35–41. https://doi.org/10.1080/15216540252774748

Robinson, C., Woo, S., Walsh, A., Nowak, A. K., & Lake, R. A. (2012). The antioxidants vitamins A and E and selenium do not reduce the incidence of asbestos-induced disease in a mouse model of mesothelioma. *Nutrition and Cancer*, *64*(2), 315–322. https://doi.org/10.1080/01635581.2012.649100

Rodrigo, R., Libuy, M., Feliú, F., & Hasson, D. (2013). Oxidative stress-related biomarkers in essential hypertension and ischemia-reperfusion myocardial damage. *Disease Markers*, *35*(6), 773–790. https://doi.org/10.1155/2013/974358

Rodríguez-Gabriel, M. A., Burns, G., McDonald, W. H., Martín, V., Yates, J. R., Bähler, J., & Russell, P. (2003). RNA-binding protein Csx1 mediates global control of gene expression in response to oxidative stress. *EMBO Journal*, *22*(23), 6256–6266. https://doi.org/10.1093/emboj/cdg597

Roos, G., Foloppe, N., Van Laer, K., Wyns, L., Nilsson, L., Geerlings, P., & Messens, J. (2009). How thioredoxin dissociates its mixed disulfide. *PLoS Computational Biology*, *5*(8). https://doi.org/10.1371/journal.pcbi.1000461

Rossi, F., & Zatti, M. (1964). Biochemical aspects of phagocytosis in polymorphonuclear leucocytes. NADH and NADPH oxidation by the granules of resting and phagocytizing cells. *Brief Reports*, *15*(1), 21–23. https://doi.org/10.1007/BF02146019

Rothstein, J. D., Bristol4, L. A., Hosler, B., Brown, R. H., & Kuncl, R. W. (1994). Chronic inhibition of superoxide dismutase produces apoptotic death of spinal neurons. *Proceedings of the National Academy of Science*, *91*(10), 4155–4159. https://doi.org/10.1073/pnas.91.10.4155

Rudyk, O., & Eaton, P. (2014). Biochemical methods for monitoring protein thiol redox states in biological systems. *Redox Biology*, *2*(1), 803–813. https://doi.org/10.1016/j.redox.2014.06.005

Rustici, G., van Bakel, H., Lackner, D. H., Holstege, F. C., Wijmenga, C., Bähler, J., & Brazma, A. (2007). Global transcriptional responses of fission and budding yeast to changes in copper and iron levels: A comparative study. *Genome Biology*, *8*(5), 1–16. https://doi.org/10.1186/gb-2007-8-5-r73

Saitoh, M., Nishitoh, H., Fujii, M., Takeda, K., Tobiume, K., Sawada, Y., Kawabata, M., Miyazono, K., & Ichijo, H. (1998). Mammalian thioredoxin is a direct inhibitor of apoptosis signal-regulating kinase (ASK) 1. *The EMBO Journal*, *17*(9). https://doi.org/10.1093/emboj/17.9.2596

Sander, H., Wallace, S., Plouse, R., Tiwari, S., & Gomes, A. V. (2019). Ponceau S waste: Ponceau S staining for total protein normalization. *Analytical Biochemistry*, *575*, 44–53. https://doi.org/10.1016/j.ab.2019.03.010

Shacter, E., Williams, J. A., Lim, M., & Levine, R. L. (1994). Differential susceptibility of plasma proteins to oxidative modifciation: Examination by western blot immunoassay. *Free*

Radical Biology and Medicine, *17*(5), 429–437. https://doi.org/10.1016/0891-5849(94)90169-4

Shergalis, A. G., Hu, S., Bankhead, A., & Neamati, N. (2020). Role of the ERO1-PDI interaction in oxidative protein folding and disease. *Pharmacology and Therapeutics*, *210*(1), 107525. https://doi.org/10.1016/j.pharmthera.2020.107525

Sian, J., Gerlach, M., Youdim, M. B. H., & Riederer, P. (1999). Hypokinetic disorder of the basal ganglia Parkinson's disease: a major hypokinetic basal ganglia disorder. *J Neural Transm*, *106*, 443–476. https://doi.org/10.1007/s007020050171

Sies, H. (1997). Oxidative stress: Oxidants and antioxidants. In *Experimental Physiology*, *82(*2), 291–295. Blackwell Publishing Ltd. https://doi.org/10.1113/expphysiol.1997.sp004024

Sies, H. (2017). Hydrogen peroxide as a central redox signaling molecule in physiological oxidative stress: Oxidative eustress. *Redox Biology*, *11*, 613–619. https://doi.org/10.1016/j.redox.2016.12.035

Sies, H., & Jones, D. P. (2020). Reactive oxygen species (ROS) as pleiotropic physiological signalling agents. *Nature Reviews Molecular Cell Biology*, *21*(7), 363–383. https://doi.org/10.1038/s41580-020-0230-3

Sikes, H. D. (2017). Redox regulation: Scaffolding H_2O_2 signaling. *Nature Chemical Biology*, *13*(8), 818–819. https://doi.org/10.1038/nchembio.2432

Singh, G., Patel, A., Tiwari, S., Gupta, D., & Prasad, S. M. (2022). Signaling molecules hydrogen sulfide (H_2S) and nitric oxide (NO): role in microalgae under adverse environmental conditions. *Acta Physiologiae Plantarum*, *44*(7), 68. https://doi.org/10.1007/s11738-022-03404-8

Singh, V. P., Poon, J., Yan, J., Lu, X., Karlsson, O., Butcher, R. J., Gates, P. J., & Engman, L. (2017). Nitro-, Azo-, and Amino Derivatives of Ebselen: Synthesis, Structure, and Cytoprotective Effects. *J. Org. Chem*, *82*(1), 313–321. https://doi.org/10.1021/acs.joc.6b02418

Smolyarova, D. D., Podgorny, O. V., Bilan, D. S., & Belousov, V. V. (2022). A guide to genetically encoded tools for the study of H_2O_2. *FEBS Journal*, *289*(18), 5382–5395. https://doi.org/10.1111/febs.16088

Sobotta, M. C., Barata, A. G., Schmidt, U., Mueller, S., Millonig, G., & Dick, T. P. (2013). Exposing cells to H_2O_2: A quantitative comparison between continuous low-dose and one-time high-dose treatments. *Free Radical Biology and Medicine*, *60*, 325–335. https://doi.org/10.1016/j.freeradbiomed.2013.02.017

Sobotta, M. C., Liou, W., Stöcker, S., Talwar, D., Oehler, M., Ruppert, T., Scharf, A. N. D., & Dick, T. P. (2015). Peroxiredoxin-2 and STAT3 form a redox relay for H_2O_2 signaling. *Nature Chemical Biology*, *11*(1), 64–70. https://doi.org/10.1038/nchembio.1695

Sotler, R., Poljšak, B., Dahmane, R., Jukić, T., Pavan Jukić, D., Rotim, C., Trebše, P., & Starc, A. (2019). Prooxidant activities of antioxidants and their impact on health. *Acta Clinica Croatica*, *58*(4), 726–736. https://doi.org/10.20471/acc.2019.58.04.20

Spitz, S. R., Dewey, W. C., & Li, G. C. (1987). Hydrogen Peroxide or Heat Shock Induces Resistance to Hydrogen Peroxide in Chinese Hamster Fibroblasts. *Journal of cellular physiology*, 13(3), 364–373. https://doi.org/10.1002/jcp.1041310308

Stancill, J., Hansen, J. P., Schmidt, E., & Corbett, J. (2022). Chronic thioredoxin reductase deficiency disrupts redox homeostasis and impairs beta-cell function. *Free Radicals Biology and Medicine*, *180*(67), 67.

Sue, G. R., Ho, Z. C., & Kim, K. (2005). Peroxiredoxins: A historical overview and speculative preview of novel mechanisms and emerging concepts in cell signaling. *Free Radical Biology and Medicine*, *38*(12), 1543–1552. https://doi.org/10.1016/j.freeradbiomed.2005.02.026

Sultana, R., & Perluigi, M. (2006). Protein Oxidation and Lipid Peroxidation in Brain of Subjects Neurodegeneration from Redox Proteomics. *Antioxidants & Redox Signaling*, *8*(11), 2021–2037. https://doi.org/10.1089/ars.2006.8.2021

Sumimoto, H. (2008). Structure, regulation and evolution of Nox-family NADPH oxidases that produce reactive oxygen species. *FEBS Journal*, *275*(13), 3249–3277. https://doi.org/10.1111/j.1742-4658.2008.06488.x

Sykiotis, G. P., & Bohmann, D. (2010). Stress-activated cap'n'collar transcription factors in aging and human disease. *Science Signaling*, *3*(112), 1–22. https://doi.org: 10.1126/scisignal.3112re3

Tabassum, N., Kheya, I., Ibn Asaduzzaman, S., Maniha, S., Fayz, A., Zakaria, A., Fayz, A., Zakaria, A., & Noor, R. (2020). A Review on the Possible Leakage of Electrons through the Electron Transport Chain within Mitochondria. *Journal of Biomedical Research & Environmental Sciences*, *1*(4), 105–113. https://doi.org/10.37871/jels1127

Tafforeau, L., Le Blastier, S., Bamps, S., Dewez, M., Vandenhaute, J., & Hermand, D. (2006). Repression of ergosterol level during oxidative stress by fission yeast F-box protein Pof14 independently of SCF. *EMBO Journal*, *25*(19), 4547–4556. https://doi.org/10.1038/sj.emboj.7601329

Talib, E. A., & Outten, C. E. (2021). Iron-sulfur cluster biogenesis, trafficking, and signaling: Roles for CGFS glutaredoxins and BolA proteins. *Biochimica et Biophysica Acta - Molecular Cell Research*, *1868*(1), 118847. https://doi.org/10.1016/j.bbamcr.2020.118847

Tay, S., Hughey, J. J., Lee, T. K., Lipniacki, T., Quake, S. R., & Covert, M. W. (2010). Single-cell NF-B dynamics reveal digital activation and analogue information processing. *Nature*, *466*(7303), 267–271. https://doi.org/10.1038/nature09145

ter Braak, B., Klip, J. E., Wink, S., Hiemstra, S., Cooper, S. L., Middleton, A., White, A., & van de Water, B. (2022). Mapping the dynamics of Nrf2 antioxidant and NFκB inflammatory responses by soft electrophilic chemicals in human liver cells defines the transition from adaptive to adverse responses. *Toxicology in Vitro*, *84*(1), 105419. https://doi.org/10.1016/j.tiv.2022.105419

Thirupathi, A., Pinho, R. A., Baker, J. S., István, B., & Gu, Y. (2020). Taurine Reverses Oxidative Damages and Restores the Muscle Function in Overuse of Exercised Muscle. In *Frontiers in Physiology*, *11*(1), 582449. https://doi.org/10.3389/fphys.2020.582449

Thurman, R. G., Ley, H. G., & Scholz, R. (1972). Hepatic Microsomal Ethanol Oxidation Hydrogen Peroxide Formation and the Role of Catalase. *Eur. J. Biochem*, *25*, 420–430. https://doi.org/10.1111/j.1432-1033.1972.tb01711.x

Toledano, M. B., & Huang, B. (2016). Microbial 2-Cys Peroxiredoxins: Insights into Their Complex Physiological Roles. *Molecules and Cells*, *39*(1), 31–39. https://doi.org/10.14348/molcells.2016.2326

Tomalin, L. E., Day, A. M., Underwood, Z. E., Smith, G. R., Dalle Pezze, P., Rallis, C., Patel, W., Dickinson, B. C., Bähler, J., Brewer, T. F., Chang, C. J. L., Shanley, D. P., & Veal, E.

A. (2016). Increasing extracellular H_2O_2 produces a bi-phasic response in intracellular H_2O_2 , with peroxiredoxin hyperoxidation only triggered once the cellular H_2O_2 -buffering capacity is overwhelmed. *Free Radical Biology and Medicine*, *95*, 333–348. https://doi.org/10.1016/j.freeradbiomed.2016.02.035

Toone, W. M., Kuge, S., Samuels, M., Morgan, B. A., Toda, T., & Jones, N. (1998). Regulation of the fission yeast transcription factor Pap1 by oxidative stress: requirement for the nuclear export factor Crm1 (Exportin) and the stress-activated MAP kinase Sty1/Spc1. *Genes and Development*, *12*, 1453–1463. https://doi.org/: 10.1101/gad.12.10.1453

Tyson, R. J., Park, C. C., Powell, J. R., Patterson, J. H., Weiner, D., Watkins, P. B., & Gonzalez, D. (2020). Precision Dosing Priority Criteria: Drug, Disease, and Patient Population Variables. *Frontiers in Pharmacology*, *11*(1), 420. https://doi.org/10.3389/fphar.2020.00420

Valko, M., Leibfritz, D., Moncol, J., Cronin, M. T. D., Mazur, M., & Telser, J. (2007). Free radicals and antioxidants in normal physiological functions and human disease. *International Journal of Biochemistry and Cell Biology*, *39*(1), 44–84. https://doi.org/10.1016/j.biocel.2006.07.001

Veal, E. A., Tomalin, L. E., Morgan, B. A., & Day, A. M. (2014). The fission yeast *Schizosaccharomyces pombe* as a model to understand how peroxiredoxins influence cell responses to hydrogen peroxide. *Biochemical Society Transactions*, *42*(4), 909–916. https://doi.org/10.1042/BST20140059

Vermot, A., Petit-Härtlein, I., Smith, S. M. E., & Fieschi, F. (2021). Nadph oxidases (Nox): An overview from discovery, molecular mechanisms to physiology and pathology. *Antioxidants*, *10*(6). https://doi.org/10.3390/antiox10060890

Vivancos, A. P., Castillo, E. A., Biteau, B., Nicot, C., Ayte, J., Toledano, M. B., & Hidalgo, E. (2005). A cysteine-sulfinic acid in peroxiredoxin regulates H_2O_2-sensing by the antioxidant Pap1 pathway. *Proceedings of the National Academy of Sciences*, *102*(25), 8875–8880. https://doi.org/10.1073/pnas.0503251102

Vivancos, A. P., Castillo, E. A., Jones, N., Ayté, J., & Hidalgo, E. (2004). Activation of the redox sensor Pap1 by hydrogen peroxide requires modulation of the intracellular oxidant concentration. *Molecular Microbiology*, *52*(5), 1427–1435. https://doi.org/10.1111/j.1365-2958.2004.04065.x

Vivancos, A. P., Jara, M., Zuin, A., Sansó, M., & Hidalgo, E. (2006). Oxidative stress in *Schizosaccharomyces pombe*: Different H_2O_2 levels, different response pathways. *Molecular Genetics and Genomics*, *276*(6), 495–502. https://doi.org/10.1007/s00438-006-0175-z

Wakabayashi, N., Itoh, K., Wakabayashi, J., Motohashi, H., Noda, S., Takahashi, S., Imakado, S., Kotsuji, T., Otsuka, F., Roop, D. R., Harada, T., Engel, J. D., & Yamamoto, M. (2003). Keap1-null mutation leads to postnatal lethality due to constitutive Nrf2 activation. *Nature Genetics*, *35*(3), 238–245. https://doi.org/10.1038/ng1248

Wan, F., Yin, J., Sun, W., & Gao, H. (2019). Oxidized OxyR up-regulates AhpCF expression to suppress plating defects of oxyR- And catalase-deficient strains. *Frontiers in Microbiology*, *10*(1), 439. https://doi.org/10.3389/fmicb.2019.00439

Whittaker, J. W. (2012). Non-heme manganese catalase - The 'other' catalase. In *Archives of Biochemistry and Biophysics*, *525*(2), 111–120. Academic Press Inc. https://doi.org/10.1016/j.abb.2011.12.008

Willstatter, R. (1932). *Discussion on Recent Advances the Study of Enzymes and their Action*. https://royalsocietypublishing.org/

Wilson, D. E., Smith, G. B., Jacob, A. L., Walker, T., Dimidschstein, J., Fishell, G., & Fitzpatrick, D. (2017). GABAergic Neurons in Ferret Visual Cortex Participate in Functionally Specific Networks. *Neuron*, *93*(5), 1058–1065. https://doi.org/10.1016/j.neuron.2017.02.035

Wong, H. S., Benoit, B., & Brand, M. D. (2019). Mitochondrial and cytosolic sources of hydrogen peroxide in resting C2C12 myoblasts. *Free Radical Biology and Medicine*, *130*, 140–150. https://doi.org/10.1016/j.freeradbiomed.2018.10.448

Wood, Z. A., Poole, L. B., Hantgan, R. R., & Karplus, P. A. (2002). Dimers to doughnuts: Redox-sensitive oligomerization of 2-cysteine peroxiredoxins. *Biochemistry*, *41*(17), 5493–5504. https://doi.org/10.1021/bi012173m

Wood, Z. A., Poole, L. B., & Karplus, P. A. (2003). Peroxiredoxin evolution and the regulation of hydrogen peroxide signaling. *Science*, *300*(5619), 650–653. https://doi.org/10.1126/science.1080405

Wu, Y. xian, Wang, Y. ying, Gao, Z. qi, Chen, D., Liu, G., Wan, B. bin, Jiang, F. juan, Wei, M. xia, Zuo, J., Zhu, J., Chen, Y. quan, Qian, F., & Pang, Q. feng. (2021). Ethyl ferulate protects against lipopolysaccharide-induced acute lung injury by activating AMPK/Nrf2 signaling pathway. *Acta Pharmacologica Sinica*, *42*(12), 2069–2081. https://doi.org/10.1038/s41401-021-00742-0

Yamamoto, X. M., Kensler, T. W., & Motohashi, H. (2018). The KEAP1-NRF2 System: A Thiol-based sensor-effector apparatus for maintaining redox homeostasis. *Physiol Rev*, *98*, 1169–1203. https://doi.org/10.1152/physrev.00023

Yu, E., Calvert, P. A., Mercer, J. R., Harrison, J., Baker, L., Figg, N. L., Kumar, S., Wang, J. C., Hurst, L. A., Obaid, D. R., Logan, A., West, N. E. J., Clarke, M. C. H., Vidal-Puig, A., Murphy, M. P., & Bennett, M. R. (2013). Mitochondrial DNA damage can promote atherosclerosis independently of reactive oxygen species through effects on smooth muscle cells and monocytes and correlates with higher-risk plaques in humans. *Circulation*, *128*(7), 702–712. https://doi.org/10.1161/CIRCULATIONAHA.113.002271

Zaffagnini, M., Marchand, C. H., Malferrari, M., Murail, S., Bonacchi, S., Genovese, D., Montalti, M., Venturoli, G., Falini, G., Baaden, M., Lemaire, S. D., Fermani, S., & Trost, P. (2019). Glutathionylation primes soluble glyceraldehyde-3-phosphate dehydrogenase for late collapse into insoluble aggregates. *PNAS*, *116*(51), 26057–26065. https://doi.org/10.1073/pnas.1914484116/-/DCSupplemental

Zavras, N., Ssiristatidis, C., Ssiatelis, A., & Koumarianou, A. (2016). Fertility risk assessment and preservation in male and female prepubertal and adolescent cancer patients. In *Clinical Medicine Insights: Oncology*. *10*, 49–57. Libertas Academica Ltd. https://doi.org/10.4137/CMO.S32811

Zhang, B., Gu, H., Yang, Y., Bai, H., Zhao, C., Si, M., Su, T., & Shen, X. (2019). Molecular mechanisms of AhpC in resistance to oxidative stress in burkholderia thailandensis. *Frontiers in Microbiology*, *10*(1), 1483. https://doi.org/10.3389/fmicb.2019.01483

Zuin, A., Vivancos, A. P., Sansó, M., Takatsume, Y., Ayté, J., Inoue, Y., & Hidalgo, E. (2005). The glycolytic metabolite methylglyoxal activates Pap1 and Sty1 stress response in *Schizosaccharomyces pombe*. *Journal of Biological Chemistry*, *280*(44), 36708–36713. https://doi.org/10.1074/jbc.M508400200

Supplementary information

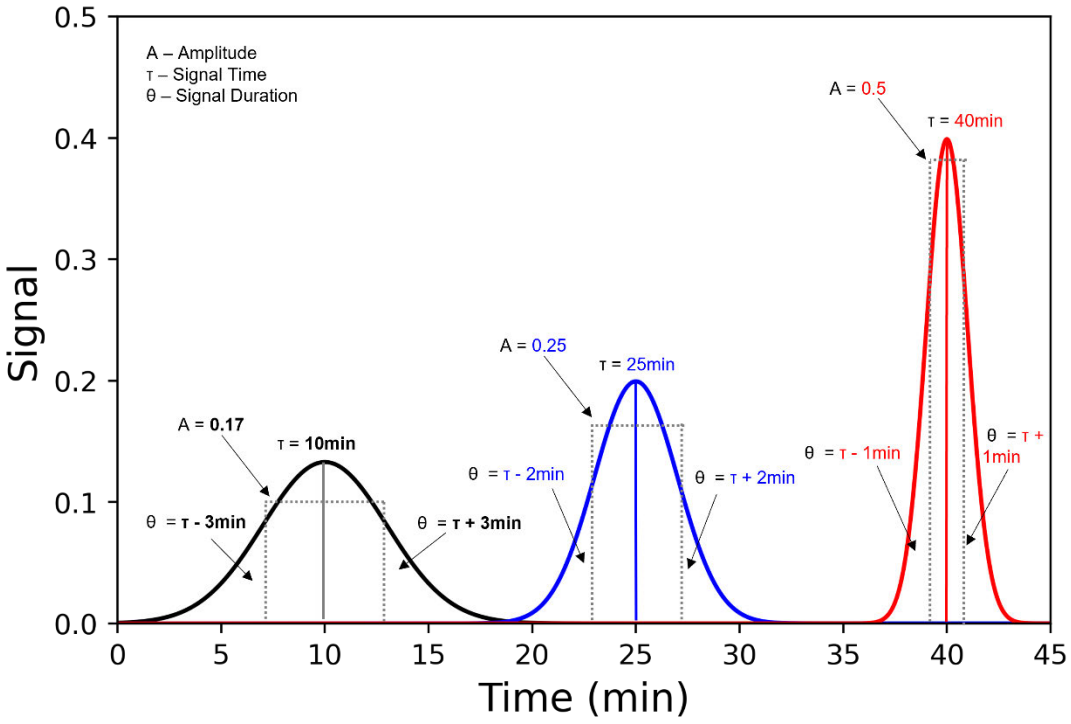

Figure S.1: Graphical representation of signalling amplitude, time and duration.

Signalling amplitude is the average concentration of signal protein over the signal duration. Hypothetical signal profiles (black, blue and red) depict higher signal duration (θ) which results in lower signal amplitude (A). Signal time (τ) measures the average time a signal protein is active and is progressively longer in each curve.

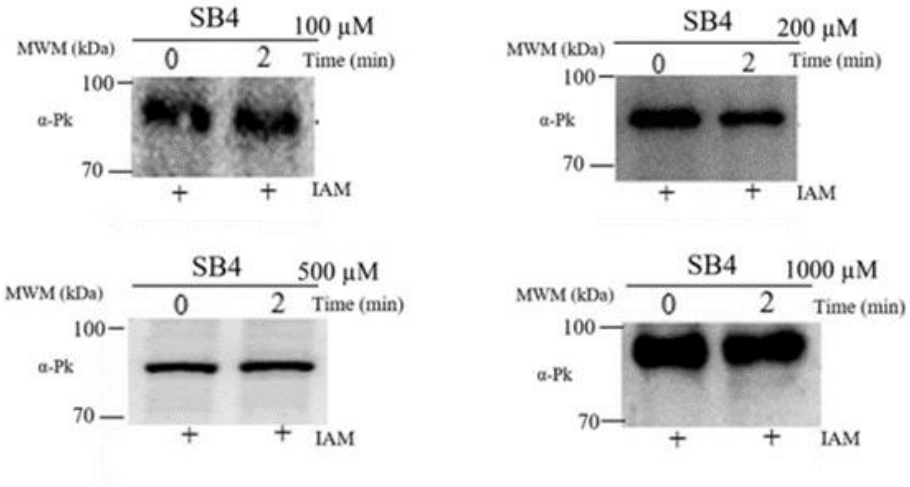

Figure S.2: Confirmation that Pap1 was exclusively oxidised by Tpx1.

An S. pombe Δtpx1 strain (Bozonot et al., 2005) was challenged with four hydrogen peroxide concentrations (100-1000 µM) for two minutes. Protein was extracted and Pap1 oxidation was examined by western blot analysis and showed no oxidation of Pap1 confirming that Tpx1 was required for Pap1 oxidation.

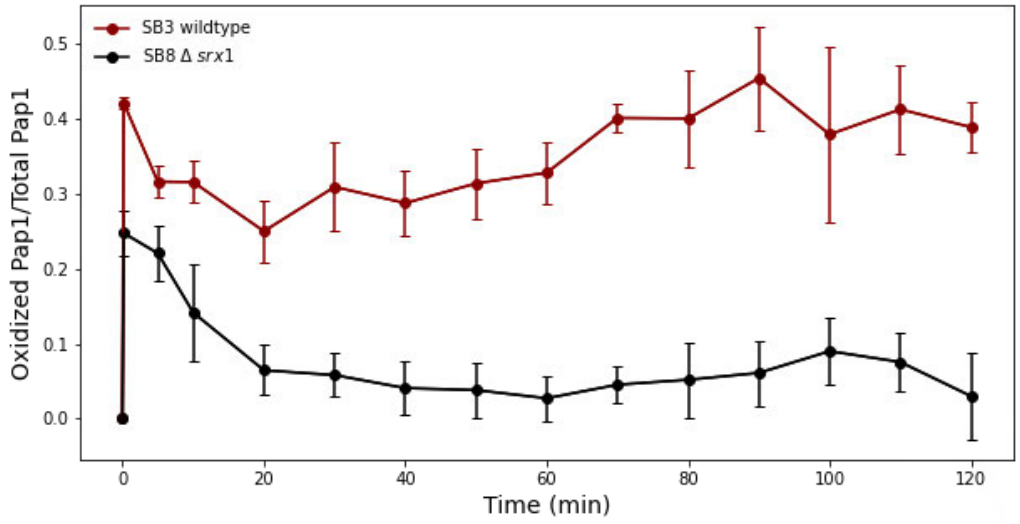

Figure S.3: Deletion of *srx1* affects the Pap1 signalling profile after exposure to hydrogen peroxide.

S. pombe cells wild-type (SB3) (red) and a Δsrx1 (SB8) (black) strain cultured to mid-exponential phase and exposed to 500 µM hydrogen peroxide the oxidation of Pap1 was determined by redox western blotting. Densitometric analysis of Pap1 oxidised and reduced bands were used to generate Pap1 signalling profiles. The data is representative of at least three independent experiments.

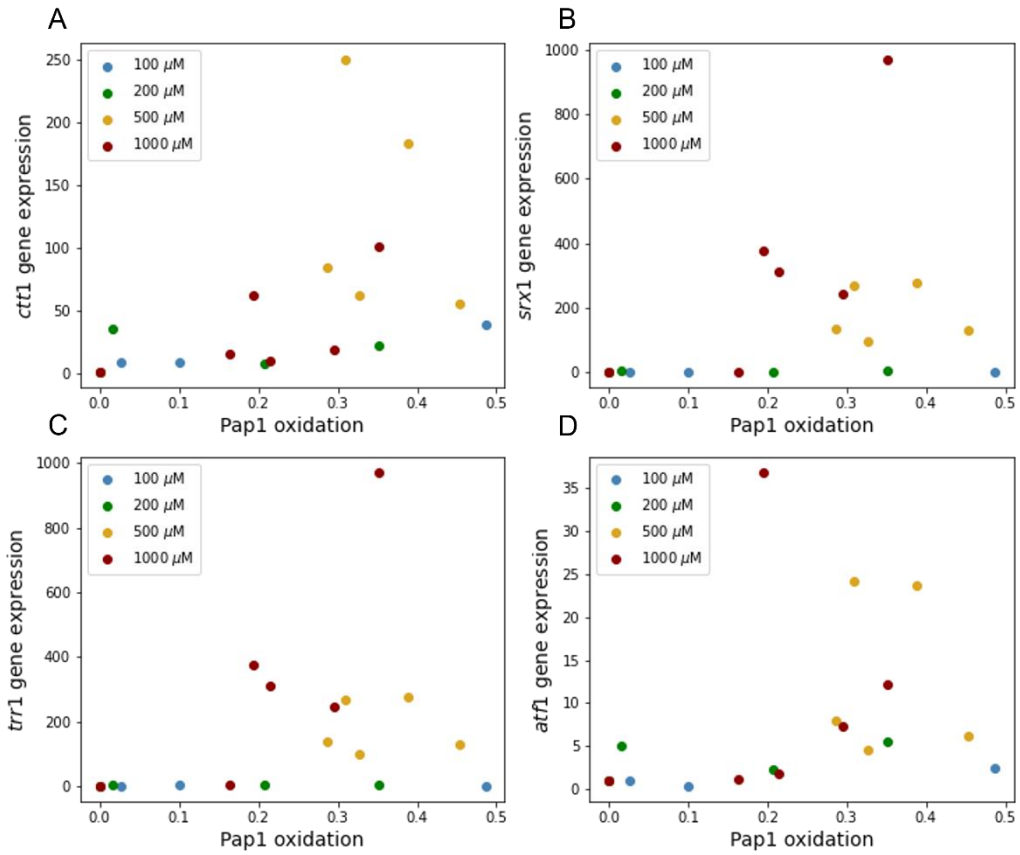

Figure S.4: Determining the relationship between fold-change induction of Pap1-regulated genes and Pap1 oxidation.

After the bolus addition of 100-1000 μM hydrogen peroxide the fold change induction of ctt1, trr1, srx1 and atf1 was determined using RT-qPCR over a 60-minute time course for 100-200 μM hydrogen peroxide and over 120 min for 500-1000 μM hydrogen peroxide. The ratio of oxidised Pap1 (oxidised/total) was determined from densitometric analysis of western blots (details in Main paper). The Pap1 oxidation ratio was plotted with the fold-change induction of mRNA at equivalent time intervals over the 60-minute or 120-minute time course.

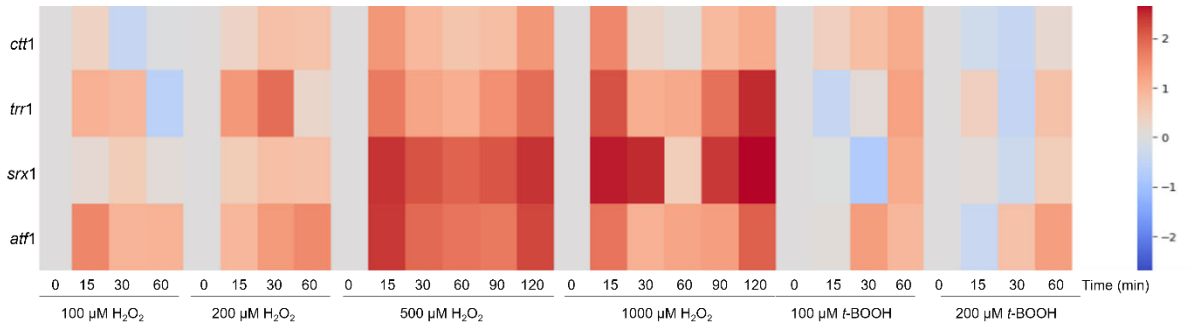

Figure S.5: Response of Pap1-regulated genes after exposure to various oxidants at different concentrations.

Wild-type S. pombe cells (SB3) exposed to 100-1000 µM hydrogen peroxide or 100-200 µM t-BOOH were monitored for the log_{10} fold change in gene expression for ctt1, trr1, srx1 and atf1 and normalised using gpd3 as the reference gene.

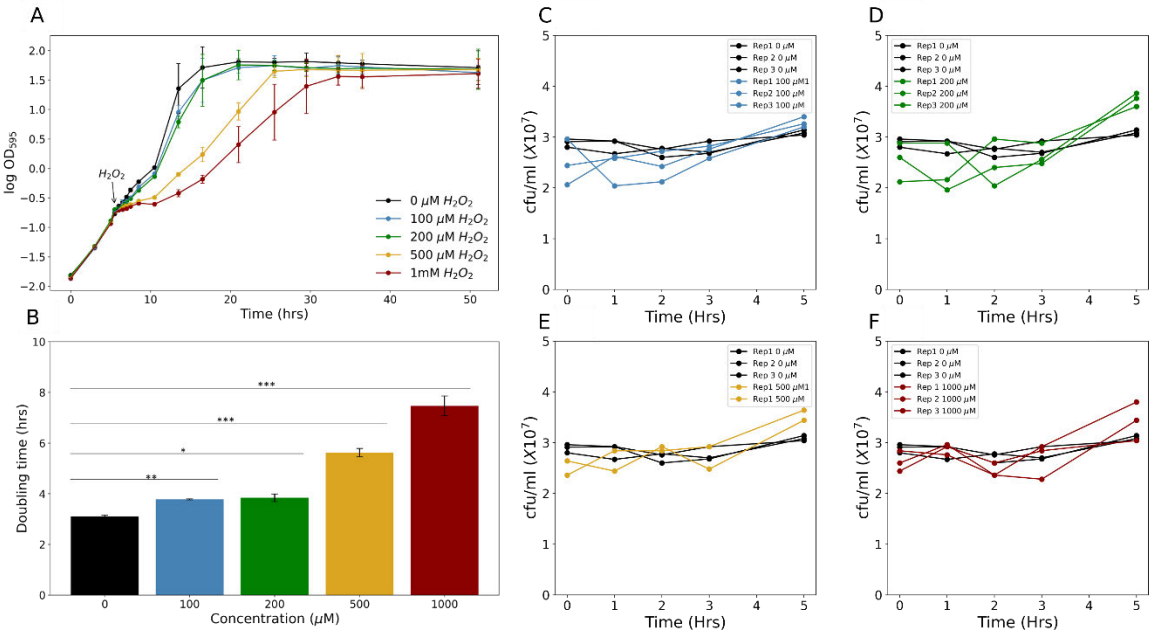

Figure S.6: The growth curves, doubling time and CFU/ml of S. pombe cells after bolus addition of hydrogen peroxide (0.1-1 mM).

*The log increase in OD595 of S. pombe cells after adding bolus concentrations of hydrogen peroxide was determined over 52 hrs in minimal medium (A) (n=3). The doubling times of the cells were then calculated and compared to the untreated cells (B). The effect of hydrogen peroxide on the doubling time was assessed using a two-tailed t-test with statistical significance denoted as *p<0.01, **p<0.001, ***p<0.0001 (n=3). The CFU/ml was determined by collecting cell samples every hr over a five-hr period and plated onto YE5S medium to assess colony growth (D-F). The experiment was carried out as three independent replications (n=3).*

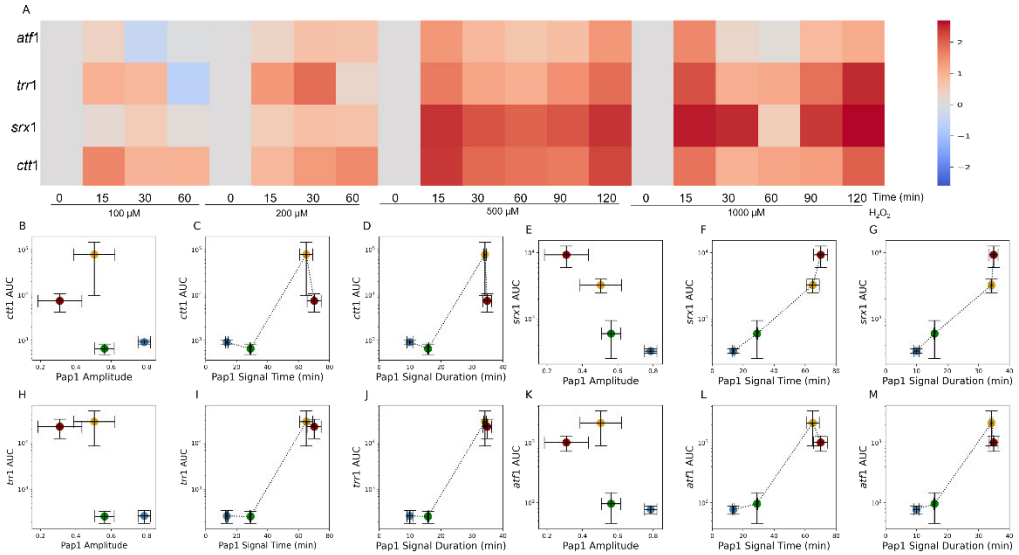

Figure S.7: Dynamics of Pap1-dependent gene induction in response to hydrogen peroxide and correlation to Pap1 dynamic profiles.

The dynamic log_{10} fold-changes in mRNA for the Pap-1 regulated genes, ctt1, trr1, srx1 and atf1, were determined by RT-qPCR following bolus treatments with 100-1000 µM hydrogen peroxide (A). The areas under the curves obtained from the dynamic gene expression profiles of ctt1, trr1, srx1 and atf1 were compared with the signal parameters obtained from the Pap1 oxidation profiles in co-response plots for 100 (blue), 200 (green), 500 (orange) and 1000 (red) µM hydrogen peroxide (B-M). The data represent the means and standard errors of at least three independent experiments.

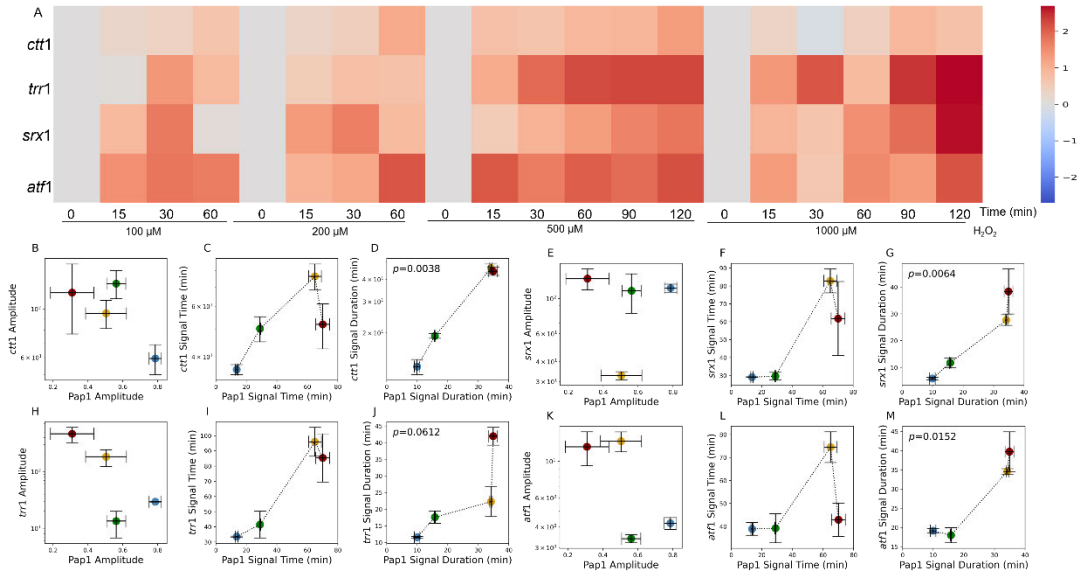

Figure S.8: Dynamics of Pap1-dependent gene induction in response to hydrogen peroxide and correlation to Pap1-activation profiles.

The dynamic log_{10} fold-changes in the mRNA of the Pap-1 regulated genes, ctt1, trr1, srx1 and atf1, were determined by RT-qPCR following bolus treatments with 100-1000 µM hydrogen peroxide (A). The signal amplitude, time and duration parameters obtained from the dynamic gene expression profiles of ctt1, trr1, srx1 and atf1 were compared with the signal parameters obtained from the Pap1 oxidation profiles in co-response plots (B-M). Deming regression was used to determine the statistical significance for the signal duration with the following p-values 0.003 (D), 0.007(G), 0.0002 (J) and 0.1025 (M). The data represent the means and standard errors of at least three independent experiments.

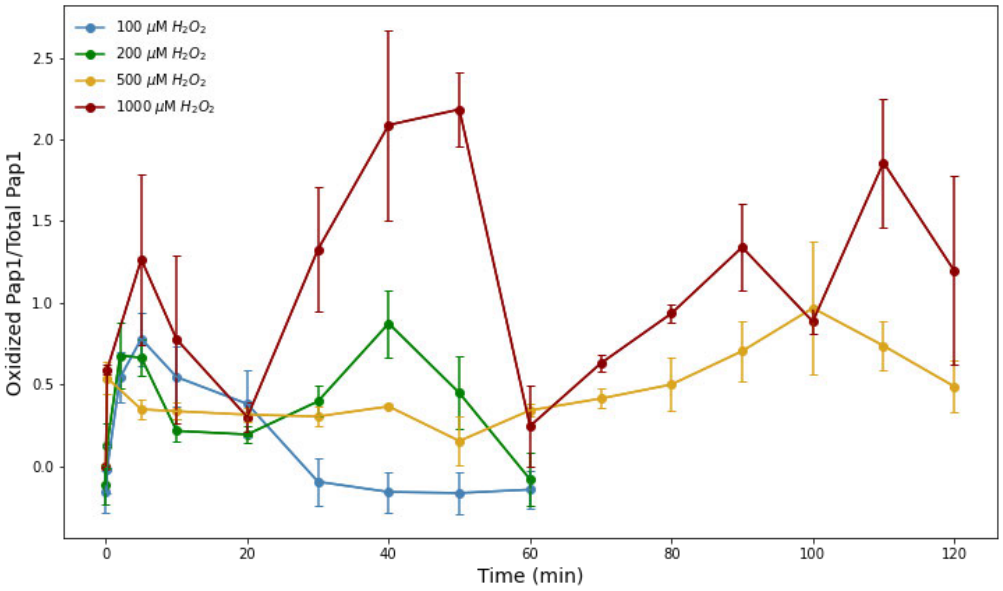

Figure S.9: Normalisation of fractional Pap1 oxidation against total Pap1 (DTT control). *S. pombe cells were exposed to 100-1000 µM hydrogen peroxide, and samples were collected and processed using western blotting. Densitometric analysis was used to quantify oxidised Pap1. To determine the fractional Pap1 oxidation, oxidised Pap1 was divided against Pap1 recovered in the DTT control (n=3).*

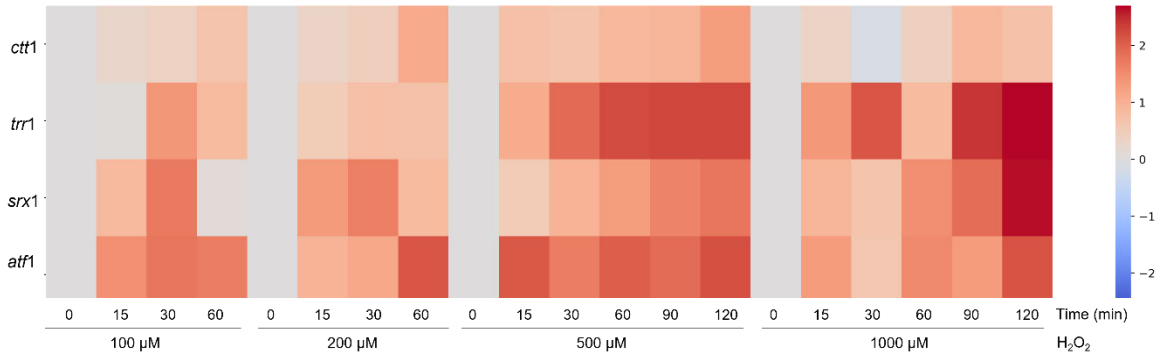

Figure S.10: Dynamics of Pap1-dependent gene induction in response to hydrogen peroxide.

The dynamic log_{10} fold-changes in the transcription of the Pap-1 regulated genes, ctt1, trr1, srx1 and atf1, were determined by RT-qPCR following bolus treatments with 100-1000 µM hydrogen peroxide and normalised against mRNA levels for the reference gene act1

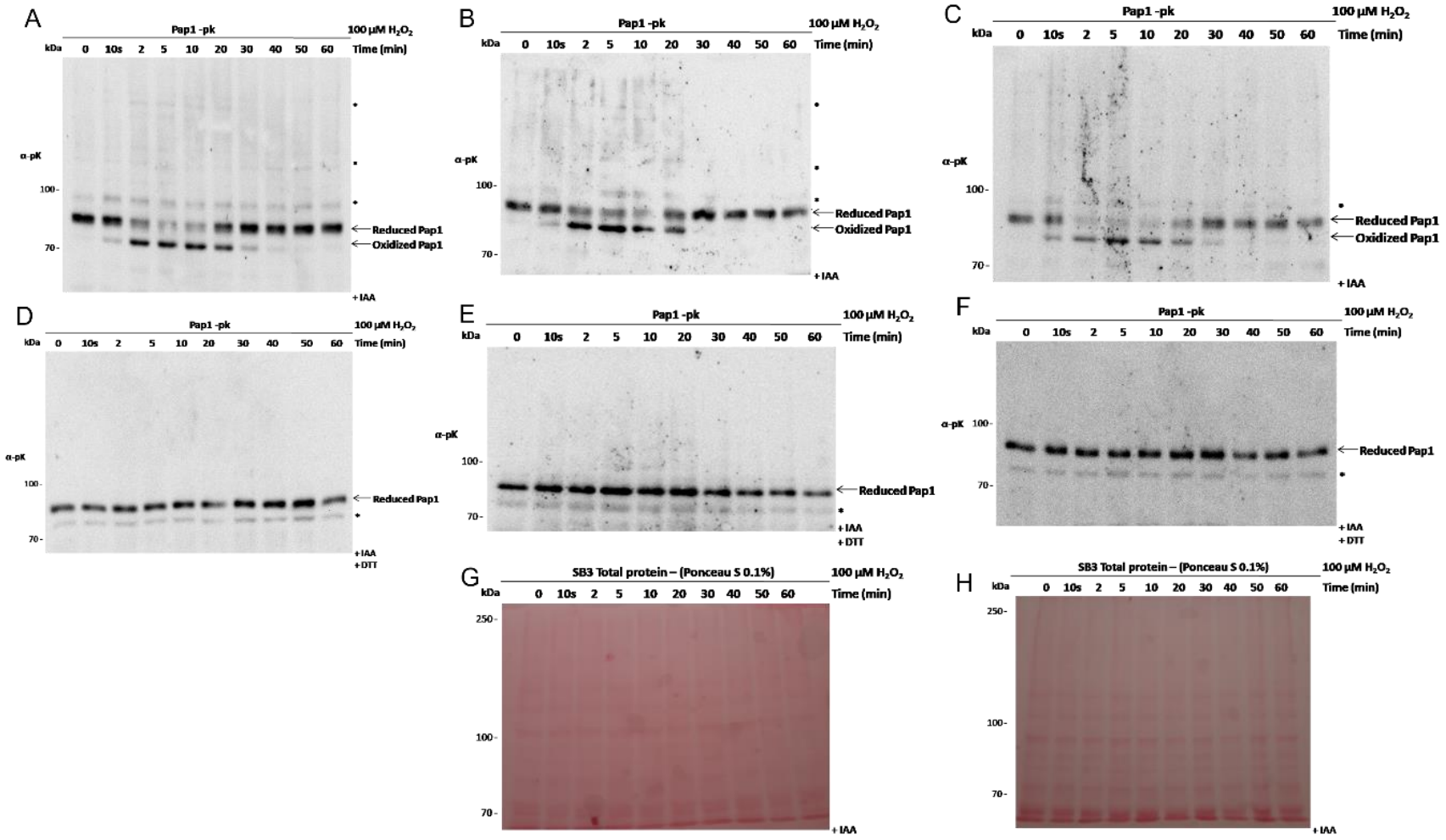

Figure S. 11: Representative Western blots of *S. pombe* cells following exposure to 100 µM hydrogen peroxide.

The blots depict Pap1 oxidized and reduced bands over a 60-minute time course (A-C), Pap1 reduced bands after DTT treatment (D-F), and blots stained with Ponceau S to observe total protein (G, H).

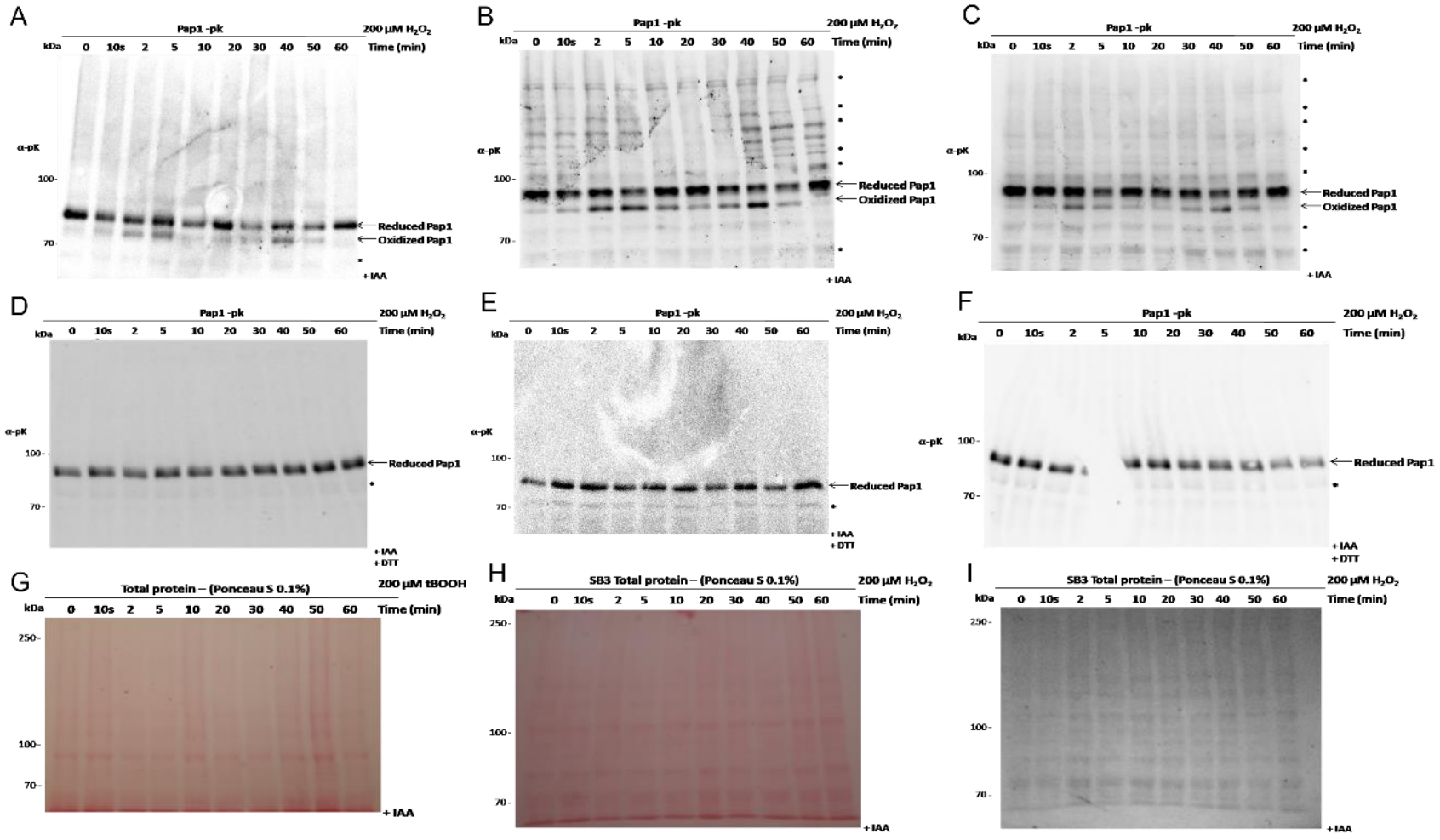

Figure S.12: Representative western blots of *S. pombe* cells following exposure to 200 µM hydrogen peroxide.

The blots depict Pap1 oxidized and reduced bands over a 60-minute time course (A-C), Pap1 reduced bands after DTT treatment (D-F), and blots stained with Ponceau S to observe total protein (G-I).

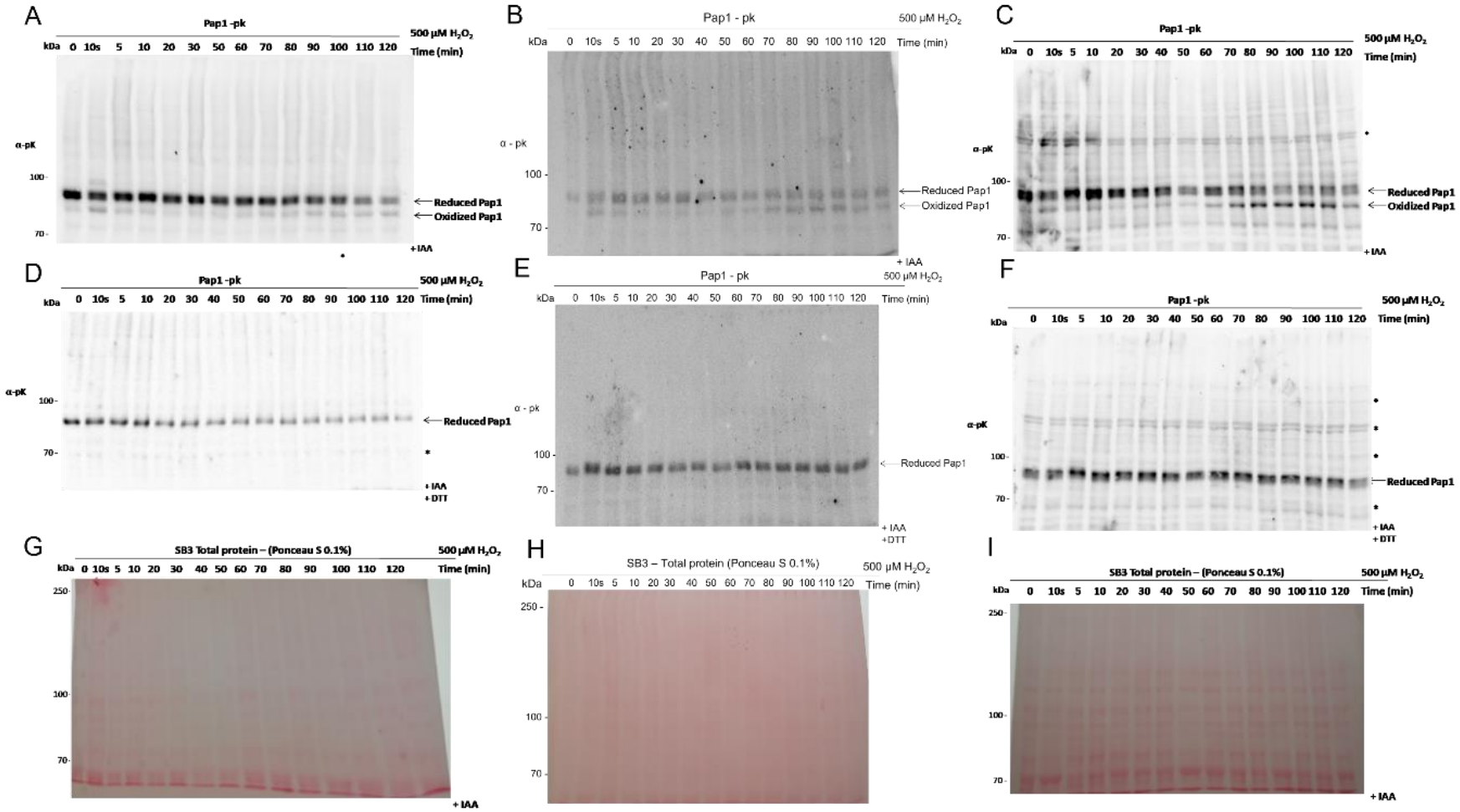
A
Pap1 -pk
500 µM H2O2
kDa 0 10s 5 10 20 30 50 60 70 80 90 100 110 120 Time (min)
α-pK
100
70
Reduced Pap1
Oxidized Pap1
+ IAA
B
Pap1 - pk
500 µM H2O2
kDa 0 10s 5 10 20 30 40 50 60 70 80 90 100 110 120 Time (min)
α - pk
100
70
Reduced Pap1
Oxidized Pap1
+ IAA
C
Pap1 -pk
500 µM H2O2
kDa 0 10s 5 10 20 30 40 50 60 70 80 90 100 110 120 Time (min)
α-pK
100
70
Reduced Pap1
Oxidized Pap1
+ IAA
D
Pap1 -pk
500 µM H2O2
kDa 0 10s 5 10 20 30 40 50 60 70 80 90 100 110 120 Time (min)
α-pK
100
70
Reduced Pap1
*
+ IAA
+ DTT
E
Pap1 - pk
500 µM H2O2
kDa 0 10s 5 10 20 30 40 50 60 70 80 90 100 110 120 Time (min)
α - pk
100
70
Reduced Pap1
+ IAA
+DTT
F
Pap1 -pk
500 µM H2O2
kDa 0 10s 5 10 20 30 40 50 60 70 80 90 100 110 120 Time (min)
α-pK
100
70
Reduced Pap1
*
+ IAA
+ DTT
G
SB3 Total protein – (Ponceau S 0.1%)
500 µM H2O2
kDa 0 10s 5 10 20 30 40 50 60 70 80 90 100 110 120 Time (min)
250
100
70
+ IAA
H
SB3 – Total protein (Ponceau S 0.1%)
500 µM H2O2
kDa 0 10s 5 10 20 30 40 50 60 70 80 90 100 110 120 Time (min)
250
100
70
I
SB3 Total protein – (Ponceau S 0.1%)
500 µM H2O2
kDa 0 10s 5 10 20 30 40 50 60 70 80 90 100 110 120 Time (min)
250
100
70
+ IAA

Figure S.13: Representative western blots of *S. pombe* cells following exposure to 500 µM hydrogen peroxide.

The blots depict Pap1 oxidized and reduced bands over a 120-minute time course (A-C), Pap1 reduced bands after DTT treatment (D-F), and blots stained with Ponceau S to observe total protein (G-I).

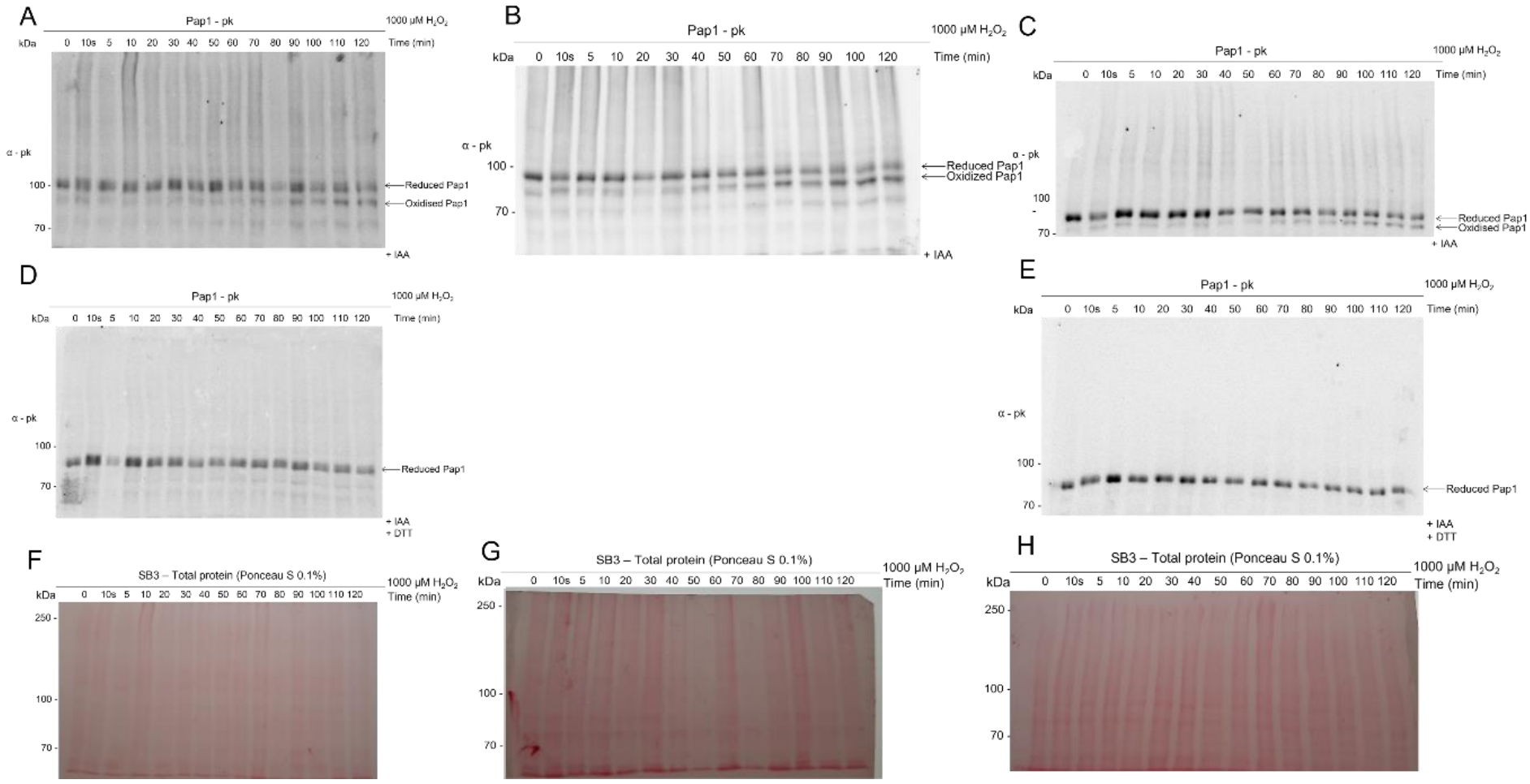

Figure S.14: Representative western blots of *S. pombe* cells following exposure to 1000 µM hydrogen peroxide.

The blots depict Pap1 oxidized and reduced bands over a 120-minute time course (A-C), Pap1 reduced bands after DTT treatment (D-E), and blots stained with Ponceau S to observe total protein (F-H).

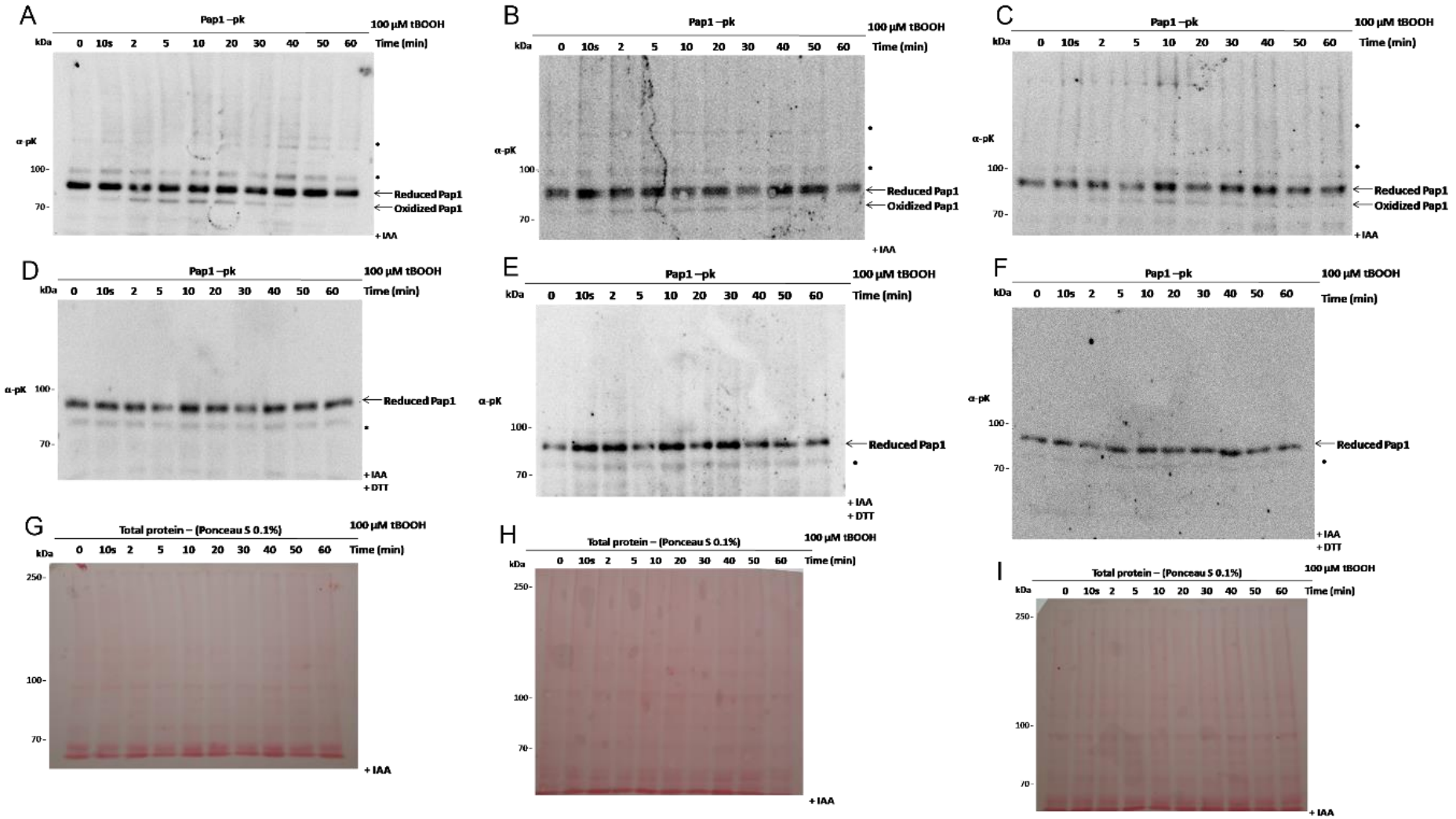

Figure S.15: Representative western blots of *S. pombe* cells following exposure to 100 µM *t*-BOOH.

The blots depict Pap1 oxidized and reduced bands over a 60-minute time course (A-C), Pap1 reduced bands after DTT treatment (D-F), and blots stained with Ponceau S to observe total protein (G-I).

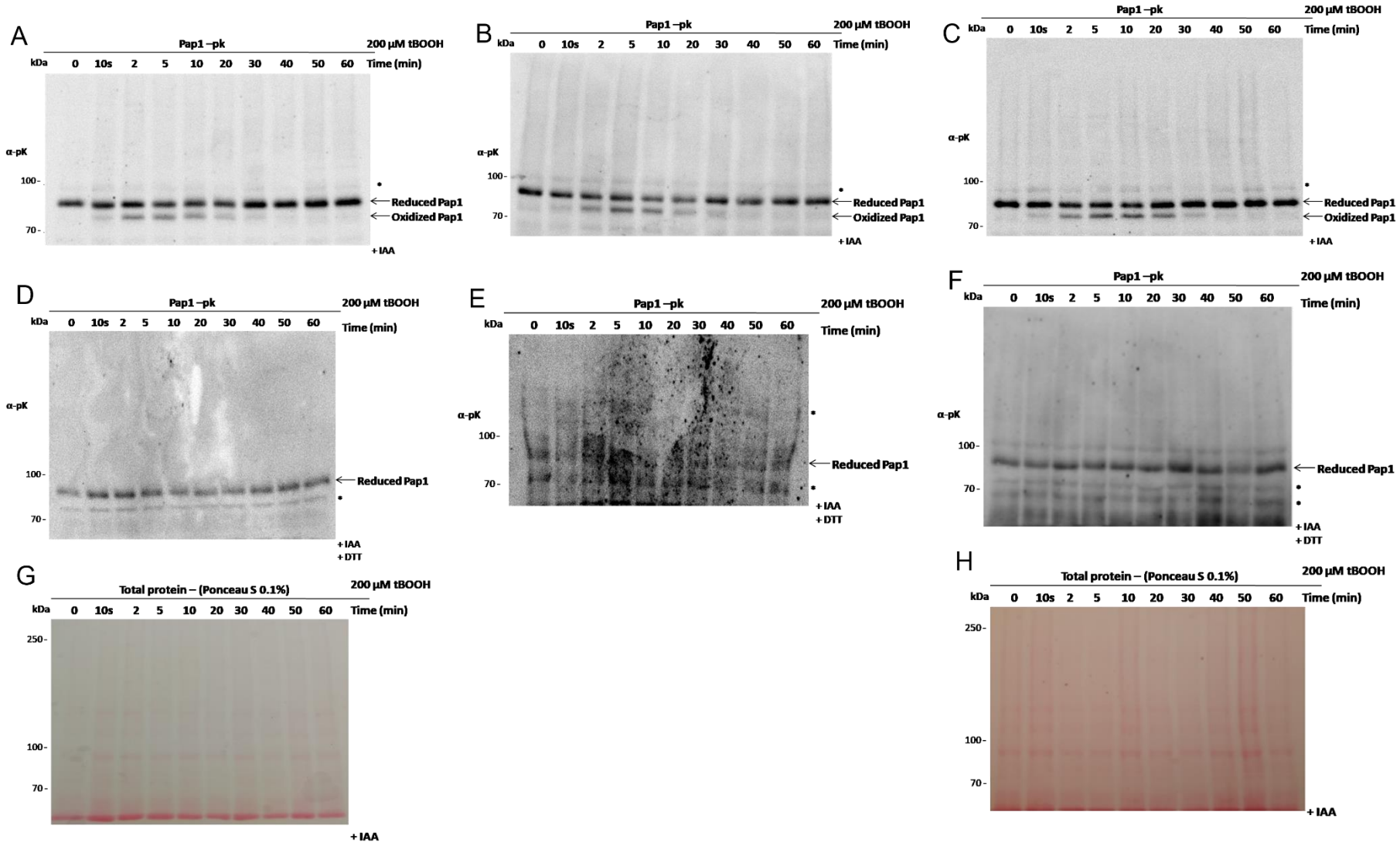

Figure S.16: Representative western blots of *S. pombe* cells following exposure to 200 µM *t*-BOOH.

The blots depict Pap1 oxidized and reduced bands over a 60-minute time course (A-C), Pap1 reduced bands after DTT treatment (D-F), and blots stained with Ponceau S to observe total protein (G-I).

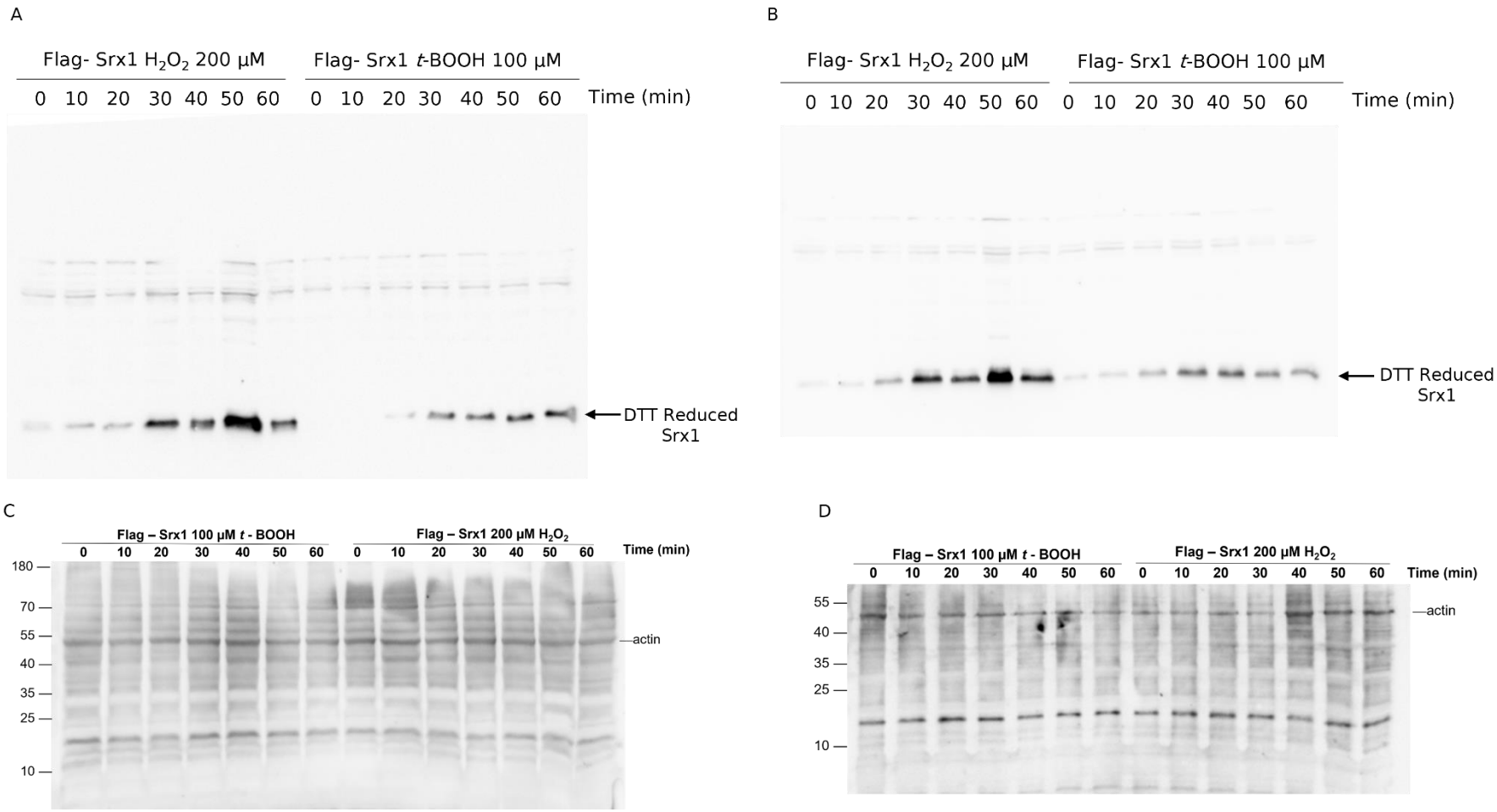

Figure S.17: Representative western blots of Flagsrx1 expression following exposure of cells expressing Flag-epitope-tagged Srx1 to 200 µM hydrogen peroxide and 100 µM *t*-BOOH.

The expression of FlagSrx1 (17~kDa) was monitored over a 60-minute time course after the bolus addition of hydrogen peroxide and t-BOOH (A-C) and actin (47~kDa) was used as a loading control (D-F).

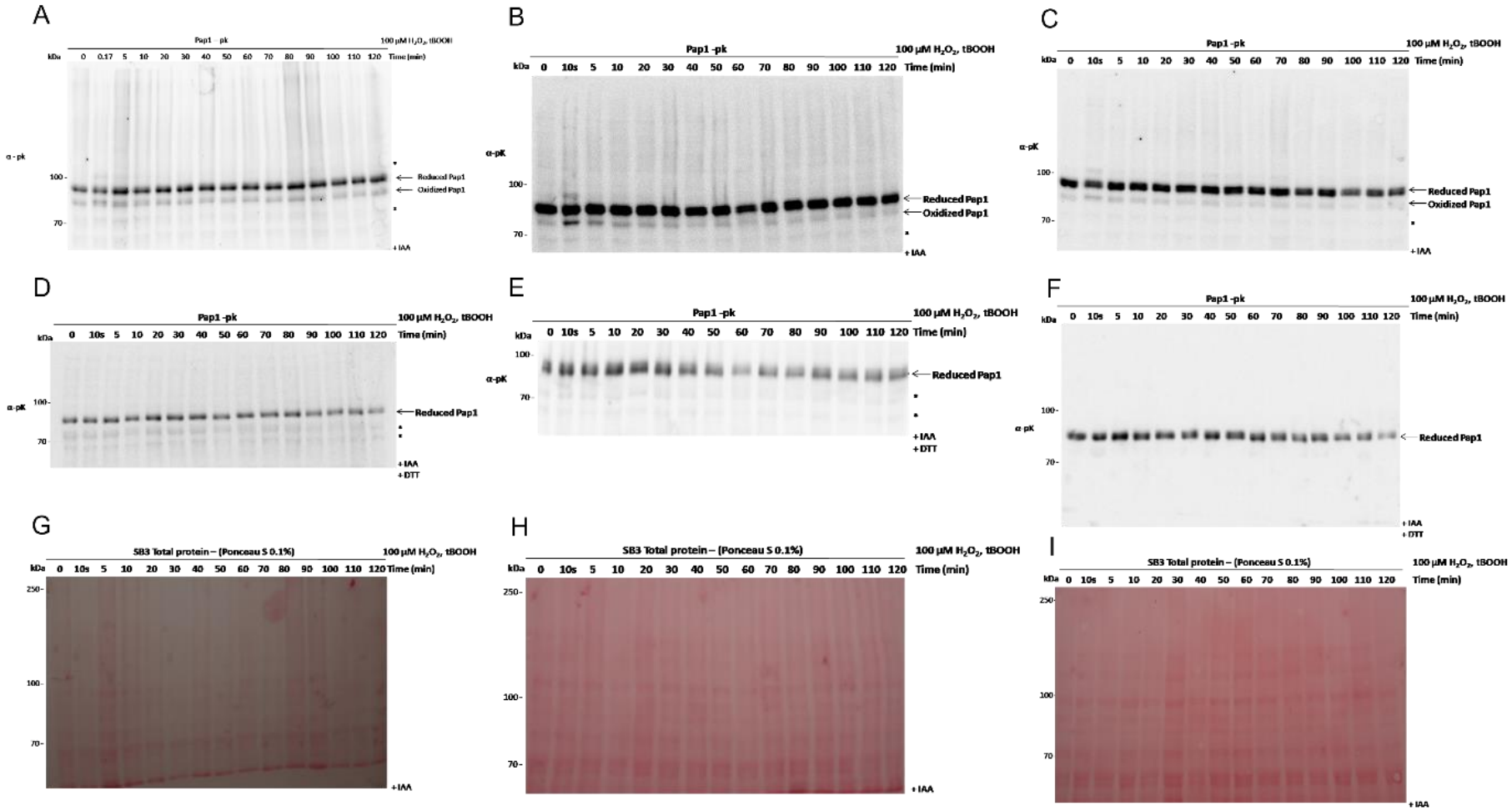

Figure S.18: Representative western blots of S. pombe cells following the co-exposure of 100 µM hydrogen peroxide and 100 µM t-BOOH. *The blots depict Pap1 oxidized and reduced bands over a 120-minute time course (A-C), Pap1 reduced bands after DTT treatment (D-F), and blots stained with Ponceau S to observe total protein (G-I).*

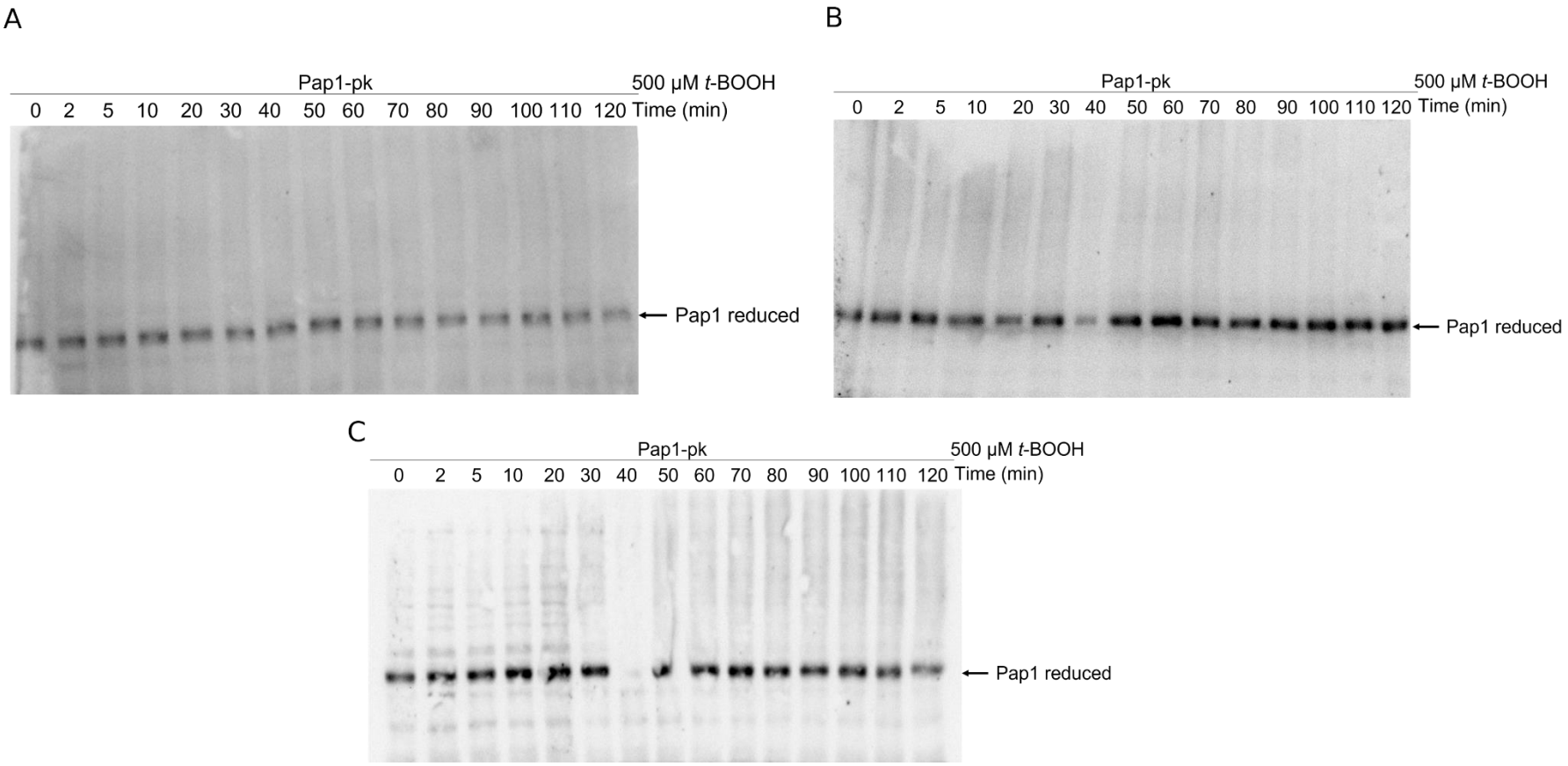

Figure S.19: Representative western blots of *S. pombe* cells following exposure to 500 μM hydrogen *t*-BOOH.

S. pombe cells were cultured to mid-exponential phase and then exposed to 500 μM t-BOOH. Samples were collected over a two-hr period from which protein was collected. The oxidation state of Pap1 was assessed by western blotting (A-C).

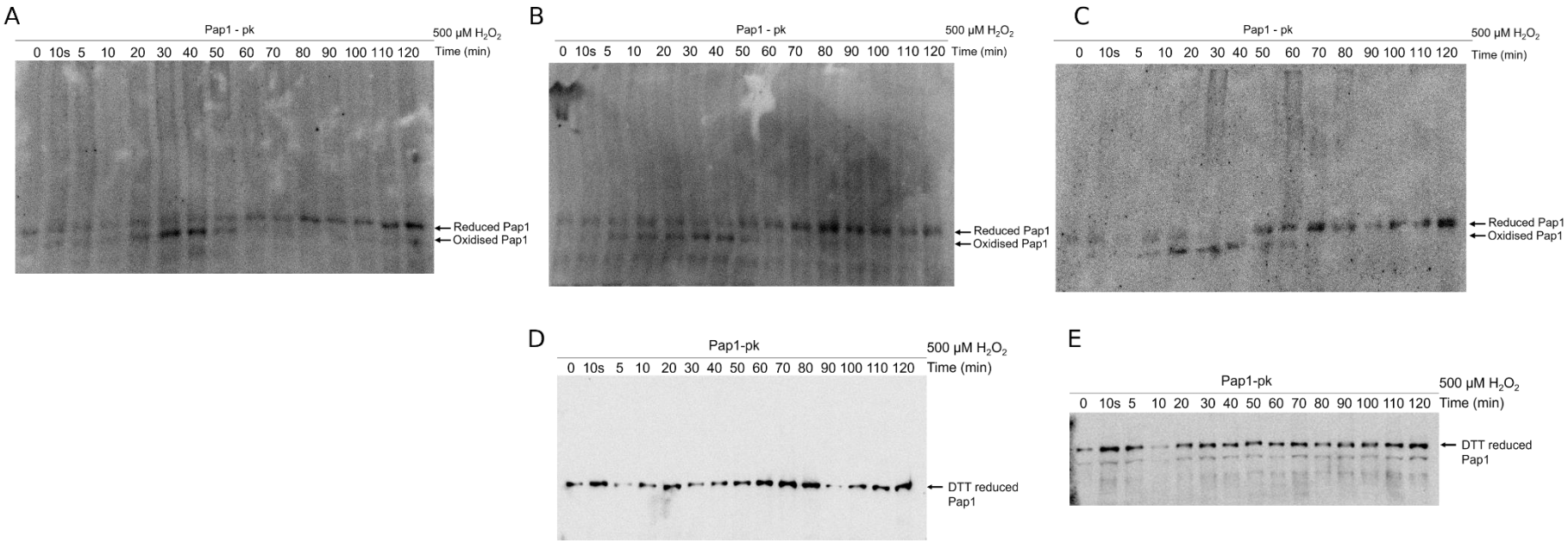

Figure S.20: Representative western blots of *S. pombe* cells following pre-exposure to 100 µM hydrogen peroxide and subsequent dosage with 500 µM hydrogen peroxide.

The blots depict Pap1 oxidized and reduced bands over a 120-minute time course (A-C), Pap1 reduced bands after DTT treatment (D-E).

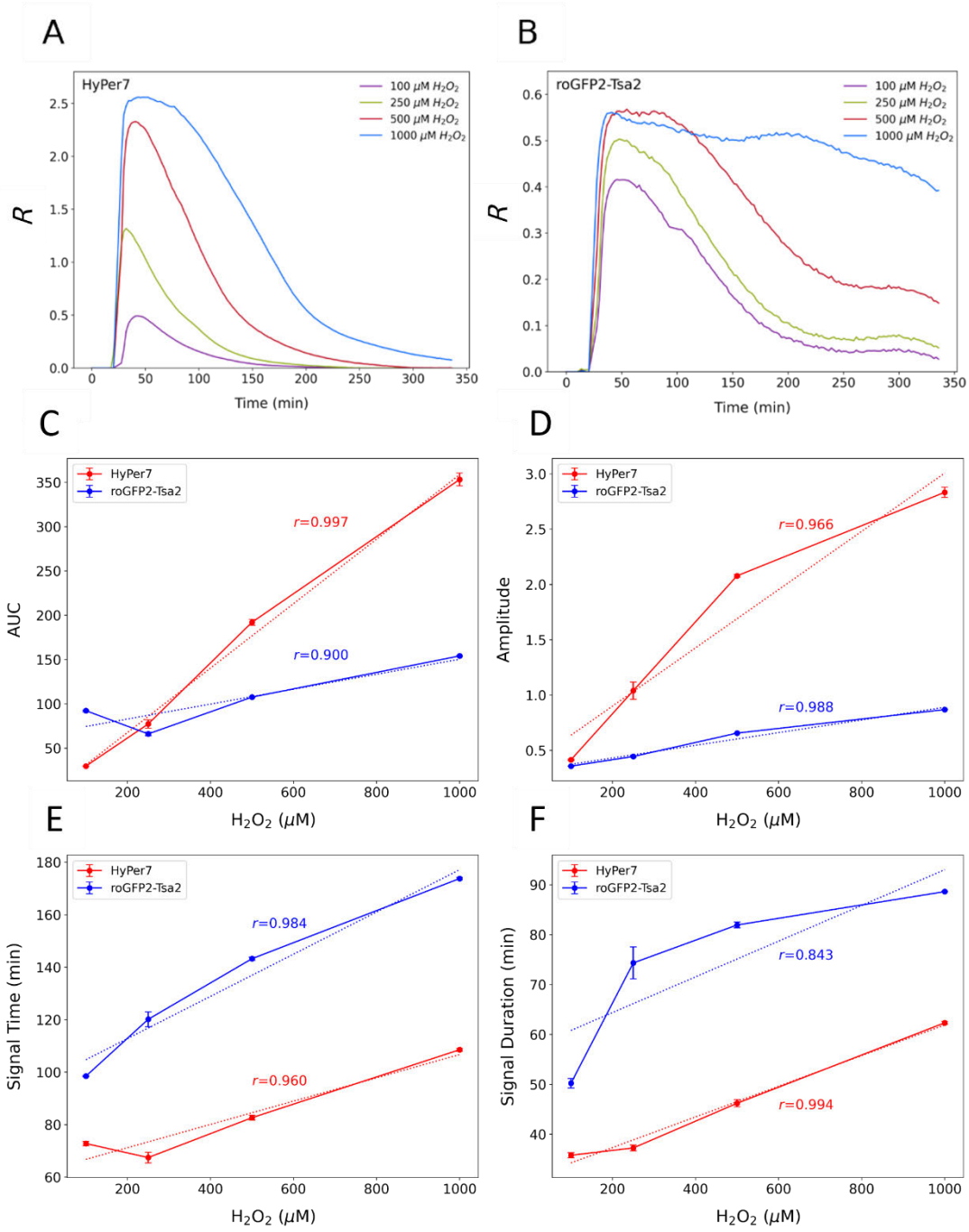

Figure S.21: The signal parameters for HyPer7 and roGFP2-Tsa2 in the same background considering a higher hydrogen peroxide detection range.

S. cerevisiae cells exposed to hydrogen peroxide ranging from 100-1000 µM and the dynamic fluorescence was measured using the genetically encoded redox sensors, HyPer7 and roGFP2-Tsa2 (A-B). The area under the curve was measured (C) and subsequently, the signalling amplitude, time and duration was calculated (D-F). The linear correlation coefficients (r2)

across the signalling parameters for HyPer7 were 0.997, 0.966, 0.960 and 0.994 and for roGFP2-Tsa2 were 0.900, 0.988, 0.984 and 0.843 respectively.

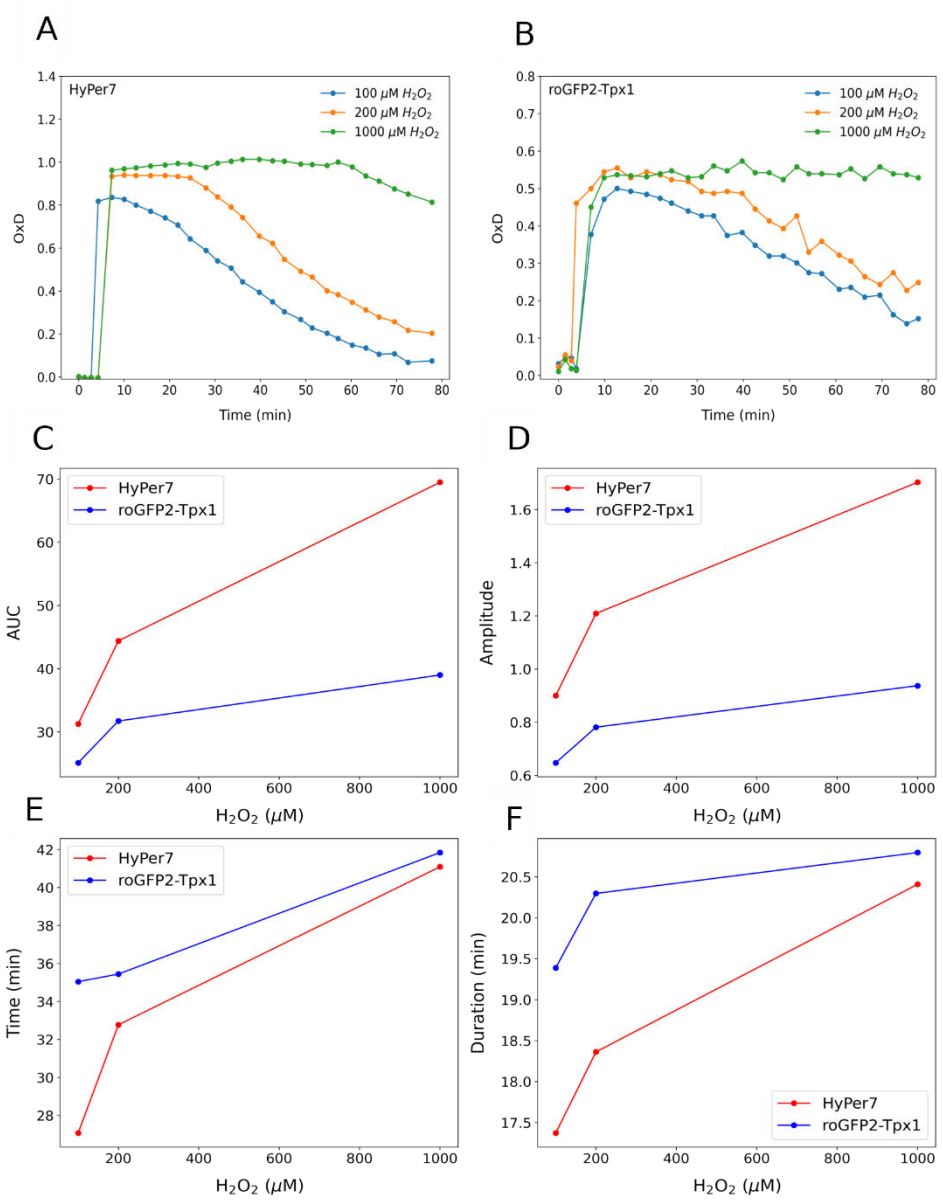

Figure S.22: The signal parameters for HyPer7 and roGFP2-Tpx1 in the same background considering a higher hydrogen peroxide detection range.

S. pombe cells were exposed to hydrogen peroxide ranging from 100-1000 µM, and the dynamic fluorescence was measured using the genetically encoded redox sensors, HyPer7 and

roGFP2-Tpx1 (A-B). The area under the curve was measured (C), and subsequently, the signalling amplitude, time and duration were calculated (D-F).

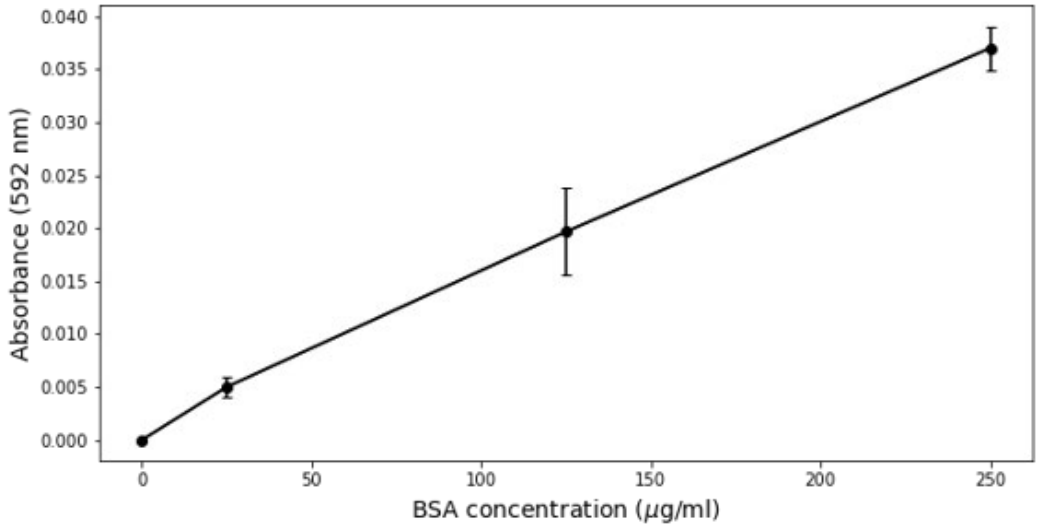

Figure S.23: BSA standard curve to determine the amount of protein to load onto SDS-PAGE gels.

A BSA standard curve ranging from 0 – 250 µg/ml was generated for S. pombe protein cell lysate samples made in IAA buffer (n=3).

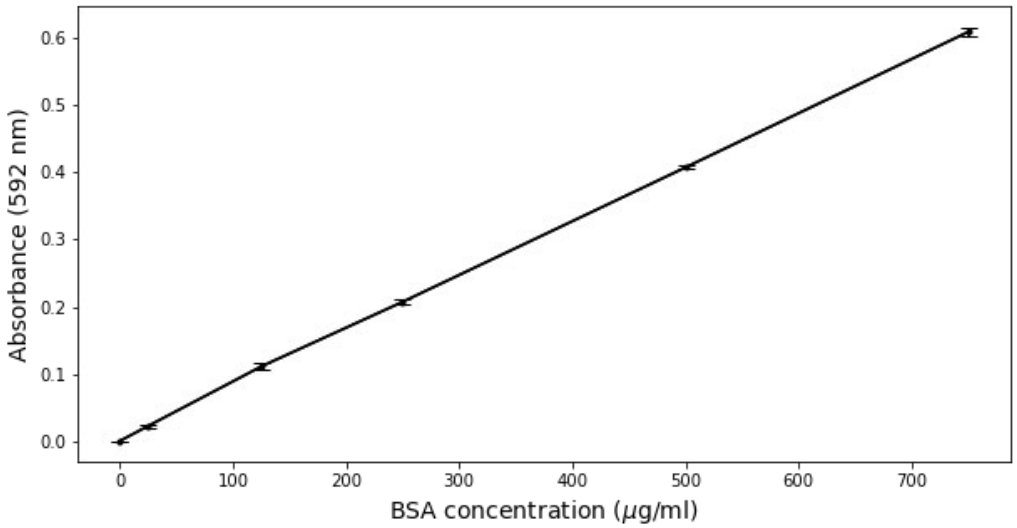

Figure S.24F: BSA standard curve to determine the amount of purified Pap1 protein.

A BSA standard curve ranging from 0 – 700 µg/ml was generated for protein samples in PBS buffer (n=3).

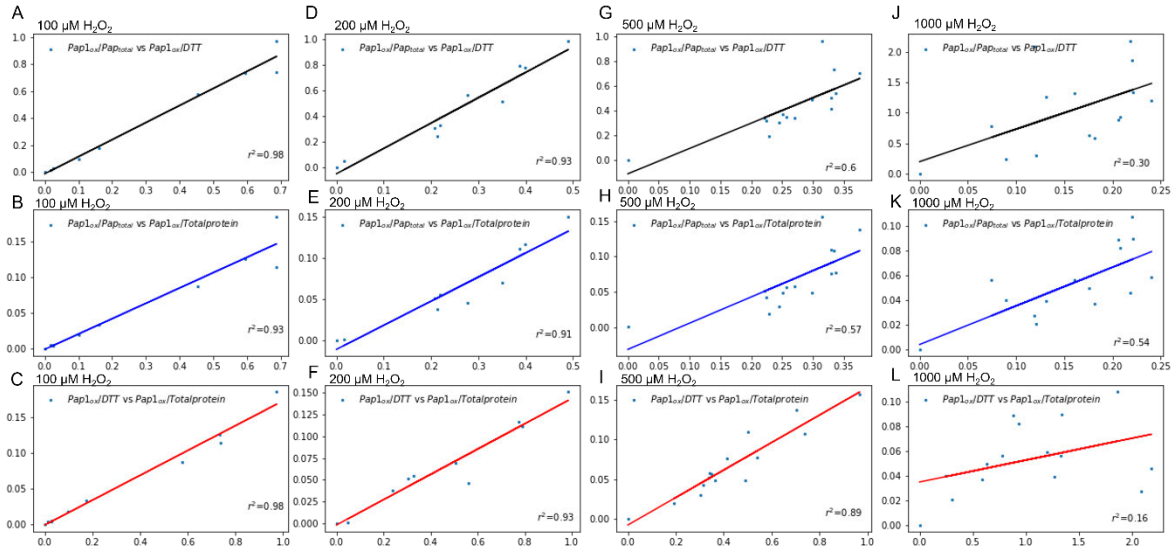

Figure S.25:Linear correlation between different normalisation techniques for signal profile generation.

The linear correlations for Pap1 oxidation after the addition of 100 µM hydrogen peroxide for normalisation with DTT, total Pap1 oxidation and total protein were r^2=0.98, r^2=0.93 and r^2=0.98 respectively (A-C). The correlations at 200 µM were r^2=0.93, r^2=0.91 and r^2=0.93 for normalisation with DTT, total Pap1 oxidation and total protein respectively (D-F). Normalisation with DTT, total Pap1 oxidation and total protein after 500 µM hydrogen peroxide exposure linear correlation values were r^2=0.6, r^2=0.57 and r^2=0.89 (G-I). The addition of 1000 µM hydrogen peroxide resulted in linear correlation values of r^2=0.3, r^2=0.54 and r^2=0.16 for normalisation with DTT, total Pap1 oxidation and total protein respectively (J-L).

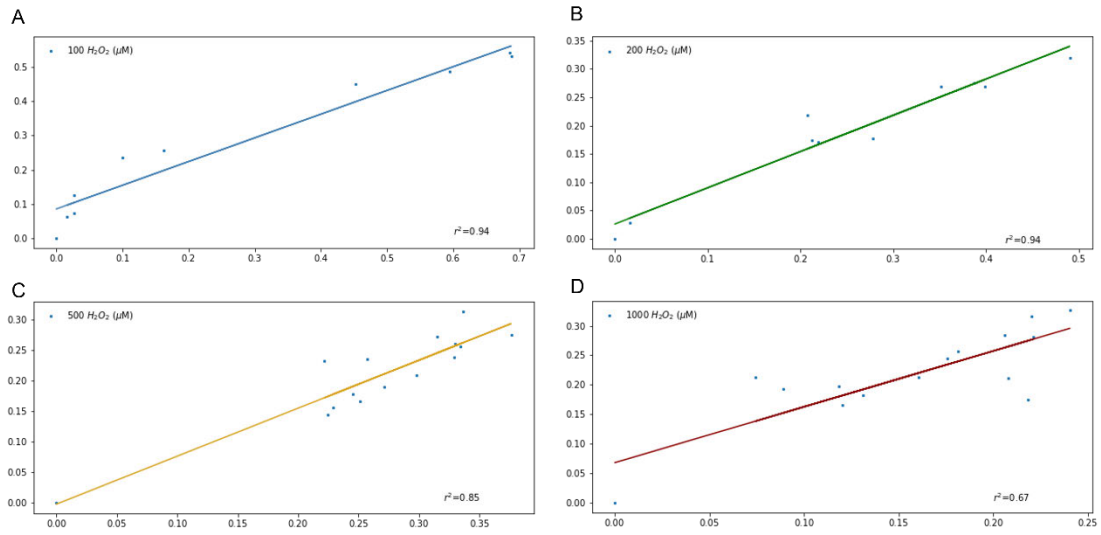

Figure S.26: The linear correlations between Pap1 oxidation profiles obtained from optimized and oversaturated western blots.

When exposed to 100-1000 µM hydrogen peroxide, Pap1 profiles from optimised western blots had significantly higher correlation values (r^2=0.94, r^2=0.94, r^2=0.85, r^2=0.67), compared to oversaturated blots (A-D).

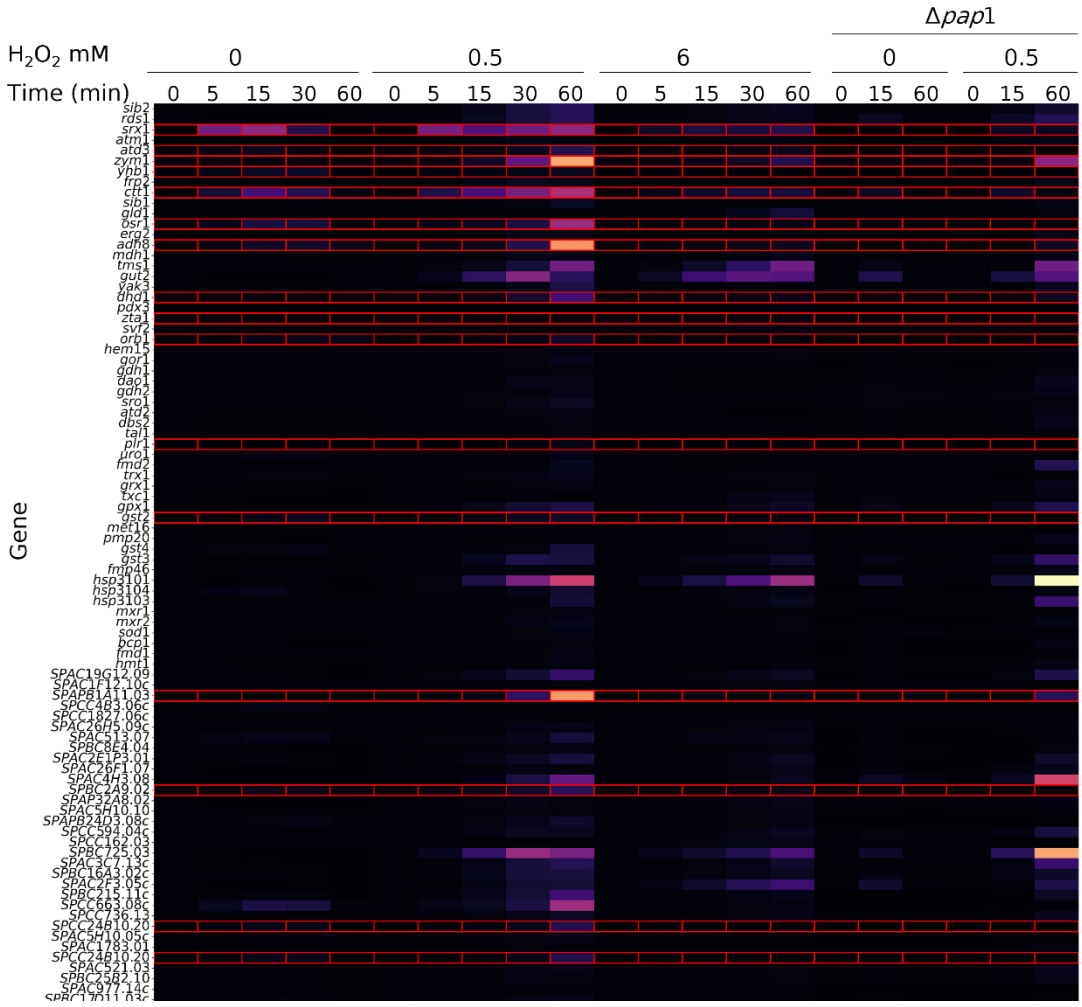

Figure S. 27: The addition of hydrogen peroxide to *S. pombe* cells and the relative gene expression of oxidoreductases genes.

Oxidoreductases function by using cofactors to reduce proteins that have been oxidized playing a critical role in cellular detoxification. In total 105 genes associated to oxidoreductase activity were upregulated at least 2-fold after exposure to 70 µM, 500 µM or 6 mM hydrogen peroxide. The Pap-regulated genes (outlined in red) that showed at least a 2-fold increase in induction after hydrogen peroxide exposure at either are zym1, yhb1, osr1, adh8, dhd1, atd3, zta1, orb1, plr1, ctt1, srx1, gst2, SPAPB1A11.03, SPBC2A9.02, SPAPB24D3.08C, SPCC1739.08C, SPBC23G7.10C, SPCC6630.08C, SPAC1F8.04C, SPCC24B10.20.

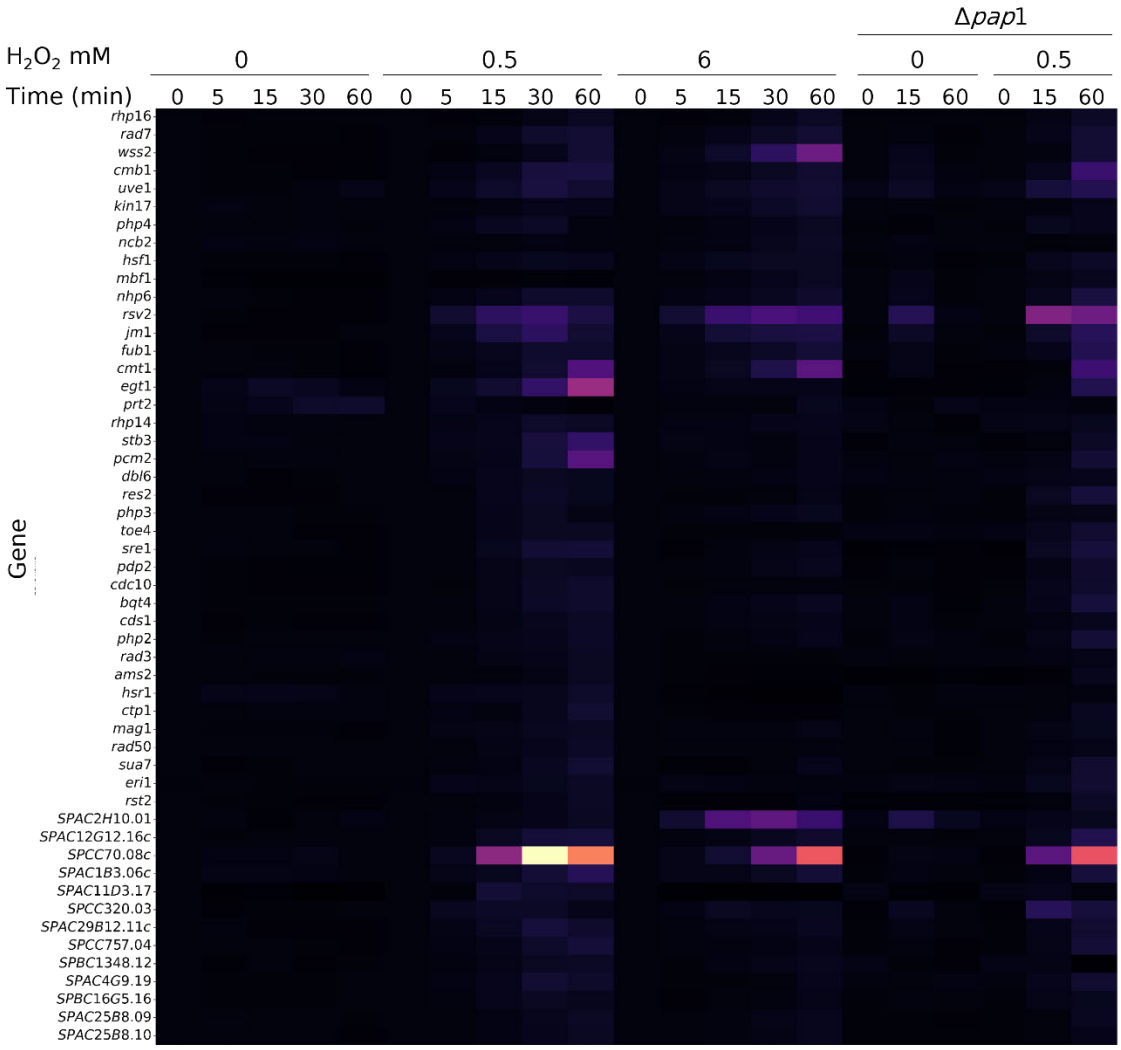

Figure S.28:The addition of hydrogen peroxide to *S. pombe* cells and the relative gene expression of DNA regulation genes.

These genes primarily function in tightly regulating the transcription of genes under various conditions. In total 55 genes were found to be upregulated in this category after exposure to 70 µM, 500 µM and 6 mM hydrogen peroxide. No genes showed downregulation in a Δpap1 strain.

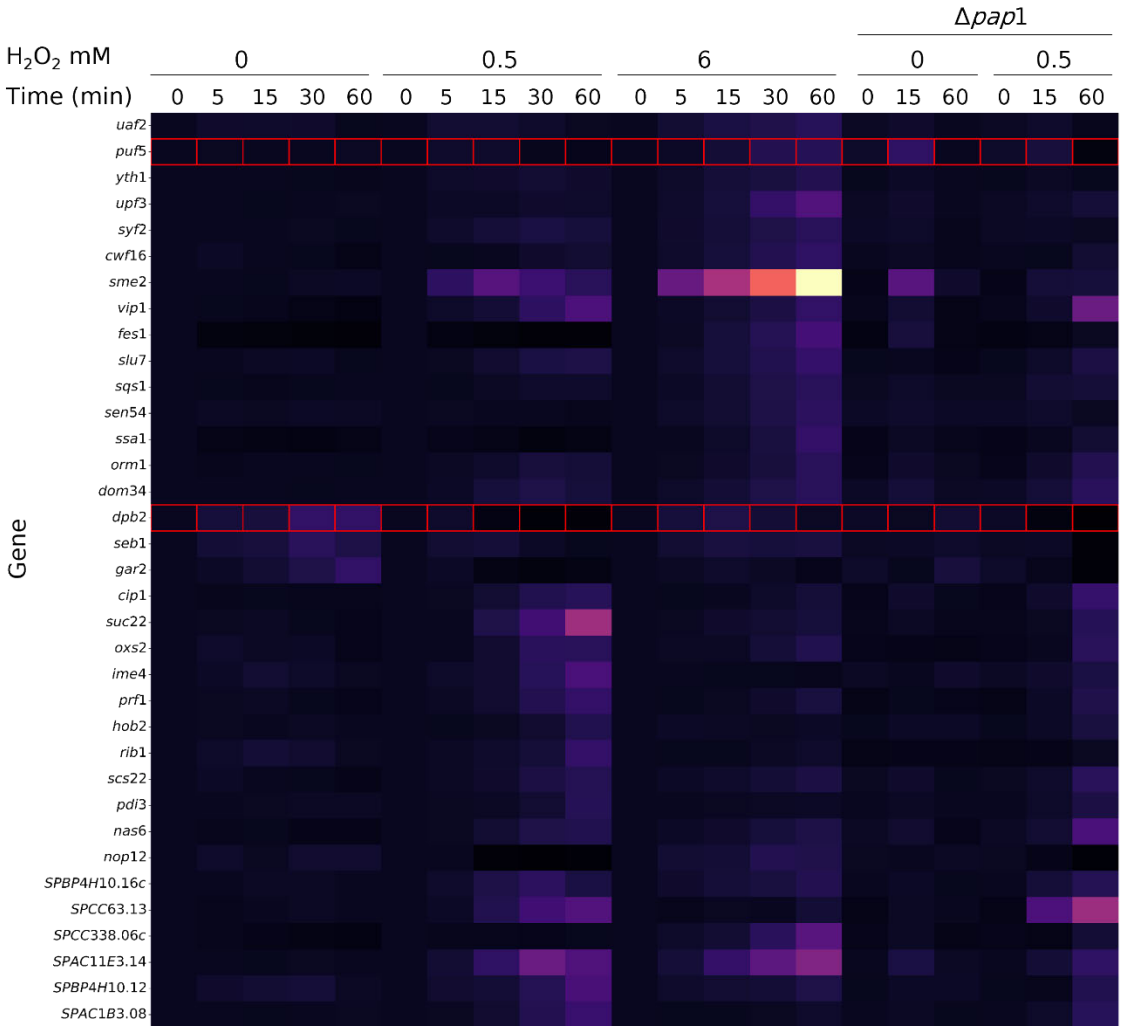

Figure S.29: The addition of hydrogen peroxide to *S. pombe* cells and the relative gene expression of genes associated to mRNA regulation.

These genes primarily function in tightly regulating the proteins that produce, process, transport and degrade mRNA transcripts. In total 38 genes were found to be upregulated in this category after exposure to 70 µM, 500 µM and 6 mM hydrogen peroxide. Of these genes, puf5 and dpb2, showed downregulation in a Δpap1 strain (outlined in red).

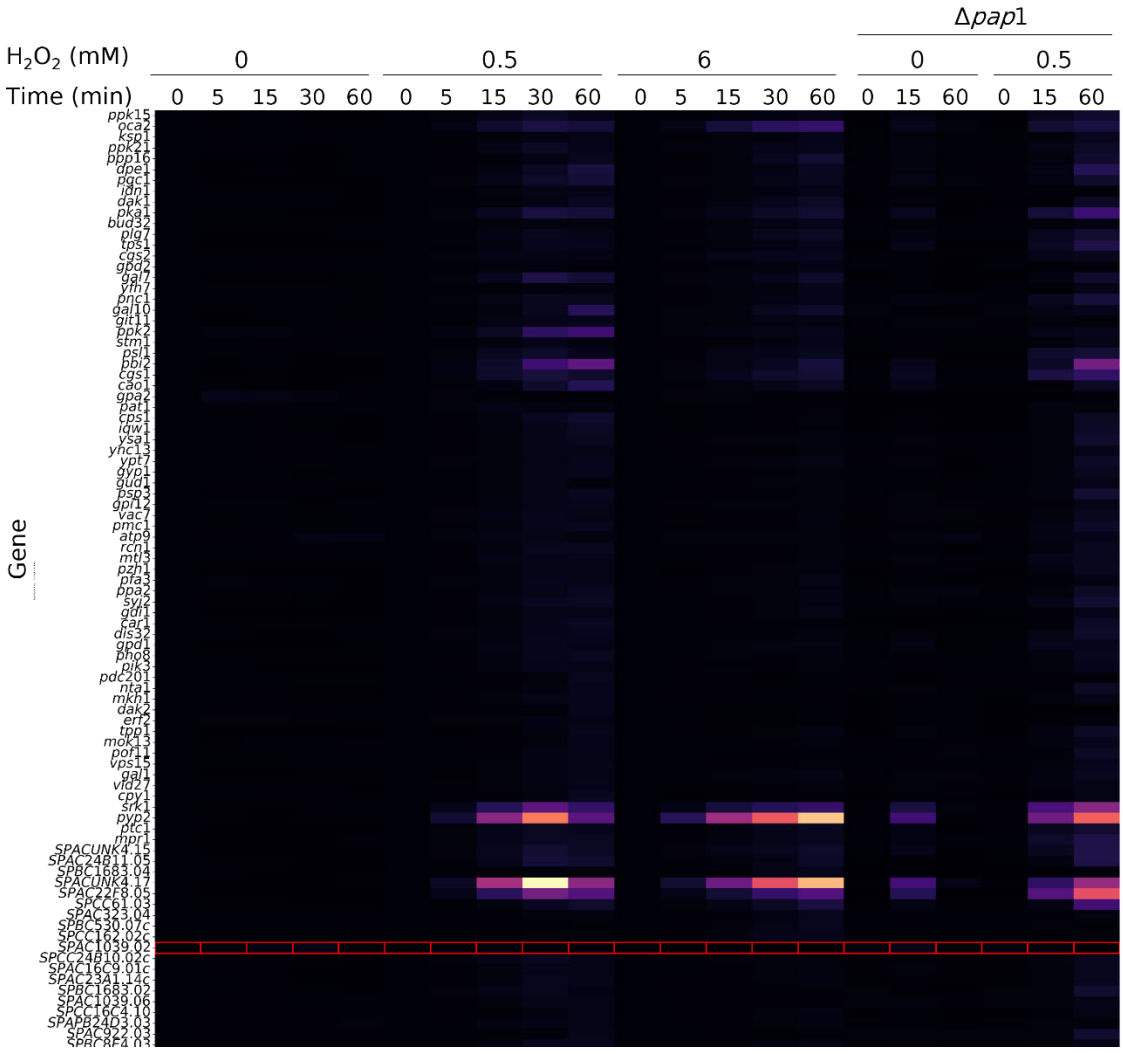

Figure S.30: The addition of hydrogen peroxide to *S. pombe* cells and the relative gene expression of genes associated to signal transduction.

These genes primarily function in tightly regulating the proteins interpret and respond to extracellular signals by relaying information from the cell surface to the nucleus. In total 95 genes were found to be upregulated in this category after exposure to 70 µM, 500 µM and 6 mM hydrogen peroxide. Of these genes, SPAC1039.02c, showed downregulation in a Δpap1 strain (outlined in red).

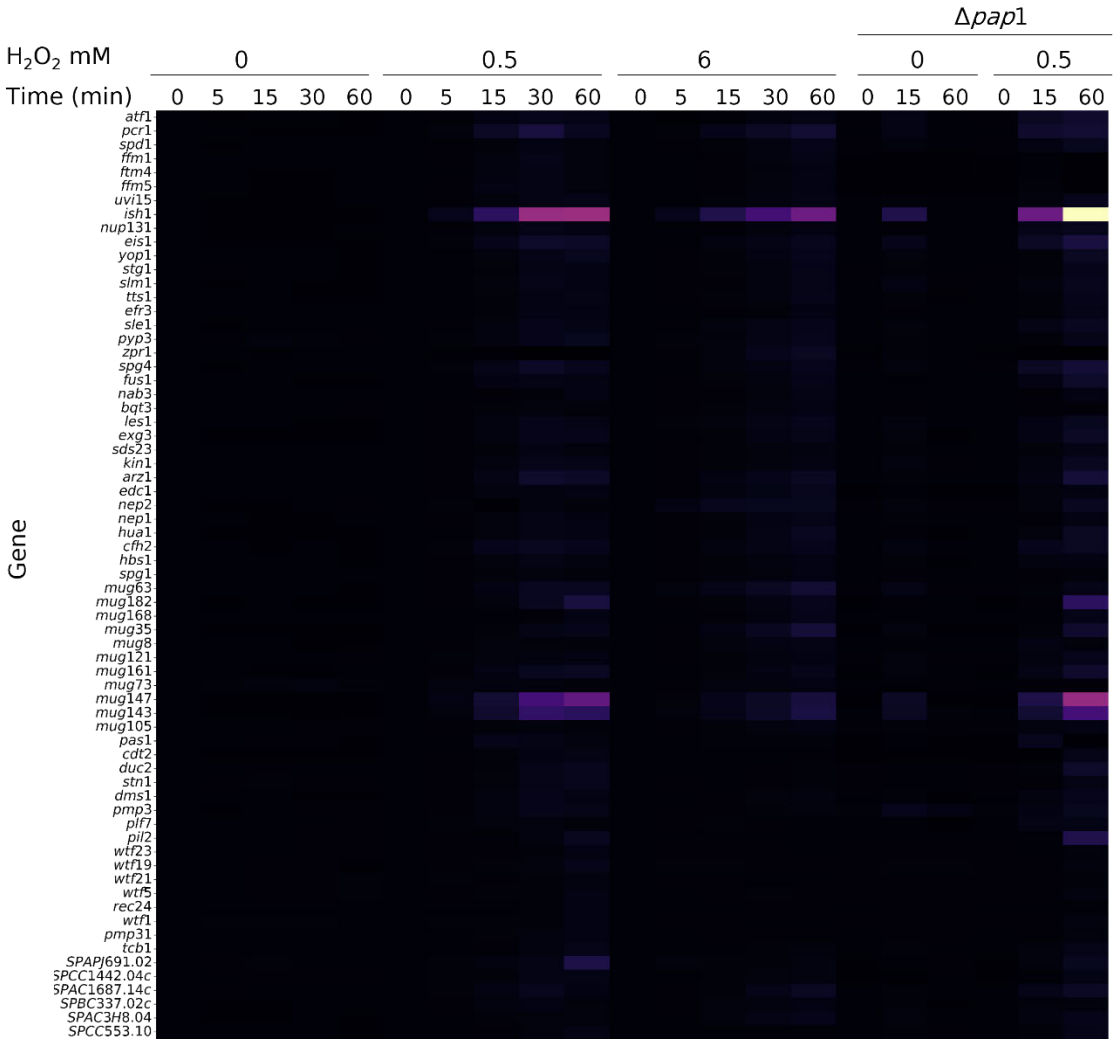

Figure S. 31: The addition of hydrogen peroxide to *S. pombe* cells and the relative gene expression of genes associated to cell cycle regulation.

These genes primarily function in tightly regulating the proteins that ensure the cell accurately replicates DNA and divides while maintaining proper growth and development. In total 78 genes were found to be upregulated in this category after exposure to 70 µM, 500 µM and 6 mM hydrogen peroxide. Of these genes sro1, aft1 and cum1 showed downregulation in a Δpap1 strain.

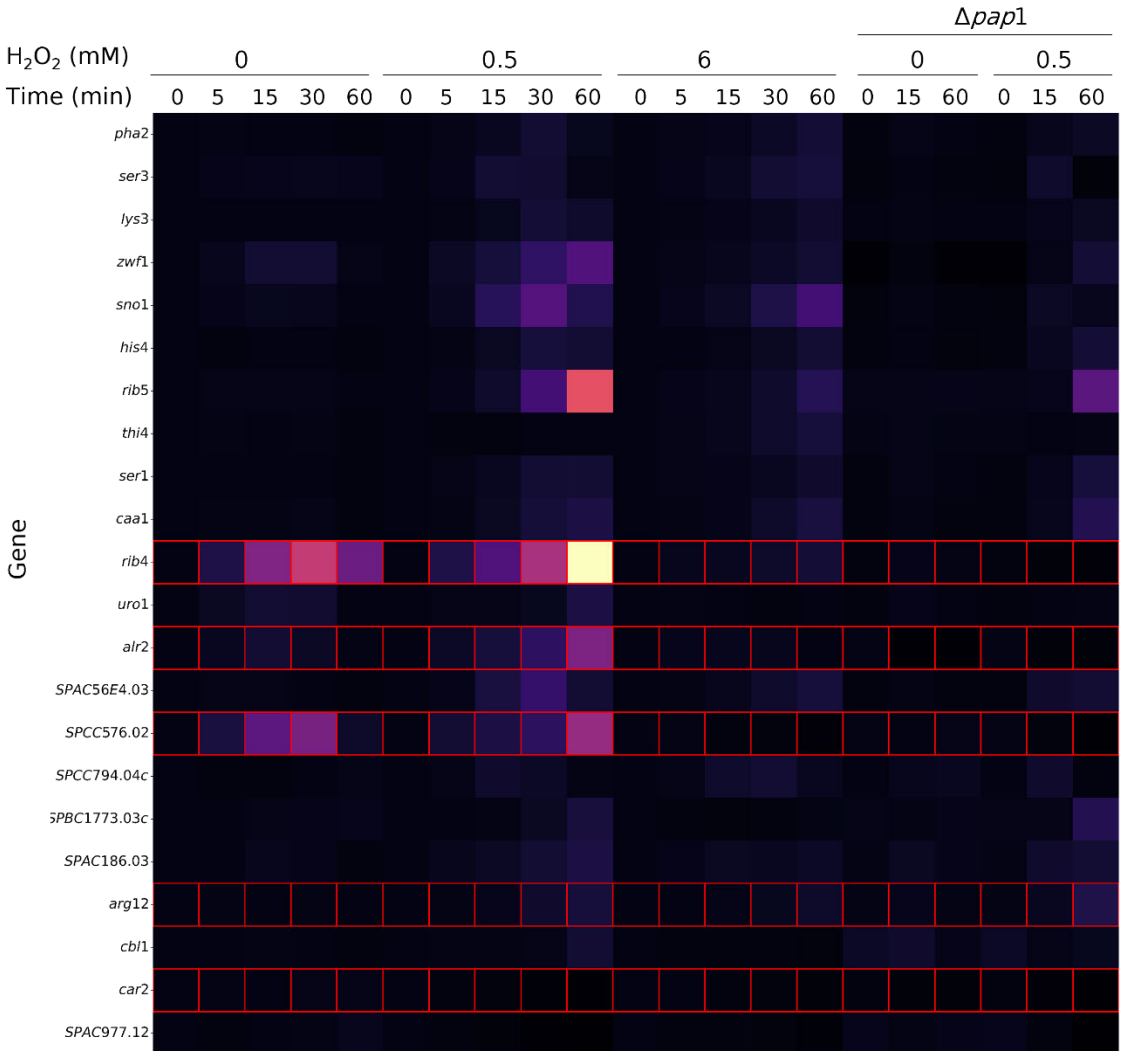

Figure S. 32: The addition of hydrogen peroxide to *S. pombe* cells and the relative gene expression of genes associated to vitamin regulation.

These genes primarily function in tightly regulating the proteins that are involved in the biosynthesis and transport of vitamins. In total 28 genes were found to be upregulated in this category after exposure to 70 µM, 500 µM and 6 mM hydrogen peroxide. Of these genes rib4, alr2, arg12, cbl1, car2, and SPCC794.02c showed downregulation in a Δpap1 strain (outlined in red).

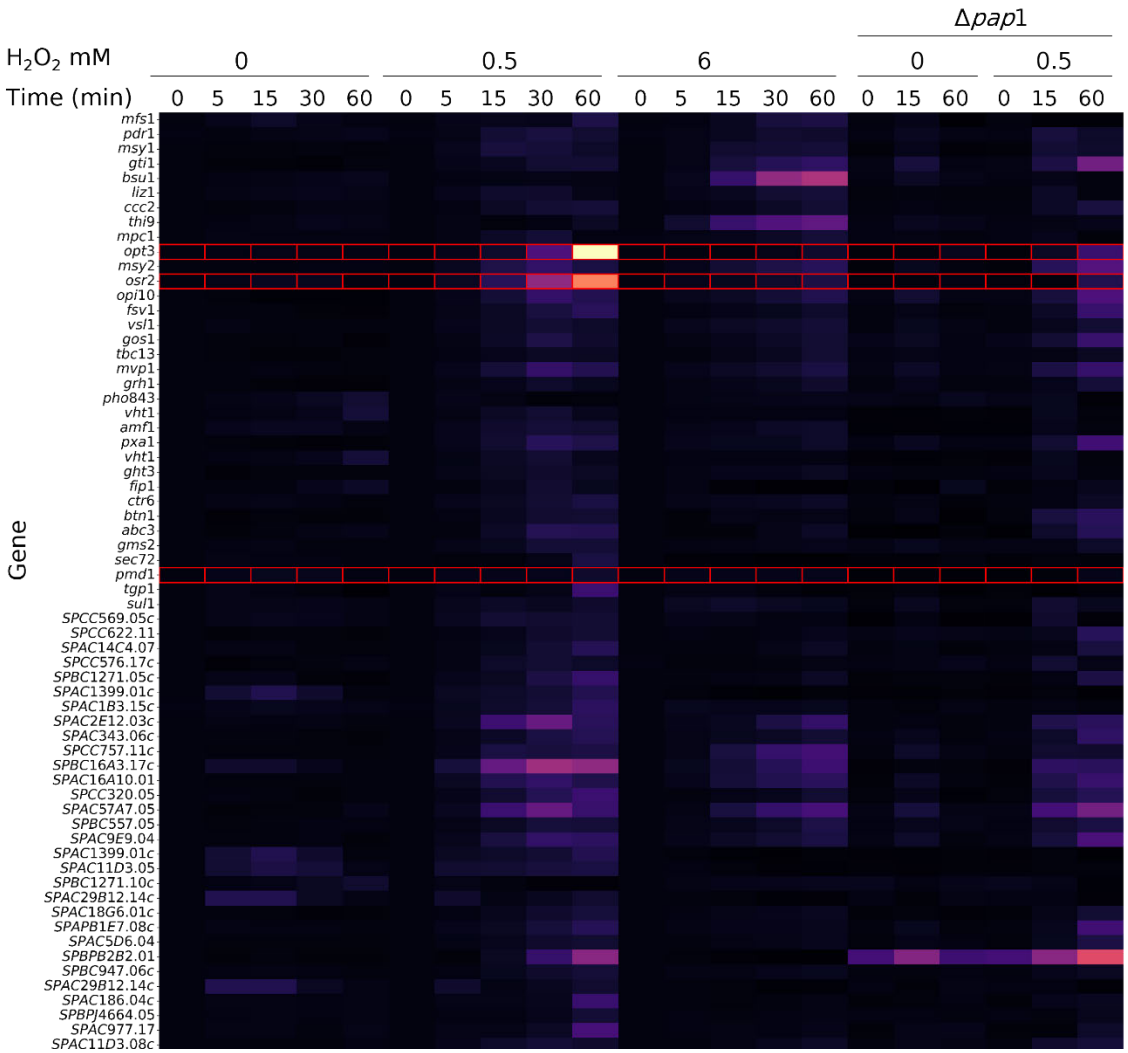

Figure S. 33: The addition of hydrogen peroxide to *S. pombe* cells and the relative gene expression of genes associated to transmembrane transport.

These genes primarily function in tightly regulating the proteins that ensure the movement of substances across cellular membrane.. In total 68 genes were found to be upregulated in this category after exposure to 70 µM, 500 µM and 6 mM hydrogen peroxide. Of these genes caf5, opt3, and osr2 showed downregulation in a Δpap1 strain (outlined in red).

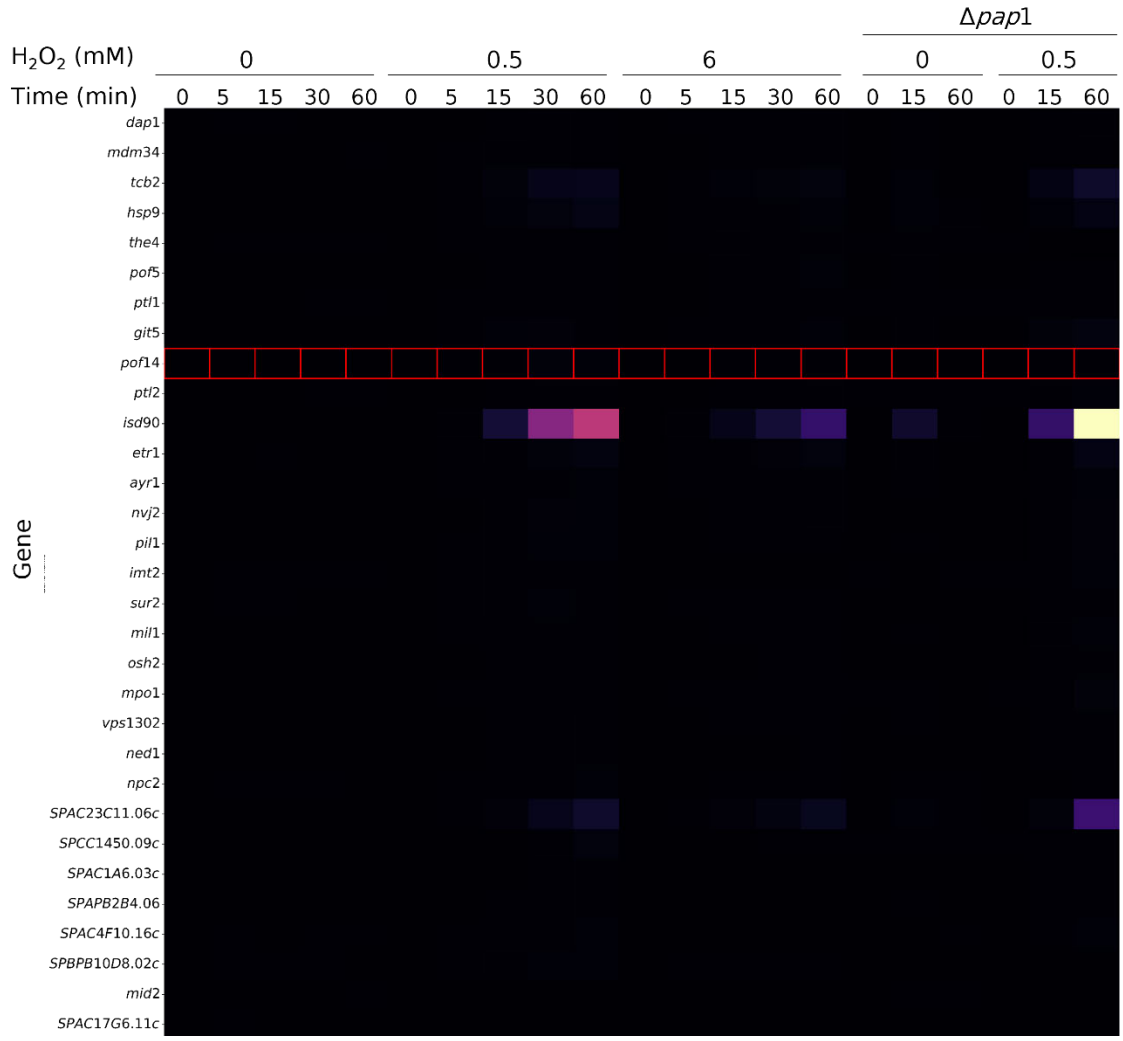

Figure S. 34: The addition of hydrogen peroxide to *S. pombe* cells and the relative gene expression of genes associated to lipid regulation.

These genes primarily function in tightly regulating the proteins that ensure the cell accurately replicates DNA and divides while maintaining proper growth and development. In total 68 genes were found to be upregulated in this category after exposure to 70 µM, 500 µM and 6 mM hydrogen peroxide. Of these genes caf5, opt3, and osr2 showed downregulation in a Δpap1 strain (outlined in red).

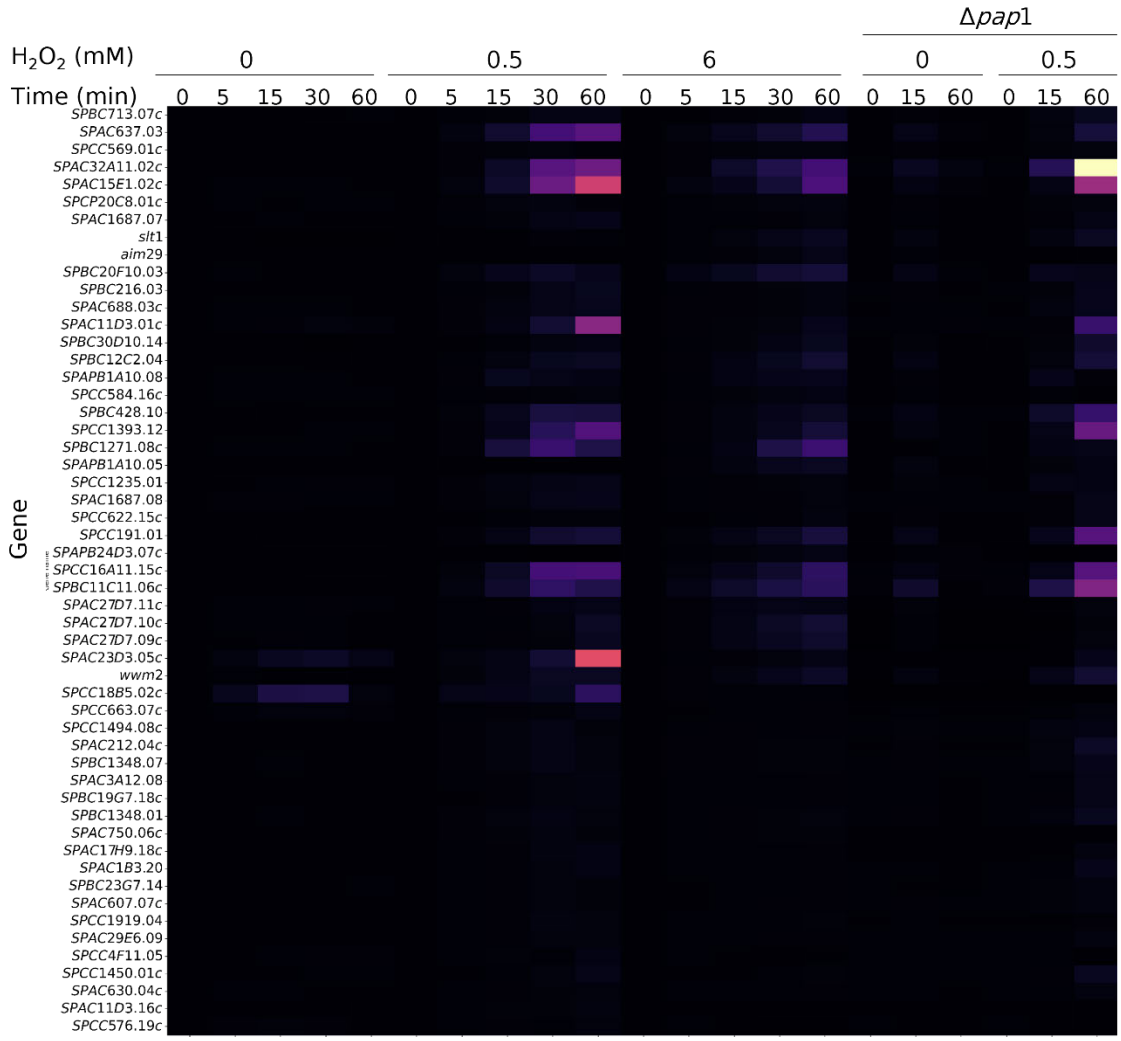

Figure S. 35: The addition of hydrogen peroxide to *S. pombe* cells and the relative gene expression of genes with unknown functions.

These genes have not been assigned a function and further investigations are required to better understand the role of these genes in oxidative stress response. In total 65 genes were found to be upregulated in this category after exposure to 70 µM, 500 µM and 6 mM hydrogen peroxide. Of these genes six showed downregulation in a Δpap1 strain.

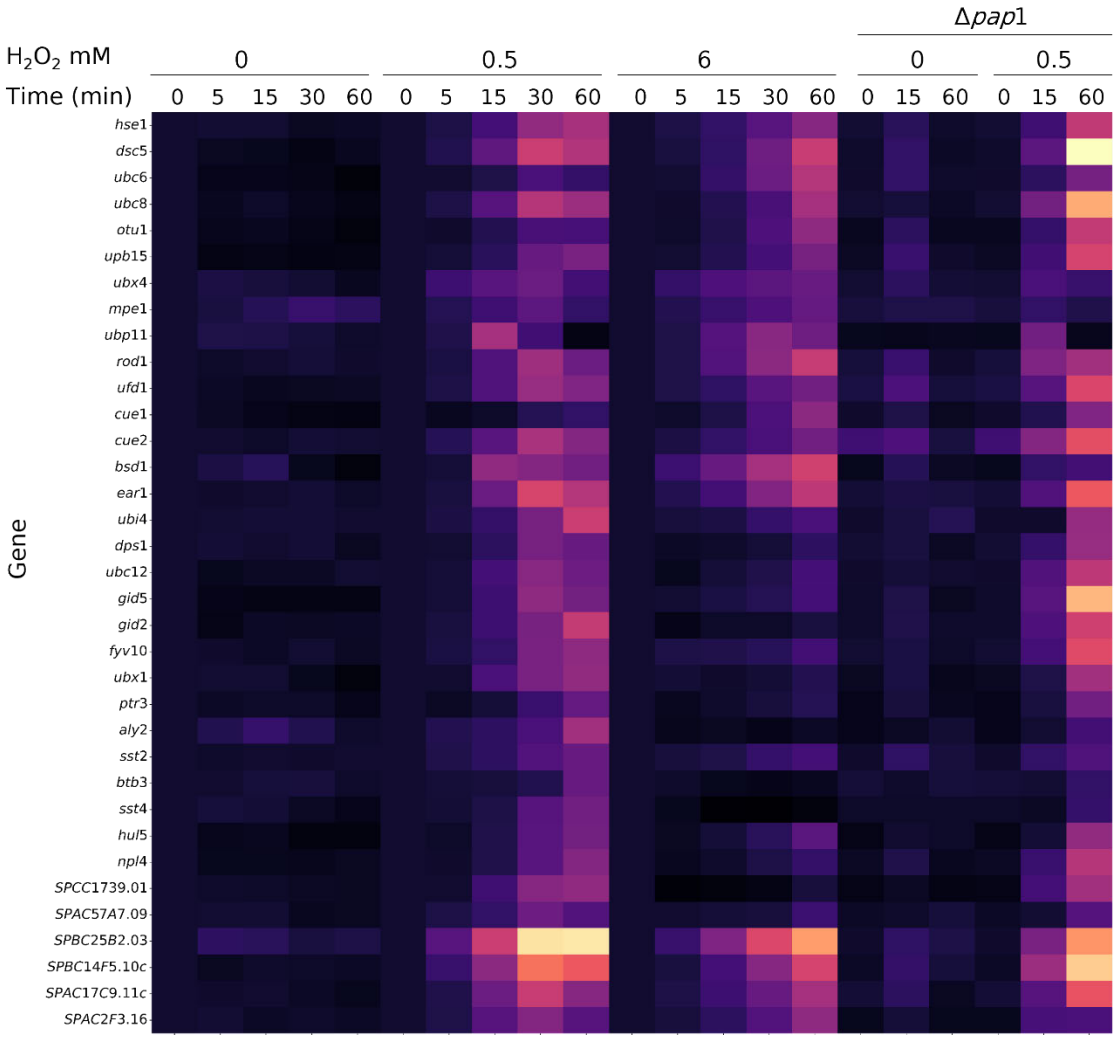

Figure S. 36: The addition of hydrogen peroxide to *S. pombe* cells and the relative gene expression of genes associated to ubiquitin regulation.

These genes primarily function in tightly regulating the proteins that are involved post-translational modifications to maintain cellular metabolic processes. In total 37 genes were found to be upregulated in this category after exposure to 70 µM, 500 µM and 6 mM hydrogen peroxide. Of these genes none showed downregulation in a Δpap1 strain.

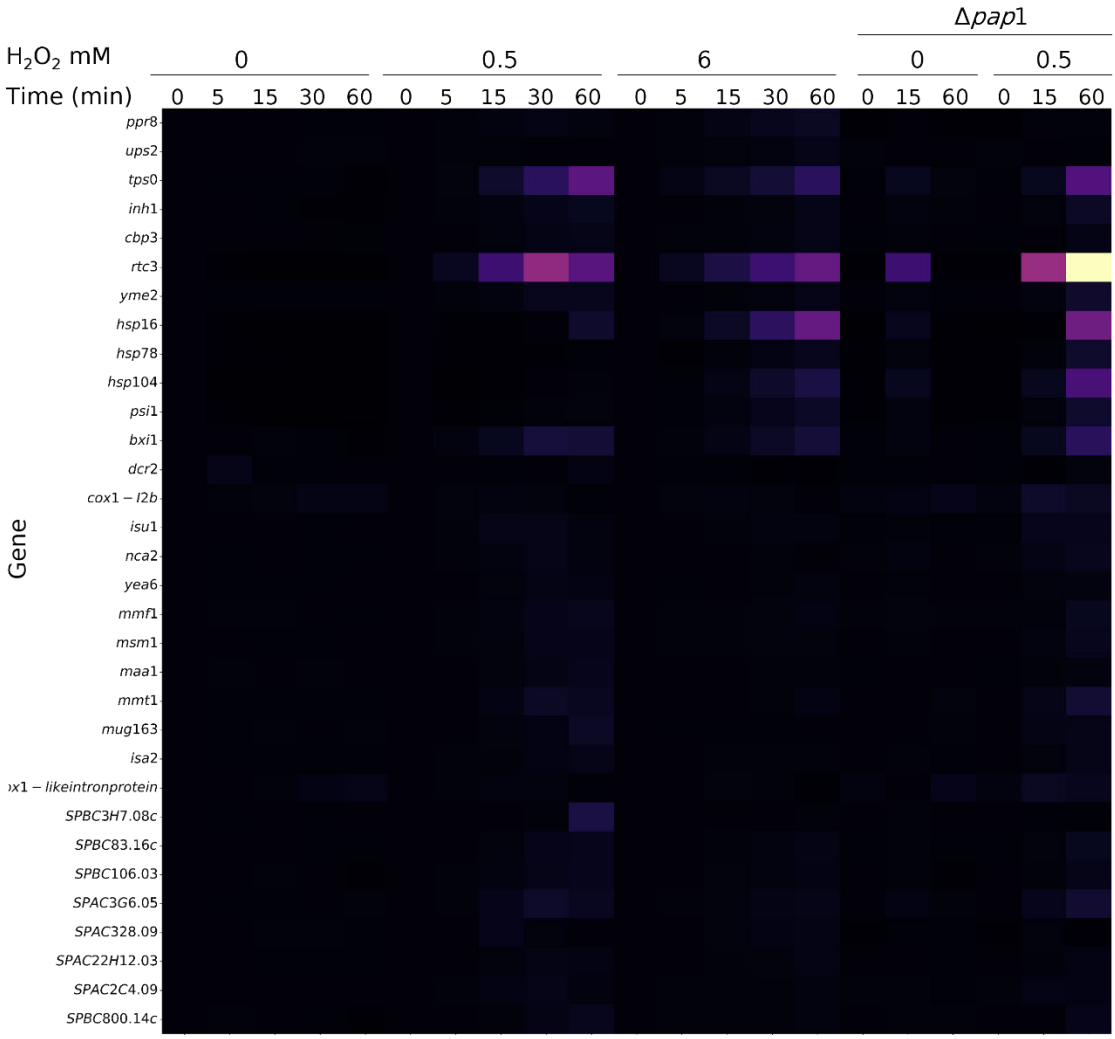

Figure S.37: The addition of hydrogen peroxide to *S. pombe* cells and the relative gene expression of genes associated to mitochondrial regulation.

These genes primarily function in tightly regulating the structure, integrity and functionality of the mitochondria. In total 35 genes were found to be upregulated in this category after exposure to 70 µM, 500 µM and 6 mM hydrogen peroxide. Of these genes none showed downregulation in a Δpap1 strain.

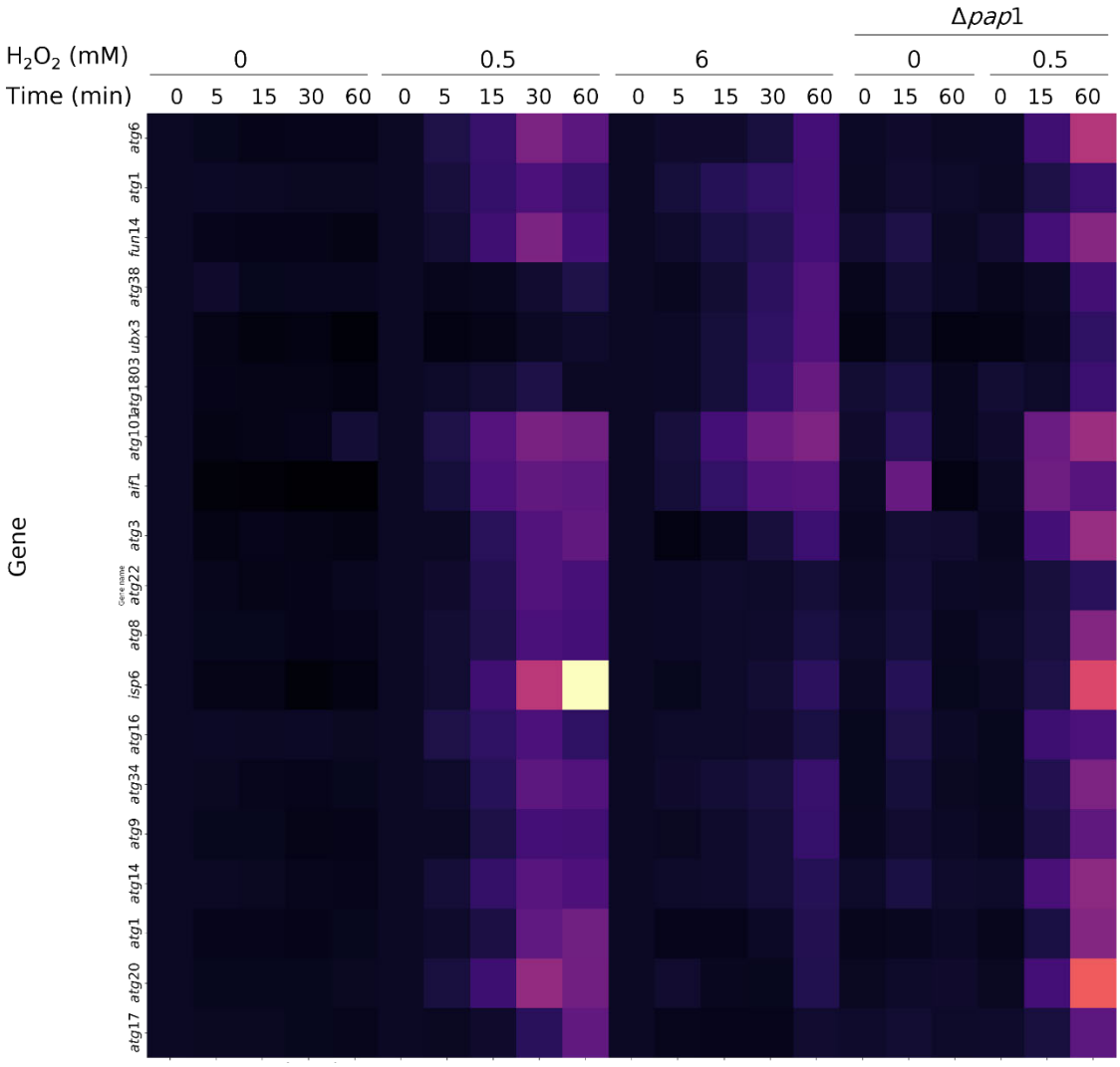

Figure S.38: The addition of hydrogen peroxide to *S. pombe* cells and the relative gene expression of genes associated to autophagy.

These genes primarily function in tightly regulating the process of autophagy and the proteins responsible for degrading and recycling damaged cellular components. In total 22 genes were found to be upregulated in this category after exposure to 70 µM, 500 µM and 6 mM hydrogen peroxide. Of these genes none showed downregulation in a Δpap1 strain.

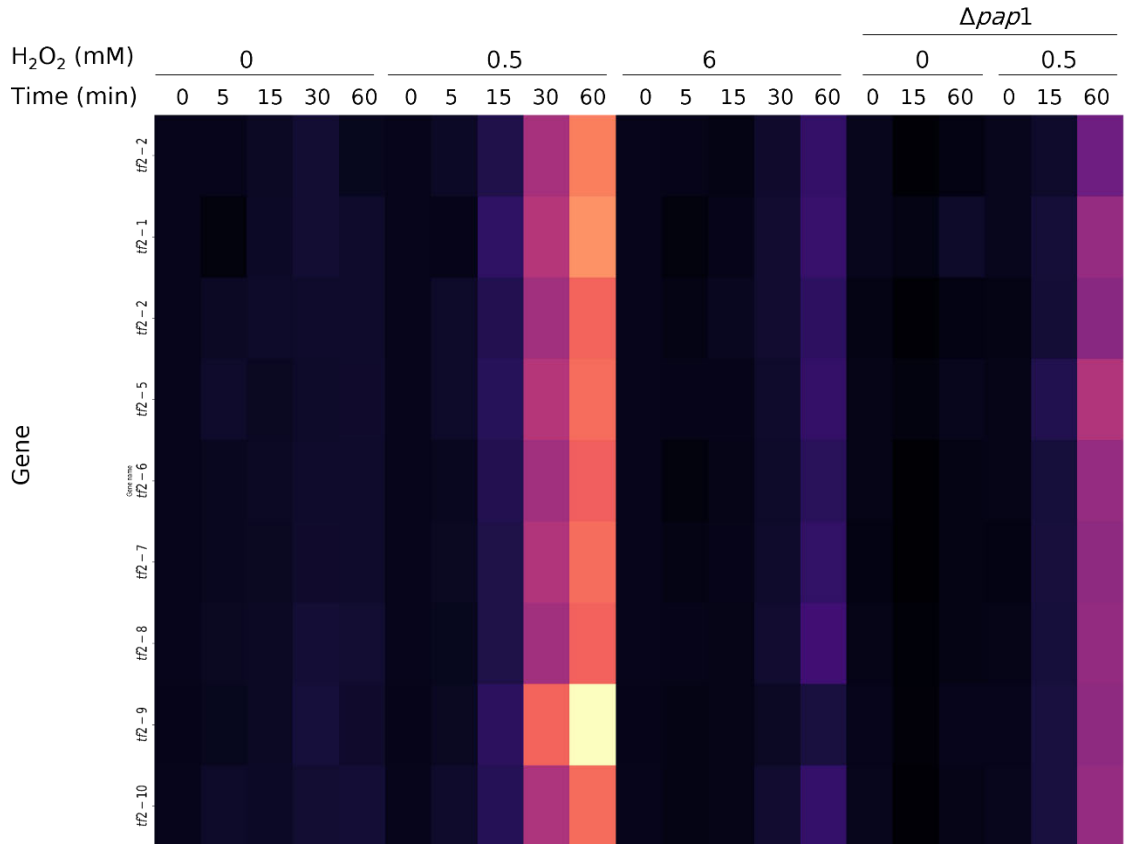

Figure S.39: The addition of hydrogen peroxide to *S. pombe* cells and the relative gene expression of genes associated to retrotransposon activity.

These genes primarily function in tightly regulating genome stability, silencing and gene regulation. In total 9 genes were found to be upregulated in this category after exposure to 70 µM, 500 µM and 6 mM hydrogen peroxide. Of these genes none showed downregulation in a Δpap1 strain.